LEABHARLANN CHOLÁISTE NA TRÍONÓIDE, BAILE ÁTHA CLIATH | TRINITY COLLEGE LIBRARY DUBLIN
Ollscoil Átha Cliath | The University of Dublin

Terms and Conditions of Use of Digitised Theses from Trinity College Library Dublin

Copyright statement

All material supplied by Trinity College Library is protected by copyright (under the Copyright and Related Rights Act, 2000 as amended) and other relevant Intellectual Property Rights. By accessing and using a Digitised Thesis from Trinity College Library you acknowledge that all Intellectual Property Rights in any Works supplied are the sole and exclusive property of the copyright and/or other IPR holder. Specific copyright holders may not be explicitly identified. Use of materials from other sources within a thesis should not be construed as a claim over them.

A non-exclusive, non-transferable licence is hereby granted to those using or reproducing, in whole or in part, the material for valid purposes, providing the copyright owners are acknowledged using the normal conventions. Where specific permission to use material is required, this is identified and such permission must be sought from the copyright holder or agency cited.

Liability statement

By using a Digitised Thesis, I accept that Trinity College Dublin bears no legal responsibility for the accuracy, legality or comprehensiveness of materials contained within the thesis, and that Trinity College Dublin accepts no liability for indirect, consequential, or incidental, damages or losses arising from use of the thesis for whatever reason. Information located in a thesis may be subject to specific use constraints, details of which may not be explicitly described. It is the responsibility of potential and actual users to be aware of such constraints and to abide by them. By making use of material from a digitised thesis, you accept these copyright and disclaimer provisions. Where it is brought to the attention of Trinity College Library that there may be a breach of copyright or other restraint, it is the policy to withdraw or take down access to a thesis while the issue is being resolved.

Access Agreement

By using a Digitised Thesis from Trinity College Library you are bound by the following Terms & Conditions. Please read them carefully.

I have read and I understand the following statement: All material supplied via a Digitised Thesis from Trinity College Library is protected by copyright and other intellectual property rights, and duplication or sale of all or part of any of a thesis is not permitted, except that material may be duplicated by you for your research use or for educational purposes in electronic or print form providing the copyright owners are acknowledged using the normal conventions. You must obtain permission for any other use. Electronic or print copies may not be offered, whether for sale or otherwise to anyone. This copy has been supplied on the understanding that it is copyright material and that no quotation from the thesis may be published without proper acknowledgement.

NOVEL PHARMACEUTICAL EXCIPIENTS

Presented by

Shane Reed Levis, B.Sc. (Pharm.)

under the direction and supervision of

Professor Patrick B. Deasy, B.Sc. (Pharm.), M.A., Ph.D., F.T.C.D., F.P.S.I.

for a

DOCTOR OF PHILOSOPHY DEGREE

at the

University of Dublin, Trinity College

Research for which was performed in the

Department of Pharmaceutics
SCHOOL OF PHARMACY

September 2000

TRINITY COLLEGE
15 DEC 2000
LIBRARY DUBLIN
Thesis
5966

DECLARATION

This thesis has not been submitted as an exercise for a degree at any other university. It is entirely the work of the undersigned author, except where duly acknowledged.

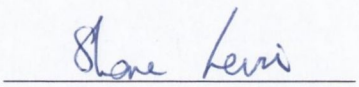

Shane Reed Levis

DECLARATION

I give my permission for the library of the University of Dublin to lend or copy this thesis upon request

Signed: Shane Lewis

To my parents, brother and sister

To Anne

ACKNOWLEDGEMENTS

First and foremost, I would like to extend my sincere thanks and appreciation to my supervisor, Professor Patrick Deasy for his invaluable and constant help, guidance and support throughout the duration of research for this thesis and in the preparation of this text. I also wish to thank the Department of Pharmaceutics for the provision of laboratory facilities. In addition, I am very grateful for the generous financial support provided by FMC Corporation and Enterprise Ireland via the Irish American Partnership Scheme and the financial awards presented to me by the ISPE and Trinity College, Dublin.

Many thanks are extended to Ron Price and Yuri Lvov of the Naval Research laboratory, Washington D.C. for their invaluable help and time spent training me in various drug loading techniques associated with the halloysite mineral. Furthermore, I would like to convey my special appreciation to Ron, his wife Cathy, and family for their very kind hospitality extended to me during my visit to the States.

I would like to thank Professor Vincent McBrierty and Dr. Chris Keely of the Department of Physics, TCD., for their advice and assistance with the DSC studies. I am also grateful to Mr David John, Mr Colin Reid and Mr Neal Leddy of the Electron Microscope Unit for their help with TEM and SEM work. Grateful appreciation is extended to Simon Marsters of NZ China Clays Ltd. for supplying a number of grades of NZ halloysite and also to Professor Hayden Murray of Indiana University for supplying a sample of Indiana halloysite. Thanks are extended to Elan Corp. for the use of their zeta sizing equipment and also to Loctite (more specifically to Dr Kenneth Broadley and Dr Seamus Grant) for the supply of a number of cyanoacrylate monomer samples and also for their technical advice and assistance in relation to using these samples in subsequent coating studies and in measuring the cyanoacrylate polymer molecular weights.

A word of thanks to the academic and technical staff of the School of Pharmacy whom I found very helpful during the course of my research. In particular, I would like to thank Dr Anne Marie Healy for her assistance in using the micromeritic equipment and Pat

Quinlan, Mary Reilly and Brian Canning for their help with sourcing materials and their assistance with the technical aspects of some of the equipment in the Department of Pharmaceutics. I am grateful to Derek Bell for his help with ordering equipment and materials as required. I would also like to acknowledge the secretarial assistance provided by Nuala Collins, especially in relation to help with image scanning. In this respect, I am also grateful to Brian Kirby.

I would like to thank all my fellow departmental colleagues for their support and friendship over the years (*in alphabetical order*): Fiona Bogan, Fiona Brennan, Stephen Byrne, Deirdre Corrigan, Abina Crean, Sally-Ann Cryan, Idris El-Mahdi, Karen Gallagher, Martina Geraghty, Brendan Griffin, Mark Hanlon, Nicole Kavanagh, Helena Kelly, Bronagh Killen, Karl Levis, Leonard McCarthy, Anthony McMahon, Rosario Mollo, Catriona Naddy, Karen O'Connor, Colleen O'Donnell, and Denis O'Driscoll.

Finally, I wish to thank my immediate family, Anne and friends for their continual support and words of encouragement.

TABLE OF CONTENTS

Title	(i)
Declaration	(ii)
Dedication	(iii)
Acknowledgments	(iv)
Table of Contents	(vi)
Presentations and publications associated with this thesis	(xv)
Summary	(xvi)

Introduction

Chapter 1.	**Introduction**		**1**
1.1	Origin and Scope of Work		1
1.2	Microcrystalline Cellulose		3
	1.2.1 Introduction		3
	1.2.2 Structure of Cellulose		4
	1.2.3 Types of Processed Celluloses		6
	1.2.4 Commercially Available Grades of MCC		7
	1.2.5 Chemical, Physical and Mechanical Properties of MCC		10
		1.2.5.1 Chemical Composition	10
		1.2.5.2 Crystallinity of MCC Powders	11
		1.2.5.3 Interaction of MCC with Water	13
		1.2.5.4 Flow Properties of MCC Powder	17
		1.2.5.5 Tensile Strength and Compactability of MCC Powders	19
		1.2.5.6 Disintegration of MCC Powder Compacts	24
1.3	Halloysite		26
	1.3.1 Introduction		26

1.3.2 Sourcing Halloysite 26
1.3.3 Origin of Halloysite 27
1.3.4 Halloysite Structure 29
1.3.5 Effect of Iron Content on Halloysite Structure 32
1.3.6 Intercalation of Halloysite 34
1.3.7 Halloysite Surface Charge 36
1.3.8 XRD Analysis and Identification of Halloysite 38
1.3.9 Applications of Halloysite 38
1.4 Indomethacin 41
1.4.1 Definition 41
1.4.2 Molecular Structure 41
1.4.3 Physicochemical Properties 42
1.4.4 UV Absorption Spectrum 43
1.4.5 Stability 43
1.4.6 Pharmacokinetic Properties of Indomethacin 43
1.4.7 Pharmacology of Indomethacin 44
1.5 Diltiazem Hydrochloride 46
1.5.1 Definition 46
1.5.2 Molecular Structure 46
1.5.3 Physicochemical Properties 47
1.5.4 UV Absorption Spectrum 48
1.5.5 Stability 48
1.5.6 Pharmacokinetic Properties of Diltiazem HCl 48
1.5.7 Pharmacology of Diltiazem HCl 50
1.6 Aims and Objectives 53

Experimental

Chapter 2. Materials **54**

Chapter 3. Methodology **57**

3.1 Particle Size Reduction of Avicel® PH-101 Powders 57

3.1.1 Size Reduction of Avicel® PH-101 by Ball Milling 57

3.1.2 De-aggregation Studies on Avicel® PH-101 using Surfactants 57

3.1.3 Size Reduction of Avicel® PH-101 by Ultrasonic Homogenisation 58

3.2 Tablet Production 59

3.3 Evaluation of Tablet 60

3.3.1 Physical Standards 60

3.3.2 Uniformity of Drug Content 60

3.3.3 Dissolution Testing 60

3.4 Extrusion-Spheronisation Process 61

3.4.1 Mixing 61

3.4.2 Extrusion 61

3.4.3 Spheronisation 62

3.5 General Methods of Spheronised Product Analysis 62

3.5.1 Sieve Analysis 62

3.5.2 Pellet Packing Density Analysis 63

3.5.3 Pellet Apparent Density 64

3.5.4 Mercury Porosimetry Analysis 65

3.6 Methods used for Powder Analysis 67

3.6.1 Particle Size Analysis by Laser Diffraction 67

3.6.2 Scanning Electron Microscopy Analysis 68

3.6.3 Mercury Porosimetry Analysis 68

3.6.4 X-ray Diffraction Analysis 68

3.6.5 BET Surface Area Analysis 69

3.6.6 DSC Sample Analysis 70

3.6.7 Thermogravimetric Analysis 71

3.7 Specific Halloysite Experiments 71

3.7.1 Zeta Potential Measurements 71

3.7.2 Removal of Allophane 72

3.7.3 Intercalation of Halloysite using Wada's Procedure 72
3.7.4 Determination of Halloysite / Cation Binding Curves 73
3.7.5 Drug Loading of Halloysite 74
3.7.6 Coating Drug Loaded Halloysite 75
3.7.7 Preparation of Solid Lipid Particles 76
3.8 Dissolution Studies 77
3.8.1 Dissolution Studies on Pellet and Powder Formulations 77
3.8.2 Calculations 78
3.8.3 Dissolution Rate Modeling 79
3.9 Statistical Methods used in Experiments 79
3.9.1 Simple Comparative Experiments 80
3.9.2 Analysis of Variance (ANOVA) 80
3.9.3 Factorial Experiments 81
3.9.4 Similarity Factor 81

Results and Discussion

Chapter 4. Preliminary Studies on Microcrystalline Cellulose 83
4.1 Preliminary Size Reduction Studies 83
4.1.1 Introduction 83
4.1.2 Surfactant Aided De-aggregation 84
4.1.3 Mechanical size Reduction Techniques 87
4.2 Preliminary Extrusion-Spheronisation Studies 94
4.2.1 Effect of Sodium Lauryl Sulphate 94
4.2.2 Effect of Other Surfactants 96
4.2.3 Effect of Increasing MCC Content 100

Chapter 5. Optimisation of MCC Size Reduction via Ultrasonic Homogenisation 103
5.1 Introduction 103
5.2 Optimisation using Factorial Analysis 104

5.2.1 Main Effects and Interactions 105
5.2.2 Day to Day Variation 108
5.2.3 Conditions for Optimal Size Reduction 109
5.3 Examination of the Effect of Cycle Number on Size Reduction and the Polydispersity Index 110
5.3.1 Effect of Cycle Number on Particle Size 110
5.3.2 Effect of Cycle Number on the Polydispersity Index 112
5.4 Examination of the Role of Three De-aggregating Agents on the Ease of Recovery of Ultrafine MCC 113
5.4..1 Introduction 113
5.4.2 Recovery of Ultrafine MCC 114
5.4.3 Re-dispersal of Ultrafine MCC 116
5.5 Conclusion 118

Chapter 6. Characterization of size reduced grades of Avicel® PH-101 119

6.1 Mercury Porosimetry of MCC Powders 119
6.1.1 Introduction 119
6.1.2 Results and Discussion 121
6.2 Specific Surface Area Measurements 126
6.2.1 Introduction 126
6.2.2 Results and Discussion 127
6.3 DSC Analysis of MCC Powders 130
6.3.1 Introduction 130
6.3.2 DSC of Pure Water 133
6.3.3 Endothermic Analysis of Hydrated MCC Powders 136
6.3.3.1 Qualitative Analysis of DSC Endotherms 136
6.3.3.2 Determination of ΔH_{endo} 138
6.3.3.3 Determination of 'non-freezable' Water Contents and Correlation with Powder Crystallinities 142

6.3.3.4 Determination of the Relative Amounts of 'Freezable' and 'Non-freezable' Water Contents 146
6.3.4 Exothermic Analysis of Hydrated MCC Powders 149
6.3.5 Conclusion 157

Chapter 7. Pharmaceutical applications of novel size reduced grades of Avicel® PH-101 159
7.1 Tableting Applications - Introduction 159
7.2 Results and Discussion 160
7.2.1 Uniformity of Weight and Thickness 160
7.2.2 Mechanical Properties of Tablets - Hardness / Friability 162
7.2.3 Compression Force / Tensile Strength Profiles 164
7.2.4 Disintegration Testing of Tablets 166
7.2.5 Drug Content Uniformity 166
7.2.6 Dissolution testing 167
7.3 Conclusion 168
7.4 Applications in Extrusion / Spheronisation - Introduction 169
7.5 Results and Discussion 171
7.5.1 Effect of Moisture Content on Pellet Yield 171
7.5.2 In Vitro Dissolution Testing of Pellets 176
7.5.3 Pellet Intra-Particulate Porosity 179
7.5.4 Mercury Porosimetry Analysis of Pellet Formulations 181
7.5.4.1 Presence of Ink-well Pores 189
7.5.5 Pellet Packing Density Analysis 191
7.6 Conclusion 193
7.7 Suspension Applications - Introduction 195
7.8 Results and Discussion 196

Chapter 8. Characterization of Halloysite **200**

8.1 Introduction 200

8.2 Sourcing Halloysite 201

8.3 Microscopic Analysis 202

8.4 Zeta Potential Measurement of Halloysite G 209

8.5 XRD Identification of Halloysite G 210

8.5.1 Intercalation of Halloysite G 212

8.6 Mercury Porosimetry of Halloysite G 217

8.6.1 Introduction 217

8.6.2 Results and Discussion 218

8.7 Specific Surface Area Measurements 224

8.8 Extrusion / Spheronisation of Halloysite G 225

8.8.1 Introduction 225

8.8.2 Results and Discussion 226

8.9 Conclusion 227

Chapter 9. Drug Loading of Halloysite **230**

9.1 Introduction 230

9.2 Ionic Binding 232

9.3 Tubular Entrapment 233

9.4 Effect of Viscosity Enhancers 235

9.5 Coating Drug Loaded Halloysite Using cationic Polymers 237

9.5.1 Chitosan Coating 237

9.5.1.1 Halloysite / Chitosan Binding studies 238

9.5.1.2 In Vitro Dissolution Testing of Chitosan Coated Halloysite 240

9.5.1.3 Burst Release Effects 244

9.5.1.4 Encapsulation Efficiencies 244

9.5.1.5 Effect of Incorporating a Cross-linker 245

9.5.2 Examination of Alternative Cationic Polymers 248

9.5.2.1 Halloysite / Eudragit E Binding Studies 248
9.5.2.2 In Vitro Dissolution Testing of Eudragit E Coated Halloysite 249
9.5.2.3 Halloysite / PEI Binding Studies 253
9.5.2.4 In Vitro Dissolution Testing of PEI Coated Halloysite 254
9.5.2.5 Encapsulation Efficiencies 257
9.6 Entrapment of Drug Loaded Halloysite within a Lipid Matrix 259
9.6.1 Introduction 259
9.6.2 Particle Size Analysis of the Solid Lipid Microparticles 261
9.6.3 Dissolution Testing and Model Fitting 263
9.6.3.1 Effect of Surfactant 265
9.6.3.2 Effect of Milling Time 267
9.6.3.3 Effect of Lipid Type 268
9.6.3.4 Effect of Dispersion Type 269
9.6.3.5 Effect of Halloysite Loading 271
9.6.4 Microscopic Examination of Solid Lipid Microparticles 272
9.6.5 Drug Encapsulation Efficiencies of Solid Lipid Microparticles 275
9.6.6 Propranolol Loaded SL Microparticles 276
9.7 Coating Drug Loaded Halloysite using Cyanoacrylate Polymers 280
9.7.1 Introduction 280
9.7.2 Results and Discussion 281
9.7.2.1 Effect of Polymerisation Reaction Time 283
9.7.2.2 Effect of Cyanoacrylate Monomer Type 285
9.7.2.3 Effect of Cyanoacrylate Monomer Concentration 288
9.7.3 Conclusion 290

General Discussion **291**

Appendices

Appendix 1:	UV absorbance spectrum for Diltiazem HCl in phosphate buffer pH 6.8	307
	UV absorbance spectrum for Propranolol HCl in phosphate buffer pH 6.8	308
Appendix 2:	Calibration curves used to determine concentration of substances in solution	309
Appendix 3:	Pressure table used with PoreSizer 9320	311
Appendix 4:	Endothermic and exothermic DSC data for hydrated Avicel® PH-101 powder samples	312
	Endothermic and exothermic DSC data for hydrated Grade X MCC powder samples	313
	Endothermic and exothermic DSC data for hydrated Grade Y MCC powder samples	314
Appendix 5:	Plots of enthalpy per gram of water as a function of water content for Avicel® PH-101, Grade X and Grade Y powders, using the endothermic data	315
	Plots of enthalpy per gram of water as a function of water content for Avicel® PH-101, Grade X and Grade Y powders, using the exothermic data	317
Appendix 6:	TG analysis of Diltiazem HCl loaded halloysite 'G' powder samples with varying residual moisture contents	319
Appendix 7:	Energy dispersive analysis plot of compacted Halloysite 'G' powder (Sample 3)	320

References **321**

PRESENTATIONS AND PUBLICATIONS ASSOCIATED WITH THIS THESIS

Oral Presentations

"Examination of potential pharmaceutical applications of a novel grade of microcrystalline cellulose", *5th European Intensive Course on New Forms and New Routes of Administration for Drugs,* Trinity College Dublin, March 1999, 4 (abstract) [S. R. Levis and P. B. Deasy]

"Examination of potential applications of a novel grade of microcrystalline cellulose in sustained drug delivery using extrusion / spheronization technology", *12th International Symposium on Microencapsulation,* the School of Pharmacy, University of London, September 1999, 18 (abstract) [S. R. Levis and P. B. Deasy]

Publications

"Production and evaluation of size reduced grades of microcrystalline cellulose", accepted by the *International Journal of Pharmaceutics,* September, 2000. [S. R. Levis and P. B. Deasy]

"Pharmaceutical applications of size reduced grades of microcrystalline cellulose", submitted to the *International Journal of Pharmaceutics,* September, 2000. [S. R. Levis and P. B. Deasy]

Summary

The research work performed in compiling this thesis can be divided into two broad areas, namely (a) the development, characterisation and examination of potential pharmaceutical applications of new de-aggregated grades of microcrystalline cellulose (MCC) and (b) the characterisation and examination of potential pharmaceutical applications of a novel tubular clay mineral, termed halloysite. MCC is a white, free flowing, tasteless powder produced by the chemical partial depolymerisation of an α-cellulose rich wood pulp at elevated temperatures in the presence of mineral acid. Because of the variation in the raw material used and the conditions of manufacture applied, different grades of MCC are available, one of the principal brands being Avicel®, common grades of which are PH-101 and PH-102. In this project novel size reduced grades of MCC were developed. Preliminary size reduction studies on Avicel® PH-101 showed that chemical de-aggregation using surfactants (a phenomenon observed by Law and Deasy, 1997) was less successful than mechanical methods. Ultrasonic homogenisation was most successful, resulting in a reduction in the average size of the Avicel® PH-101 grade to 10-15 μm. The effect of the production parameter, cycle number, on the mean particle size and the polydispersity index of the MCC suspensions was investigated. Size reduced MCC grades in combination with various de-aggregating agents were recovered using a spray-dryer.

Novel grades X and Y, consisting of size reduced MCC and size reduced MCC in combination with sodium lauryl sulphate (SLS), respectively, were characterised and examined for tabletting applications. Characterisation studies included morphological examination using SEM techniques, particle size determination, estimation of powder bed porosities and specific surface areas using mercury porosimetry and nitrogen adsorption techniques, respectively, and investigation of the interactions between the MCC polymer grades and water using differential scanning calorimetry. Physical parameters determined for the novel grades were compared to those of the original Avicel® PH-101 grade. Both grades proved inferior to the currently available Avicel® PH-101 and PH-102 grades for a tableting application involving paracetamol. Powdered grades X and Y had poor flow

properties, forming tablets with poor uniformity of weight, low hardness values, high levels of friability and longer disintegration times. Flow properties of Grade X were slightly better due to the reduced static effects induced by SLS whose presence decreased tablet hardness.

Six novel size reduced grades of MCC were investigated as spheronisation aids in an application involving Indomethacin. All consisted of size reduced MCC in combination with two different levels of 3 de-aggregation agents namely SLS, sodium citrate and sodium hexametaphosphate. All grades produced pellets with higher yields in the desired size range (850-1180 μm) compared to Avicel® PH-101. Analysis of the in vitro dissolution data using the similarity factor (f_2) indicated that only those pellets incorporating the novel grade combined with SLS resulted in enhanced drug release retardation, relative to those incorporating Avicel® PH-101, which could be explained in terms of reduced pellet intra-particulate porosity. All pellets illustrated excellent flow properties with Hausner ratios less than 1.2 and Carr's indices lower than 10%.

The second section of the project was principally concerned with the physical characterisation of halloysite and examination of its potential use in sustained drug delivery of diltiazem hydrochloride, mainly achievable due to its unique tubular morphology. The powder properties of the mineral were characterised using a number of techniques such as specific surface area analysis, intrusion mercury porosimetry, both scanning and transmission electron microscopy, XRD analysis and surface charge analysis using a zeta-sizer. Various physical and chemical clean-up procedures were applied to the mineral to remove debris, and increase the proportion of intact tubules and the specific tubular volume available for drug entrapment. The halloysite 'G' grade, which was sieved through a 125 μm sieve, without any alkali treatment, proved to be the best candidate for further drug loading, entrapment and sustained release studies.

Halloysite, being an expandable mineral, is amenable to intercalation and the ability of the mineral to incorporate drug within the 'inter-layer' space was examined, but proved

disappointing. The main space available for drug entrapment was shown to be within its tubular lumen and to a lesser degree by binding of cationic drug to anionic binding sites on the mineral's surface by ionic forces. The release of drug entrapped within its core lumen was further retarded by coating the drug loaded mineral with various polymeric coatings ranging from cationic polymers such as polyethyleneimine, chitosan and Eudragit E to various alkylcyanoacrylate polymers, in which latter group polymerisation of the coating was induced by the presence of residual water. Delay in entrapped drug release was also achieved by forming drug loaded halloysite particles into lipid microparticles. Release of drug from these systems was further reduced by substituting the drug candidate with Propranolol Hydrochloride, a compound with a lower intrinsic aqueous solubility. This work confirms that halloysite has considerable potential for novel sustained drug delivery systems.

Chapter 1

Introduction

1.1 ORIGIN AND SCOPE OF WORK

The quality of medicinal products depends not only on the active ingredients present and production processes, but also on the performance and quality of the excipients. Until recently, there has been considerable 'historical' underestimation of the role played by the excipient, as was discernible in the definition of the traditional concept which regarded it simply as a substance that facilitates the administration and preservation of the active principle (Pifferi *et al.*, 1999). The classical excipient was generally considered to be inert from a chemical point of view and also inactive in pharmacological and toxicological terms. Contrary to this, the excipient is in fact fundamental to guarantee the safety and efficacy of the final pharmaceutical product (Pifferi, 1995), changing the traditional concept into the more up-to-date one of functional agent, i.e. one that can fulfill several functions within the pharmaceutical formulation. Depending on the final product and its intended route of administration, the excipients must guarantee the stability of the dosage form, the precision and accuracy of the dosage, as well as modifying, when necessary, its organoleptic characteristics (smell, taste, swallowability and local tolerability) so as to improve the patients' compliance (Pifferi *et al.*, 1999). Furthermore, interest in modified release dosage forms is another factor that spurs demand for more sophisticated excipients that can fulfill specific functions within the formulation, permitting the optimisation of plasma concentrations of the active, thus increasing efficacy and the added value of the medicinal product.

In this thesis, two novel excipient classes were examined as potential candidates offering improved functionality within the pharmaceutical technology sector. The first, a modified size reduced grade of microcrystalline cellulose (MCC) was developed on the basis of observations of Deasy and Law (1997) that sodium lauryl sulphate caused fragmentation of MCC into small crystallites affecting drug release and other properties. Subsequent correspondence with FMC (the major manufacturer of pharmaceutical grade MCC worldwide, marketed under the trade name Avicel®) led to the sponsorship of this work. Patents covering aspects of the manufacture of MCC have lapsed and because of the large demand for the relatively expensive excipient by pharmaceutical Companies, other excipient manufacturers in Europe and Asia have commenced marketing the material. As a result it is important that FMC respond to such competition by developing new grades of MCC with unique or improved functionality, thus ensuring the Company preserves its dominant position in the market, despite increasing competition.

Interest in the second excipient, termed halloysite, originated as a consequence of correspondence with Ron Price of the Naval Research Laboratory in Washington D.C. The mineral, being tubular in nature, has the potential to entrap active ingredients within its core lumen, thereby creating a sustained release mechanism. The sustained release of tetracycline and other anti-fouling agents encapsulated within lipid micro-tubular structures, rigidised by electroless deposition of metals, was reported by Price *et al.* (1991) and Schnur *et al.*, (1994). Subsequent work by Price, extended the above work to examine use of the above mineral as a cheaper alternative to the lipid structures, and its application in this area became the subject of a recent patent (Price and Gaber., 1997). Work to date, has concentrated mainly on marine and other non-pharmaceutical applications of halloysite and so it is the intention of this project to investigate its potential pharmaceutical applications, more specifically, in the area of sustained drug delivery.

1.2 MICROCRYSTALLINE CELLULOSE

1.2.1 Introduction

In 1938, Anselme Payen, on the basis of careful chemical analysis and intelligent scientific intuition suggested that the cell walls of a large number of plants were composed of the same substance, which he termed cellulose (Nevell and Zeronian, 1985). Even though cellulose is the most abundant naturally occurring polymer, it is never found pure in nature, the cotton fibre being probably its purest natural source which seldom contains more than about 5% of other substances after allowances have been made for adsorbed water. The morphological structure of the cotton fibre is illustrated in Fig. 1.2a. More commonly in leaves, plant stalks, wood and the like it is associated with other substances such as lignins and hemicelluloses, both being present in considerable quantities (Nevell and Zeronian, 1985), i.e. wood generally contains (on a dry basis) between 40 and 55% cellulose, 15 and 35% lignin and 25 and 40% hemicelluloses. Lignins are complex hydrocarbon polymers with both aliphatic and aromatic constituents, whereas hemicelluloses comprise a group of polysaccharides which remains associated with the cellulose after the lignin has been removed by using aqueous alkali. Hemicellulose differs from cellulose in that it contains a wide variety of different sugar units, while cellulose consists of only 1,4,-β-D-glucopyranose. In addition, hemicellulose undergoes considerable chain branching whereas cellulose is a linear polymer and the degree of polymerisation (DP) of cellulose is nominally 10-100 fold greater than most hemicellulose materials (Keely, 1996).

Vegetable fibers comprise the sole source of industrial and pharmaceutical celluloses used at the present time, billions of tons being produced annually by photosynthesis. The most common sources for industrial use are wood pulp and cotton lint. The production of cellulose, however, is not confined solely to the vegetable kingdom and is also present in the outer mantle layers of some marine organisms of the Tunicata class (Nevell and Zeronian, 1985). A polymer known as Tunicin present in the mantle is regarded as a form of cellulose. In addition bacterial cellulose has been known for a long time.

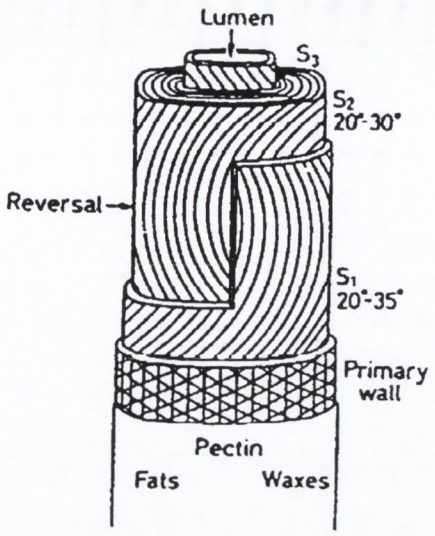

Figure 1.2a. Morphological structure of the cotton fibre (Nevell and Zeronian, 1985). The primary wall (*ca.* 0.5 μm thick) contains about 50% cellulose micro fibrils in an interlaced network. The secondary wall consists of an outer S_1 and inner S_2 layer, each containing cellulose fibres in spiral patterns. The S_2 layer constitutes 95% approx. of the entire weight of the cotton fibre. The lumen wall (S_3) is not easily detected and surrounds the central channel of the fibre containing nitrogenous deposits.

1.2.2 Structure of Cellulose

Pure cellulose (denoted α-cellulose) consists of a linear polymer chain of repeating sugar units, the sugar units consisting of the same sugar namely 1,4,-β-D-glucopyranose (anhydroglucose). The glucose units are linked by 1,4,-β glucosidic bonds. The empirical formula for cellulose is $(C_6H_{10}O_5)_n$, where n has a value of 500 or more. Fig. 1.2b illustrates the cellulose chain in (a) the conventional and (b) the Haworth projections.

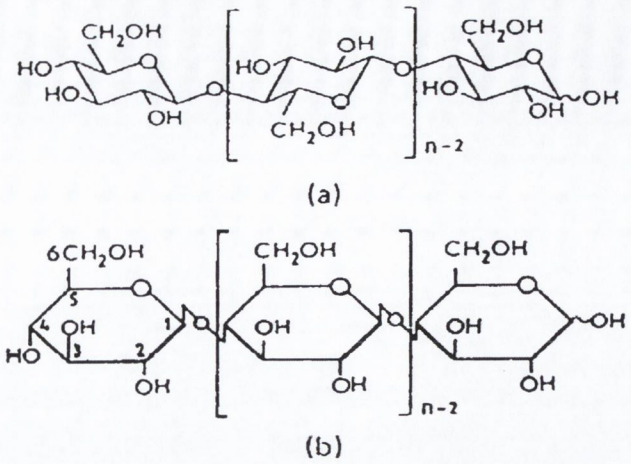

Figure 1.2b. The cellulose polymer chain showing the anhydroglucose repeat units connected via 1,4,-β glucosidic bonds (Krässig, 1985).

Cellulose chains (when fully extended) can be viewed as flat ribbons with numerous hydroxyl sites projecting laterally outwards, which are available for inter and intra molecular hydrogen bonding. In addition, the presence of the oxygen in the pyranose ring facilitates intra-molecular bonding, which produces enhanced stiffness and high temperature stabilisation of cellulose. A direct consequence of hydrogen bonding is that the cellulose chains tend to establish parallel arrangements with intra-chain hydrogen bonding, forming crystallite strands that result in the fibrous nature of cellulose. In the original fibre, each long cellulose chain weaves through or exists in several crystalline and amorphous areas as illustrated in Fig. 1.2c. This type of structure gives strength, extensibility and toughness to the original fibre. This supermolecular polymeric structure of cellulose is frequently referred to as the 'fringe-micellar' concept, where the micelles are crystalline embedded in an amorphous matrix. The hydrogen-carbon bonds contribute hydrophobic sites in the cellulose molecule, whereas the hydroxyl groups contribute hydrophilic sources. It is this well ordered distribution of hydrophobic and hydrophilic sites which largely determines the super-molecular structure of the polymer and many of its physical and chemical properties.

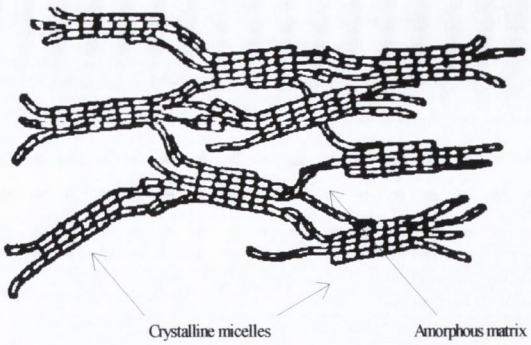

Figure 1.2c. Fringe-micellar (fibrillar) model of fibre structure of cellulose (Krässig, 1985).

1.2.3 Types of Processed Celluloses

Processed cellulose can be classified into two main groups, those that are microcrystalline and that are microfine. Microcrystalline cellulose (MCC) is obtained essentially from wood pulp. It is formed by a combination of process techniques involving initially the acid hydrolysis and milling of the cellulose present in the pulp followed by a subsequent spray-drying process (Bolhuis and Lerk, 1973). The acid hydrolysis in this reaction is heterogeneous and attacks predominantly the more accessible amorphous regions between the crystallites of the cellulose chain, forming a highly crystalline version of the polymer, i.e. the so-called microcrystallites. If the cellulose pulp is allowed to hydrolyse for a sufficiently long period of time in the presence of acid under suitable conditions, a 'level-off' molecular weight (M_w) is attained, i.e. a minimum chain length (expressed in DP units) is achieved. More recently, Bergfeld *et al.* 1996, patented a technique allowing for the more environmentally friendly partial hydrolysis of cellulose and capable of producing level-off cellulose. This is achieved by subjecting cellulose pulp to hydrolysis in a pressurized reactor using water under a gas pressure of 0.1 to 60 bar of oxygen and/or carbon dioxide, measured at 20°C, at a temperature of 100° to 200°C for a sufficient period of time. The partial hydrolysis is preferably under a gas pressure of 0.5 to 30 bar and in a temperature range from 140° to 180°C. The DP of MCC at this stage is less than 350 (European Pharmacopeia, 1996) and yields a crystallite less than 200 nm approx. in

length and 40 nm in width. When such MCC is dispersed in an aqueous phase, colloidal gels are produced, such materials being generally marketed as gelling or suspending agents (ie Avicel RC/CL grades). If the above hydrolysis reaction is allowed to proceed to various intermediary points and by varying the spray-drying process conditions, white powders of varying average particle sizes and differing degrees of crystallinity can be obtained, these powders having different pharmaceutical applications.

The other processed form of cellulose, referred to as micro-fine cellulose, differs from MCC due to its significantly higher amorphous content (i.e. the MCC product has a higher crystallinity and lower molecularity than the micro-fine cellulose product (Podczeck and Révésv, 1993). The microcrystalline form is characterised by a crystallinity of about 60 to 80% (Doelker *et al.*, 1987), whereas the micro-fine celluloses have a crystallinity of about 15 to 45% (Doelker *et al.*, 1987). Acid hydrolysis is not used in the production of the micro-fine version and it is solely the product of physical milling of purified cellulose, the mechanically de-aggregated product being subsequently separated from the sediment formed. According to Nevell and Zeronian, 1985, under milling conditions where sufficient mechanical energy can be localised in the cellulose crystallites, the covalent bonds are broken causing the cellulose fibers to be ground eventually to an amorphous powder (which is referred to as Cellulose II upon wetting).

1.2.4 Commercially Available Grades of MCC

The preparation of MCC was first patented in the beginning of the 1960's by Battista and Smith (US Patent 2978446, 1961; US Patent 3141875, 1964) of the American Viscose Company. The first product was put onto the market as a pharmaceutical excipient, to be used essentially in tableting applications, in 1963 under the trade name Avicel® (now sold by FMC Corp.). Since then a considerable number of different grades of the material have been developed and marketed both by FMC and also by newer competing companies. A schematic representation of the stages involved in the production of the pioneering Avicel® product is illustrated in Fig. 1.2d.

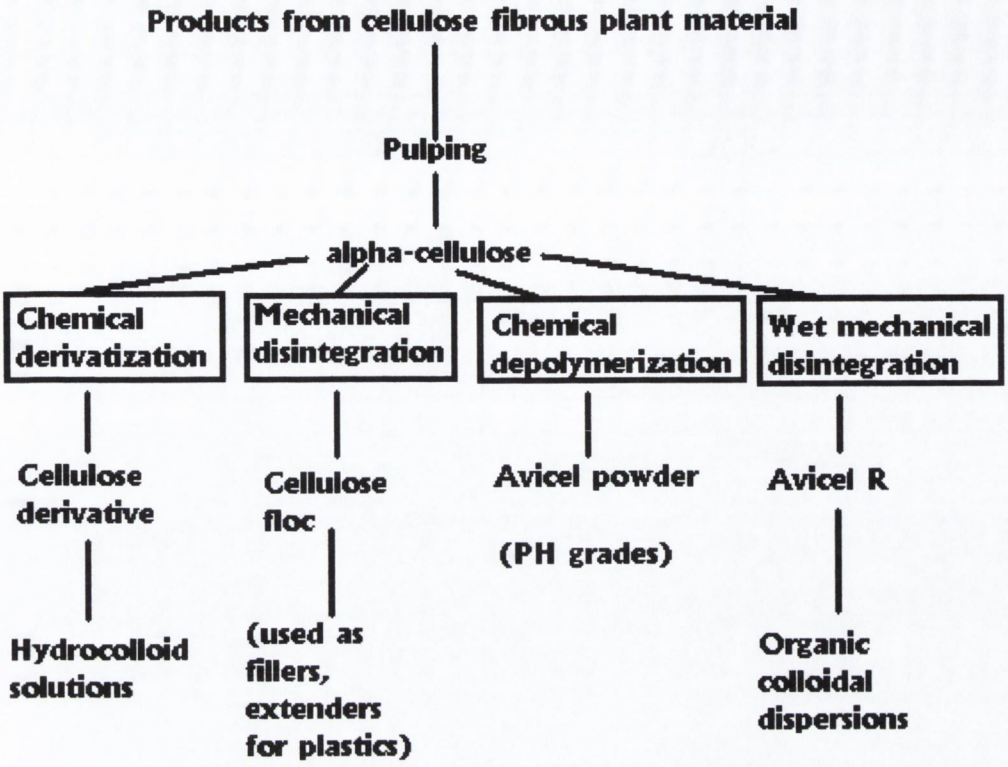

Figure 1.2d. Schematic representation of steps involved in Avicel® production (Company literature)

The full range of the Avicel® products currently being marketed by FMC Corp. is illustrated in Tables 1.2a and 1.2b, in addition to some of the more popular products that are currently coming online from its competitors. In the case of the Avicel® range, products include the free-flowing, white powder PH grades which are normally used in tableting applications and to a lesser degree in extrusion/spheronisation applications. Colloidal grades (i.e. Avicel® RC/CL products) are water dispersible and are marketed for use in liquid formulations as suspending aids. These colloidal grades are co-processed mixtures of MCC and sodium carboxymethylcellulose (NaCMC), the NaCMC functioning as a dispersion aid and protective colloid.

Table 1.2a. Different brands and grades of 'powdered' microcrystalline cellulose available commercially.

Brand (Manufacturer)	***Grade***	***Mean Particle Size (μm)****	***Moisture Content (%)****
Avicel	PH-101	50	<5.0
(FMC)	PH-102	100	<5.0
	PH-103	50	<3.0
	PH-105	20	<5.0
	PH-112	100	<1.5
	PH-200	180	<5.0
Emcocel		56	<5.0
(Mendell)			
Pharmacel	101	50	<5.0
(DMV)	102	100	<5.0
Unimac	MG-22	105	<5.0
(Unitaka Rayon)	MG-100	38	<5.0

*All values quoted were extracted from the respective company literature

Table 1.2b. Grades of 'colloidal' microcrystalline cellulose.

Brand (Manufacturer)	***Grade***	***NaCMC (% range)****	***Moisture Content (%)****	***Drying Method***
Avicel	RC-501	7.1-11.9	<6.0	Bulk
(FMC)	RC-581	8.3-13.8	<6.0	Bulk
	RC-591	8.3-13.8	<6.0	Spray
	CL-611	11.3-18.8	<6.0	Spray

*All values quoted were extracted from the respective company literature

1.2.5 Chemical, Physical and Mechanical Properties of MCC

1.2.5.1 Chemical Composition

As mentioned previously, pure microcrystalline cellulose consists entirely of α-cellulose bound together to form a linear polymeric chain. Despite this, impurities are present due to the fact that the source used to manufacture MCC (i.e. wood pulp) typically contains other materials such as lignins and hemicelluloses. Landin *et al.* 1993a, performed a study to examine the effect that country of origin had on the properties of MCC. The study involved comparing four brands of MCC, all similar to Avicel PH-101 (produced in Ireland) but which were produced by different manufacturers in Finland (Emcocel), India and Japan (Unimac MG 100). Their chemical compositions were shown to vary considerably as regards both lignin content and their total and relative quantities of hemicellulose sugars, suggesting that different woods were used as raw materials. More specifically, the mannose/xylose ratios suggested that the Indian and Japanese brands were derived from hardwood, whereas the Irish and Finnish brands were derived from softwood (Baehr *et al.,* 1991). In addition, striking differences in non-cellulose contents were observed, suggestive of manufacturing processes of significantly different intensities, ranging from the Indian brand with the highest lignin and hemicellulose sugar contents to the Japanese brand with the lowest.

The same authors (Landin *et al.,* 1993b) performed a subsequent study to examine the effect of batch variation and source of pulp on the nature of the impurities present in various MCC powders. Their studies focused on the Emcocel brand of MCC and all three batches examined were shown to contain significant quantities of impurities again derived from the wood of origin. Hydrolysis with trifluoroacetic acid (TFA), which primarily breaks down the hemicellulose surrounding the cellulose fibers in wood was shown to release small quantities of xylose and mannose from xylans and mannans respectively; a small quantity of glucose was also present, probably due to the peeling of the external layers of cellulose fibers. According to the authors, the mannose/xylose ratios for all three batches reflected their coniferous origin. Hydrolysis with sulphuric acid to break down the

cellulose fibers themselves produced larger quantities of xylose and especially mannose, probably derived from the hemicellulose trapped among the fibers. The influence of the process conditions was evident by the batch produced using atypical process conditions having considerably less hemicellulose but considerably more lignin than the standard product, while the influence of pulp source was evident in the greater hemicellulose content and lower lignin content of the batch produced using a different pulp to normal.

1.2.5.2 Crystallinity of MCC Powders

Evidence, previously discussed, of variation in the chemical composition of some of the MCC grades that are commercially available at present is illustrative of the differing levels of intensities of the manufacturing processes used for their production. This also has an important impact on their respective crystallinities, a more rigorous hydrolysis treatment preferentially forming a more highly crystalline product, whereas less rigorous process regimes have the opposite effect. The crystallinity of MCC has been reported to vary widely from one manufacturer to another and from lot to lot (Doelker *et al.,* 1987). These results were confirmed by the investigations of Landin *et al.* (1993a,b), which pointed to the Finnish brand examined as being the most crystalline, followed by the Irish, Japanese and Indian brands, with crystallinities ranging from 96.2% to 81.7%, using the method of Nelson and O'Connor (1964). In addition, they also used an infrared spectroscopy technique to estimate MCC crystallinities, the calculated values being lower in this case relative to the previous XRD technique. They concluded that this variation between techniques could explain the disparity among the reported crystallinities of MCC (Nakai *et al.,* 1977; Soltys *et al.,* 1984), but because both techniques correlated well, were still valid for comparing different MCC powders.

For all four brands, X-ray diffractograms illustrated peaks at 15, 16 and 22.6° 2θ, being characteristic of cellulose Type I. In addition, the Japanese brand also had peaks at 12 and 20° 2θ,, being characteristic of cellulose Type II (see Fig. 1.2e). Since native cellulose is cellulose I, the cellulose II content confirmed that the Japanese brand had undergone the most vigorous mechanical manufacturing process.

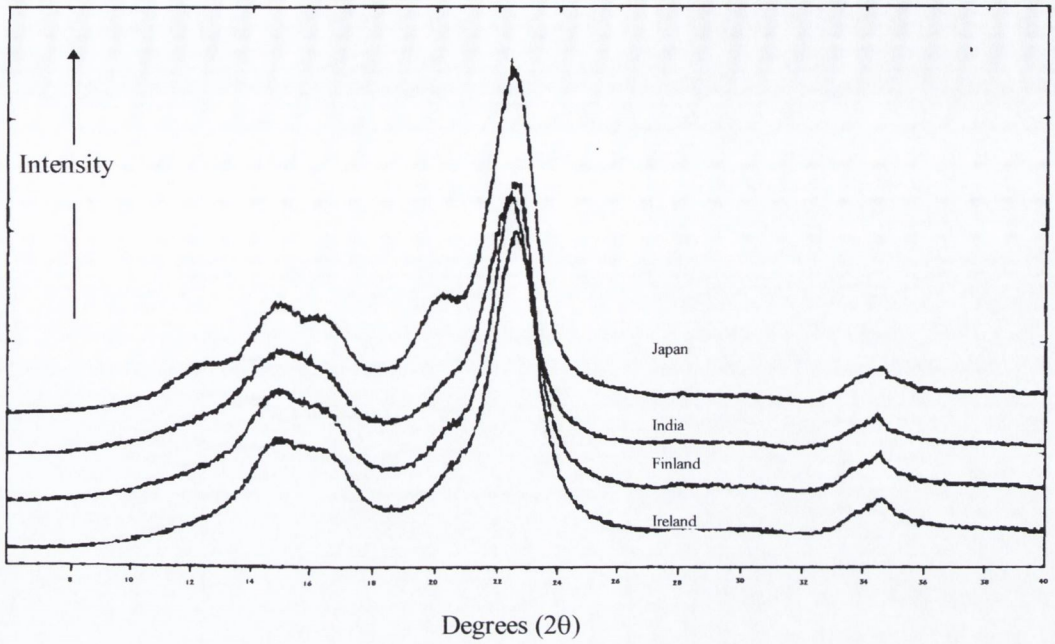

Figure 1.2e X-ray diffractograms of 4 brands of MCC powder obtained from 4 different countries of origin, namely Japan, India, Finland and Ireland (Landin *et al.*, 1993a).

Results from the study performed on the three batches of Emcocel (Landin *et al.*, 1993b) illustrated that the standard product was the most crystalline, while the least crystalline product was obtained from the non-standard pulp. This indicates that the origin of the pulp can also have an important effect on the overall crystallinities of the final product, even though similar process conditions may have been used.

In contrast, however, Rowe *et al.* 1994, measured the crystallinities of samples of microcrystalline cellulose from different batches obtained from a variety of different sources and detected the existence of very obvious batchwise variation, this being of a magnitude that neutralised any effect differences in the source/origin of the material may have had. They therefore concluded that differences seen in the processing of these materials (especially granulation and extrusion) must be due to properties other than crystallinity. Such differences may be due to differences in macroscopical features such as

particle size and shape as suggested by Parker and Rowe (1991) or differences in the lignin and hemicellulose content as suggested by Landin *et al.* 1993, or even due to a complex interaction of both, yet this still remains to be confirmed.

1.2.5.3 Interaction of MCC with Water

The interaction between water and pharmaceutical excipients is very important for numerous reasons, including product stability (chemical, physical and microbiological) and the control of drug release. An extensive literature exists on the interaction between MCC and water, the interaction being examined by many techniques including sorption isotherms (Morrison and Dzieciuch, 1959; Nakai *et al.,* 1977; Hollenbeck *et al.,* 1978; Zographi *et al.,* 1984; Khan and Pilpel, 1987), differential scanning calorimetry (Khan and Pilpel, 1986; Fielden *et al.,* 1988), microcalorimetry (Hollenbeck *et al.,* 1978; Fielden *et al.,* 1988) and dielectric spectroscopy (Khan and Pilpel, 1987).

The evidence presented to-date leads to the conclusion that water binds to celluloses by a three stage process from a molecular point of view. Initially, the water binds tightly to the anhydroglucose units and in addition, links adjacent units, i.e. two hydrogen bonds per water molecule. Following this, some of the initial bonds between the water and the cellulose molecules break with the addition of extra water molecules to bind at the now vacant anhydroglucose sites. In this situation there is the involvement of more water molecules with one hydrogen bond existing per water molecule. Finally, hydrogen bonds establish between water molecules, corresponding to a more loosely bound region of sorbed water. The above mechanism is represented diagrammatically by Khan and Pilpel (1987), this diagram being illustrated in Fig. 1.2f. Examination of the three dimensional spacing of the cellulose structure by Khan and Pilpel (1987), showed that the most exposed hydroxyl group is the carbon-6 hydroxyl (6-OH). This they concluded is the one most likely to be involved in hydrogen bonding with water molecules. A similar bonding mechanism has been proposed for the binding of water to starch (Van den Berg, 1981).

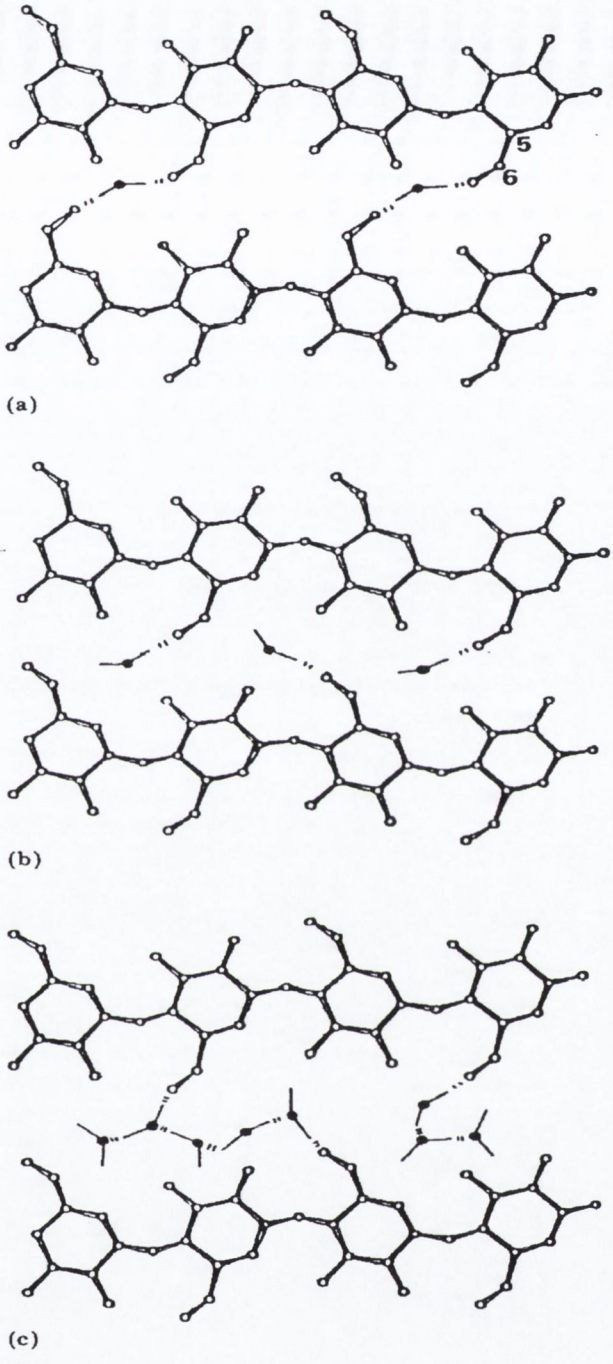

Figure 1.2f. Diagrammatic representation of proposed three stage interaction between cellulose and water (Khan and Pilpel, 1987).

Studies performed by Blair *et al.* (1990), using a combination of gravimetric and calorimetric studies of water vapour sorption to MCC, further confirmed the above

proposed mechanism. Examination of the kinetics of the water/MCC interaction show that they do not approximate to first order, as in the case of a simple sorption process. Instead the profile fits into three regions, illustrating an initial rapid sorption corresponding to the binding of one water molecule between two anhydroglucose moieties (~10% water content). This is followed by a very slow stage coinciding with the breaking and reforming of water and anhydroglucose bonds (which occurs at 19% approx. water content) and then a final rapid stage equating to the formation of a more loosely bound region of water. It is important to note that the three stages of this sorption process are not entirely discrete and instead there is some overlap between them.

A number of models have been developed to explain the interaction of the MCC powder with water in the specific application of extrusion/spheronisation. One such model is the concept of MCC as a 'sponge' as suggested by Fielden *et al.* (1988), where it is proposed that the cellulose particles provide the ability to hold water as a 'sponge'. The ability of cellulose to hold water is well known, as discussed above, and is considered to occur in two ways. Part of the water is localised closely and tightly to the cellulose fibers in pores in the amorphous regions, and part is localised in a more loose arrangement between the fibers (Stamm, 1964; Stone and Scallen, 1968). The exact nature of the interaction is thought to be very complex. A schematic representation of the interaction of water with the macro cellulose structure is provided by Li *et al.* (1992), and is presented in Fig. 1.2g. According to the 'sponge' model, during the extrusion process, the hydrated cellulose 'sponge' is compressed causing water to squeeze out and lubricate the particles flowing through the extruder (Newton, 1998). Variations in the performance of different sources of MCC are associated with the different interactions between the particular grade of MCC and water due to different pore structures and crystallinities. After extrusion, the volume of the 'sponges' increases and the extrudate appears apparently dry and brittle, allowing it to be chopped into short lengths for the spheroniser. Subjecting these cylinders to the forces of spheronisation again compresses the 'sponges' and allows for deformation of the soft structures.

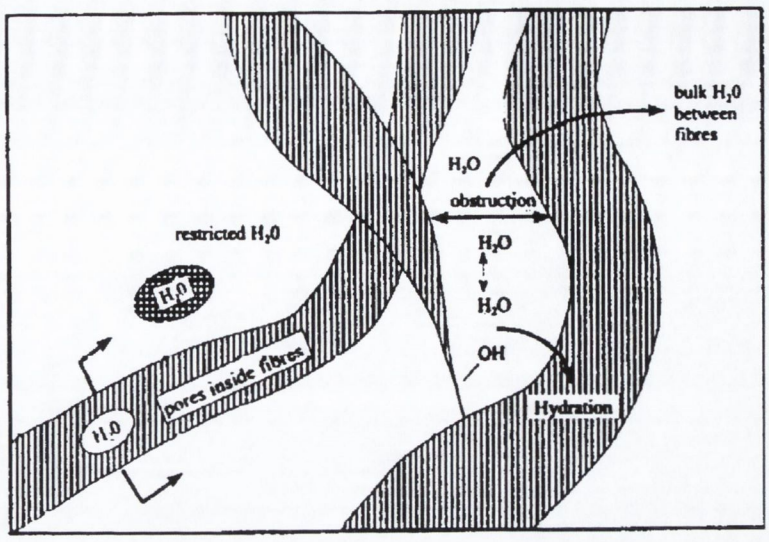

Figure 1.2g Schematic illustration of water in cellulose samples. There are two types of water: (a) loosely adsorbed bulk water located between the fibres with obstruction and hydration interactions with the fibres and (b) restricted water tightly bound to the amorphous and porous regions of the fibre.

The alternative model, referred to as the crystallite gel model, proposes that the MCC particles in the formulation are broken down into smaller particles by shear forces acting on the particles during extrusion (Kleinbudde, 1997). It is suggested that with increasing shear stress, the process proceeds so that finally single crystallites of colloidal size occur, due to breaking of some of the secondary valence bonds, and that these crystallites in the presence of water form a gel and it is this gel network which aids both extrusion and spheronisation. The crystallite network rearranges to form a coherent percolating network structure, due to the formation of new contact points, and the original particles can no longer be identified.

Despite the above, there are numerous observations that both models find difficult or fail to explain. According to Kleinbudde (1998), the surface of pellets prepared from MCC of different particle sizes are comparably smooth, whereas, the 'sponge' model would indicate that larger particles should result in pellets with a less smooth, raspberry-like surface. In addition, it has been observed that wet pellets tend to shrink during drying

(Kleinebudde, 1994), whereas, the sponge model would suggest no change in shape or porosity when subjected to drying. There are also a number of counter arguments to the gel/crystallite model. In this case, colloidal grades of MCC would be expected to be more effective as excipients, but instead the opposite is true (Kleinebudde, 1997). Furthermore, as Fielden (1998) points out, it is possible to form pellets from some formulations without any extrusion process, simply by adding water, mixing and placing on the spheroniser plate (Chapra *et al.* 1995), however according to the crystallite-gel model no gel would be formed in such situations.

An important property of MCC when being used as an extrusion aid is its ability to readily bond to itself when a wet mix of the powder is dried. This phenomenon is referred to as autohesion and is defined as the mutual interdiffusion of polymer end chains across the particle-particle interface of high molecular weight polymers resulting in a stable link. According to Kleinebudde (1997), hydrogen bonds are formed in the amorphous ends of the crystallites of MCC during drying by autohesion resulting in the formation of a stable matrix of high strength. Despite the above, other research (Evans and Luner, 1989) has shown from coagulation of MCC dispersions that there is clear evidence that the aggregates are held together by van der Waals attractions and not hydrogen bonds. As a result, there is no present universal agreement on which mechanism is exactly responsible.

1.2.5.4 Flow Properties of MCC Powder

The flowability of MCC is evaluated differently by different authors. Livingstone (1970) reported that MCC powder flows quite well, whereas, Mendell (1977) stated that it exhibited the poorest flowability of all the vehicles examined.

(a) Effect of particle size and shape

Bolhuis and Lerk (1973) showed that the flow properties of MCC were dependent upon the size and the morphology of the MCC particles. They determined an approximation of

the fluidity of the material from the coefficients of variation of upper punch force and of tablet weight. Their results indicated that the MCC grade (Avicel PH-101) had poor flow properties which were attributable to its typical match-stick-like structure of the particles as was evident from scanning electron microscopy. The Avicel PH-102 grade, with a larger average particle size, exhibited much better flow properties because of its granular form. It was to address the problem of poor flowability of Avicel PH-101 that FMC introduced the PH-102 grade. The effect of MCC particle size on its flow properties was further confirmed by Doelker *et al.* 1995, where the flow properties of 6 Avicel® MCC grades were determined. The MCC grades differed in terms of average particle size ranging from 37 μm for the PH-105 grade to a maximum of 145 μm for the PH-200 grade, these sizes representing the weight geometric mean diameter. From the results they were able to show a direct correlation between powder flowability and particle size, i.e. no flow was detected for the PH-105 grade using the vibratory hopper technique, whereas a maximum flow of 13.3 g/sec was determined for the largest PH-200 grade. In all cases, as one would logically expect, the flow rates ranked inversely to that of the determined Hausner ratios, defined as the ratio of tapped powder bed density to poured powder bed density.

(b) Effect of moisture content

Amidon *et al.* 1995, examined the effect of moisture content on the flow properties of MCC powder (Avicel PH-101), the flow properties being measured using a simplified shear cell. From this study they were able to calculate the shear cell index, n, it being a measure of powder flow. An index value greater than 1 indicates deviation from linearity and the greater the value, generally the poorer flowing the material is. In general materials with n values greater than 1.1 are not very free flowing. According to the authors results, the n value for Avicel PH-101 was less than 1.1 up to 3% approx. moisture content (see Fig. 1.2h), and a clear increase in this index value was observed with increasing moisture content, i.e. increased moisture reduced the powder flow properties.

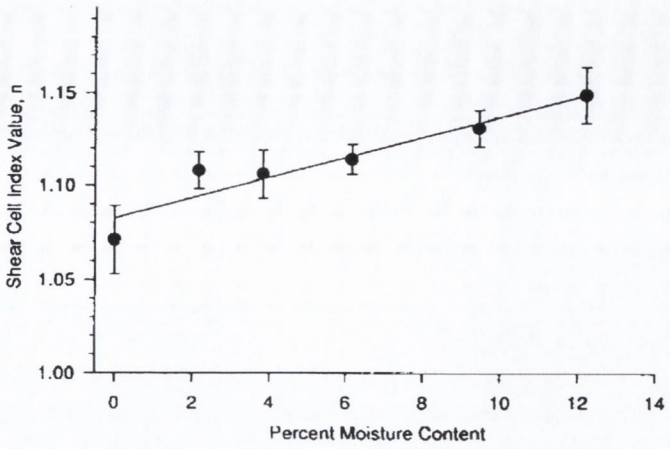

Figure 1.2h. Shear cell index value, n, of microcrystalline cellulose as a function of moisture content (Amidon *et al.*, 1995)

(c) Effect of lubricants

Because of the less than ideal flow properties of some of the commercially available grades of MCC, especially the Avicel PH-101 grade, lubricants are frequently added into formulations intended for tableting. As well as lubricants being incorporated to improve powder bed flow, they also reduce friction between the tablet material and the die wall, thereby reducing problems such as die sticking and capping of tablets (Salpekar and Augsberger, 1974). Podczech *et al.* 1996, stated that lubricant incorporation improves flow properties by reducing the friction between powder particles. In their study, they observed magnesium stearate to form a film around the MCC particles thereby causing less shearing of the material to occur at the point of contact of the MCC particles with the surrounding area during sliding. In the case of magnesium stearate, at an optimal concentration, the lubricant by adhering to the particles can alter their shape, i.e. change needle-like particles to a more spherical form with a reduced surface area, less friction and better flow properties.

1.2.5.5 Tensile Strength and Compactability of MCC Powder

Khan and Pilpel (1986) performed a study to examine the tensile strength of a packed bed of MCC powder. They observed that there was a much greater increase in the tensile

strength of the powder when the moisture content was increased from 5.2 wt% to 15 wt% than from 0 to 5.2 wt%. This they claimed was due to the phenomenon of low levels of moisture (< 3 wt% approx.) being internally chemisorbed into the cellulose structure and therefore was not available on the surface of the particles, thereby not affecting the bonding forces between them and hence the tensile strength of the bed. At higher moisture levels (ie > 5.2 wt%), however, the tensile strength was shown to increase, probably due to the development of liquid bridges (pendular bonds) between the surfaces of neighbouring particles. It is due to this phenomenon that most of the commercially available grades of MCC have not more than 5 wt% residual moisture content (see Table 1.2a). In the same study, Khan and Pilpel examined the effect of increasing particle size on MCC powder bed tensile strength. Larger particle sized powders resulted in a reduced tensile strength due to the larger particles having fewer potential sites in a given cross-sectional area for pendular bonds to form between the particles.

A direct consequence of the high tensile strength observed for MCC powder beds is its ability to be directly compressed in the 'dry' state to form very hard and durable compacts. It is generally regarded as the best excipient for direct tableting (Doelker *et al.,* 1987). The superior bonding properties of Avicel® are also attributable to the filamentous structure of the cellulose micro-crystals (Bolhuis and Lerk, 1973). The typically match-stick-like particles are mechanically interlocked and bonded by hydrogen bridges under compression. Very dense compacts are formed primarily through the material's ability to plastically deform with very minimal fragmentation of the particles occurring (Williams *et al.,* 1997; Yu *et al.,* 1989). According to Yu *et al.* 1989, when the applied pressure increases beyond the elastic limit of the MCC material, particles start to deform plastically, the mechanism involving particle shearing and squeezing, which is believed to facilitate the filling of gaps and pores. Air trapped in the bed can also escape more readily. The same study also showed that MCC has reduced elastic nature, especially when compared to other compressible materials such as paracetamol. This is important, as if during compression the stored elastic energy is excessive, then during decompression this energy

is available to destroy the areas of true contact that are formed during compression. This results in the formation of a weaker bonded compact.

(a) Effect of MCC particle size on compact strength

Doelker *et al.* 1995, when looking at the compactability of various Avicel® MCC grades, differing in terms of their average particle size, observed that the strongest compacts were obtained with the finest powder grades (i.e. Avicel PH-105). In the case of the other grades, the differences observed were so small, that they could be considered of identical compactability, especially when taking into account the well-known inter-batch variability. Therefore a general effect of particle size on MCC compactability could not be observed.

(b) Effect of moisture content on MCC compact strength

Because the compressibility and compactability of MCC is related to the tensile strength of its powder bed, it is not surprising that they are significantly affected by the level of moisture present. According to Williams *et al.* 1997, storage of MCC at elevated humidity conditions adversely affects its compaction properties. They investigated the compaction properties of MCC from six different sources, which consisted of both 50 μm and 100 μm grades. Their results demonstrated that storing compacts at different humidity levels (i.e. 30%, 50% or 75% relative humidity) had a significant influence on the tensile strength (TS) of the respective MCC compacts. The magnitude of TS decreased as the humidity was increased for all 50 μm grades of MCC with similar trends occurring for the 100 μm grades. The rate of decrease of TS as a function of humidity level was less for the 50 μm grades of MCC than for the 100 μm grades. Malamataris *et al.* 1991, also investigated the influence of moisture on the mechanical properties of MCC and observed similar results to Williams and coworkers, (1997). According to Bolhuis *et al.* 1985, the amount of water sorbed caused by storage at elevated humidity conditions is directly related to the reduction in crushing strength of MCC compacts and Doelker (1993) stated that these moisture-mediated changes in MCC containing tablets are an important concern. A number of reasons have been given for the effect of increasing moisture reducing MCC tablet compactability. Bassam *et al.* 1990, stated that it was due to the lubricating action

of water, which facilitates the slippage and flow of individual micro-crystals of MCC. More recently, Doelker (1993) and Amidon *et al.* 1995, produced evidence that disruption of the hydrogen bonds and subsequent reduction of compact tensile strength was responsible, similar to the observations of Khan and Pilpel (1986), describing the effect of moisture on MCC powder bed tensile strength. Their results (Doelker, 1993; Amidon *et al.*, 1995) showed that below moisture levels of 3% approx., the effect of moisture was to increase the tablet bond, however at moisture contents >3%, disruption of the hydrogen bonds occurs which cross link the hydroxyl groups. As a result an increase and then peak in the tensile strength of the compacts was observed up about 3% moisture content, followed by a significant decrease as the moisture content was increased further, indicating the presence of an optimum intermediary moisture content (see Fig. 1.2i).

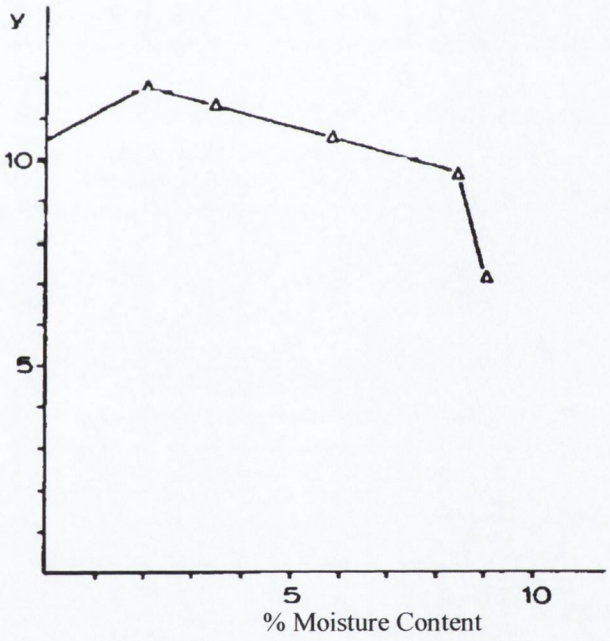

Figure 1.2i. Diametral crushing force (Y x 10 N) of Avicel PH-101 compacts as a function of percentage moisture content (Doelker, 1993).

Radebaugh *et al.* 1989, stated that this observed increase in the compactability of MCC powders when the moisture content was increased up to a level of 3 to 5% approx. was probably due to this moisture tightly binding to the amorphous regions of the cellulose polymer and thereby plasticizing it. Plasticization usually causes measurable changes in

the viscoelastic properties of a material making it less elastic and more susceptible to compaction. Radebaugh and coworkers (1989), observed from their data that when the MCC powder used to make up the compacts was plasticized with available water prior to compression and compaction, the elastic modulus (measure of elasticity) of the material decreased to a moisture content of 5% approx., at which point a plateau was achieved. When the water was added to the MCC powder after compression and compaction, plasticization was not observed due to the reduced ability of the water to distribute itself within the compacted powder. At very high humidity levels, Williams *et al.*,1997, observed that the ability of MCC to plastically deform, decreased.

(c) Effect of lubricants on MCC compact strength

Lubricants are frequently incorporated with MCC powders when being used in tableting applications for reasons mentioned previously in Section 1.2.5.3. The presence of lubricants, however, poses disadvantages, causing undesirable changes in properties, most notably a decrease in tablet strength (Alpar *et al.*, 1969; Jarosz and Parrott, 1984). This decrease in strength has been attributed to the weaker bonds resulting after compression between lubricant-lubricant molecules rather than the stronger excipient-excipient bonds (De Boer *et al.*, 1978), i.e. the strongest bonds are formed between clean surfaces. Studies by Rowe (1988), indicated that when MCC is compacted with magnesium stearate as a lubricant, strong adhesive interactions cause a film to be formed over the MCC excipient. This film is extensive as the shearing of the system (induced by compression) causes the magnesium stearate to spread further until a monomolecular film is formed. This decreases the number of strong cohesive interactions between the excipient particles causing a decrease in tablet compact strength. Not all lubricants follow this mechanism and results from the same study by Rowe (1988) indicate that when polytetrafluoroethylene is used as a lubricant, there are poor adhesive interactions between it and the MCC excipient, and so it tends to concentrate in the interstitial pores between the MCC particles. Therefore the excipient cohesive forces remain relatively strong and unchanged and hence there is little decrease in compact strength. Stearic acid was shown to have properties somewhere between these two extremes.

As well as the ability of lubricants to reduce compact strength being dependent upon the relative attraction between the MCC excipient and lubricant molecules, Doelker *et al.* 1995, showed that this ability is also dependent upon the flowability of the MCC powder. In this study the effect of lubricant incorporation on the tensile strength of compacts consisting of different Avicel® MCC powder grades was examined, the results illustrating the existence of a sequence of susceptibility between the different grades, this sequence being Avicel® PH-200>>PH-112=PH-102>PH-103=PH-101>PH-105. The PH-200 grade was the most susceptible to the effects of lubricant incorporation. The authors concluded that this order of susceptibility is again determined by the completeness of the lubricant surface film formation, which in this case is dependent upon the flowability characteristics of the powders, which as described previously is dependent upon both mean powder particle size and moisture content.

1.2.5.6 Disintegration of MCC Powder Compacts

The disintegration phenomenon has been the subject of extensive investigations and as an outcome of these researchs, two principal mechanisms have been proposed (Gayot-Hermann, 1992). One mechanism refers to the swelling of disintegrants, which results in the development of a swelling force. The other mechanism refers to the annihilation of the intermolecular bonds, which results in the development of a repulsion force. According to both mechanisms, the development of a disintegration force is needed to produce disintegration.

In the case of MCC, there is extensive literature describing the penetration and uptake of water into MCC compacts (Lerk *et al.,* 1979; van Kemp *et al.,* 1986; Ferrari *et al.,* 1986). In these instances, MCC has been shown to take up an amount of water which is significantly greater than the initial void volume of the compacts. This rapid water uptake is not due only to capillary forces but also illustrates that pore widening and extensive swelling of the powder bed occurs (Carmella *et al.,* 1984a; Ek *et al.,* 1995). Ferrari *et al.* 1986, performed studies to investigate the plausibility of the bond annihilation

phenomenon caused by the development of a repulsion force, by evaluating changes in tablet tensile strengths in media of different dielectric constants. From their data they concluded that the annihilation/weakening of intermolecular bonds, due to environmental changes in dielectric constant may play a role in disintegration, however the media must first initially be capable of penetrating the compacts, and then the mechanical stress created is likely to be the most decisive mechanism in promoting disintegration. They, similar to Carmella *et al.* (1984b) and Ek *et al.* (1995), detected the development of a force within the compacts which they linked to the swelling of the material. Despite the above observations, MCC is commonly believed to be a non-swelling material, however, even a small increase in particle volume is capable of developing a high swelling force (Carmella *et al.,* 1984b). Ferrari and coworkers (1986) observed that a relatively limited particle swelling occurred for MCC (~40% in water), yet was accompanied by a high swelling force.

The disintegration properties of MCC are affected by the presence of lubricants (Sixsmith, 1976; Rowe, 1987). This is essentially due to the typically hydrophobic nature of the lubricants used such as magnesium stearate. Even though such an agent is only needed mainly at the interface of the compact and the die wall, it must be distributed throughout the tablet, thereby tending to make the compact more hydrophobic. Due to this hydrophobic nature they reduce the previously described ability of water to penetrate the compact.

1.3 Halloysite

1.3.1 Introduction

Halloysite is a 1:1 type layer silicate being a member of the kaolin group of minerals. Unlike other minerals of this type, halloysite can assume a variety of particle (crystal) shapes. It also has the ability to exist in a hydrated (endellite) and dehydrated state (metahalloysite), the empirical formula of each being $Al_2Si_2O_5(OH)_4.2H_2O$ and $Al_2Si_2O_5(OH)_4$, respectively. The most common morphology is that of an elongated hollow tubule, but the occurrence of short tubular, spheroidal and tabular (platy) forms has been widely reported (Carson and Kunze, 1970, Dixon and McKee, 1974, Tazaki, 1982, Churchman and Theng, 1984, Noro, 1986, Bailey, 1990).

1.3.2 Sourcing Halloysite

The principal commercial source of halloysite deposits are in New Zealand and are exploited by New Zealand China Clays Ltd., (a subsidiary company of Ceramaco Corporation Ltd.). The deposits were initially discovered in the early 20th century, but it was not until the 1960's that a systematic exploration and development programme was performed over various volcanic areas of the North Island, leading to the confirmation of these large resources in Northland and several smaller resources in the Coromandel region (Harvey, 1996). Three commercially significant halloysite resources were confirmed by these studies at Maturi Bay, Mahimahi and Maungaparerua. New Zealand China Clays Ltd. was established in 1969 to process the halloysite and develop both local and export markets in ceramics and other applications. Currently, virtually 100% of the New Zealand production is exported to most of the top white-ware manufacturers throughout the world.

Other commercial sources of halloysite include Japan and South Korea. In Japan, the Gaerome clays, with visible quartz grains, consist of an ill-sorted sedimentary clay mixture of kaolinite, halloysite, aquartz and feldspar, and occurs in Pliocene sediments in Seto (Aichi Pref.) and Tayimi-Toki (Gifu Pref.) areas in the vicinity of Nagoya in central Japan.

This area is one of the country's main centers of ceramic production. Other sources of poorer grades produced by hydrothermal weathering of lavas, include the Omura mine to the north of Nagasaki, and the Okuchi mine in the north-western area of Kagoshima Prefecture in southern Kyushu. In South Korea, there are many producers of halloysite clays, but the two largest are believed to be the Taemyung mine at Keumseo, Kyongsangnam and the Hankukyoeub mine at Samka, Kyongsangnam (Harvey, 1996). These deposits consist of both hydrated and dehydrated halloysite along with quartz, cristoballite and occasionally feldspar. The halloysite is thought to have formed by hydrothermal alteration caused by circulating surface waters.

Other minor sources include the Czech Republic, from a deposit near Michalova for the production of heavy clayware refractories, ceramic insulators, paper rubber filling and sugar refining. In France, Ste. Argiles Rares et Silice Industrielle du Perigord is reported to produce up to 2000 t.p.a. for use as a component in ceramic porcelain, from a deposit located in the Dordogne. In the USA, deposits are found in Indiana, the Dragon mine in Utah (now closed), and a deposit located about 80 km north of Reno, exploited by the Nevada cement company.

1.3.3 Origin of Halloysite

Halloysite is a product of soil mineral weathering. In New Zealand, it arises due to the weathering of rhyolitic tephras, in which situation volcanic glass alters to allophane, which on ageing crystallises to cylindrical halloysite. Kirkman, 1975, suggested the following weathering sequence based on the observed distribution of allophane and halloysite in various clay fractions:

feldspar and glass

⇓

allophane

⇓

poorly crystallised halloysite (short squat cylindrical particles)

⇓

well crystallised halloysite (tubular halloysite; endellite)

⇓

metahalloysite (dehydrated halloysite)

This weathering sequence also agrees with that proposed for Japanese volcanic soils, but has been observed to occur at a faster rate when compared to the New Zealand deposits (Kirkman, 1975). Kirkman (1977) observed that in New Zealand, allophane dominates clay fractions of tephras up to about 13,000 years of age, whereas the clay fractions of tephras between 13,000 and 42,000 years of age contain small but increasing amounts of halloysite. It is only the very much older clay fractions to which well-ordered halloysite is restricted. According to Kirkman (1977) active organic cycles induced by high soil humus contents could dramatically increase the rate of formation and alteration of the clay minerals. Kirkman (1977) also examined the crystal growth patterns of the halloysite mineral, observations of which also implied that development of halloysite crystals begins within very small volumes of the allophanic matrix, the cylindrical halloysite particles beginning to crystallise from allophane after about 11,000 years, and that the initially very small and poorly formed particles grow slowly with age and improve in crystallinity. During the transformation, most of the aluminium originally present in the allophane becomes incorporated into the 1:1 lattice, the silica being provided from percolating water within the immediate environment. The extent to which halloysite is formed by the above weathering process is determined by factors such as the concentration of silica (Si) in the soil solution and the soil temperature (Farmer *et al.,* 1979).

Because of the mechanism by which halloysite is formed, small levels of amorphous allophane are still present in conjunction with even very well-developed cylindrical tubes, mainly being associated within the central core lumen of the mineral. This was revealed by experiments performed by Kirkman (1977) which involved attempting to dissolve the halloysite tubular layers in hot alkali (2% Na_2CO_3) over periods of 30, 60 and 120 min, in an effort to reveal further details of its layered structure. TEM observations indicated that the layers of the exterior of the cylinders did not dissolve, with the diameter of the tubes

remaining approximately constant. Instead, it was the centers of the particles which became progressively less electron dense corresponding to the dissolution of the intrinsically associated amorphous allophane.

1.3.4 Halloysite Structure

Halloysite was originally described and named by Berthier in 1826 and from that time until 1934 the mineral was regarded as an amorphous substance with no characteristic shape. In 1934, X-ray studies performed by Hofmann, Endell and Wilm (1934) indicated its crystalline nature. It was not until the mineral was examined with the electron microscope that Shaw and Humbert (1941) observed from electron micrographs that the mineral typically occurred as split rods. This theory was revised later by Kelley and Shaw (1942) who concluded from observations that the mineral was a rod-shaped ellipsoid and in the same year by Kelley and Page (1942), who described halloysite as "needle-shaped crystals". It was work performed by Bates *et al.*, (1950), which deduced its currently accepted tubular structure. These publishings remain the definitive paper on halloysite to date (Price and Gaber, 1997).

Bates *et al.*, 1950, showed from electron microscopy and a series of mathematical calculations that halloysite exists in the form of hollow tubes, many of which are split longitudinally or have collapsed to form laths or ribbons. Structural considerations led to the hypothesis that the halloysite crystals existed as well developed tubes and that the strain induced by dehydrating the mineral (to form metahalloysite), causes the tubes to collapse, split and commonly unroll. They were able to explain the above physical phenomena which occurred upon mineral dehydration, in terms of its inherent structure.

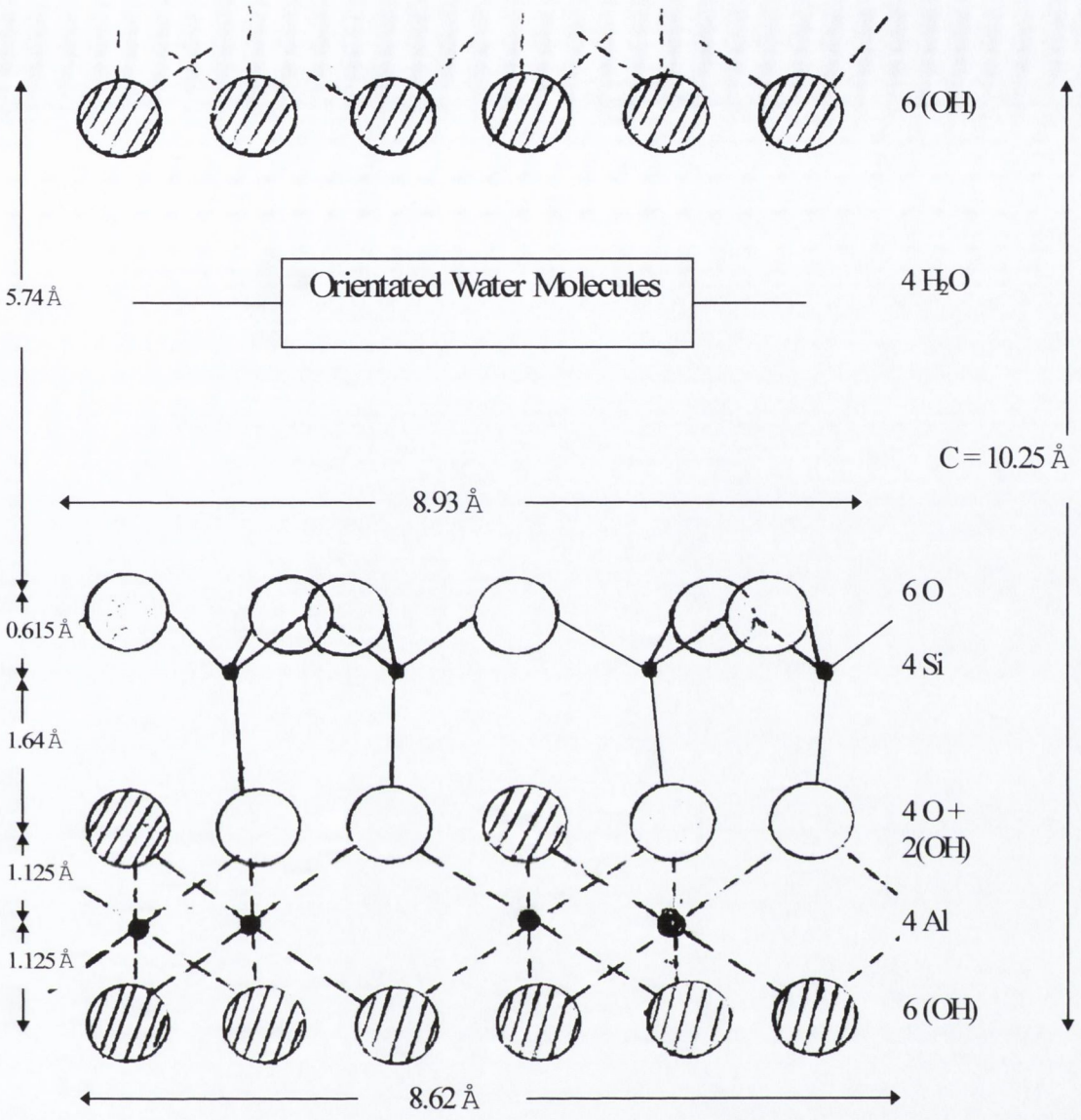

Figure 1.3a. Structure of hydrated halloysite (endellite) according to Hendricks, 1938.

Fig. 1.3a illustrates the structure of hydrated halloysite (endellite) as proposed by Hendricks (1938). Similar to the other minerals in the kaolin group, a 1:1 structural unit is present, consisting of a modified octahedral gibbsite sheet (alumina) bonded to a tetrahedral silicon-oxygen sheet. In the mineral gibbsite the six hydroxyl ions on one side of the unit cell occupy a distance of 8.62 Å in the b direction, while in the silicon-oxygen sheet, the corresponding six oxygen ions occupy a distance of 8.93 Å. Thus, as Pauling (1930) pointed out, the two sheets which compose the structure are not a perfect fit. The

mineral consists of several of the previously described units, one on top of the other in the c direction as illustrated in Fig. 1.3a. In the hydrated version of the mineral (endellite), the distance between each repeating unit in the c direction is 5.74 Å due to the presence of an intercalated layer of water. This distance is wide enough to behave as a buffer, alleviating the stretching forces to which the hydroxyl ions in the gibbsite sheet (width = 8.62 Å) are subjected to by the adjacent expanded oxygen atoms (width = 8.93 Å). The six hydroxyl ions are, therefore, free to approach the normal spacing of 8.62 Å, while the six oxygen ions on the opposite side of the same unit occupy a distance of 8.93 Å.

Bates *et al.*, 1950, deduced that by assuming that the "vertical bonds" in the c direction within the unit remain of equal length relative to each other, a curvature must result, such as that shown in exaggerated form in Fig. 1.3b. They calculated the inner diameter to be 250.8 Å (i.e. 2 X 125.4 Å), using simple mathematical calculations, this value being of the same order of magnitude as the inner diameter of the smallest sample tubes measured by them using electron microscopy techniques.

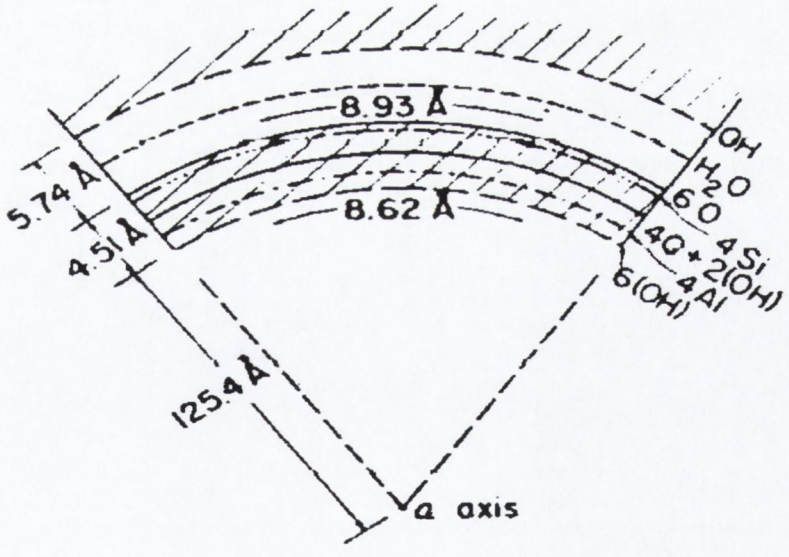

Figure 1.3b. Diagrammatic representation of the proposed curved arrangement of endellite (halloysite) layers according to Bates *et al.*, 1950.

When the halloysite mineral is dehydrated to metahalloysite, the intercalated water layer, mentioned previously, is removed. As a result, the buffering effect of the water no longer exists and the distance between the adjacent units in the c direction (see Fig. 1.3b) shrinks to less than 3 Å, (previously 5.74 Å). As a result, the six oxygen ions of the unit apparently 'stretch' the opposing hydroxyl ions to fit the cell dimension of 8.93 Å. As a consequence of this, the curved sheets tend to become planar, resulting in longitudinal splitting or collapse of the tubes. Once started, Bates *et al.,* 1950, concluded that a split would continue along the length of the tube. Unrolling also further relieves the strained condition. The fact that splitting or unrolling of tubes occurs upon dehydration, explains the relative irreversibility of the process. It is important to note, however, that not all tubes undergo splitting, unrolling or collapse with dehydration, as in many crystals the tubular structure is sufficiently strong to prevent opposing oxygen and hydroxyl layers of adjacent units from coming together, when the intervening layer of orientated water molecules is removed.

Kaolinite differs form halloysite due to the fact that even though its chemical composition is similar to halloysite, it is almost invariably planar in nature. In this instance the lateral misfit that occurs within the halloysite structure is corrected by the rotation of alternate silica tetrahedra in opposite directions (Radoslovich, 1963). In hydrated halloysite, however, tetrahedral rotation is blocked by the presence of interlayer water (Bailey, 1990).

1.3.5 Effect of Iron Content on Halloysite Structure

Studies have shown that the morphology of the halloysite mineral is not only affected by the mechanism involved in its generation, but can be influenced by the level of iron (Fe^{3+}) that has substituted the aluminimium ions (Al^{3+}) within the gibbsite sheet. Noro (1986) showed that the curvature of halloysite crystals decreases with an increase in Fe_2O_3 content, with the data of their study indicating that the halloysite crystals approach a platy form above 3.5 to 4% Fe_2O_3. Hexagonal platy halloysite has been discovered in Japan, the

first being found in an altered Tuff at Ookusa, Komaki City, Aichi Prefecture, Central Japan. Examination of this platy halloysite by Noro (1986) showed that its most characteristic property is its large Fe_2O_3 content. Kunze and Bradley (1964) and de Souza Santos *et al.,* (1966) also reported that their platy halloysites were rich in Fe_2O_3 (8.25 and 1.42%, respectively). Nora (1986) was able to show that this phenomenon occurred due to substitution of the aluminium ion by the larger iron ion, the ionic radii of each being 53 and 64.5 pm, respectively. Therefore, the size of the octahedra in halloysite (gibbsite) increases by ~6% when Al^{3+} is replaced by Fe^{3+}. The expansion of the octahedra decreases the mismatch between the octahedral sheet and the tetrahedral sheet, described previously, and consequently the crystal may take on the platy form above 3.5 to 4% Fe_2O_3.

Based on the above phenomenom, Soma *et al.,* (1992), suggests that it seems conceivable that when the structural Fe_2O_3 exceeds ~4%, the lateral dimension of the octahedral sheet in the b direction would become so large, as to cause it to curl around the tetrahedral sheet. The possibility of such a "reversal" in layer rolling has been suggested by the results of Churchman and Theng (1984) for an iron rich spheroidal halloysite sample from New Zealand. Spheroidal halloysites, however, do not present a clear cut case in that their structural Fe content may be either relatively high or low (Tazaki, 1982, Churchman and Theng, 1984, Noro, 1986, Johnson *et al.,* 1990). In this instance, iron does not appear to dictate particle morphology. Rather spheroidal shape probably relates more to mechanisms of formation than to structural factors (Bailey, 1990). These general conclusions are supported by the results of X-ray photoelectron spectroscopy (XPS) analysis performed by Soma *et al.,* 1992.

XPS data (Soma *et al.,* 1992) further suggests that the layers within a halloysite crystal are built up like "onion skins", similar to what Kohyama *et al.,* 1982, envisaged and that their chemical composition varies from layer to layer. This type of layer heterogeneity may partly arise from the preferential leaching of outer crystal surfaces, the exact nature of

which depends upon the chemical composition of the ambient solution as crystallisation progresses.

1.3.6 Intercalation of Halloysite

As mentioned previously, naturally occurring halloysite (endellite) is present in its hydrated form with the water molecules forming a specific layer between adjacent 1:1 silica/gibbsite building units. According to Sudo and Shimoda (1978), the term "intercalation" has been used to describe the phenomenon in which there is an intrusion of a material (in this case water) into the interlayer region of the clay mineral. This intercalation reaction with halloysite is not limited solely to water, and occurs with various salts and other organic compounds. In the period 1956-1959, it was noticed that various salts are specifically absorbed within the interlayer region. For the purpose of emphasizing this particular process, in the case of the formation of salt-clay complexes, the term "intersalation" has been proposed (Andrew *et al.*, 1960).

Wada (1961) and Andrew *et al.*, (1960) reported that clay minerals of the kaolin group can form a complex with potassium acetate, which was expanded to include halloysite in further studies (Wada, 1965). In the case of halloysite, the experiment was performed by grinding potassium acetate with the mineral in an agate mortar for about 15-30 min and then allowing the ground material to stand for about 24 hr. Potassium acetate was adsorbed by the repetitive interlayer region as a well orientated mono-molecular layer, resulting in expansion of the height of the hydrated unit structure from ~10 Å to ~14 Å. The crystal model structure of the halloysite-potassium acetate complex is shown in Fig. 1.3c. When this complex is washed with excess water, the potassium acetate readily dissolves in the water causing a contraction of the spacing back to ~10 Å from 14 Å.

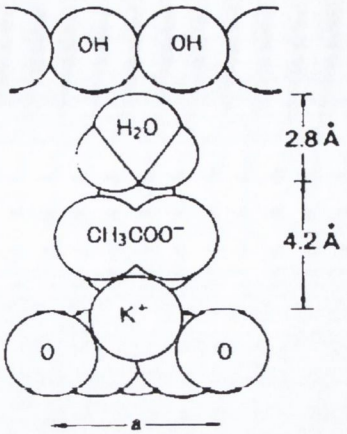

Figure 1.3c. Crystal structural model of the kaolinite-potassium acetate complex (Wada, 1961).

Subsequent studies have been aimed at forming new complexes, (Weiss *et al.,* 1963, 1966, Carr and Chih, 1971). The data of Carr and Chih, (1971), suggest that particle morphology might be important in determining the reactivity of different halloysites towards organic compounds. Churchman and Theng (1984), examined various mineralogical factors affecting complex formation. They observed that when the interlayer space of halloysite has already been expanded by water, as in the case of fully hydrated samples, the rate and extent of intercalation depend more on the properties of the organic species than on the mineralogy of the clay. Carr and Chih (1971), observed that in general an organic compound will only form a complex with halloysite provided it is relatively small, contains two functional groups (preferably -OH and/or $-NH_2$) and has one functional per two carbon atoms, and do not generally include cyclic or aromatic types. With partially and completely dehydrated halloysite, however, complex formation is influenced by the particle size, crystallinity and iron content of the mineral. A large particle size, a high degree of crystallinity and a low iron content are all conducive to complex formation. According to Churchman and Theng (1984), the iron content of halloysite also appears to affect particle shape. Low structural iron contents are associated with long tubular particles, intermediate contents with short and/or wide tubes, and high contents with spheroidal and other non-tubular forms.

1.3.7 Halloysite Surface Charge

Bailey (1990) pointed out that water is encouraged into the interlayer spaces within the halloysite structure due to the presence of exchangeable cations bound to its surface. The determined cation exchange capacity of the mineral confirmed that the mineral must have a net negative surface charge. This was confirmed by electrophoretic experiments performed by Tari *et al.*, 1999, using a Zetasizer.

A number of hypotheses have been proposed to describe the existence of this negative charge. Bailey (1990) suggested that it was due to the aluminium for silica substitutions in the tetrahedral sheet, i.e. due to the presence of a 4-coordinate Al (Al(IV)). Newman *et al.*, 1994, showed, however, using "high-field" and "medium-field" solid state ^{27}Al MAS NMR spectroscopy on six halloysite samples, that of the six, Al(IV) was found to be present in only five, the contents of which were very low (<1%). This indicated little evidence for the presence of this tetrahedrally coordinated Al being responsible.

At present, it is generally accepted that the net negative surface charge arises due to a combination of the non-stoichiometric substitution of octahedral Al^{3+} by Fe^{3+} and the acidic and amphoteric properties of the silica and gibbsite sheets, respectively. X-ray photoelectron spectroscopy has provided good evidence to show that halloysites carry a negative charge on the basal or 'face' surface of their crystals, arising from the non-stoichiometric replacement of Al^{3+} by Fe^{3+}, as mentioned above (Soma *et al.*, 1992). The substitution is non-stoichiometric in that the loss of Al is disproportionately higher than the gain in Fe, the result being the creation of a positive layer-charge deficiency. Since this charge is intrinsic to the layer structure, its sign and magnitude are independent of pH. In addition, since it is the silica side of the 1:1 unit that is exposed on the mineral's surface, an additional negative charge is created on its surface over a substantial range of pH values, due to its ionisation as illustrated by Eqn 1.3a. Exposure of the silicon oxide to water (similar to the aluminium oxide) causes the formation of surface hydroxyl groups, which can be ionised. Because silica is an acidic oxide, the second reaction on the right hand side of Eqn. 1.3a is dominant over a wide range of pH values.

$$\left[Si-OH_2^+ \xleftarrow{H^+} Si-OH \xrightarrow{OH^-} Si-O^-\right] \qquad \text{Eqn. 1.3a}$$

By contrast, the net charge on the crystal edges, which is essentially composed of gibbsite (alumina), can be either negative or positive with changes in pH due to the amphoteric nature of alumina. The amphoteric nature of the edge surface can be ascribed to the protonation and deprotonation of -OH groups coordinated with exposed Al ions under acid and alkaline pH conditions, respectively. This process is represented by the scheme in Fig. 1.3d, (Theng and Wells, 1995a).

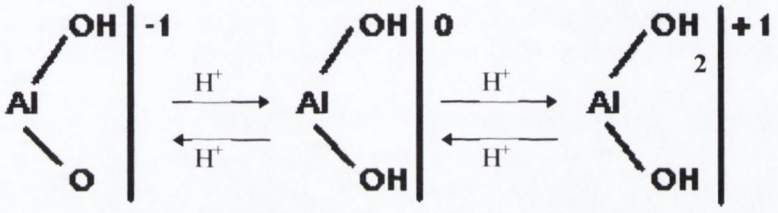

Alkaline side of PZC | Point of zero charge (PZC) | Acid side of PZC

Figure 1.3d. Illustration of amphoteric nature of alumina, as present in the edge surfaces of halloysite tubules.

At the point of zero charge (PZC; pH ~6), the edge surface charge is essentially uncharged, while at pH values above and below the PZC, it will be negatively and positively charged, respectively. As the pH decreases below the PZC, the magnitude of the positive charge on particle edges increases progressively. At high pH values, particles tend to repel each other since the charge on both the edge and face surfaces are negative. When the pH reduces, the surface charge remains relatively constant, or decreases only to a limited degree, whereas the edge becomes progressively positive, thereby reducing the

overall net surface negative charge of the mineral. This has important implications for the binding of the mineral with cationic molecules.

1.3.8 XRD Analysis and Identification of Halloysite

Several characteristics facilitate the X-ray identification of halloysites. According to Brindley and Brown (1980), the 10 Å-form (hydrated; endellite) is recognised by the broad 10.1 Å 001 diffraction peak which collapses to about 7.2 Å (7 Å-form) when heated for an hour at around 100°C; the conditions are not critical. This easy collapse of the basal spacing differentiates 10 Å halloysites from other clays with basal spacings near 10 Å. The 003 reflections (d = 3.40 Å) of the 10 Å form is then replaced by the 002 reflection (d = 3.60 Å) of the 7 Å-form (dehydrated metahalloysite).

As mentioned previously, halloysites, especially the hydrated form (endellite) are capable of forming complexes with various salts and organic compounds. Formation of these complexes can be detected by XRD analysis if the interlayer space is expanded greater than 2.8 Å, which is the expansion due to the presence of water. This is reflected in an overall expansion of the 1:1 gibbsite/alumina unit to greater than 10 Å, and is consequently detected by XRD analysis as the presence of a peak > 10 Å (or less than 8.78° 2θ using Bragg's Law).

1.3.9 Applications of Halloysite

The principal use of halloysite to-date is in the ceramics industry. Its use in ceramics dates back to antiquity. Korea has used halloysite as a major component of its highest quality whiteware for many centuries, this technology being subsequently adopted and adapted by Japanese porcelain manufacturers. Halloysite was also amongst the earliest clay minerals to be used as catalysts (Harvey, 1996). Halloysites from the Dragon mine, Utah, were used as a base for some of the initial oil cracking catalyst studies, early in the 20th century. Further developments in activated clays and synthetic catalysts have constrained its use in these applications, but small tonnages are still used.

Njopwouo *et al.,* 1987, demonstrated the ability of halloysite and other minerals (kalolinite) to behave as a catalyst on the polymerization of styrene. They observed that all clays, when pretreated with acid, effectively catalysed the thermal polymerization of styrene, the catalytic activity of which depended upon its concentration in the reaction medium. It was concluded from the study that it was the ability of the clay to exchange cations that enabled it to easily fix protons on its surface, and it was these fixed surface protons which were responsible for its catalytic action.

A recent study performed by Theng and Wells (1995b) also showed that with respect to New Zealand, the halloysite rich clay from the Bay of Islands region shows considerable promise as a bleaching agent. As the natural material is acidic, relatively little HCl was required to achieve optimum performance. A potential commercial use of this bleaching property is in decolourizing butter, the authors observing the preference by some overseas markets for a pale, whitish product, from which the carotenoid pigments and a range of flavour compounds have been removed.

Halloysite has sometimes been referred to as 'poor man's kaolin' since in many of its applications other than ceramics its properties are inferior to those of kaolinite. Such applications include paper filling, paper coating and paint pigment.

More recently halloysite has been examined as a potential excipient in various sustained chemical delivery applications, especially various antifouling agents such as tetracycline. In this regard it has become the subject of a recent patent (Price and Gaber, 1997), in which hollow ceramic or organic tubules function as a method for the delivery of an active agent at a controlled rate. The active agent is contained within the lumen of the microtubule, being typically adsorbed onto its inner surface. The microtubule is defined as being a mineral tubule such as halloysite, cylindrite, boulangerite or imogolite, with an inner diameter of less than 0.2 μm.

Similar work by Price in conjunction with other coworkers (Schnur *et al.*, 1994) examined the controlled release applications of various biological agents such as tetracycline from tubular lipid microstructures of similar dimensions to halloysite, which had been rigidised and made impermeable by subjecting them to a metallization process. The controlled release from these small rigid hollow cylinders was described in terms of diffusion. In this case, the diffusion of the encapsulant to the media is affected by the diameter of the cylinders and the concentration gradient. The effective porosity of the cylinder is reflected in the cylinder inner diameter as long as the walls of the cylinder are relatively impermeable to solutes. If the encapsulant is mixed with a polymeric carrier (P1) (different from that of the coating P2), then factors affecting the release of the encapsulant into the external environment are as follows, as illustrated diagrammatically in Fig. 1.3e:

1. the permeation of the encapsulant into the carrier polymer (P1)
2. the porosity of the carrier polymer P1
3. the concentration gradient between P1 and P2
4. the porosity of the exterior polymer coating P2
5. the permeation of the encapsulant in the polymeric coating P2
6. the concentration gradient between the polymeric coating P2 and external environment/media

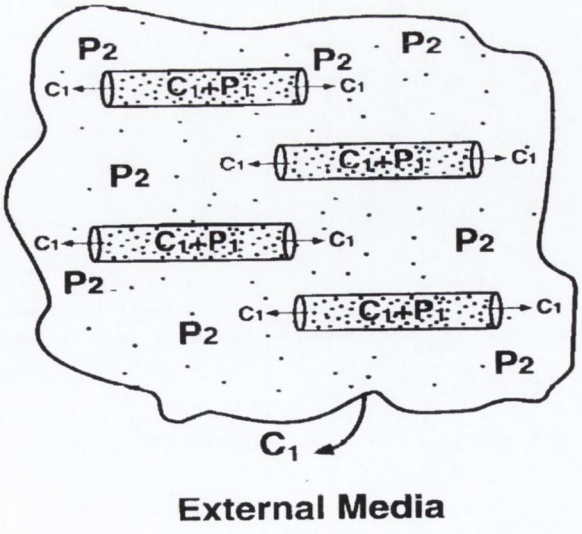

Figure 1.3e. Release from hollow cylinders (Schnur *et al.*, 1994).

1.4 INDOMETHACIN

1.4.1 Definition

Indomethacin has been shown to exist in three polymorphic forms denoted as the α, β and γ forms (Yamamoto, 1968). Form I (γ-form) indomethacin presents the highest melting point and lowest solubility, and is also the most thermodynamically stable form. For this reason, it is the principal form used in pharmaceutical applications, the sodium trihydrate salt being used less frequently. Both forms I and II (α-form) indomethacin were reported to be equally biologically available and active (O'Brien *et al.*, 1984). Form I was used for the purposes of this thesis.

1.4.2 Molecular Structure

The molecular structure of indomethacin is shown in Fig. 1.4a. The drug is structurally and pharmacologically related to suldinac. It is referred to chemically as 1-(*p*-chlorobenzoyl)-5-methoxy-2-methylindol-3-yl) acetic acid (Merck Index, 1996). It has a molecular weight of 357.78 and structural formula $C_{19}H_{16}ClNO_4$ (United States Pharmacopoeia (USP), 1995).

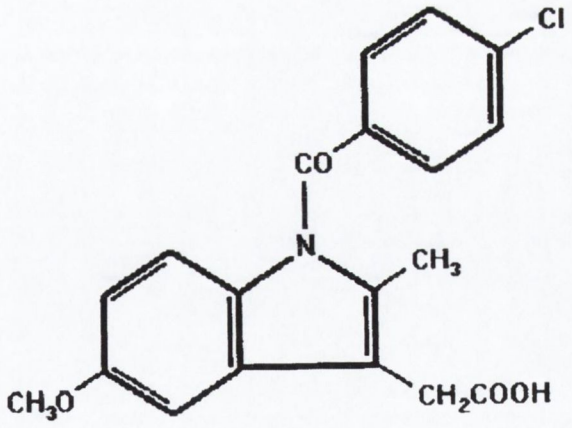

Figure 1.4a. Molecular structure of indomethacin.

1.4.3 Physicochemical Properties

Indomethacin is a pale yellow to yellow-tan, crystalline powder that is odourless or almost odourless and tasteless.

An extensive literature has been reported for the solubility of Indomethacin. According to the Pharmaceutical Codex (1994), it is very slightly soluble in water, soluble at 20°C in 50 parts of alcohol, in 45 parts of ether and in 30 parts of chloroform. O'Brien *et al.* (1984), generated a Table quoting solubility data of the various polymorphic forms for the drug in various solvents and aqueous buffer systems (see Table 1.4a). Table 1.4a illustrates the drug's pH dependent solubility, with solubility increasing with pH, which is related to the ionisation of its carboxyl group, the pKa of which is 4.5. Much work has been performed to increase its dissolution, enhanced dissolution being observed with an amorphous glassy form of indomethacin (Corrigan *et al.*, 1985; Fukuoka *et al.*, 1986).

Table 1.4a Solubility data reported for indomethacin (O'Brien *et al.*, 1984).

Solvent	Temp. (°C)	Solubility
Water	25	0.40 mg/100 ml[a]
Water	25	0.41 mg/100 ml[b]
Water	25	0.42 mg/100 ml[c]
Water	RT	Practically insoluble
Phosphate buffer pH 5.6	25	3 mg/100 ml[a]
Phosphate buffer pH 5.6	25	5 mg/100 ml[b]
Phosphate buffer pH 6.2	25	11 mg/100 ml[a]
Phosphate buffer pH 6.2	25	16 mg/100 ml[b]
Phosphate buffer pH 7.0	25	54 mg/100 ml[a]
Phosphate buffer pH 7.0	25	80 mg/100 ml[b]
Ethyl alcohol (95%)	RT	1 in 50
Chloroform	RT	1 in 30
Ether	RT	1 in 45
Methanol	25	32 mg/g
Benzene	25	4 mg/g
n-butanol	25	19 mg/g
sec-butanol	25	27 mg/g

[a]Form I, [b]Form II, [c]Form III, RT = Room Temperature

1.4.4 UV Absorption Spectrum

The USP (1995) lists a UV absorbance maximum at 318 nm in methanolic 0.1N hydrochloric acid. The E(1%, 1cm) calculated by O'Brien *et al.* (1984), at the above maximum wavelength is 182, in methanolic 0.1N HCl.

1.4.5 Stability

In general, when formulated products incorporating the indomethacin are stored at room temperature, they remain stable for at least 5 years. Its colour increases in intensity when exposed to strong direct sunlight, indicating a light sensitivity, however, degradation is only slight. Despite this, light resistant containers should be used as a precaution to minimise this discolouration process. Indomethacin is stable in neutral or slightly acidic media, but is decomposed by strong alkali where it undergoes alkaline hydrolysis to *p*-chlorobenzoate and 2-methyl-5-methoxy-indole-3-acetate, these products being also primary metabolic products. Its half-life at room temperature is 200 hr approx. in pH 8.0 buffer and is reduced to 90 min approx. in pH 10.0 solutions.

1.4.6 Pharmacokinetic Properties of Indomethacin

Indomethacin is rapidly and almost completely absorbed from the GI tract in healthy adults (UpJohn Company literature, 1985). Following oral administration, bioavailability is virtually 100%, with 90% of a single dose being absorbed within 4 hr. When it is taken with food or aluminium and magnesium hydroxide antacids, peak plasma concentrations of the drug may be slightly decreased or delayed, however, the clinical significance of this effect has not been established (Thuss *et al.*, 1986).

Indomethacin has a plasma half-life of about 4.5 hr and is about 99% bound to plasma proteins. It crosses the blood-brain barrier in small amounts and appears to freely cross the placenta (Day *et al.*, 1984). It is metabolised in the liver and undergoes enterohepatic re-circulation, i.e. its disappearance from plasma proteins appears to be biphasic with a half-life of 4 hr approx. during the initial phase and 2.6 to 11.2 hr during the second phase; variations in terminal plasma half-life may be due to individual differences in enterohepatic

circulation of the drug (Ellison *et al.*, 1985). Indomethacin is metabolised in the liver to its glucuronide conjugate and to desmethyl, desbenzoyl and desmethyl-desbenzoyl metabolites and their glucuronides. These metabolites do not possess any anti-inflammatory activity. The conjugate products pass into the bile and are then excreted into the intestine. Here they can be excreted into the faeces, or the drug conjugate can be hydrolysed back to the parent drug by the action of the enzyme β-glucuronidase, which is then re-absorbed through the gut wall to re-enter the liver via the hepatic portal vein, thus continuing the cycle.

Approximately 33% or more of a typical 25 mg oral dose of indomethacin is excreted in the faeces principally as desmethylated metabolites in their unconjugated forms. 1.5% of faecal drug excretion occurs as indomethacin. Renal excretion of the drug also occurs in addition to biliary and metabolic elimination. About 60% of a typical 25 mg oral dose is excreted via urine in 48 hr as unchanged indomethacin and its desmethyl and desbenzoyl products, appearing predominantly in its conjugated form, ie about 30% of urinary drug excretion occurs as indomethacin and its glucuronide, with the balance consisting of metabolites and their glucuronides.

1.4.7 Pharmacology of Indomethacin

Indomethacin has pharmacological actions similar to those of other NSAIDS, exhibiting anti-inflammatory, analgesic and antipyretic activity. The exact mechanisms have not been clearly established, but many actions appear to be principally associated with inhibition of prostaglandin synthesis, by inhibiting the enzyme cyclo-oxygenase, which catalyses the formation of prostaglandin precursors (endoperoxides) from arachidonic acid (Yeh *et al.*, 1982). Inflammation is reduced by decreasing the release of mediators from granulocytes, basophils and mast cells. Indomethacin also acts by decreasing the sensitivity of vessels to bradykinin and histamine, affecting lymphokine production from T-lymphocytes, and reversing vasodilation.

Indomethacin is administered orally or rectally for anti-inflammatory and analgesic effects in the symptomatic treatment of active stages of moderate to severe rheumatoid arthritis (including acute flares of chronic diseases), osteoarthritis and ankylosing spondylitis. It is also used orally and rectally for symptomatic treatment of acute gouty arthritis and acute painful shoulder (bursitis and/or tendinitis). Extended release products are not recommended for use in the treatment of acute gouty arthritis. It may cause serious adverse effects and should not be used as a simple analgesic or antipyretic. Indomethacin, as its sodium trihydrate form, is used in the treatment of patent ductus arteriosus in premature neonates.

Adverse effects have been estimated to occur in 30 to 60% of patients treated with indomethacin and serious reactions requiring discontinuance of the drug occur in 10% approx. of patients. Most adverse reactions appear to be dose related and mainly involve the CNS and GI tract (Procianoy *et al.*, 1980). Headache is the most frequent adverse effect, occurring in at least 10% of patients treated with the drug, with dizziness also being common, occurring in 3-9% of patients. GI disturbances most frequently reported include nausea, with or without vomiting and dyspepsia (including indigestion, heartburn and epigastric pain), which occur in about 3-9% of patients. Dyspepsia may occur at any time during treatment and is not always dose related; peptic ulceration with bleeding may occur and is usually, but not always accompanied by dyspepsia. Blood dyscrasias, particularly thrombocytopaenia occur rarely. Bronchospasm may be precipitated in patients suffering from or with a previous history of bronchial asthma or allergic diseases. Rashes including purpuric eruptions are uncommon.

Indomethacin is currently available as conventional capsules (25 mg/50 mg), ophthalmic suspensions (10 mg/ml), oral suspensions (25 mg/ml) and suppositories (50 and 100 mg) which are normally administered in 2-4 divided doses daily and sustained release capsules (75 mg) which are administered once and/or twice daily. To reduce GI effects of the drug, all oral preparations should be administered after food or with antacids, extended

release products being administered and swallowed intact. Daily dose levels of the drug may be increased to 200 mg if the drug is well tolerated (Pharmaceutical Codex, 1994).

1.5 DILTIAZEM HYDROCHLORIDE

1.5.1 Definition

Diltiazem hydrochloride (HCl) belongs to the benzothiazepine class of compounds. It was initially synthesised in the laboratories of Tanabe Seiyaku Co., Ltd., in Japan and was granted its first patent in 1969. Since its introduction into medical use it has gained wide acceptance as an anti-anginal and anti-hypertensive agent due to its calcium channel blocking activity. Because most currently available calcium channel blocking agents are dihydropyridines, diltiazem HCl, like verapamil has been referred to as a nondihydropyridine calcium channel blocking agent. No polymorphs of the drug have been reported to date.

1.5.2 Molecular Structure

The accepted chemical name for diltiazem HCl is (2S-cis)-3-(acetloxy-5-[2-(dimethylamino)ethyl]-2,3-dihydro-2-(4-methoxy-phenyl)-1,5-benzothia-zepin-4(5H)-one monohydrochloride. It possesses two asymmetric carbons and is supplied as the dextrorotatory cis isomer for use in pharmaceutical applications (Mazzo *et al.*, 1994). The molecular formula and molecular weight of diltiazem HCl are $C_{22}H_{26}N_2O_4S.HCl$ and 450.98 respectively. Its chemical structure is shown in Fig. 1.5a.

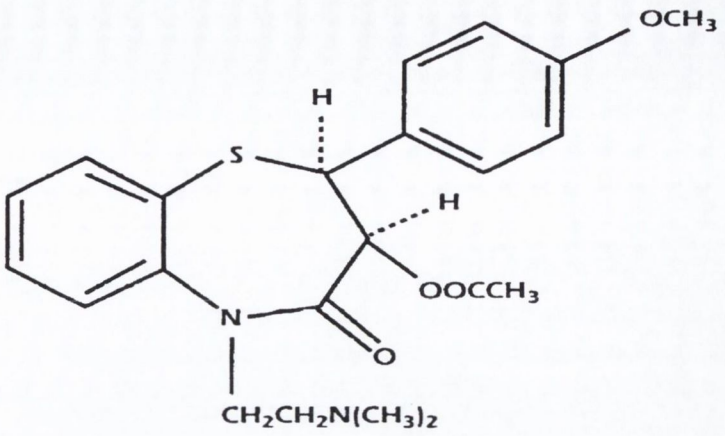

Figure 1.5a Molecular structure of diltiazem base.

1.5.3 Physicochemical Properties

Diltiazem HCl is a white to off-white crystalline powder. It is odourless and has a bitter taste.

The solubility of diltiazem HCl in a variety of solvents is presented in Table 1.5a (Mazzo *et al.*, 1994). The solubilities are indicated in terms of current USP (1995) definitions.

Table 1.5a Solubilities of diltiazem hydrochloride at 25°C.

Solvent	Solubility
Chloroform	Freely soluble
Formic acid	Freely soluble
Methanol	Freely soluble
Water	Freely soluble
Dehydrated alcohol	Sparingly soluble
Benzene	Practically insoluble
Ether	insoluble

According to Yang and Fassihi, (1997), its saturated solubility in aqueous solution at room temperature is greater than 50% w/v. The pH of a saturated aqueous solution of diltiazem HCl in water is 3.0. A 1% (w/w) solution of the drug in water has a pH of 4.2.

1.5.4 UV Absorption Spectrum

Mazzo *et al.*, (1994), determined the UV absorption spectrum of diltiazem HCl in 0.1 N HCl (aq) using a Beckman DU-6-spectrophotometer. The absorption spectrum obtained was characterised by maxima at approximately 205 nm and 236 nm. The absorptivity in absorbance units for a 10.1 μg/ml solution in a 1 cm cell was calculated to be 0.954 at 205 nm and 0.556 at 236 nm.

1.5.5 Stability

In the solid state diltiazem HCl is reported to be highly stable (Mazzo *et al.*, 1994). Storage of the drug under conditions of room temperature and 33% or 79% relative humidity for 57 days did not cause any physical or chemical degradation. It was stable after 3 weeks of storage under conditions of 44°C/75% relative humidity. Storage for three weeks at 40°C/75% relative humidity with exposure to UV light did not affect its chemical stability, but did cause a slight colour change (yellowing). For this reason it should be stored in light resistant containers.

When in solution (aqueous buffer pH 1-7), diltiazem HCl undergoes hydrolysis to the deacetyl product. It is most stable at pH 5. The decomposition follows pseudo-first order kinetics; estimating the room temperature shelf-life of the solution to be 42 days or 15.8 days at pH 5 or 2 respectively, by extrapolation. Exposure of the aqueous buffered solutions of the drug at pH 2 or 7 to UV radiation caused more degradation as compared to the same solutions protected from light, demonstrating the light sensitivity of the compound in solution.

1.5.6 Pharamacokinetic Properties of Diltiazem HCl

Upon oral administration of diltiazem HCl (in conventional tablet form), approximately 80% of the dose is rapidly absorbed from the GI tract. Despite this, only about 40% of the oral dose reaches the systemic circulation as unchanged drug since it undergoes extensive metabolism on first pass through the liver. Oral administration of the solution reached peak plasma levels 38 min after dosing (Mazzo *et al.*, 1994). It has been

reported to be 70 to 85% plasma protein bound, but only 30 to 40% bound to albumin. It is also lipophilic and therefore has a large volume of distribution (3-8 l/kg).

It illustrates dose dependent non-linear pharmacokinetics; this non-linearity of the drug area under the curve (AUC) being the result of dose dependent first-pass metabolism. Following oral administration in healthy individuals it has a plasma half-life of 2 - 11 hr, however, plasma half-life of unidentified metabolites may be increased to about 20 hr. Half-life may be slightly prolonged after multiple dosing (Buckley *et al.,* 1990), due to saturation of the hepatic first pass metabolism. Following a single IV injection of the drug in healthy adults, pharmacokinetics are dose proportional over a dosage range of 10.5 - 21 mg with a half-life of 3 - 4 hr approx. Following continuous infusion (10 - 15 mg/hr), the plasma elimination half-life increases to 4 - 5 hr. Plasma half-life of the drug may be increased in geriatric patients, but is unchanged or only slightly increased in patients with renal impairment. Liver cirrhosis has been shown to reduce its apparent clearance and to prolong its half-life.

As mentioned, diltiazem HCl is extensively metabolised, pre-dominantly due to hepatic metabolism, with only trace amounts (0.1 - 4%) of unchanged drug being eliminated in the urine. The three major metabolic pathways are O-deacetylation, N-demethylation and O-demethylation which produce several active and at least 5 inactive metabolites via the Cytochrome P450 enzyme systems. The principal six metabolites are illustrated in Fig. 1.5b. Desacetyl diltiazem and N-monodemethyl diltiazem undergo further biotransformation to form desacetyl N-monodemethyl diltiazem, desacetyl N,O-didimethyl diltiazem and desacetyl O-demethyl diltiazem. Desacetyl diltiazem, N-monodemethyl diltiazem, desacetyl N-monodemethyl diltiazem and desacetyl diltiazem N-oxide are the most abundant in the plasma. The most abundant metabolites in the urine are N-monodemethyl diltiazem and desacetyl N,O-didimethyl diltiazem. N-monodemethyl diltiazem is excreted unconjugated. The other metabolite is excreted in urine as the glucuronide or sulphate conjugate. N-monodemethyl diltiazem and desacetyl diltiazem are active metabolites which are not as potent as the parent compound.

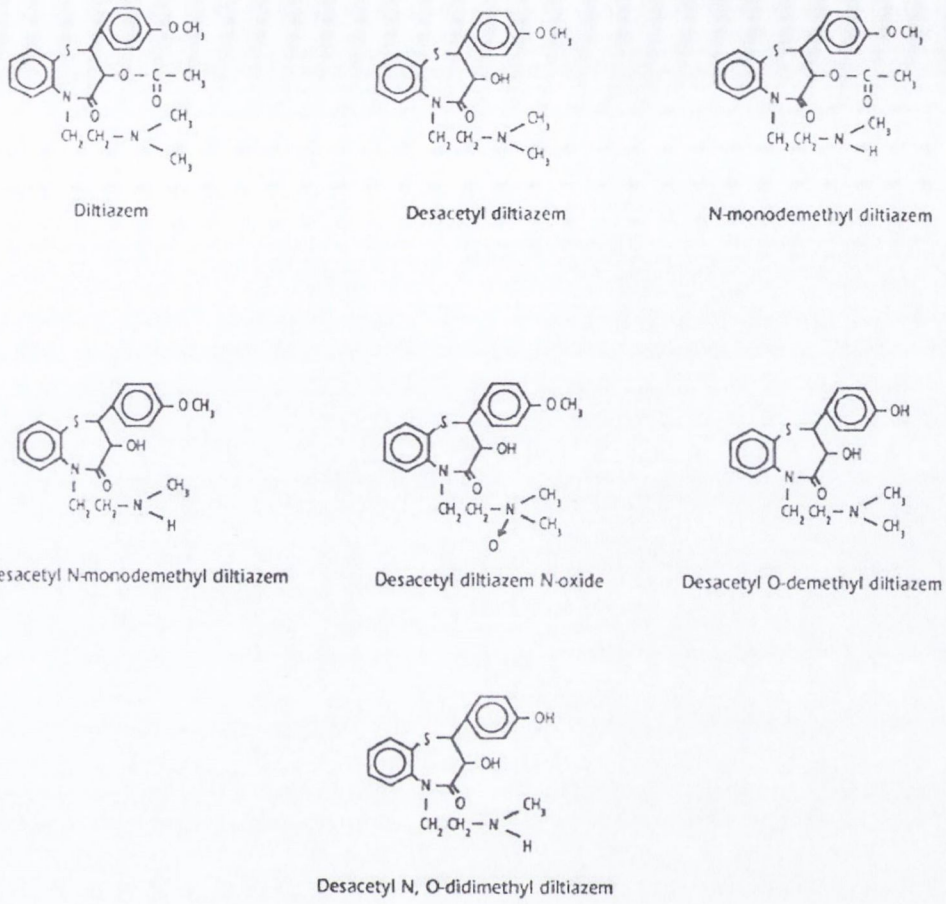

Figure 1.5b Diltiazem and its six main metabolites found in man (Mazzo *et al.*, 1994).

1.5.7 Pharmacology of Diltiazem HCl

The principal physiological action of diltiazem HCl is to inhibit the transmembrane influx of extra-cellular calcium ions across the membranes of myocardial cells and vascular smooth muscle cells, without changing serum calcium concentrations. The exact mechanism whereby it inhibits calcium ion influx across the slow calcium channels is not known, but is thought to inhibit ion-control gating mechanisms of the channel, deform the slow channel, and/or interfere with the release of calcium from the sarcoplasmic reticulum. By inhibiting calcium influx, it inhibits the contractile processes of cardiac and vascular smooth muscle, thereby dilating the main coronary and systemic arteries and decreasing myocardial contractility.

Diltiazem HCl is a calcium influx inhibitor similar to verapamil and nifedipine, but in contrast also has substantial inhibitory effects on the cardiac conduction system, acting principally at the atrio-ventricular (AV) node, with some effects on the sinus node. The drug increases AV nodal refractoriness by binding to calcium channels; binding is enhanced during depolarisation and the drug tends to unbind in a time-dependent manner during repolarisation. Therefore, when heart rate is increased (e.g. tachycardia), calcium channel bound drug increases as a result of a greater number of depolarisations and shorter diastolic periods (limiting drug unbinding). This frequency dependent effect of diltiazem HCl on the AV nodal conduction allows it to selectively decrease heart rate during tachyarrythmias involving the AV node, while having little or no effect on normal AV nodal conduction at normal heart rates.

Diltiazem HCl is used in the management of Prinzmetal variant angina (drug of choice), chronic stable angina pectoris, supraventricular tachycardias and hypertension. In the management of chronic stable angina pectoris, the drug appears to be as effective as beta-adrenergic blocking agents (i.e. propranolol) and/or oral nitrates, however it should only be used to treat this condition when the patient can not tolerate adequate doses or is refractory to these drugs. When used as an antihypertensive agent, it has been used as monotherapy or in combination with other classes of antihypertensive agents. Drug therapy in the management of hypertension must be individualised and adjusted based on the degree of blood pressure elevation, severity of the disease (i.e. presence of target organ damage), response to therapy and tolerance to side effects.

In therapeutic dosage, diltiazem HCl is usually well tolerated. Serious adverse reactions requiring discontinuance of therapy or dosage adjustment are rare, however GI disturbance, skin eruptions and bradycardia may result in discontinuance in about 1% of patients. Nausea, the most common GI disturbance, occurs in up to 3% of patients receiving diltiazem HCl, with other effects such as constipation, diarrhoea, vomiting and dyspepsia occurring less frequently. Approximately 1-5% of patients experience adverse

nervous system effects such as headaches, somnolence and abnormal dreams. Rash has been reported in about 1% of patients receiving the drug. A generalised rash characterised by leukocytoclastic vasculitis has also been reported, but a casual relationship to the drug has not been established.

Diltiazem hydrochloride is currently available as conventional tablets and capsules (60 and 90 mg) which are normally administered on a twice daily basis. Sustained release capsule and tablet formulations (60, 90, 120, 180, 300 mg) are also available, which may be administered once or twice daily in the case of the 60, 90, 120 and 180 mg preparations and once daily only for the 300 mg product. The maximum daily dose is 360 mg. The preparations may be taken with or without food.

1.6 AIMS AND OBJECTIVES

The following points broadly outline the intentions of this research work:

- to develop novel size reduced grades of MCC with improved functionality for use in pharmaceutical applications.
- to characterise physical properties of these novel grades with particular reference to the dynamics of their interaction with water.
- to assess the potential use of these novel MCC grades as functional excipients in three pharmaceutical applications, namely tableting, extrusion/spheronisation and suspensions.
- to characterise physical properties of the tubular halloysite mineral such as particle size and morphology, surface charge, surface area and tubular volume.
- to examine a number of mechanisms by which the mineral can be loaded with drug, examples of which include ionic binding and tubular entrapment.
- to examine the potential use of the tubular halloysite mineral as a novel functional excipient in the area of sustained drug delivery.
- to examine the potential of various coating systems (i.e. cationic polymers, lipids) to further modify the drug release properties from the loaded mineral.

Chapter 2

Materials

In general, reagent grade chemicals were used in the production and *in vitro* testing of products. The qualities or grades of materials listed here are those quoted by the manufacturer. Most of these correspond in quality, though not by name, to either the General Purpose Reagent (GPR) or Analar Grade used by BDH Chemicals (UK).

Description	***Batch or Lot***	***Supplier***
Acetic acid (glacial)	Lot: 119H3456	Sigma Chemicals
Apiezon-H™ vacuum grease		Gec Alsthom (M&I) Ltd.
Avicel® PH-101	Lot: 6712C	FMC Corp., Ireland
Avicel® PH-102	Lot: 7717C	FMC Corp., Ireland
Avicel® RC-581	Lot: B713C	FMC Corp., Ireland
Avicel® RC-591	Lot: D718C	FMC Corp., Ireland
Benzalkonium Chloride	Lot: 298364 1190	Fluka Chemika
Buffer soln. pH 4.00	Lot: 51910	Riedel-de-Haën
Buffer soln. pH 7.00	Lot: 71250	Riedel-de-Haën
Buffer soln. pH 9.00	Lot: 97F2	Riedel-de-Haën
Cetrimide	Lot: 40503	Aldrich Chemicals
Chitosan (medium Mol. Wt.)	Lot: 06126MN	Aldrich Chemicals
Citric acid monohydrate	Lot: 33160	Riedel-de Haen, Germany
Crillet 4	B/N: EO.0111	Croda Chemicals Ltd.
Cyanoacrylate (n-butyl)	Lot: 2266-52A	Loctite, Ireland

Cyanoacrylate (iso-butyl)	Lot: 2395/78	Loctite, Ireland
Cyanoacrylate (octyl)	Lot: 2395/71	Loctite, Ireland
Diltiazem HCl	B/N: 150406	Profarmaco
Eudragit E 100	Lot: 01-80203	Röhm Pharma, Germany
α-Glucose	Lot: K24104846	Merck
Glutaraldehyde (25% aq. soln)	Lot: 68H0099	Sigma Chemicals
Glycerol	Lot: K25433793	Merck
Halloysite 'G'	B/N: 12/98	NZ China Clays Ltd.
Halloysite 'MM'	N/A	NZ China Clays Ltd.
Halloysite 'ultrafine'	N/A	NZ China Clays Ltd.
Helium gas		Air Products
Heptane	B/N: 9L03JA	Rathburn Chemicals Ltd.
n-Hexane	HPLC Grade	Lab-Scan Analytical Sciences
High Pressure Fluid		Micromeritics Instrument Corporation
High Vacuum Grease		Dow Corning
Hydrochloric acid (37% w/w; 1.18 g/ml)	Lot: K26014952-901	AnalaR
Indium standard	Lot: WE 1239	Mettler
Indomethacin	20 μm	Ind. Chimica Farmaceutica Italy
α-Lactose monohydrate	Granulac® 200 type D80/200 mesh	Meggle, Germany
Mercury	Triple distilled (GPR^{++})	BDH Laboratory Supplies
Methanol (HPLC grade)	B/N: 31950/2578	Scharlau
Nitrogen gas		Air Products
Novata E	Batch No: 12182	Henkel
Paracetamol	Granular	FMC Corp., USA
Pluronic F68		Pechiney Ugine Kuhlmann Ltd.
Polyethylene glycol (MW 400)	Lot:60H0463	Sigma Chemicals

Polyethyleneimine (50 wt% aqueous soln)	Mol. Wt. 25,000	Aldrich Chemicals
Polyvinyl pyrrolidone (K29/32)	Batch No: 4E386	GAF Great Britain Ltd.
Potassium acetate	Lot: 34H0619	Sigma Chemicals
Potassium chloride	Lot: K25691637-906	BDH Chemicals, UK
Precirol ATO5	Lot: 84863	Gattefossé, France
Propranolol hydrochloride	B/N: 128140	Finechem, England
Reference material for Gemini 2370 (Kaolinite)	P/N 004-16819-00	Micromeritics Instrument Corporation
Reference material for PoreSizer 9320 (Silica-Alumina)	P/N 004-16822-00	Micromeritics Instrument Corporation
Sodium acetate	Lot: 108H01471	Sigma Chemicals
Sodium citrate B.P.	Lot: 924515	Aldrich Chemicals
di-Sodium hydrogen phosphate-12-hydrate	Lot: K91147473-934	Merck, Germany
Sodium hydroxide	Lot: 60500	Riedel-de-Haën
Sodium lauryl sulphate	Lot: 87H0671	Sigma Chemical Co., USA
Sodium polymetaphosphate	Lot: JR01112ER	Aldrich Chemicals
Stearic acid	Lot: 2003134	Merck, Germany
Sulphadimidine B.P.		Allied Pharmaceutical. Distributors Ltd., Dublin
Tetrahydrofuran	B/N: 7L06JA	Rathburn Chemicals Ltd.
Tween 20	Lot: 63H0481	Sigma Chemical Co., USA
Water	Distilled, deionised	
Zeta-Potential Transfer Standard	Batch No: 269901	Malvern Instruments Ltd (UK)

Chapter 3

Methodology

3.1 PARTICLE SIZE REDUCTION OF AVICEL® PH-101 POWDERS

3.1.1 Size Reduction of Avicel® PH-101 by Ball Milling

0.3 g of Avicel® PH-101 powder was accurately weighed out and transferred to a 10 ml volumetric flask. Suitable quantities of sodium lauryl sulphate were also weighed out and transferred to the volumetric flask as indicated in Table 4.1c. The sample was made up to final volume using distilled water. The contents of the flask were transferred to a RETSCH® vibratory ball mill and milled in the wetted state under the conditions listed in Table 4.1c.

3.1.2 De-aggregation Studies on Avicel® PH-101 using Surfactants

Physical mixes of Avicel® PH-101 and various surfactants were made up using the general formulae shown in Table 3.1a. 80 g water was added to each powder mix, which was subsequently allowed to hydrate in a temperature controlled water bath at appropriate temperatures. Following hydration, the mixes were removed from the water bath, filtered and dried using a forced circulation oven (Memmert Type UL40, Germany) for at least 48 h at 50°C.

Table 3.1a. Composition of the powder mixes and the experimental conditions under which they were tested.

I.D. Key	Time for hydration (hr)	Surfactant Content (g)	MCC Content (g)	Water content (g)	Temp. (°C)
		SLS			
S1	48	1	19	80	37
S2	48	2	18	80	37
S3	16	1	19	80	37
S4	16	2	18	80	37
S5	48	1	19	80	25
S6	48	2	18	80	25
S7	16	1	19	80	25
S8	16	2	18	80	25
		Tween 20			
P1	48	1	19	80	37
P2	48	2	18	80	37
P3	16	1	19	80	37
P4	16	2	18	80	37
P5	48	1	19	80	25
P6	48	2	18	80	25
P7	16	1	19	80	25
P8	16	2	18	80	25
		Cetrimide			
C1	48	1	19	80	37
C2	48	2	18	80	37
C3	16	1	19	80	37
C4	16	2	18	80	37
C5	48	1	19	80	25
C6	48	2	18	80	25
C7	16	1	19	80	25
C8	16	2	18	80	25
		Controls			
Control 1	48	-	20	80	37
Control 2	48	-	20	80	37
Control 3	16	-	20	80	25
Control 4	16	-	20	80	25

3.1.3 Size Reduction of Avicel® PH-101 by Ultrasonic Homogenisation

5% and 10% aqueous Avicel® PH-101 suspensions were prepared using distilled water. Appropriate quantities of SLS (5% w/w) were dissolved in a small volume of distilled water and added as indicated in Table 4.1d, in Chapter 4. The suspensions were

homogenised using variable cycle runs, using a 'Minisonic' homogeniser, produced by Ultrasonics Ltd., Shipley, Yorks, England.

3.2 TABLET PRODUCTION

100 g powder mixes of the required materials were blended together in a cube mixer for 15 min at 40 rpm. The blends were then compressed immediately to minimise the risk of segregation. At the outset, compression was achieved using a Manesty single punch, hand operated tablet press (Model 1B 179) fitted with a 12.5 mm flat-faced punch and die set. The tablet press was adjusted to produce a compression weight of 550 mg approx. (300 mg approx. Paracetamol). The average breaking strain was adjusted to the equivalent of 10 Kp units approx. The adjusted die cavity depth and compression level were kept constant during the compression of all subsequent powder batches.

In order to obtain better control of the compression pressure, an IR press was used subsequently. Powder weights of 400 mg were compressed using the press at a number of compression forces namely, 1000, 2000, 3000, 4000, and 5000 kg using a 13 mm flat-faced punch and die set. Tablet tensile strengths were determined for each tablet compressed under the variable compression forces using the following equation.

$$\sigma = {}^{2P}\!/\!_{\pi DE} \qquad \textbf{Eqn. 3.2a}$$

where σ is the average tensile strength (kg/cm^3)

P is the average tablet hardness (kg/cm)

D is the average tablet diameter (cm)

E is the average tablet thickness (cm)

3.3 EVALUATION OF TABLETS

3.3.1 Physical Standards

A Schleuniger Pharmatron hardness tester (model 6D) was used. Thickness was determined using an optical micrometer (Graticules Ltd, Tonbridge, Kent, UK). 20 tablets were rotated 100 times in an Erweka Copley Friabilator (TA 20) to evaluate friability. Distintegration times were determined as described in the BP using an Erweka Copley Disintegration tester (ZT 44).

3.3.2 Uniformity of Drug Content

20 tablets from each batch were weighed and powdered. A quantity of the powder containing 0.15 g paracetamol was added to 50 ml of 0.1 M NaOH, diluted with 100 ml of water and shaken for 15 min. Sufficient water was added to produce 200 ml. This was filtered, and 10 ml of the filtrate diluted to 100 ml with water. 10 ml of the resulting solution was added to 10 ml of 0.1M NaOH, diluted to 100 ml with water and the absorbance of the resulting solution measured at the λ_{max} of 257 nm. The drug content of $C_8H_9NO_2$ was calculated taking 715 as the value of A (1%, 1 cm) at the λ_{max}, 257 nm.

3.3.3 Dissolution Testing

Dissolution testing was performed using Apparatus II of the BP (Erweka Copley Dissolution tester, DT 6). The dissolution rate was determined in 1000 ml of McIlvaine buffer pH 6.8 equilibrated at 37°C ± 0.5°C and stirred at 100 rpm. The paddles were kept 23-27 mm above the base of the vessel. Samples were withdrawn every 5 min over the initial 15 min, every 15 min for the next 45 min and then every 30 min over a total dissolution time of 120 min. Fresh dissolution medium was added in each case to replace the withdrawn samples. The sample was then filtered via a 5 ml syringe, through a 13 mm 0.45 μm pore size Gelman membrane filter (type Supor®-450). Each 5 ml sample was diluted to 10 ml using the same buffer medium. 0.5 ml of this resulting solution was then diluted to 10 ml again using the same buffer. The first 5 ml of sample was used to rinse

out the Hellma quartz ultra-violet (UV) cell, having a 1 cm light path, and the remainder was read at 257 nm using a Shimadzu UV 160 spectrophotometer with McIlvaine buffer pH 6.8 as the reference solution.

For subsequent UV readings, the sum of X% of the previous values was added to the new value to give a corrected reading; this sum of the X% adjustments was to account for the previous sample removed from the bulk medium. The calculation of the X value is shown by Eqn. 3.3a. Standards were prepared in the medium used to cover the concentration of drug which could be expected and a calibration curve was produced from which the absorbance readings could be converted to concentration values. The dissolution results represent the mean of three determinations.

$$X = \frac{\text{Sample volume}}{\text{Volume of dissolution medium}} \times 100 \qquad \textbf{Eqn. 3.3a}$$

3.4 EXTRUSION-SPHERONISATION PROCESS

3.4.1 Mixing

Powders were placed in the bowl and mixed at speed 1.0 using a "K" shaped mixing arm (Kenwood Chef excel, UK). The powders were pre-blended for 10 min and mixing was continued for a further 4 min after adding the required amount of water. The mixer was stopped every 2 min to scrape any powders accumulating high on the side-wall of the mixing bowl back into the mix. The granulating liquid, water, was added gradually to the powders via a syringe. The wet mass was placed into an airtight container and allowed to stand overnight for at least 12 hr to allow the powders and water to reach equilibrium.

3.4.2 Extrusion

The wet mass was extruded using a rotary gravity-fed cylinder-type extruder (Alexanderwerk Type GA65, Germany) fitted with a 7.0 cm diameter, 14.8 cm long perforated cylinder. The perforations were 1 mm in diameter, and the cylinder wall was 4

mm thick. The perforations were spread evenly and centrally over 8.3 cm length of the cylinder wall. The perforated cylinder was located against a solid cylinder in the extruder and was capable of rotating from 20 to 100 rpm.

3.4.3 Spheronisation

The extrudate was spheronized on a 4 inch (120 mm) diameter spheronizer (Caleva Model 120, UK) using a cross hatch friction plate. The spheronized pellets were collected and dried in a forced air circulation oven (Memmert Type UL40, Germany) for at least 48 hr at 40°C to constant weight.

3.5 GENERAL METHODS OF SPHERONIZED PRODUCT ANALYSIS

The physical properties of pellets that were examined include size distribution and pellet apparent density determinations. The size distribution of a batch of pellets was measured by sieve analysis, while pellet apparent density determinations were obtained by measuring the volume occupied by a known weight of pellets in a standard graduated cylinder. The surface morphology of pellets was revealed by scanning electron microscopy.

3.5.1 Sieve Analysis

Sieve analysis was performed using a nest of standard sieves. The sieves were placed on top of each other, the largest aperture sieve at the top with decreasing apertures as the sieve nest approached the base plate. The sieve apertures used were 1680, 1180, 850, and 300 μm. A batch of pellets was placed onto a nest of Endecott sieves, which was securely mounted on an Endecott test sieve shaker (1 MK11, UK). The sieve shaker was set to agitate the nest for 10 min, during which time the pellets fell through the sieves until the aperture was smaller than the size of the individual pellets. The sieves were subsequently separated and their retained fractions weighed. The weight of each fraction was expressed as a percentage of the weight of dry solids added to the sieves. In this thesis, the desirable size range of pellets was taken to be between the 850 and 1180 μm and any spheronized product occurring within this range is referred to as "pellets". Pellets occurring above this

size are described as "large pellets", while any product occurring below this size range is referred to as "fines".

3.5.2 Pellet Packing Density Analysis

The packing density was regarded as an important characteristic of the spheronized pellets. This could influence ultimately the size of capsule shells to be used in the final dosage form. Packing density would depend primarily on pellet size distribution, pellet shape and tendency for pellets to adhere to one another. The pellets may pack in such a way as to leave big gaps between their surfaces, resulting in a lower packing density. On the other hand, very spherical pellets may sift between each other to give higher packing values. The packing density of pellets was determined by carefully pouring pre-weighed samples of pellets into 100 ml graduated cylinders and the "poured volume" was noted. The 'tapped volume' was determined after manually dropping the cylinder from a height of approximately 2 cm onto a hard surface 500 times at 2 s intervals. The pellets were considered to be closely packed at this stage. The respective poured and tapped densities were calculated as follows:

$$\rho = \frac{w}{V} \qquad \textbf{Eqn. 3.5a}$$

where ρ is the determined density,

w is the weight of pellets and

V is the volume occupied by the pellets.

Poured and tapped density ratios were calculated from the poured volume and tapped volume values, from which Carr's indices and Hausner ratios could be derived according to the Equations 3.5b and 3.5c below.

$$\text{Carr's index} = \frac{\rho_{B\,\max} - \rho_{B\,\min}}{\rho_{B\,\max}} \times 100\% \qquad \textbf{Eqn. 3.5b}$$

$$\text{Hausner ratio} = \frac{\rho_{B\max}}{\rho_{B\min}} \qquad \textbf{Eqn. 3.5c}$$

where $\rho_{B\max}$ is the tapped density and

$\rho_{B\min}$ is the poured density.

3.5.3 Pellet Apparent Density Analysis

A 25 ml density bottle (BS733, Jay Tec, UK) was washed, dried and weighed (W_1). The bottle was filled with distilled water and placed in a water bath maintained at 25°C until no water emerged from the stopper. After drying the outside of the bottle it was again weighed (W_2) and its volume (V) calculated from the formula:

$$\textbf{Volume of the bottle (V)} = \frac{W_2 - W_1}{0.9971} \quad \textbf{cm}^3 \qquad \textbf{Eqn. 3.5d}$$

where 0.9971 g/cm^3 is the density of water at 25°C. The bottle was then emptied, cleaned and filled with hexane. Hexane was chosen as none of the pellet formulation components was soluble in it. The above procedure was repeated and the weight of the bottle filled with hexane noted (W_3). The density of hexane (ρ_H) at 25°C was then determined as follows:

$$\rho_H = \frac{W_3 - W_1}{V} \quad \textbf{g/cm}^3 \qquad \textbf{Eqn. 3.6e}$$

4 g of pellets were placed in the density bottle, which was again left at 25°C until hexane ceased to emerge from the stopper, at which time the outside of the bottle was dried and its weight noted (W_4). The above procedure was repeated and an average of three readings taken. An apparent density was calculated as follows:

$$\textbf{Vol. of hexane displaced by 4 g of pellets (Y)} = \frac{W_3 - W_1}{\rho_H} - \frac{W_4 - W_1 - 4}{\rho_H} \quad \textbf{cm}^3$$

$$\rho = \frac{4}{Y} \ \textbf{g/cm}^3 \qquad \textbf{Eqn. 3.5f}$$

where ρ is pellets apparent density.

Intraparticle porosity($\in_{intraparticle}$) of the pellets may then be computed from a knowledge of the true density of the materials and pellet density (Martin, 1993; Kleinebudde, 1994). The porosity is given by the equation:

$$\in_{\textbf{intraparticle}} \textbf{(\%)} = 1 - \frac{\rho_g}{\rho}.100 \qquad \textbf{Eqn. 3.5g}$$

where ρ_g is the pellets apparent density and

ρ is the true density of the materials.

3.5.4 Mercury Porosimetry Analysis

Mercury porosimetry was performed using a Micromeritics 9320 Poresizer (semiautomated) with associated software.

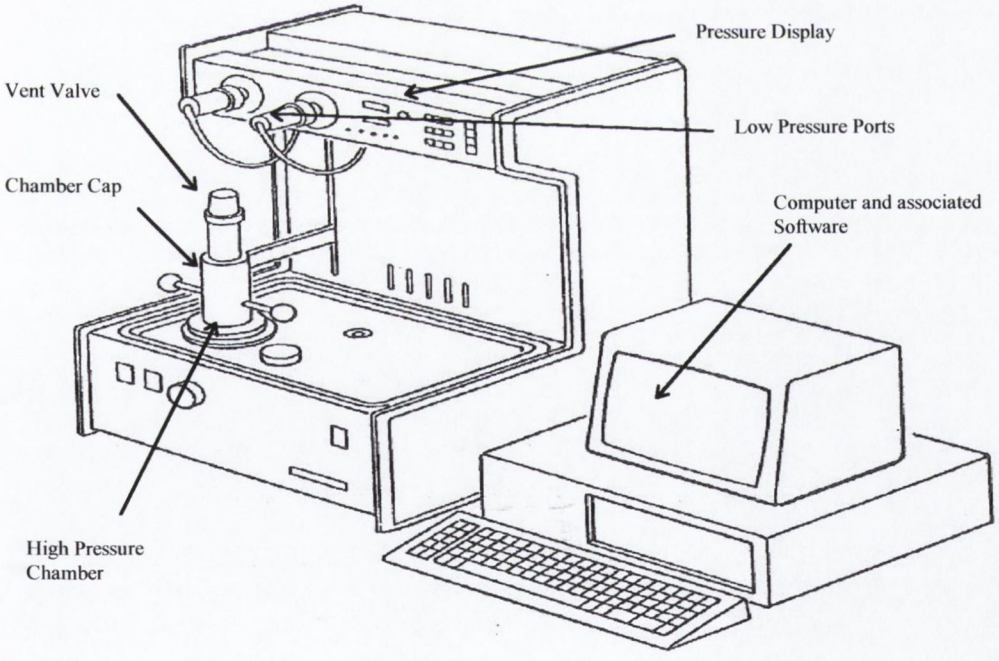

Fig. 3.5a Illustration of PoreSizer 9320 system.

The measurements were performed on pellet samples using a 3 cm^3 "powder sample" penetrometer (sample weight 350 mg +/- 10%), illustrated in Fig. 3.5b, below. Samples were dried to constant weight using a vacuum oven set at 80°C and removed just prior to analysis.

Penetrometers were calibrated (by filling with mercury under pressure) prior to use to obtain an accurate measurement of penetrometer volume.

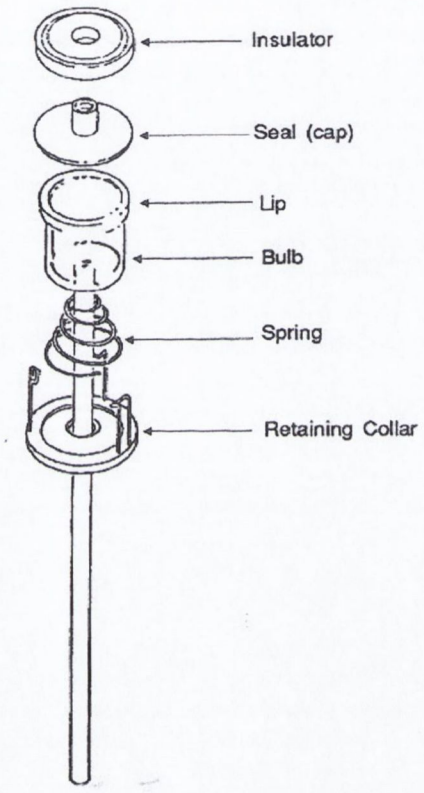

Fig. 3.5b. Illustration of penetrometer components.

Intrusion pressures between 0.5 and 30,000 p.s.i. were used, corresponding to pore diameters between 360 μm and 0.006 μm. The low pressure analysis (0.5 to ~20 p.s.i.) was done semiautomatically while the high pressure analysis (~20 to 30,000 p.s.i.) was automatically controlled. The pressure table used for the high pressure analysis is illustrated in Appendix 3.

The advancing and receding contact angle for the mercury was taken to be 130.0 degrees. The surface tension was taken as 485.0 dyn/cm. Mercury density was dependent on room

temperature (Micromeritics PoreSizer 9320 Operator's Manual V2.02, 1992). Other variables (e.g. penetrometer stem volume and maximum head pressure) were a function of the penetrometer used. The equilibration mode of analysis was used with an equilibrium time of 10 s.

3.6 METHODS USED FOR POWDER ANALYSIS

3.6.1 Particle Size Analysis by Laser Diffraction

The particle size of powder samples were measured using a Malvern 2600c (Malvern, USA) laser diffraction particle analyser with a 300 mm lens attached, which is capable of measuring particles in the size range 5.8 to 564 μm. All particle size measurements quoted in this thesis refer to the d_{50} value (i.e. d[v,0.5]), which is defined as the median diameter of volume distribution. Two methods of analysis were applied, namely dry powder analysis and powder-in-liquid analysis. All measurements were repeated 3 times and the results were averaged.

(a) Dry Powder Analysis

Powder samples of approximately 10 g were placed into the feed tray of a Dry Powder Feeder (PS64, Malvern, USA). The feed rate was controlled in order to distribute the powder into a dispersing air jet, which was sucked across the path of the laser beam by a vacuum. The resultant scattering from all particles present in the beam gave a measurement of the particle size distribution, which was calculated by the sizer software.

(b) Powder-in Liquid Analysis

A small quantity of dispersion was prepared by sonicating (BranSonic 220, USA) 0.3 g approx. of the powder sample with 10 ml of water in a sealed beaker for 1 min, stirring with a magnetic stirrer afterwards to maintain a uniform dispersion. Whilst the dispersion was stirred, a sample was taken by pipette and rapidly added to the small volume presentation unit (MS1-S, Malvern, USA) containing fresh dispersant (water). The MS1-S consists of a free-standing stainless steel re-circulating unit with a built-in stirrer to keep

the samples suspended and a pump to circulate the sample to the measurement cell with a total sample volume of 50 to 80 ml. This method of analysis was used to measure the individual particles by breaking down cohesive particle aggregates by prior ultrasonic treatment of an aqueous suspension of microcrystalline cellulose particles.

3.6.2 Scanning Electron Microscopy (SEM) Analysis

SEM was used to evaluate selected samples of powder. The samples from each batch of powder were mounted on an aluminium stub using double-sided sticky tape. The powders were coated with a thin film of gold in a Polaron SC500 sputter coater (UK). The samples were then examined using a LEO Stereoscan S-360 scanning electron microscope (UK). The analysis allowed an examination of the size and surface appearance of the particles in the powder sample. The effects of certain processing on the appearance and size of the fine particles could be observed and estimations of particle dimensions could be made.

Elemental analysis was also performed at different spots in the specimen so that the elemental content could be obtained. This was done using the Energy Dispersive Analysis of X-rays (EDAX) system attached to the SEM.

3.6.3 Mercury Porosimetry Analysis

Mercury porosimetry was also performed on powder samples using the Micromeritics 9320 Poresizer (semiautomated) with associated software. The measurements were performed on powder samples using a 5 cm^3 "powder sample" penetrometer (sample weight 250 mg +/- 10%). Samples were again dried to constant weight using a vacuum oven set at 80°C and removed just prior to analysis. The same intrusion pressure table was used for the powder sample analysis as for the pellet sample analysis, as illustrated in Appendix 3.

3.6.4 X-ray Diffraction Analysis

X-ray diffraction (XRD) patterns were obtained using a Siemens D500 X-ray powder diffractometer. Powdered samples were studied by placing a thin layer of the powder in

conventional cavity mounts. The samples were scanned in all cases from 5 to 40° 2θ. A 1.00° dispersion slit, a 1.00° antiscatter slit, and a 0.15° receiving slit were used. The Cu anode X-ray was operated at 40 kV and 20 mA in combination with a Ni filter to give monochromatic CU Kα X-rays (λ = 1.5418 Å).

3.6.5 BET Surface Area Analysis

Surface area analysis was performed using a Micromeritics Gemini 2370 Surface Area Analyser with nitrogen as the adsorptive gas. The Gemini system is a balanced adsorption apparatus which uses a technique known as SMART (a sorption method using adaptive rate technology), i.e. adsorbate gas is supplied to the sample at exactly the rate that the sample can adsorb it (Camp and Stanley, 1991).

Moisture was removed from the samples prior to the surface area measurement by placing them in a vacuum oven for 24 hr at 70°C at a pressure of -500 mbar. Subsequently, samples were degassed using a Micromeritics FlowPrep 060 Degasser. The FlowPrep uses a flowing gas (helium), which is passed over a heated sample (70°C) to remove moisture and other contaminants.

The Gemini analyser consists of two tubes of matched internal volume, one of these tubes contains the sample while the other one is empty. Large-bulb tubes containing longer filler rods were used with the powder samples. These filler rods (hollow glass rods) reduce the amount of gas above the sample and hence act to minimise the pressure 'noise' caused by the boiling of the liquid nitrogen and lead to more precise measurement. The filler rods achieve an improved baseline performance by reducing the random pressure fluctuations caused by slight temperature variations at or near the liquid nitrogen surface. By displacing most of the gas from this gradient region, the filler rods leave less gas to expand and contract in response to temperature changes. Without the random pressure fluctuations, the Gemini system can then achieve a much closer balance of pressures and more precise gas uptake measurement.

Powdered sample was added to the large-bulb sample tube to within 1/8 inch of the top of the bulb. An equal volume of inert material having negligible surface area was added to the balance tube (3 mm solid glass beads were used). A long filler rod was worked into

each tube through the materials until both rods were resting on the bottom of the tubes (Stephens, 1992). Approximate volume balance was attained, confirmed by the ΔFree Space value in the range -0.5 to +0.5 cm^3 in all cases.

Helium was used for free space measurement, while nitrogen was used as the adsorptive gas.

The saturation pressure (P_o) was measured each day. The operating parameters used for each system are indicated in Table 3.6a below.

Table 3.6a. Operating conditions used in the determination of the BET surface area of materials by the Gemini 2370 Surface Area Analyser

Sample ID	Evacuation rate (mm Hg/min)	Evacuation time (min)	Equilibration time (s)
Avicel® PH-101	500	3	10
Grade X	500	3	10
Grade Y	500	3	10

BET multipoint surface areas were determined. The volume of nitrogen adsorbed at six relative pressure points between 0.05 and 0.3 units was measured. This is the range to which the linearity of the BET plot is usually restricted (Sing et al., 1985). The BET multipoint area was calculated using either five or six of the measured points (i.e. the surface area was calculated with all six points and then recalculated omitting the first point or the last point; whichever result gave the highest correlation coefficient, for the fit of the BET plot, was selected).

Analyses were performed at least in duplicate.

3.6.6 DSC Sample Analysis

Microcrystalline cellulose sample batches (Avicel® PH-101, Grade X and Grade Y) of various hydration levels were prepared by adding a pre-determined weight of HPLC grade water to 5 g approx. of the microcrystalline cellulose grade in sealed glass bottles. The bottles and their contents were periodically agitated (by stirring) and allowed to equilibrate

for at least one week. Following this equilibration step, 6-8 mg approx. of the hydrated cellulose samples was accurately weighed out and transferred to dry aluminium DSC pans and sealed hermetically. It was important that the pans were dry in order to achieve an adequate seal at the interface. The hermetically sealed pans were left for a further period of time (approx. 1-2 weeks) before testing to facilitate re-equilibration after transfer from the sample bottle. DSC studies were performed in a Perkin-Elmer DSC 7 calorimeter equipped with a thermal analysis station. The instrument was calibrated by standard procedures. An empty aluminium pan was used as reference. DSC traces were recorded at a fixed scanning rate of 10 K/min for both the cooling and heating cycles. Endotherms were obtained from the cooling cycle performed within the temperature range of 25°C to minus 60°C, while exotherms were obtained from the heating cycle performed in the reverse temperature range as above.

Following DSC analysis, the pan was removed, weighed to determine if any weight losses had occurred (which would have indicated an inappropriately sealed pan), pierced and then dried in an oven set at 60°C to constant weight to determine the actual water content.

3.6.7 Thermogravimetric Analysis

Thermogravimetric analysis (TGA) was performed using a Mettler Toleda TC15 TA controller. Analysis was performed in the temperature range 30°C to 250°C using a heating rate of 10K/min. The sample weights used were between 5 to 10 mg approximately. Nitrogen gas flowed over the open crucibles containing the sample as the analysis was performed. The percentage weight losses incurred during the heating cycle were estimated using the STAR^e software.

3.7 SPECIFIC HALLOYSITE EXPERIMENTS

3.7.1 Zeta Potential Measurements

Electophoretic experiments were performed with a Zetasizer 3000 (Malvern Ltd, UK). This instrument uses a photon correlation spectroscopy technique that enables particle size and zeta-potential measurements. The zeta-potential was detected from the motion of

particles caused by a dc external electric field supplied to a very dilute suspension of the halloysite sample (0.1 mg/ml) in an aqueous electrolyte solution (0.001M KCl). Measuring the rate of motion (electrophoretic motility) and using the Smoluchowski equation, the zeta-potential of the particles was determined. pH adjustments were done with aqueous solution of 0.1M HCl or 0.1M NaOH. The pH was measured with a pH meter (AGB 2000), calibrated with buffer solutions (pH 4, 7, 9). Double de-ionised water (filtered through a 0.2 μm filter) was used to prepare the aqueous KCl, HCl and NaOH solutions. Prior to each measurement, the operating conditions were checked and adjusted using a calibrated latex solution (zeta-potential = -50 ± 5 mV) supplied by the instrument manufacturer.

3.7.2 Removal of Allophane

A suitable quantity of an aqueous 0.5M NaOH solution was added to the halloysite clay sample until the mass of NaOH was 2% by weight. The mixture was heated at 60°C for 8 hr approx., after which the NaOH soln was filtered off, followed by re-suspending the halloysite in deionised water. The halloysite sample was rinsed and filtered several times to ensure that the NaOH was fully washed out, followed by drying in a forced air circulation oven for 48 hr at 50°C to constant weight. The dried caked powder mass was ground using a mortar and pestle and sieved through a 125 μm sieve prior to further analysis.

3.7.3 Intercalation of Halloysite using Wada's Procedure (Wada, 1961)

A small sample of the halloysite clay (20 g approx.) was ground with 16 g approx. potassium acetate. The clay was ground using a mortar and pestle for 20 min while monitoring it continuously to guard against "balling-up" of the clay/KOAc mixture which may pick up moisture from the air and then tend to escape grinding. Following XRD analysis, the clay/KOAc sample was washed by shaking several times with distilled water and then centrifuged to separate it from the bulk of the water, which was decanted off. The clay (not allowed to dry out) was then exposed to various organic liquids or aqueous

solutions of organic solids in sample tubes, upon which XRD analysis was performed at various time intervals (1 day; 21 days) to examine for evidence of intercalation.

3.7.4 Determination of Halloysite / Cation Binding Curves

(a) Using Viscosity Measurements

A 0.2% w/v chitosan solution in buffer medium (see below) was prepared and 20 ml was mixed with appropriate quantities (2, 4, 6, 8, 10, 12, 14, 16, 18 & 20 ml) of an aqueous halloysite suspension (0.1% w/v), with the total sample volume being maintained at 40 ml using buffer medium. Buffer solutions (pH 2.8 and 4.5) consisting of 0.1M acetic acid and 0.1M sodium acetate were used to prepare the chitosan solution and the halloysite suspensions. Total chitosan concentration was fixed at 0.1% w/v in all samples. The sample solutions were then incubated at 37°C for 48 hr in a temperature controlled reciprocating water bath (Model 25, Precision Scientific, Illinois, USA), set to shake at 50 rpm. After incubation, the samples were centrifuged for 20 min at 3000 rpm (Sanyo Harrier 15/80 Centrifuge; Model MSB080 CX1.5). The viscosity of the supernatant solution was determined at 37°C using a suspended level viscometer (Ubbelohde viscometer size 1, Technico, UK). The viscometer was placed vertically in the viscometer bath in a position so as to maintain the top of the sample 2 mm below the top of the water level in the bath. After the flow times of the sample were determined, the average of three determinations were used to calculate the specific viscosity (η_{sp}) using Eqn 3.9a below:

$$\eta_{sp} = \frac{t - t_0}{t_0} \qquad \textbf{Eqn. 3.7a}$$

where t is the sample flow time at 37°C, and

t_0 is the solvent (buffer) flow time at 37°C

(b) Using UV Analysis

Halloysite / cation binding curves were investigated for the drug, Diltiazem HCl, and two cationic coating polymers, namely Polyethyleneimine (PEI) and Eudragit E, using the UV analysis technique. 100 mg samples of halloysite 'G' powder (< 125μm) were added to 100 ml conical flasks. 50 ml of the aqueous cationic solutions, containing various amounts of the cation (i.e. 5 to 160 mg for Diltiazem HCL; 2 to 30 mg for PEI; 2.5 to 80 mg for Eudragit E) were added to each powder sample and stirred for 20 min at 500 rpm. 5 ml samples were taken and filtered through 0.2 μm filters (Gelman, USA) to remove the particulate material. UV analysis was performed using a Shimadzu UV-160 spectrophotometer set at the appropriate wavelength (i.e. 236 nm for Diltiazem HCL; 209 nm for PEI; 229 nm for Eudragit E). The concentrations in mg/ml of cation in solution were calculated for each sample using the appropriate calibration curve illustrated in Appendix 2. The difference in concentration of the cation solution before and after interaction corresponded to the amount bound to the halloysite mineral. All measurements were performed in triplicate.

3.7.5 Drug Loading of Halloysite

1.5 g of the halloysite 'G' clay sample was weighed out and 1.5 ml of the drug solution (Diltiazem HCl, 40% w/v in distilled water; Propranolol HCl, 20% w/v in methanol) was mixed with it. The wetted halloysite powder was placed in a sealed desiccator vessel, and a vacuum applied (vacuum suction pressure approx. 30 mm Hg) for 30 s, until all the gas bubbles were removed, as illustrated in Fig. 3.7a. The vacuum was removed, and reapplied two more times as above, to ensure that the drug solution had fully displaced all the air present in the mineral tubules. The drug loaded samples were then dried in a forced air circulation oven for at least 24 hr at 50°C to constant weight. The dried powders were removed from the oven, ground down using a mortar and pestle and sieved through a 125 μm sieve to separate any large aggregates.

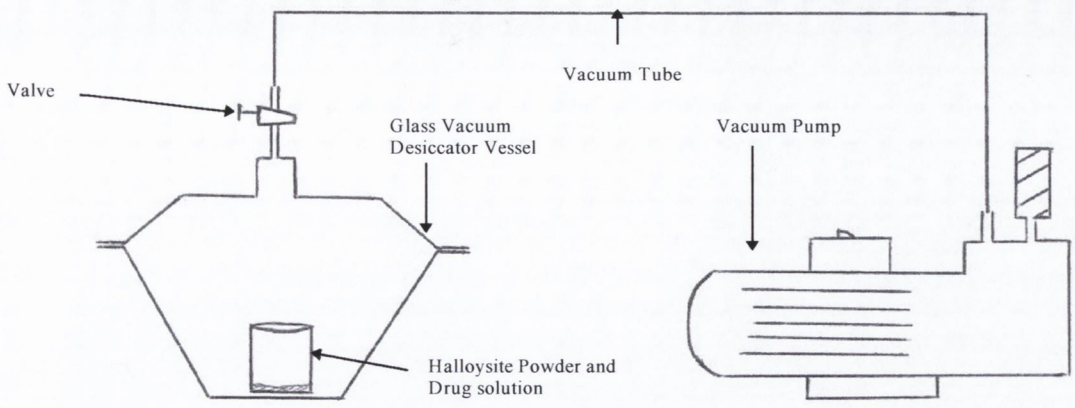

Figure 3.7a. Illustration of apparatus used to drug load the halloysite powder.

3.7.6 Coating Drug Loaded Halloysite

3.7.6.1 Charge Neutralisation

Appropriate quantities of the dried drug loaded halloysite powder were weighed out and added to 100 ml conical flasks. 50 ml quantities of aqueous solutions of the coating material (i.e. chitosan, PEI, Eudragit E at various concentrations - see Chapter 9) were added and the mixtures were stirred at a fixed rate of 500 rpm for 2 min to allow the charge neutralisation reaction between halloysite and the coating material to occur. The cross linking agent (glutaraldehyde 10 & 20% w/v), if used, was added at this stage. The suspensions were then transferred to 50 ml centrifuge tubes and centrifuged at 3000 rpm for 10 min. After centrifugation, the supernatant was discarded, and the sediment removed and dried in a forced air circulation oven for 24 hr at 50°C to constant weight. The dried powder cake was ground back to a fine powder using a mortar and pestle, and sieved through a 125 μm sieve.

3.7.6.2 Polymerisation using Cyanoacrylate Monomers

5 & 10% v/v solutions of the cyanoacrylate monomers (octyl, n-butyl and isobutyl) were prepared in heptane. 20 ml volumes of these solutions were placed into clean, dry 100 ml conical flasks, and 3 g of the drug loaded halloysite powder was carefully added. The suspensions were allowed to stir at 500 rpm, at room temperature, for fixed time periods (i.e. 30 min, 3 hr & 8 hr), during which time surface polymerisation occurred (see Fig. 7.3b). The reaction was quenched by filtering off the excess heptane solvent and drying the encapsulated halloysite powder in a forced circulation oven for at least 24 hr at 50°C. The dried powder cake was ground to a fine powder and sieved through a 125 μm sieve.

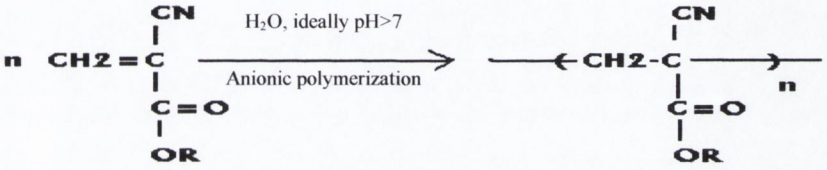

Figure 3.7b. Polymerization of 2-cyanoacrylate monomer units.

3.7.7 Preparation of Solid Lipid Particles

Solid lipid particles were prepared using both the "cold dispersion" and the "hot dispersion" technique.

3.7.7.1 'Cold Dispersion' Technique

The lipid (Novata E, Precirol AT05) was melted and dispersed with the drug loaded halloysite powder (<125 μm), using a magnetic stirrer. The lipid was cooled rapidly with liquid nitrogen, entrapping the halloysite core material. The cooled, loaded lipid particles were ground down using a mortar and pestle to a fine powder, with the aid of liquid nitrogen, which retained it in a brittle, easily crushable state. The ground lipid was finally sieved through a 600 μm sieve. Under the 'cold dispersion' technique, the sieved lipid powder was dispersed in an aqueous surfactant solution and emulsified using an Ultra-turrax stirrer T25 (Janke & Kunkel GmbH & Co., Staufen, Germany) at temperatures of 5

to 10°C approx. below the melting point of the lipid. The shearing forces created by the ultra-turrax blade size reduced the solid lipid particles.

The lipid particles were lyophilized using a freeze-drying apparatus (Hetosicc, Heto lab equipment, Denmark). The solid lipid (SL) dispersion containing the cryoprotectant (5% w/v) (glucose) was frozen in a 100 ml round bottomed flask, by spinning it while immersed for 10 min in a chilled polyethylene glycol bath. The samples were freeze-dried for 24 hr at a temperature of - 25°C at maximum vacuum, followed by a drying period of 1-5 days at room temperature at maximum vacuum. Reconstitution of the lyophilized products in de-ionised water was performed by shaking and subsequent sonication (5 min, 220 W, Bransonic, USA).

3.7.7.2 'Hot Dispersion' Technique

The "hot dispersion" technique was very similar to the "cold technique", however, in this case the halloysite encapsulated lipid particles were dispersed in the aqueous surfactant (Pleuronic F68) solution at temperatures above the melting point of the lipid (i.e. at 80 to 90°C), using an Ultra-turrax stirrer T25. The lipid particles obtained were lyophilized as before.

3.8 DISSOLUTION STUDIES

3.8.1 Dissolution Studies on Pellet and Powder Formulations

The dissolution studies were performed using an Erweka DT6 K (Germany) dissolution tester. 1000 ml of each dissolution medium was placed into each of the 6 dissolution vessels. The water bath maintained the dissolution medium at 37°C for the duration of the experiment. For the dissolution of the pellets, the pellets being tested were contained in baskets, which were rotated at 100 rpm and kept 23 to 27 mm above the base of the vessel (A189, Apparatus I, British Pharmacopoeia, 1998). In the case of the powder samples, the powder was initially loaded into empty tea-bags and sealed at the opened end by thread, before being placed into the baskets.

5 ml samples were withdrawn at intervals over 8 hr and were replaced with 5 ml fresh dissolution medium maintained at 37°C. Samples were taken at times 0.25, 0.5, 0.75, 1, 1.5, 2, 2.5, 3, 4, 5, 6, 7, 8 hr. The sample was taken from a point half-way up the side of the vessel. The samples were then filtered through a 0.45 μm membrane filter (type Gelman, USA) and were analysed in a Shimadzu UV-160 spectrophotometer (Japan) set at the appropriate wavelength. The repeated removal of sample from the dissolution medium was accounted for in the subsequent calculations.

The various dissolution media were achieved using McIlvaine buffer as shown in Table 3.8a below (Pharmaceutical Handbook, 1980), as confirmed with a calibrated pH meter.

Table 3.8a Composition of McIlvaine buffer systems

pH	Disodium hydrogen-orthophosphate dodecahydrate (g/L)	Citric acid monohydrate (g/L)
6.8	55.3	4.8
3.2	17.7	15.8

3.8.2 Calculations

The absorbances of standard Indomethacin solutions at pH 6.8 were measured at wavelength 318 nm. The absorbances of standard Diltiazem HCl solutions were measured at 236 nm at both pH 3.2 & 6.8, while the absorbances of standard Propranolol HCl solutions were measured at pH 6.8 at wavelength 292 nm. The absorbance values *vs.* their respective concentrations in mg/ml were subjected to linear, least squares regression analysis, resulting in a linear calibration curve. The calibration equations are illustrated in Appendix 2. The concentrations, in mg/ml of Indomethacin, Diltiazem HCl and Propranolol HCl in solution, were calculated for each sample using the appropriate calibration equation. The results were presented as percentage drug released, having assayed the products for the actual drug loading.

The MCC pellet formulations were assayed for Indomethacin content by grinding an appropriate quantity of the pellets (1 g approx.) into a fine powder using a mortar and pestle. A suitable quantity of the powder was placed into a 500 ml volumetric flask and made up to the mark using the appropriate buffer solution. The powder suspension was stirred at 500 rpm using a magnetic stirrer, while placed in a heated water bath maintained at 37°C. 5 ml samples were taken at daily intervals after the initial 5 days and the drug content determined by UV analysis at the appropriate wavelength. This was continued until the determined drug contents were similar for two consecutive days or started to decrease, drug contents at this point equating to 100% release. Similar procedures were used for estimating Diltiazem HCl and Propranolol HCl loadings in the polymer coated halloysite preparations and the solid lipid microparticles, however no prior grinding was necessary in these instances.

3.8.3 Dissolution Rate Modeling

The release data of Diltiazem hydrochloride and Propranolol hydrochloride from the coated drug loaded halloysite samples were fitted to various drug release kinetic models to ascertain which model gave the best fit. The criteria for which the model was selected is based on the calculated R^2 values obtained for data fitted to the respective models.

(a) Zero-Order Kinetics

Zero-order kinetics was calculated from the linear regression treatment of the data of drug release (%) versus time. The rate constant (k, (hr^{-1})) was the slope of the line.

(b) Higuchi (Matrix) Model

The data of percentage drug release was plotted versus the square root of time, followed by linear regression analysis.

3.9 STATISTICAL METHODS USED IN EXPERIMENTS

The statistical analyses used in the experiments were compiled with the aid of a statistical package (Microsoft Excel).

The 'randomization' of experimental runs has been found to guarantee inferential validity in the face of unspecified disturbances, and 'blocking' eliminates the unwanted sources of variability (Box *et al.*, 1978). Hence all the runs within an experiment were conducted in a fully randomized order and whenever appropriate, 'blocking' was used to reduce error.

3.9.1 Simple Comparative Experiments

Simple comparative t-tests were applied to situations when two independent samples were involved. The standard error was calculated using a pooled estimate of the sample variance. The hypothesis was tested with t-ratio complying with a student's t-distribution having n-1 degrees of freedom, where n is equal to the sample number for each sample group. The t ratio for two sample means is given below:

$$t = \frac{\overline{Y}_2 - \overline{Y}_1}{S_D} \qquad \textbf{Eqn. 3.9a}$$

where t is the t ratio

$\overline{Y}$ is the mean of sample 1

$\overline{Y}_2$ is the mean of sample 2 and

S_D is the estimated standard error of the mean difference.

All tests were conducted at 0.05 level of significance.

3.9.2 Analysis of Variance (ANOVA)

In the above section, the two sample t-test was used to measure the means of two different groups. The t-test can, however, be generalised to permit comparisons between more than two sample means. This generalisation is called analysis of variance (ANOVA). Hence ANOVA is the statistical procedure used for an overall test for more than two sample means for quantitative data. The ANOVA tables encountered in the result sections are divided into the following columns:

Source	is the source variation
df	is the degrees of freedom
SS	is the sequential sum of squares
MS	is the adjusted mean squares
F	is the *F*-statistic and
p	is the *p*-value which is the probability associated with the *F* statistic

The *F*-statistics in an ANOVA table are based on the adjusted sums of squares, which are equivalent to the adjusted mean squares multiplied by the respective degree of freedom. The *F*-statistic is calculated by dividing the mean square value for the respective term by the mean square value for residual error. A high *F*-statistic associated with a low *p*-value (<0.05) would be considered significant.

3.9.3 Factorial Experiments

Full factorial experiments were designated by the following nomenclature:

$$N = L^K \qquad \textbf{Eqn. 3.9b}$$

where K is the number of variables,
L is the number of variable levels and
N is the number of experiment runs.

An example of a 2^3 factorial experiment design layout or 'matrix' that was used is presented in Table 5.2a. The levels of variables were coded at the low (-) and high (+) levels for convention. The experiment allowed the determination of the main effects of each variable and interaction between factors.

3.9.4 Similarity Factor

According to FDA guidelines, dissolution profiles of new formulations can be compared to approved preparations using a similarity factor (f_2):

$$f_2 = 50 \text{ Log } \left\{ \left[1 + \frac{1}{n} \sum_{t=1}^{n} \left(R_t - T_t \right)^2 \right]^{-0.5} .100 \right\} \qquad \textbf{Eqn. 3.9c}$$

where R_t and T_t are the percent dissolved at each time point for reference (R) and test (T) products. An f_2 value between 50 and 100 suggests that the two dissolution profiles are similar and the mean dissolution profiles are assumed to differ by no more than 15% at any time point (Tang and Gan, 1998).

Chapter 4

Preliminary Studies on Microcrystalline Cellulose

4.1 Preliminary Size Reduction Studies

4.1a INTRODUCTION

Deasy and Law (1997) observed that the anionic surfactant, sodium lauryl sulphate (SLS), appeared to reduce the rate of drug release when incorporated into spheronized pellets containing the drug Indomethacin, in conjunction with Avicel® PH-101. They performed further experiments to verify the above observation. These involved making up physical mixes containing MCC (Avicel® PH-101) and two different concentrations of SLS, which were hydrated for specified times, followed by subsequent drying and qualitative examination using SEM techniques. From the results of this qualitative analysis, she concluded that the incorporation of the surfactant resulted in de-aggregation of the crystal aggregates in the microcrystalline cellulose powder.

Based on the above anomalous result, we aimed to produce a surfactant aided de-aggregated grade of microcrystalline cellulose (MCC), using Avicel® PH-101 as the starting material. The initial stages of our work involved replicating the experimental techniques performed by Law using SLS. In addition, other surfactants were also used at different concentrations to see if the phenomenon could be repeated using these. The other surfactants used were Cetrimide and Tween 20, the first being cationic in nature, while Tween 20 is non-ionic. Docusate sodium, another anionic surfactant was contemplated for use in place of sodium lauryl sulphate, but it was decided against this

after consideration of their relative physical properties, i.e. SLS avoids the problem of hygroscopicity and also has a significantly higher aqueous solubility.

Thus, the initial aim of the experiment was to confirm that the incorporation of different surfactants as physical mixes with Avicel® PH-101 caused de-aggregation of MCC crystals. In addition, using factorial analysis, we aimed to determine if this phenomenon was influenced by the actual type of surfactant used, by the temperature, and also by the time, i.e. was there an aqueous interaction, temperature and time dependence involved in the de-aggregation phenomenon? From the statistical analysis of the results, it was finally hoped to determine conditions that would optimize the de-aggregation process, with the ultimate view to assessing its potential use for development as a new pharmaceutical excipient.

4.1.2 SURFACTANT AIDED DE-AGGREGATION

(a) Size Reduction Studies on Original Batch of Avicel® PH-101

In this preliminary study, the experimental procedure involved making up a number of different physical mixes according to the experimental design described in Chapter 3.1.2. Each of the recovered powdered mixes were quantitatively analyzed regarding particle size. Qualitative analysis was performed on some of the samples, using SEM techniques, at a number of different magnifications. A control was also prepared, which involved treating MCC under similar conditions, but in the absence of any surfactant.

The particle size analysis results for the dry powders are illustrated in Table 4.1a. The analysis of each dry powder was repeated in triplicate and the results averaged. The results that are quoted in the following Table are these averaged values.

Table 4.1a. Median particle size results for the treated powders.

Powder sample I.D. Key	Median Particle Size (μm)	Powder sample I.D. Key	Median Particle Size (μm)	Powder sample I.D. Key	Median Particle Size (μm)
S1	50.64	C1	53.49	P1	55.84
S2	54.51	C2	52.68	P2	53.88
S3	51.16	C3	52.17	P3	55.66
S4	48.04	C4	51.41	P4	57.42
S5	55.24	C5	53.16	P5	55.48
S6	54.19	C6	52.29	P6	55.48
S7	54.97	C7	52.48	P7	55.61
S8	53.72	C8	52.82	P8	55.32

The results for the controls are listed in Table 4.1b.

Table 4.1b. Median particle size results for the control powders.

Powder sample I.D. Key	Median Particle Size (μm)
Control 1	54.14
Control 2	50.98
Control 3	54.40
Control 4	56.45

The results arising from the quantitative analysis illustrate that no significant reduction in particle size occurred in the Avicel® PH-101 crystal aggregates, when treated with the three different surfactants. The proposed de-aggregation that was observed by Deasy and Law (1997) using sodium lauryl sulphate was not observed by us, even when the experiment was repeated under similar experimental conditions. Since no significant reduction in particle size (i.e. de-aggregation) occurred, there was no point in applying factorial statistical analysis as the phenomenon that we were attempting to optimize was not shown to occur. A number of the powdered samples were analyzed further qualitatively using SEM, in an attempt to provide more insight into what actually happened to the original microcrystalline aggregates upon treatment. The SEM micrograph (Fig. 4.1a) for one of the Avicel® PH-101 controls illustrated crystal aggregates, which appear to consist of bundles of individual crystallite structures bound together in a relatively loose arrangement. The approximate average size of these aggregates is 50-60 μm. Dispersed amongst these aggregates are a number of individual

crystallites, which are smaller in size. This is in agreement with observations made by Ek *et al.*, 1994, who stated that microcrystalline cellulose powders consist of two types of particles, individual particles and their agglomerates. The combination of these large aggregates and the smaller individual crystallites contribute to a more monomodal particle size distribution, ranging between approx. 5-300 μm (see Fig. 4.1c). In this distribution, the greatest proportion of the MCC particles were around 50-60 μm in size, with the % proportion of particles decreasing in the upper and lower size ranges.

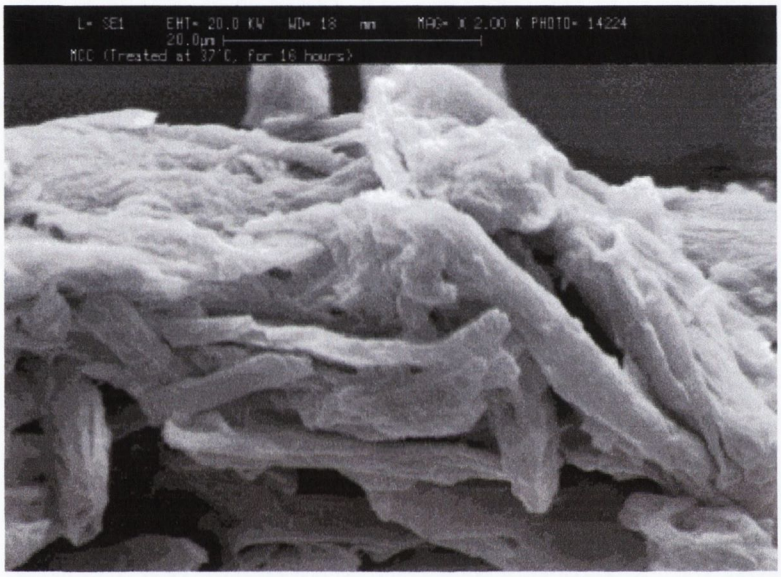

Figure 4.1a. Scanning electron micrograph of MCC (Avicel® PH-101) (magnification X 2000)

When the microcrystalline cellulose was treated with the surfactants, the SEMs illustrate that, rather than causing de-aggregation, they appear to finely coat the aggregates instead. This coat gives the impression of rigidising or solidifying the apparently loosely bound arrangement of crystallites in the MCC aggregates. This coating effect is clearly apparent in the SEM micrograph for Avicel® PH-101 treated with 10% w/w sodium lauryl sulphate, as illustrated in Fig. 4.1b.

Figure 4.1b. Scanning electron micrograph of MCC (Avicel® PH-101) treated with 10% SLS (magnification X 2000).

(b) Examination of an Alternative Batch of Avicel® PH-101

Following the results obtained from the previous experiment, it was decided to repeat the experiment, using a different batch of the MCC powder, to see if perhaps the phenomenon was batch dependent. In this case, the experiment was repeated on a much smaller scale using only SLS. If the alternative batch proved to be successful, then the full scope of experiments would be repeated as previously indicated. Again, however, the other batch illustrated no significant reduction in particle size following treatment with the surfactant under the different conditions.

4.1.3 MECHANICAL SIZE REDUCTION TECHNIQUES

Because of the lack of success achieved with the initial experiments, in terms of surfactant induced MCC de-aggregation, we decided to examine other mechanical techniques that might offer some potential for particle size reduction of MCC.

(a) Wet grinding

The first technique investigated was wet grinding. The RETSCH® 'Vibratory Ball Mill' was chosen as being potentially the most efficient mill available for achieving particle size reduction below 50 μm in the wet state. An alternative mill, the RETSCH® 'ultra-centrifugal mill' was also available, but this one is limited to particle size reduction in the dry state only. Table 4 lists the different preliminary experiments that were performed on Avicel® PH-101 powder, using the RETSCH® vibratory ball mill. A number of parameters were altered, while keeping others constant, to get an approximate estimation of which factors have an important influence on the final desired particle size reduction.

These preliminary experiments would allow us to design a more comprehensive factorial experiment, thus enabling us to investigate the overall influence of each factor and whether or not there is an interaction between any of them.

Parameters investigated during the preliminary experiments included:

(1) Vibration frequency: Two levels - low (60); high (80)

(2) Grinding time: 5 min and 10 min.

(3) Presence or absence of surfactant (SLS).

The results obtained from the preliminary experiments are listed in Table 4.1c as follows.

Table 4.1c. Parameters examined and results obtained from preliminary wet grinding analysis performed on MCC (Avicel® PH-101) powder.

Grinding Frequency (Hz)	Grinding Time (min)	SLS Content (%) (relative to MCC Content)	Median Particle Size (μm)
-	-	-	56.39
60	5	-	39.02
60	10	-	30.23
80	10	-	27.86
60	10	5	44.96

The particle size of the powder which underwent no grinding was 56.39 μm approx., which is in agreement with Company literature values. In all cases, grinding, irrespective of the conditions, caused particle size reduction. The extent of the particle size reduction appeared to be time dependent, i.e. the average particle size decreased from 56.39 μm to 39.22 μm during the first 5 min of milling, and by a further 9 μm approx. over a further 5 min period. It is important to note that, as the milling time progresses and size reduction progresses, the main stress required to cause fracture increases, through depletion of cracks, while the magnitude of the available local stress decreases. Because of diminishing local stress and increasing aggregation, increases in energy expenditure are useless, and size reduction reaches some practical milling limit.

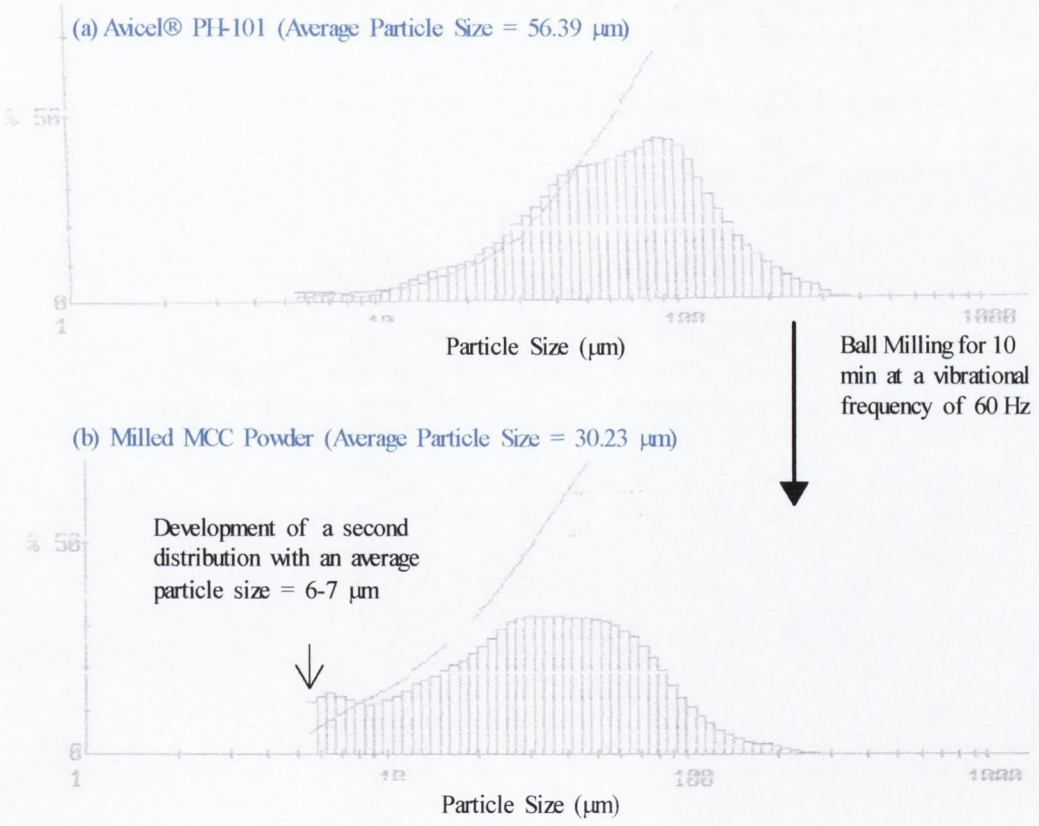

Figure 4.1c. Particle size histograms illustrating the conversion of (a) the monomodal size distribution of Avicel® PH-101 to (b) typically a bimodal size distribution, via milling for 10 min using a vibrational ball mill.

Another feature evident from the frequency distribution curves (see Fig. 4.1c) is the progression, from the previously mentioned monomodal particle size distribution, to one that is bimodal in nature. The original monomodal distribution is positioned with a median size between 50-60 μm, but with continued milling the overall percentage of particles in this upper modal distribution reduced in magnitude, with a second distribution developing around 6-7 μm. In this bimodal distribution, as well as a large proportion of the particles having an average size of 50 μm approx., there is an increasing proportion of the particles in the ground powder with a median size of 6-7 μm. With progressive milling the proportion of these smaller crystallites should increase.

The extent of the particle size reduction also appears to be dependent upon the vibration frequency, (i.e. milling equal quantities of MCC powder for 10 min at a vibrational frequency of 60 and 80 Hz results in a size reduction to 30.23 and 27.86 μm, respectively), although the results from these tests suggest that the duration of milling is the most important factor.

An important feature is the fact that the inclusion of the surfactant (SLS) does not exert any desired influence on the overall size reduction process. In fact, it appears to have the opposite effect, and instead retards the particle size reduction. This may be due to the fact that, with its inclusion, combined with the agitatory effect associated with the milling, a foam is formed, which is sufficiently viscous to support and disperse the Avicel® PH-101 powder. This may exert a protective property against the compaction stresses experienced during milling.

Five percent SLS was subsequently added to Avicel® PH-101 powder, which had been ground previously for 10 min at the lower vibration frequency (60 Hz), after which it was dispersed using a magnetic stirrer to ensure homogeneity and then measured using the Malvern. The resulting median particle size was measured to be 29.41 μm, which is very close to 30.23 μm, the particle size of Avicel® PH-101 powder treated in a similar fashion

with the exclusion of the surfactant. Therefore, it would appear from these studies that the post grinding inclusion of surfactant has little or no effect on the overall particle size. It may, however, prove beneficial during subsequent drying of the powder, by reducing the tendency for re-aggregation of the individual MCC particles.

This grinding technique illustrated the first signs of significant size reduction in the original Avicel® PH-101 powder. Despite this, there were a number of disadvantages associated with it. Firstly, the process was time dependent and very slow, taking up to 10 min for any significant size reduction. This tardiness would indicate that a large amount of energy is required during the process, making it inefficient from an economic point of view. Further to this point, is the fact that the sample quantities capable of being milled were very small (i.e. 5-10 g approx.) and so it would take quite a long time to produce adequate quantities of size reduced material, to allow for further characterisation and application studies. Due to the above listed advantages, we decided to examine a further technique for possible size reduction.

(b) Ultrasonic Homogenisation

We decided to look at the potential of ultrasonic homogenisation in size reducing Avicel® PH-101 particles, arising from its current application in forming 'nanosuspensions' by high pressure homogenisation of drug suspensions (Müller *et al*, 1998). The equipment used for the production of the above nanosuspensions was a piston-gap homogeniser Lab 60 (APV Homogeniser GmbH, Lubeck, Germany). In our lab, we investigated a related piece of equipment called a 'Minisonic' homogeniser, produced by Ultrasonics Ltd., Shipley, Yorks, England.

A number of preliminary experiments were performed to investigate its potential in this area. For these tests, 5% and 15% aqueous MCC suspensions were prepared. The different suspensions were passed several times through the homogeniser and the particle

size of the material was measured, after variable treatment runs in the wetted state, using the Malvern.

The results from these preliminary tests are listed in Table 4.1d.

Table 4.1d. Experimental parameters and results obtained from preliminary ultrasonic homogenisation tests on MCC (Avicel® PH-101) powder.

MCC Concentration (%)	No. passes through Homogeniser	SLS Content (%) (relative to MCC Content)	Median Particle Size (μm)
5	-	-	65.37
5	1	-	28.40
5	2	-	20.74
5	5	-	15.48
5	10	-	13.12
5	25	-	11.04
5	10	5	14.33
10	5	-	15.28
10	10	-	13.00
10	2	5	20.20

It appeared from the above preliminary results that the percentage of MCC in the suspension had little impact on the final particle size. The most important factor, in terms of size reduction, appeared to be the number of times that the suspension is actually passed through the homogeniser. The greatest level of size reduction occurred during the initial 5 runs, whereas further passes did not cause further significant size reduction. Again, particle size reduction via this method seemed to follow a transition from a monomodal to a bimodal distribution.

In this case, the inclusion of SLS appeared to have a negligible effect in terms of size reduction, but further studies would have to be performed to investigate any beneficiary effects in preventing particle re-aggregation, when we subsequently attempted to spray-dry the size reduced powder.

This technique has a number of advantages over the previously tested 'wet grinding' technique. It is very fast and is capable of milling large quantities, in a relatively short time period. In general, 0.5 litres of suspended material passes through the homogeniser in 30 sec approx., which is for a laboratory scale model. The homogenisation step could easily be scaled-up and applied in the commercial manufacture of a size reduced grade of MCC.

Since this technique proved so successful relative to wet grinding, based on our preliminary results, we decided to devote our attention to it in further studies, with the intentions of developing a sized reduced product for further characterisation and application studies. The optimisation of MCC size reduction, via ultrasonic homogenisation, is examined in greater detail in Chapter 5.

4.2 Preliminary Extrusion/Spheronization Studies

4.2.1 EFFECT OF SODIUM LAURYL SULPHATE

As mentioned in Section 4.1b, we were unable to replicate the de-aggregation phenomenon, induced by the inclusion of sodium lauryl sulphate as physical mixes with MCC, as reported by Deasy and Law (1997). The phenomenon may have arisen, as a consequence of their technique employed in sample preparation for SEM examination. As a result, we decided to repeat Deasy and Law's extrusion-spheronisation experiments to confirm that the enhanced delayed drug release observed by her, arising from the inclusion of SLS into the pellet formulations, was observed.

Three different pellet formulations were prepared, using the extrusion spheronisation technique, the formulae of which are illustrated in Table 4.2a.

Table 4.2a. Percentage composition of pellet formulations containing 0%, 1.25% and 2.5% SLS examined *in vitro* for a sustained release effect.

	Indomethacin	SLS	MCC	Lactose
Control	30%	0%	20%	50%
SLS A	30%	1.25%	20%	48.75%
SLS B	30%	2.5%	20%	47.5%

Following their preparation, the individual pellet formulations were evaluated by dissolution testing in McIlvaine buffer at pH 6.8. The absorbance data (measured at 318 nm) obtained following the dissolution testing, was converted to the percentage amount of drug released using an appropriate calibration curve. The data for each formulation was plotted on a suitable curve, to graphically illustrate the results (see Fig. 4.2a).

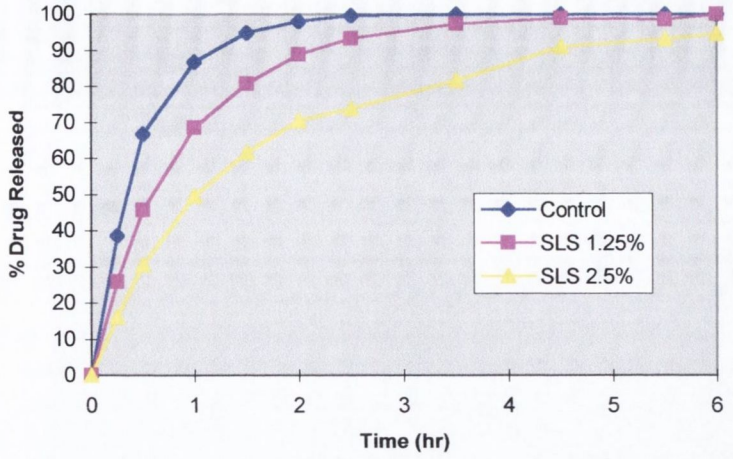

Figure 4.2a. Dissolution of Indomethacin from pellets containing 0%, 1.25% and 2.5% SLS, in pH 6.8 McIlvaine buffer, for 6 h at 37°C.

The profiles obtained for the three products are very similar to those obtained for preparations tested by Law. The dissolution profile for the spheronized preparation, which does not contain any SLS (i.e. Control), illustrated the fastest rate of drug release, reaching complete release at a much earlier time than for the other two preparations.

Thus, these results confirm that the inclusion of the surfactant SLS into the spheronized formulations resulted in a reduced drug release. The magnitude of this retardation in drug release appears also to be concentration dependent, i.e. as the concentration of the surfactant present in the formulation increased, the dissolution rate is observed to decrease, as illustrated by SLS 1.25% and SLS 2.5% profiles.

These results further confirm the presence of an interactive phenomenon existing between the surfactant and the microcrystalline cellulose, which appears to augment its retarding matrix effect, thereby reducing the release of the drug from the intact pellets. A potential reason for this arises from further studies detailed in Chapter 7. Studies on novel grades of MCC in extrusion/spheronisation illustrate that pellets incorporating the size reduced grade, combined with SLS, also have further delayed drug release. These pellets also illustrate a reduced porosity, so it is possible that the SLS has the potential to produce less

porous pellets. This would delay dissolution medium penetration into the pellet cores and hence ultimate drug dissolution and release into the immediate environment.

4.2.2 EFFECT OF OTHER SURFACTANTS

The aim of this section of the study was to investigate if the retarded drug release phenomenon, as observed for SLS, is a general phenomenon for other classes of surfactants, or solely a unique property of SLS. Two alternative surfactants were used, each belonging to a different class. Cetrimide was chosen as a suitable cationic surfactant and Tween 20 was chosen as a suitable non-ionic representative.

(a) Pellets containing Cetrimide

Again, three different pellet preparations were prepared using the extrusion-spheronisation technique, the formulae of which are illustrated in Table 4.2b.

Table 4.2b. Percentage composition of pellet formulations containing 0%, 1.25%, and 2.5% Cetrimide, examined *in vitro* for a sustained release effect.

	Indomethacin	**Cetrimide**	**MCC**	**Lactose**
Control	30%	0%	20%	50%
Cetrimide A	30%	1.25%	20%	48.75%
Cetrimide B	30%	2.5%	20%	47.5%

The pellet formulations were then evaluated by dissolution testing, after which appropriate dissolution profiles were produced and shown in Fig. 4.2b.

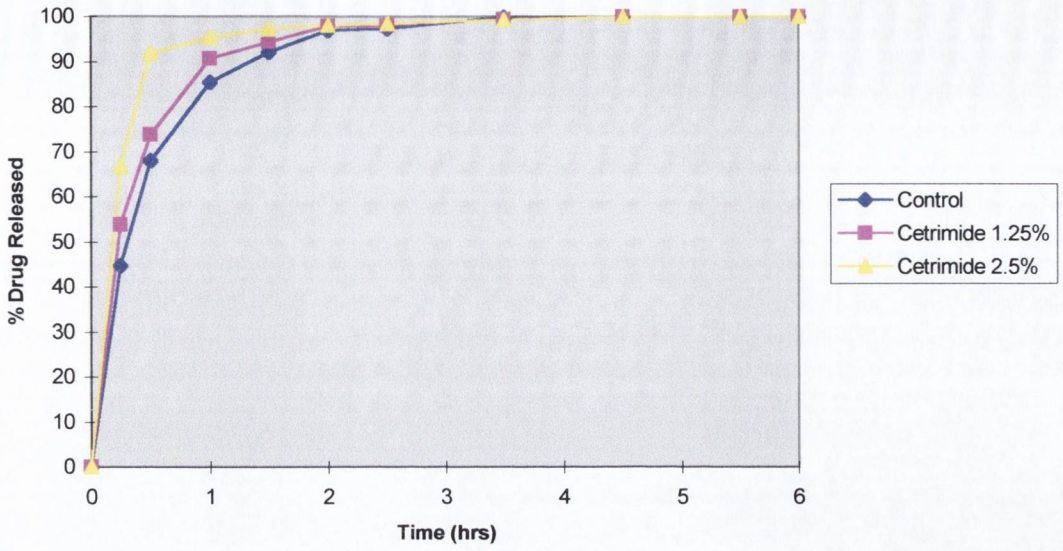

Figure 4.2b. Dissolution of Indomethacin from pellets containing 0%, 1.25% and 2.5% Cetrimide, in pH 6.8 McIlvaine buffer, for 6 h at 37°C.

The dissolution profile obtained for the control pellet preparation is similar to that produced for the same control preparation in the previous experiment, with 100% drug release occurring after 3.5 h approximately. The incorporation of the cationic surfactant, Cetrimide, resulted in an increase in the rate of drug release from the pellets. This increase in drug release rate appears to be concentration dependent, with higher surfactant concentrations increasing the release rate. Cetrimide, thus has the opposite effect on indomethacin drug release from extruded spheronized pellets relative to the previously examined surfactant, SLS. As a result, the delayed phenomenon cannot be generalised for all surfactants.

Cetrimide appears to increase drug release rate from the pellets, by promoting their disintegration in the dissolution medium. Examination of the basket contents during the dissolution test showed that the Cetrimide containing pellets fragmented much more quickly into powdered particles, relative to the control pellets, which retained their integrity for a much longer period of time. It would appear that this fragmentation process resulted in loss of the matrix system present in the pellets, which is responsible for

their sustained release effect. The increase in the particle surface area exposed to the disintegration medium, arising from the fragmentation, would also have an effect.

Visual examination of the Cetrimide containing pellets indicated that a large proportion of them were more cylindrical in shape than spherical. Sieve analysis of the pellets also indicated that there was a very high percentage yield in the 'pellet' fraction, i.e. greater than 85%. This evidence would suggest that a more spherical product may be produced, if more water was used in the original pellet formulation (i.e. perhaps a 30% level as opposed to the 25% used).

(b) Pellets containing Tween 20

Three different pellet formulations were prepared using the extrusion/spheronisation technique, the formulae of which are illustrated in Table 4.2c.

Table 4.2c. Percentage composition of pellet formulations containing 0%, 1.25% and 2.5% Tween 20, examined *in vitro* for a sustained release effect.

	Indomethacin	**Tween 20**	**MCC**	**Lactose**
Control	30%	0%	20%	50%
Tween 20 A	30%	1.25%	20%	48.75%
Tween 20 B	30%	2.5%	20%	47.5%

Again, each of the pellet formulations was evaluated by dissolution testing, under similar conditions to before, the dissolution profiles of which are illustrated in Fig. 4.2c.

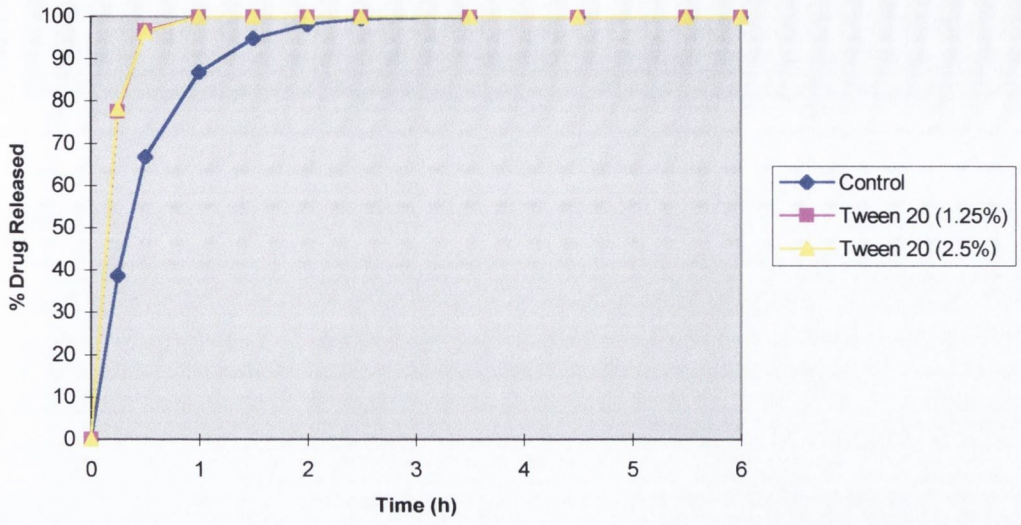

Figure 4.2c. Dissolution of Indomethacin from pellets containing 0%, 1.25% and 2.5% Tween 20, in pH 6.8 McIlvaine buffer, for 6 h at 37°C.

The results obtained from the dissolution experiment are very similar to those obtained from the previous experiment incorporating Cetrimide, i.e. the drug release rate was increased by the incorporation of the non-ionic surfactant, Tween 20. In this case, however, the release profiles for both of the Tween 20 pelletized formulations were very similar, if not superimposable, indicating that the increase in drug release rate does not appear to be as surfactant concentration dependent as in the case of Cetrimide. Again, observation of the pellets during the dissolution test suggests a similar reason for the increased drug release rate relative to the control. Significant fragmentation of the pellets was observed from a very early stage (15 min approx.), destroying the retardant matrix effect and also increasing the exposed particle surface area available for promoting drug dissolution.

The results from both of the above studies indicate that the retardant drug release phenomenon from pelletized drug formulations is only observed for the anionic surfactant, SLS, as observed by Law and Deasy (1997). This is because the inclusion of SLS does not cause pellet fragmentation, upon subsequent addition to the dissolution media, unlike

pellets incorporating Cetrimide and Tween 20. In addition, as suggested earlier, SLS may also reduce pellet porosity, thus reducing drug release.

4.2.3 EFFECT OF INCREASING MCC CONTENT

After we had eliminated the effect that other surfactants might exert on drug release from pelletized formulations, we decided to investigate if the incorporation of SLS, while simultaneously increasing the amount of MCC in the formulations, would have any pronounced effect on drug release. Since our primary concern was to maximise the retardant effect, only the higher surfactant concentration (2.5%) was chosen for the purposes of this experiment. While the MCC content was increased, the content of lactose used was proportionately decreased. The water levels used for hydration of the mixed powder mass had to be increased also, with increasing MCC content, in order to produce a suitably plastic mass for extrusion-spheronisation. For this purpose, the following equation (Eqn. 4.1) derived by Wan *et al.,* (1993) was used as an aid to predict appropriate water levels.

$$L_i a + M_i b = c \qquad \textbf{Eqn. 4.1}$$

where L_i is the weight of lactose (g), M_i the weight of MCC (g), a, the amount of water required by 1 g of lactose, b the amount of water required by 1 g of MCC, and c, the amount of water (g) required to form spheroids with a modal fraction in the size range of 0.7-1.0 mm. For formulations of MCC and lactose 200 mesh, by solving suitable equations, they calculated the averaged values of a and b to be 0.2 and 0.8 respectively.

Table 4.2d illustrates the formulations prepared:

Table 4.2d. Percentage composition of pellet formulations containing increasing levels of MCC (Avicel® PH-101) powder examined *in vitro* for a sustained release effect.

I.D. Key	Indomethacin (%)	MCC Content (%)	SLS Content (%)	Lactose Content (%)	Actual Water Content (%)	Predicted Water Content (%)
L1	30	20	2.5	47.5	25	25.5
L1	30	30	2.5	37.5	35	31.5
L3	30	40	2.5	27.5	45	37.5
L4	30	50	2.5	17.5	50	43.5
L5	30	67.5	2.5	0	55	54

Each formulation then underwent dissolution testing as before and the respective profiles are illustrated in Fig. 4.2d.

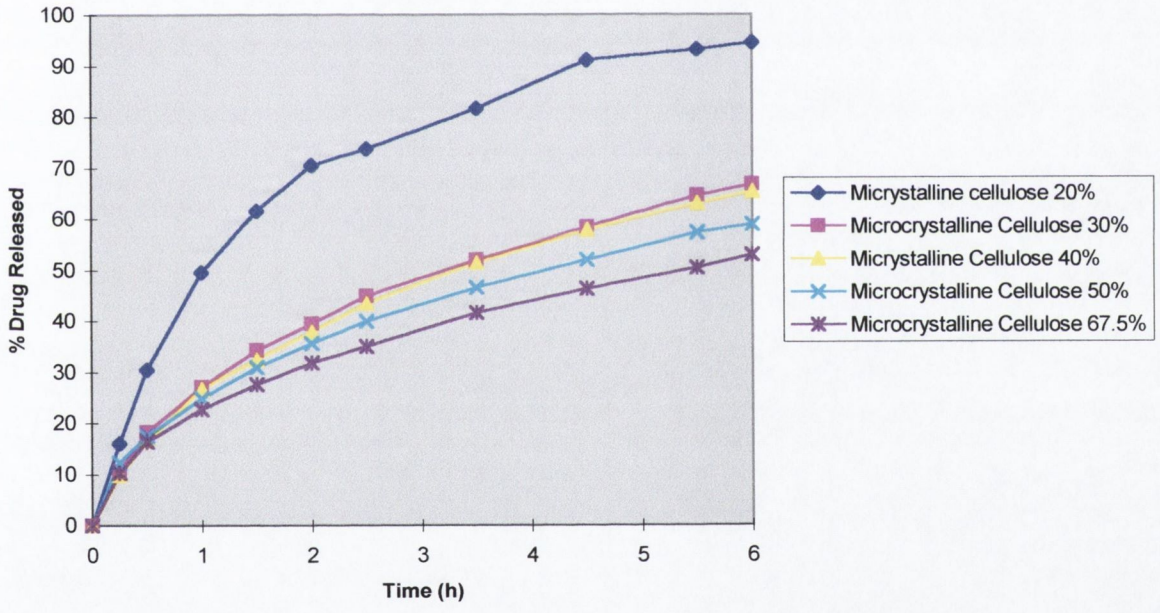

Figure 4.2d. Dissolution of Indomethacin from pellets containing increasing levels of MCC, in pH 6.8 McIlvaine buffer, for 6 h at 37°C.

It is evident from Fig. 4.2d, that, as the MCC content is increased in the formulations, drug release is further retarded. As a result, the most hindered drug release is observed for the formulation consisting of 67.5% MCC and the absence of lactose. In this case 50% approx. of the drug has been released from the pellets after 6 h of testing. The main

reason for this is that the water soluble lactose levels are reduced and replaced with the water insoluble MCC matrix. Examination of the pellets in the baskets during the test confirmed that they maintained their integrity for the entire duration, showing no signs of fragmentation. The fact that the matrix remains intact helps to account for the more sustained release effect.

Chapter 5

Optimisation of MCC Size Reduction via Ultrasonic Homogenisation

5.1 INTRODUCTION

A classical approach to experimentation is to investigate the effects of one experimental variable, while keeping all others constant. A well-known example would be the investigation of the relationship between the volume of a gas and pressure and temperature. This approach is valid provided the underlying laws relating cause and effect are known with some certainty. However, in many cases, such knowledge is not available and it is not known, which of the many variables that might affect the outcome of an experiment, will prove the most important and hence justify more extensive study.

Furthermore, it is possible that variables may interact with each other. Thus, the magnitude of the effect caused by altering one factor will depend on the magnitude of the other factors. An experimental design, which investigates the effect of one factor, while keeping all other factors at a constant level, is unlikely to disclose the presence of such interactions.

Factorial design is a system of experimental design which is intended to avoid such difficulties. It provides a means whereby the factors involved in a reaction or a process can be evaluated simultaneously and their relative importance assessed. It is thus a means of separating those factors which are important from those which are not. The technique

can be applied to many pharmaceutical problems, and it forms the basis of many tests which seek to find an optimum solution.

There are many techniques available for particle size reduction some of which are mentioned in Chapter 4. A very elegant method is the use of high pressure homogenisation which offers the opportunity of scaling-up to industrial production.

5.2 OPTIMISATION USING FACTORIAL ANALYSIS

Preliminary experiments performed in Chapter 4 illustrate that the percentage of MCC in the suspension and the inclusion of SLS have a negligible impact on the size reduction, relative to the cycle number. Whether they are statistically insignificant or not was determined by the factorial experiment that follows.

The optimisation of the homogenisation process was examined statistically using a suitably designed factorial experiment. The contributory factors that were considered to have a potentially important influence were surfactant presence, number of cycles through the homogeniser and suspension concentration. The different levels of these factors are listed below:

Factor A: Surfactant concentration 0% (-); 1% (+).
Factor B: Homogenisation cycles 1 (-); 5 (+).
Factor C: Suspension conc. 5% (-); 10% (+).

As a result a full 2^3 factorial experiment was performed. The experiment was performed in duplicate, so that an estimate of the standard error could be calculated. An entire run of experiments, represented by the expanded array in Table 5.2a, was performed in one day so that the entire experiment was carried out in two blocks. This enabled us to determine if there was any day to day variation. Experiments performed within the same day were performed in a random manner, so as to eliminate any unknown sources of bias.

Table 5.2a. Expanded array for full 2^3 factorial experiment examining the effect of SLS content, MCC suspension content and number of homogenisation cycles on size reduction of Avicel® PH 101 powder.

Design Point	A	B	C	AB	AC	BC	ABC	Results
1	-	-	-	+	+	+	-	ý 1
2	+	-	-	-	-	+	+	ý 2
3	-	+	-	-	+	-	+	ý 3
4	+	+	-	+	-	-	-	ý 4
5	-	-	+	+	-	-	+	ý 5
6	+	-	+	-	+	-	-	ý 6
7	-	+	+	-	-	+	-	ý 7
8	+	+	+	+	+	+	+	ý 8

5.2.1 Main Effects and Interactions

Each effect was calculated by multiplying its column of signs (as illustrated in the above expanded array) by the column of ýi's, summing and dividing by 4 (half the number of design points). The results obtained are shown in Table 5.2b.

Table 5.2b. Results (median particle sizes) and summary statistics for the homogenisation study.

Results (A) μm	Results (B) μm	$\acute{y}_i$	S_i^2
27.25	27.21	27.23	0.0008
27.78	28.02	27.9	0.029
16.28	16.47	16.38	0.018
17.20	18.13	17.77	0.266
24.69	24.23	24.46	0.106
25.2	24.92	25.06	0.039
115.35	16.01	15.68	0.218
17.19	17.06	17.13	0.0085

The main effects and interactions were calculated to be as follows:

A = +1.03 AB = +0.39 ABC = +0.083

B = -9.43 AC = -0.0025

C = -1.73 BC = +1.07

They are illustrated graphically in Fig. 5.2a.

The random error variance was estimated as follows:

$$S^2 = \frac{\sum S_i^2}{8} = 0.086$$

The standard error of the effect was estimated as follows:

$$\text{SE (effect)} = \sqrt{\frac{4S^2}{n}} = \sqrt{\frac{4(0.086)}{16}}$$

$$= 0.146$$

An effect is considered to be statistically significant if the effect is outside ± 2.31 (based on 8 degrees of freedom) X (S.E.)

$\Rightarrow \pm 2.31 \text{ X } 0.146$

$\Rightarrow \pm 0.34$

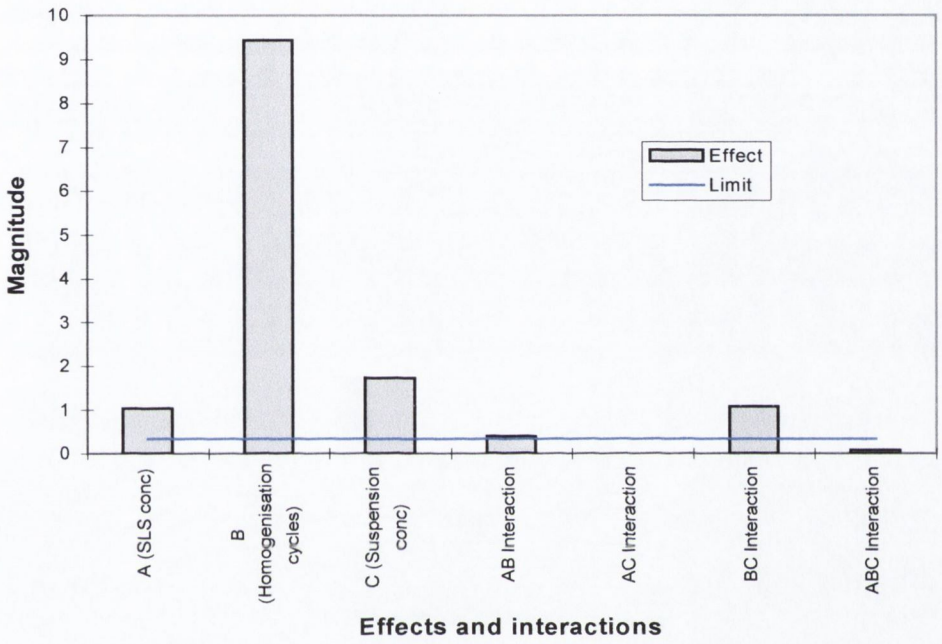

Figure 5.2a Illustration of the magnitude of each of the main effects and the interactions between them. The blue line illustrates the level above which the calculated effects and interactions are real. (NB - all effects are illustrated as being positive for ease of presentation).

This suggests that Factors A, B, and C all have a statistically important effect on the overall particle size of the MCC powder following homogenisation. Of all the factors, Factor B (ie the number of homogenisation cycles) is undoubtedly the most influential. By increasing the number of cycles from 1 to 5, there is a significant reduction in the MCC particle size which is desirable. The inclusion of surfactant (Factor A) again has an undesirable effect, in that it reduced the magnitude of size reduction. This can be explained by the fact that the cavitation and shearing forces, experienced during the

process, cause the SLS to form a foam, which disperses the powder, and thereby protects the MCC particles against the full impact of the stresses.

Increasing the concentration of the MCC suspension had a desirable effect also on particle size reduction. This may be explained by the greater local concentration of particles dispersed in the water augmenting the stresses involved. Despite this, we decided to stick to the lower suspension concentrations, as the higher suspension concentration tended to block the nozzle of the spray drier, when it was subsequently used to evaporate off the water and dry the size reduced powder.

5.2.2 Day to day Variation

As previously mentioned, the experiment was blocked so that each replicate was performed on a different day. This enabled us to determine if there was significant day to day variation within the experiment, and to obtain a more appropriate measure of random variation.

SS (error) = SS (within rows) - SS (between days)

SS (within rows) = S^2 X degrees of freedom

$$= 0.086 \text{ X } 8 \quad = \quad 0.688$$

SS (between days) = $8 \sum (\acute{y}_j - \acute{y})^2$

Where $\acute{y}_j$ = mean yield on day (j) and $\acute{y}$ is the overall mean. The multiplier 8 is used, as each mean $\acute{y}_j$ is based on 8 observations.

$$\Rightarrow \text{SS (between days)} = 8[(21.37-21.44)^2 + (21.50-21.44)^2]$$

$$= 0.068$$

SS (error) = 0.688 - 0.068 = 0.62

df (error) = df (within rows) - df (between days)

= 8-1=7

Our adjusted S^2, based on 7 degrees of freedom

$$\Rightarrow S^2 = \frac{SS(error)}{7} = \frac{0.62}{7} = 0.088$$

This is very similar to the original estimate of the random error variance, which suggests that day to day variation is negligible. Hence, the previous conclusions in relation to the main effects and interactions previously discussed are still valid.

5.2.3 Conditions for Optimal Size Reduction

Since optimisation of the homogenisation process required producing the greatest size reduction, optimal conditions would be achieved using the higher homogenisation cycle level, using the higher suspension concentration and absence of surfactant. As previously mentioned, the lower suspension concentration was chosen as it did not block the spray dryer during further processing.

The average particle size of the optimally size reduced product, at the above design point, was 16.38 μm. A 95% confidence interval for the long run average under these conditions is:

$16.38 \pm t_{0.025} \sqrt{\frac{S^2}{2}}$ with t and S^2 as 8 degrees of freedom.

$$\Rightarrow 16.38 \pm 2.31 \sqrt{\frac{0.086}{2}}$$

$\Rightarrow 16.38 \pm 0.48$ μm.

This size reduced product was then dried using a Büchi Mini spray dryer (B-190), using an inlet temperature of 124°C and an outlet temperature of 63°C. The dried powder was collected and was further tested, versus other currently available grades of MCC (ie Avicel® PH-101 and Avicel® PH-102), for any improved functionality in a number of pharmaceutical applications. These applications included:

1. Use as an adjuvant in tabletting.
2. Use as a spheronisation aid in extrusion/spheronisation techniques.
3. Use as a suspending agent in suspensions.

The results of the above investigations are discussed in Chapter 7.

5.3 EXAMINATION OF THE EFFECT OF HOMOGENISATION CYCLE NUMBER ON SIZE REDUCTION AND THE POLYDISPERSITY INDEX OF MCC

5.3.1 Effect of Cycle Number on Particle Size

The particle size of the size reduced powders was measured as before using the Malvern 2600c series. The powders were analysed in their wetted state. The results, shown in Fig. 5.3a, illustrate the influence of homogenisation cycle number on the reduction of the Avicel® PH-101 powder, prepared as aqueous suspensions at two concentrations, namely 5% and 10%. The particle size values plotted on the graph are the d_{50} values, determined using the Malvern software.

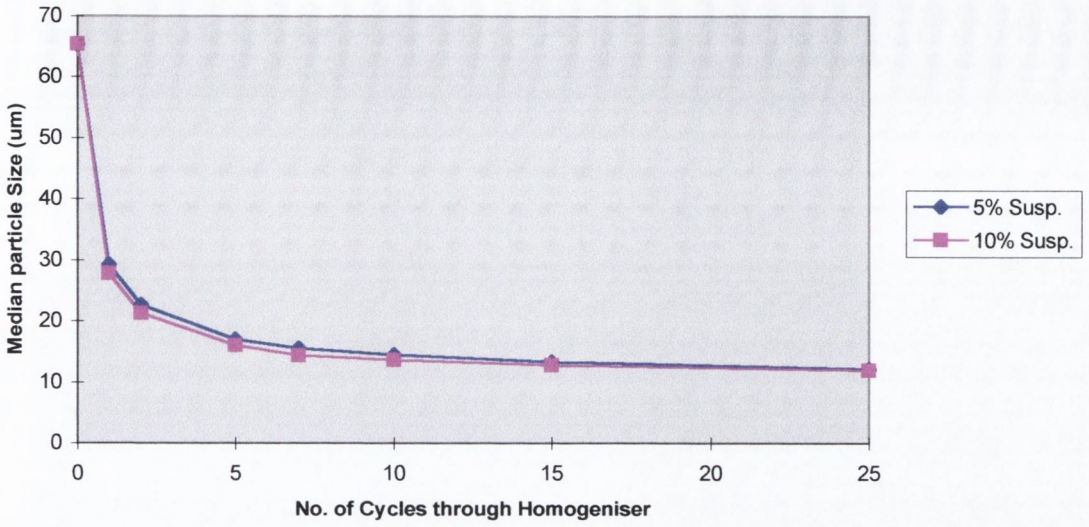

Figure 5.3a. Effect of homogenisation cycle number on the magnitude of size reduction of 5 and 10% MCC (Avicel® PH-101) aqueous suspensions.

The application of the student's t-test, using 2 degrees of freedom and a 95% confidence interval at each cycle point, illustrated that no statistically significant difference existed between the 5% and 10% suspensions. Visual observation of the graph confirms that the curves are virtually superimposable. The 10% suspension may have undergone slightly greater size reduction due to the increased attrition and cavitation forces, induced by the greater local concentration of MCC particles. The greatest level of reduction occurs up to cycle number 5 and levels off after that. This is in agreement with the results of Müller and Peters, 1998, who prepared nanosuspensions of poorly soluble drugs, using high pressure homogenisation. They concluded that the homogenisation process reduced the mean particle size, which decreased clearly up to cycle number 5 and remained unchanged when increasing the cycle number to 10. In our case, further cycles above cycle number 5 did cause further size reduction, but this was negligible, relative to the size reduction produced up to cycle no. 5.

5.3.2 Effect of Cycle Number on the Polydispersity Index

A second graph (see Fig. 5.3b) was plotted to illustrate the effect of homogenisation cycle number on the width of the size distribution (i.e. the polydispersity index) of the particles. This required plotting the difference between the d_{90} and the d_{10} values of the homogenised powders at each cycle number. Again, this was performed for the 5% and 10% aqueous Avicel® suspensions, between which no statistically significant differences were shown to occur using the student's t-test at 2 d.f. and a 95% C.I.

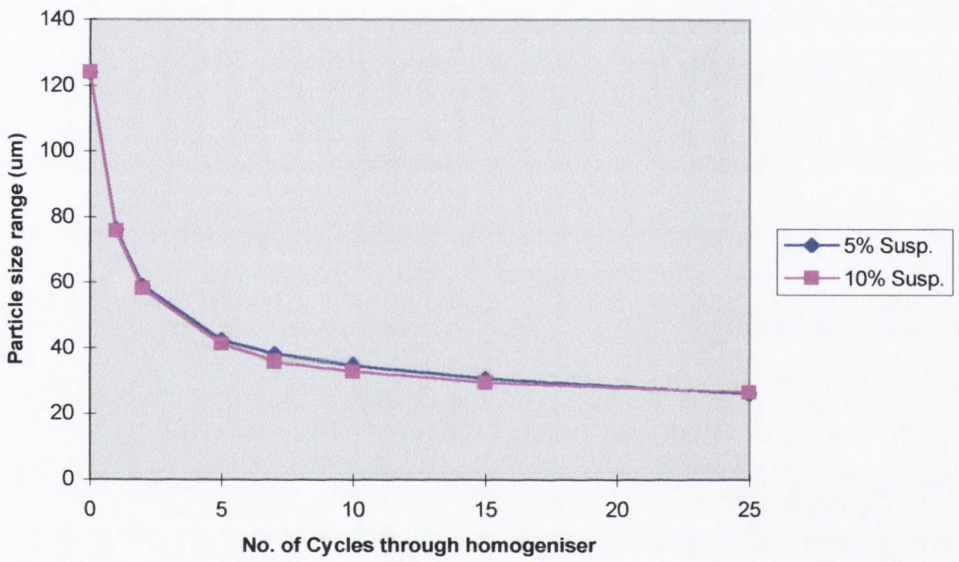

Figure 5.3b. Effect of homogenisation cycle number on the size polydispersity of 5 and 10% MCC (Avicel® PH-101) aqueous suspensions.

These curves differ slightly from the previous ones in that significant reduction in the particle size range occurs up to ca. cycle number 10, after which further, but only slight, reduction occurs up to ca. cycle number 25. This again agrees with the results of Müller and Peters (1998), who concluded that the PI (polydispersity index) decreases until ca. cycle number 9. These results indicate that despite reaching the maximum degree of dispersion at ca. 5 cycles, that higher cycle numbers are conducive to a more monodisperse product.

5.4 EXAMINATION OF THE ROLE OF THREE DE-AGGREGATING AGENTS ON THE EASE OF RECOVERY OF ULTRAFINE MCC

5.4.1 Introduction

The aim of this section was to examine the role of a number of de-aggregating agents on the ease of recovery of an ultra-fine grade of MCC. These were used in combination with a mechanical de-aggregating process, namely ultrasonic homogenisation, the benefits of which, in producing size reduction of MCC powder suspensions, are evident from previous experiments. It was hoped that the presence of small quantities of de-aggregating agents would have a two-fold effect. Firstly, their presence was intended to prevent re-aggregation of the size reduced MCC powder, during subsequent recovery from the aqueous suspension by spray-drying. Secondly, they were intended to augment the re-dispersal of the recovered MCC powders, when re-constituted with an aqueous medium.

The three potential de-aggregating agents chosen were sodium lauryl sulphate, sodium hexametaphosphate and sodium citrate. Sodium lauryl sulphate (SLS) was chosen, based on an observation by Deasy and Law (1997) that this anionic wetting agent has the ability to promote fragmentation of the MCC used as a spheronisation aid into small crystallites. These observations were illustrated by scanning electron microscopy. SLS is known by a large number of synonyms and is a widely used excipient in pharmaceutical formulation and technology applications, at typical concentrations of between 1% and 2%. It has some potential to cause irritation to skin and eyes, but this is mainly evident at higher concentrations i.e. 10-20% (Handbook of Pharmaceutical Excipients, 2000).

The second excipient chosen was sodium hexametaphosphate. It is a mixture of polymeric meta phosphates - not a hexamer. It is stable in water but dissolves slowly. This point was considered, when it was used in preparing aqueous suspensions with MCC, i.e. it was given suitable time to dissolve completely. Aqueous solutions possess dispersing and deflocculating properties (Merck, 1996). Its estimated acceptable daily dietary intake is

up to 70 mg as phosphorous per kg body weight (Report of FAO/WHO Expert Committee on Food Additives, 1964).

The final excipient chosen as a potential dispersing agent is sodium citrate BP. It is soluble in 1.3 parts water (Merck, 1996), the aqueous solution being slightly alkaline to litmus (pH 8). Again, at low levels, it is relatively safe to be used as an excipient in pharmaceutical formulations - i.e. LD_{50} orally in rats is 1.0 to 2.7 g/kg (Handbook of Pharmaceutical Excipients, 2000). It has been used as a sequestering agent and for this reason may prove useful as a dispersing agent, when combined with microcrystalline cellulose.

5.4.2 Recovery of Ultrafine MCC

Three potential dispersing agents were chosen as described in the introduction, namely sodium lauryl sulphate (SLS), sodium hexametaphosphate (NaHMP) and sodium citrate (NaCit). Each excipient was examined at two levels (i.e. 6.25% and 12.5% of the MCC solid content in each suspension). These levels were chosen, as they most realistically reflect levels that would ultimately be incorporated into powder mixtures used to produce pellet formulations using extrusion/spheronisation technology. The general experimental formulae used are shown in Table 5.4a.

Table 5.4a: General experimental formulae used in the size reduction studies of MCC using ultrasonic homogenisation.

I.D. Key	Dispersing Agent	Concentration of Dispersing agent (%)	MCC Content (g)
SRP A	SLS	6.25	25
SRP B	NaHMP	6.25	25
SRP C	NaCit	6.25	25
SRP D	SLS	12.5	25
SRP E	NaHMP	12.5	25
SRP F	NaCit	12.5	25

The initial stages of this investigation involved preparing coarse pre-dispersios of MCC suspended in a number of aqueous solutions, containing different types and levels of potential de-aggregating agents. Each suspension was size reduced by homogenisation using 5 cycles. This cycle level was chosen as previous results, described in Section 5.3.1, indicated that the greatest level of size reduction occurred during the initial 5 runs, whereas further passes did not cause significant further size reduction.

As mentioned in the methodology, the particle size distributions of the six powder suspensions were determined, the results of which are expressed in Table 5.4b. The values quoted are the d_{50} values, which are the 50% cumulative undersize values obtained by the computer software and the units used are microns.

Table 5.4b: Results of size reduction studies of MCC suspensions, using homogenisation incorporating 5 cycles.

	SRP A	SRP B	SRP C	SRP D	SRP E	SRP F
	14.74	14.18	13.94	14.83	14.44	14.36
	14.88	14.10	14.07	14.93	14.37	14.48
	14.75	14.07	14.16	14.84	14.38	14.32
	14.71	14.4	14.47	15.06	14.21	14.3
	14.59	14.22	14.51	15.11	14.21	14.32
	14.73	14.33	14.38	15.11	14.29	14.47
	14.32	14.26	14.15	14.92	14.32	14.35
	14.28	14.35	14.25	14.96	14.24	14.45
	14.40	14.30	14.26	15.01	14.26	14.36
Total	131.4	128.21	128.19	134.77	128.72	129.41
Mean	14.6	14.25	14.24	14.97	14.3	14.38
Variance	0.0463	0.0128	0.0349	0.0112	0.0066	0.0048

The above results were analyzed statistically, using ANOVA. The results from this analysis are illustrated in Table 5.4c.

Table 5.4c: ANOVA for results of size reduction studies of MCC suspensions, using homogenisation incorporating 5 cycles.

ANOVA						
Source of Variation	SS	df	MS	F	P-value	F crit
Between Groups	3.677548	5	0.73551	37.87671	1.51E-15	2.408513
Within Groups	0.932089	48	0.019419			
Total	4.609637	53				

ANOVA (Table 5.4c) confirmed that there is a statistically significant difference between the particle size distributions of the six size reduced suspensions. Since a significant difference was shown to exist, the student's t-test was appropriate to show the individual differences between the paired combinations. The student's t-test was performed with 16 degrees of freedom and a probability of $p = 0.05$. The results of this test showed that preparations SRP A and SRP D were the most significantly different. Both contained SLS as the dispersing agent and did not result in size reduction to the same degree as the other four preparations. The slight hindrance to size reduction may be due to the formation of a foam, the effects of which were described previously.

5.4.3 Re-dispersal of Ultrafine MCC

Following spray-drying of each powder sample, appropriate amounts were re-constituted using distilled water and re-examined, using the Malvern for re-dispersal abilities. The particle size analysis results are shown in Table 5.4d.

Table 5.4d. Results of particle sizes of re-constituted powders recovered by spray-drying.

	SRP A	SRP B	SRP C	SRP D	SRP E	SRP F
	11.32	11.07	10.83	11.21	10.71	10.4
	11.29	11.07	11.00	11.25	10.62	10.42
	11.34	11.04	11.08	11.27	10.64	10.43
	11.29	11.14	10.99	11.00	10.62	10.41
	11.17	11.08	11.32	11.31	10.67	10.46
	11.29	11.10	11.04	11.01	10.64	10.45
Total	67.7	66.5	66.26	67.05	63.9	62.57
Mean	11.28	11.08	11.04	11.18	10.65	10.43
Variance	0.0035	0.0011	0.0256	0.0184	0.0012	0.0005

Again ANOVA was applied to the collected data, the results of which are illustrated in Table 5.4e.

Table 5.4e: ANOVA of results of particle size of re-constituted powders recovered by spray-drying.

ANOVA						
Source of Variation	SS	df	MS	F	P-value	F crit
Between Groups	3.300822	5	0.660164	78.58061	2.58E-16	2.533554
Within Groups	0.252033	30	0.008401			
Total	3.552856	35				

ANOVA confirmed that there was a statistically significant difference between the re-constituted powders. This difference again existed, mainly between the SLS containing preparations and the other four, and may be explained as before. This was illustrated, using the student's t-test with 10 degrees of freedom and P = 0.05. The results indicate that all the powders are amenable to re-dispersion, i.e. any aggregates that may have formed during spray-drying were easily reversed with the simple stirring process, after re-constitution. This experiment thus illustrates that a micro-fine grade of MCC (10 μm

approx.) is achievable, with the incorporation of the de-aggregating agents SLS, NaHMP and NaCit, through a simple two-step process of homogenisation followed by spray-drying.

The average particle size of the re-constituted MCC was lower than that prior to spray-drying, in the case of all preparations. This may be due to a slight partitioning effect occurring along the glass columns of the spray-dryer apparatus, during the drying process, i.e. substantial quantities of powder were lost by adherence to the vessel walls, especially the main Büchi column. Only the powders collected in the final collection vessel were used in the subsequent re-dispersal studies. Inherent in the sedimentation process is the fact that larger particles will sediment out from a fluid before the finer ones, or alternatively, the finer particles are more likely to reach the final collecting vessel. This would explain the slight shift downwards in the average particle size of the powders recovered.

5.4.4 Conclusion

All six preparations facilitated the preparation of a microfine grade of MCC. Thus, all six powders were further examined for their potential as extrusion/spheronisation aids in the production of spherical pellets, as described in Chapter 7. The resultant pellets were characterized, using a number of physical measurements (i.e. porosity, density, retarded drug release, surface smoothness, etc.) to see if any significant differences could be established between the 6 powders.

Chapter 6

Characterization of Size Reduced Grades of Avicel® PH-101

6.1 Mercury Porosimetry of MCC Powders

6.1.1 Introduction

Mercury Porosimetry was introduced into the field of pharmaceutical technology by Strickland *et al.,* (1956), where they measured the apparent density of granulates, using a simple mercury Porosimeter with a pressure range of 20 - 150 KN/m^2. Since then, the use of the technique has increased significantly, both to measure the pore distribution of tablets (Selkirk and Ganderton, 1970a and 1970b) and to study similarly the porosity, particle size and surface area of powder systems (e.g. Carli and Motta, 1984, Smith and Schentrup, 1987, and Zouai *et al.*, 1996).

Mercury Porosimetry was used to examine the porous structure of three grades of microcrystalline cellulose, namely Avicel® PH-101, Grade X (size reduced MCC) and Grade Y (size reduced MCC incorporating 1% SLS). The aim of this section was to evaluate the correlation between the particle size and porous structure of the three powders. Previous work performed by Zouai *et al.,* (1996), illustrated the highly porous nature of Avicel® PH-102, which is a grade of MCC with a larger average particle size relative to Avicel® PH-101 (Company Literature).

The porous characteristics of the three powders were determined by examining the pore size distribution of the powders, as reflected in plots of the cumulative pore volume

intruded by mercury versus the pore diameter (calculated from the applied pressure using the Washburn Equation), or plots of the incremental intrusion volume versus pore diameter. Cumulative pore size distributions are illustrated in Fig. 6.1f, whereas the incremental pore volumes are shown in Figs. 6.1c, 6.1d and 6.1e. In all cases the pore diameter is represented on a log scale. This is because, if the data was plotted on an arithmetic scale, the data at the high diameter range would be expanded and would be compressed over the low diameter range. This would result in a loss of information about Hg intrusion into the fine pores of the sample material. The relevant quantitative results (i.e. total intrusion volumes, % porosity, etc.) of these porosimetric studies are listed in Table 6.1a. The percentage porosity values for the powders are determined from Equation 6.1a.

$$P_{pc} = \frac{100(V_{tot})}{V_b} \qquad \textbf{Eqn. 6.1a}$$

where

P_{pc} = percentage porosity

V_{tot} = total intrusion volume

V_b = sample bulk volume (volume after the largest open pores have been filled)

$= V_{pen} - V_{Hg}$

where V_{pen} = total internal penetrometer volume

V_{Hg} = volume of mercury occupying the remaining space

6.1.2 Results and Discussion

Table 6.1a. Quantitative Results of Porosimetric Study of Avicel® PH-101, Grade X and Grade Y microcrystalline cellulose powders.

	Avicel® PH-101	Grade X	Grade Y
Ave. Particle Size of Raw Material (μm)	56.39	12.62	10.58
Hg Total Intrusion Volume (ml/g)	1.616	2.253	2.030
Median Pore Diameter Volume (μm)	16.561	3.230	3.205
Bulk Density (g/ml)	0.464	0.326	0.366
Porosity (%)	74.9	73.5	74.3

Total mercury intrusion for the three grades of MCC powders are illustrated in Table 6.1a above. Intrusion values for Grades X and Y are very similar, showing averages of 2.25 and 2.03 ml/g respectively. However, in the case of Avicel® PH-101, the total intrusion is lower with an average of 1.62 ml/g. This can be explained bythe fact that Avicel® PH-101 powder consists of irregular particles (as confirmed by its broad histogram from Malvern studies, illustrated in Chapter 4) and so the smaller particles fill extra-particulate pores that exist between the larger particles, creating an overall lower free space available for mercury intrusion. The novel size reduced grades however, have a smaller, more uniform size distribution (again as confirmed by Malvern and SEM studies; see Figs. 6.1a and 6.1b for examples of scanning electron micrographs of Grade X and Grade Y, respectively) and so the packing properties are not as good. This is reflected by the differences in bulk density values between the different grades, i.e. 0.464 g/ml for Avicel® PH-101 and 0.326 and 0.366 g/ml for Grades X and Y, respectively.

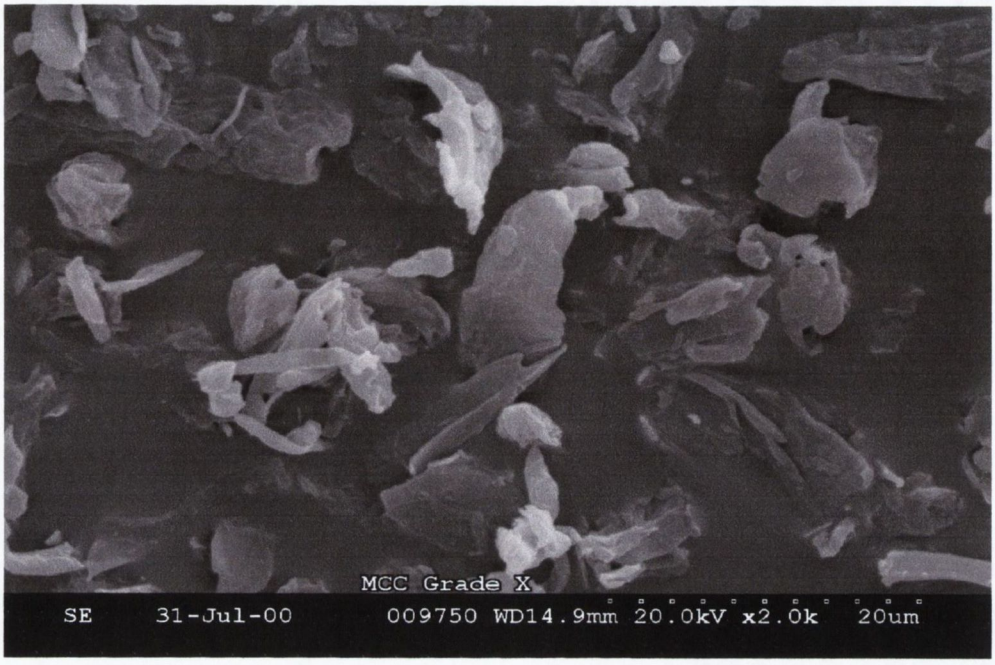

Figure 6.1a Scanning electron micrograph of Grade X MCC powder (magnification X 2000).

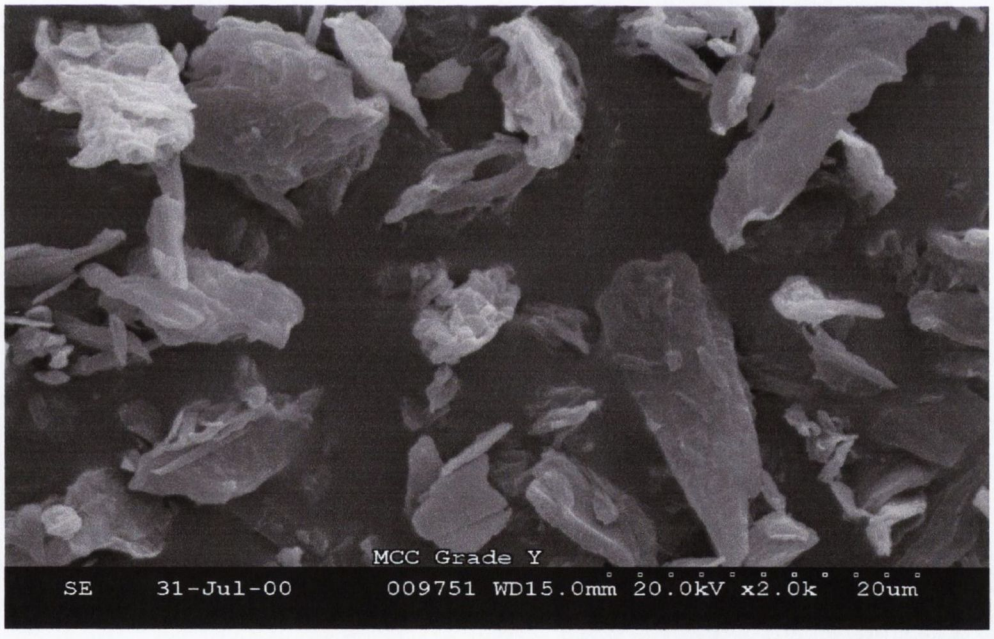

Figure 6.1b Scanning electron micrograph of Grade Y MCC powder (magnification X 2000).

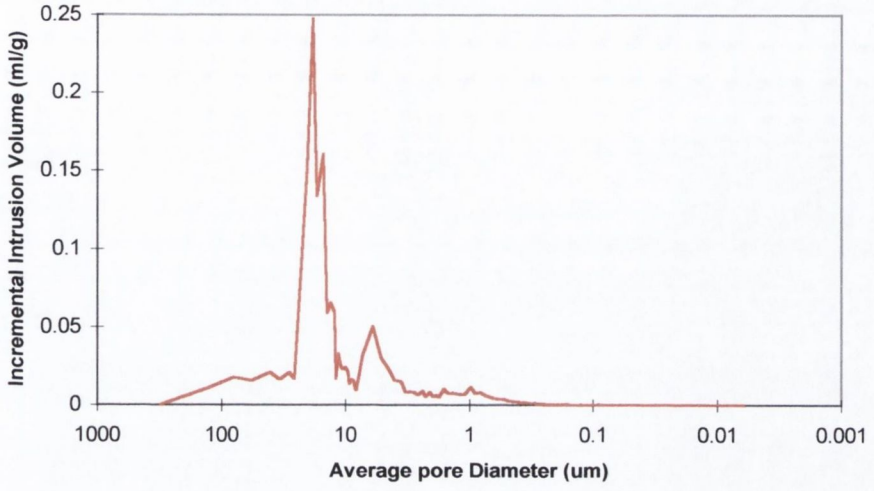

Figure 6.1c. Incremental mercury intrusion curve for Avicel® PH-101.

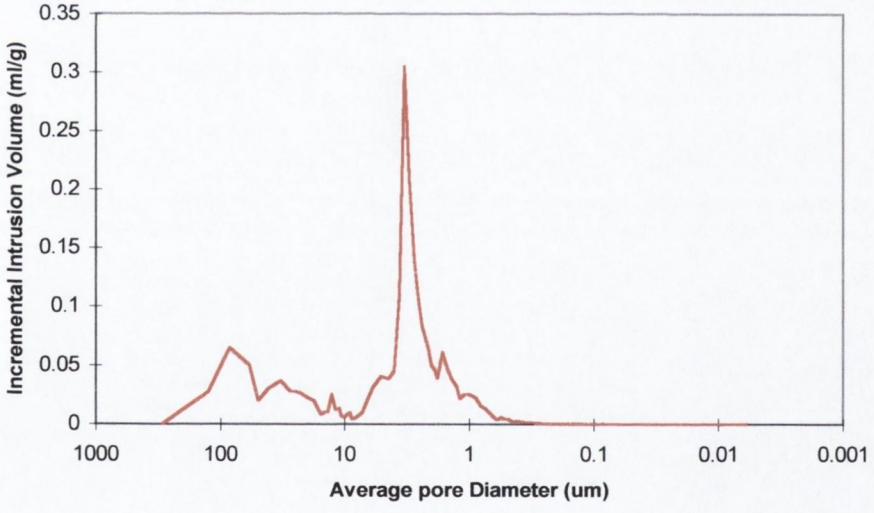

Figure 6.1d. Incremental mercury intrusion curve for Grade X MCC powder.

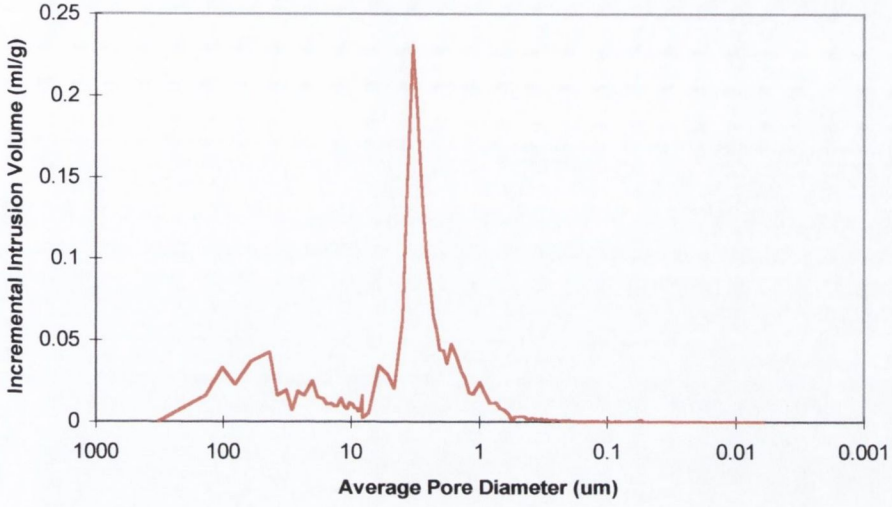

Figure 6.1e. Incremental mercury intrusion curve for Grade Y MCC powder.

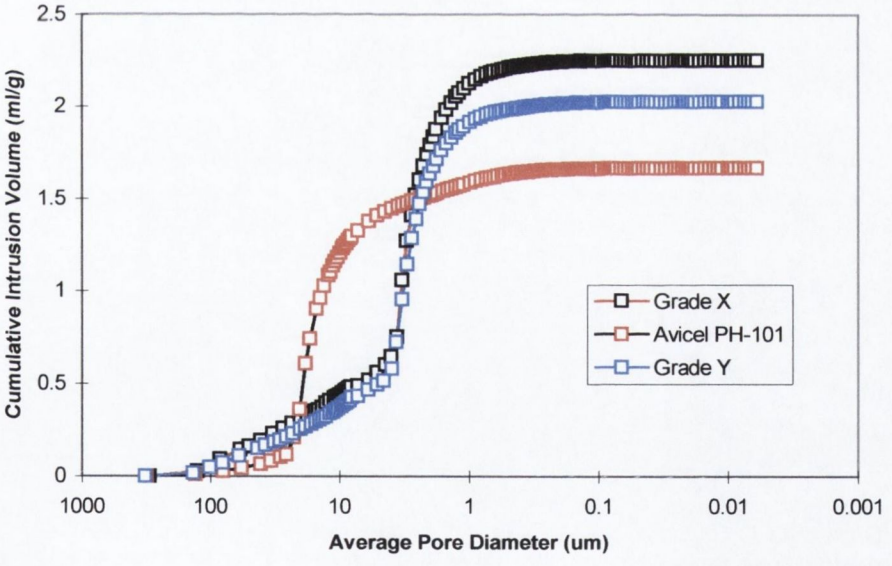

Figure 6.1f. Cumulative mercury intrusion curves for Avicel® PH-101, Grade X and Grade Y microcrystalline cellulose powders.

The median pore diameters for the three powder grades are also shown in Table 6.1a. The average values are 16.56 μm for Avicel® PH-101 and 3.23 and 3.21 for Grades X and Y, respectively. It is very evident that the median pore diameter is significantly greater for Avicel® PH-101 than for the novel grades. This is in agreement with results published by Zouai *et al.*, (1996), and was explained by Hausner (1967), that, when a powder mass consists of fine particles (i.e. Grades X and Y), pores between the particles will also be fine, whereas on the other hand, if the powder mass consists of coarser particles (i.e. Avicel® PH-101), the voids between the particles will similarly be coarser. Hence, pore size is a function of particle shape and size.

The incremental intrusion curves show a bimodal distribution for all three powder grades (illustrated in Figs. 6.1c, 6.1d and 6.1e). Coarse pores were observed in the range of ~ 12 to 400 μm, whereas finer pores were seen to exist in the range 1 to 12 μm. In both cases, these pores correspond to interparticulate voids within the powder mass. These results agree with the works of Le Thiesse (1989), who stated that the overall porosity of microcrystalline cellulose is essentially interparticulate, and Marshall and Sixsmith (1974), who observed that interparticulate porosity of MCC correspond to a void size range of 8 to 0.8 μm. They observed also, intraparticulate pores with size ranges of ~ 0.003 μm. However, we were unable to achieve pressures capable of penetrating pores of this size with our equipment and so they were undetected.

The incremental intrusion plots of Avicel® PH-101 do, however, differ from those of Grades X and Y in terms of the relative proportion of pores between 1 to 12 μm and 12 to 400 μm, respectively. Avicel® PH-101, consisting of coarser particles, has the majority of its pores in the upper range with an average of 17 μm approx., corresponding to its median pore diameter previously quoted, whereas both Grades X and Y, have predominantly greater intrusion in the lower size range. This is evident in Figs. 6.1c, 6.1d and 6.1e.

The shape of the cumulative intrusion *vs.* pore diameter curves are typically sigmoidal for all three powder samples, as illustrated in Fig. 6.1f. In the case of Avicel® PH-101, a sharp increase in intrusion volume occurs, when the pressure becomes high enough to fill pores in the range ~10 to 30 μm, whereas the sharp increase is observed at the lower range of 1 to 6 μm for both Grades X and Y. The total pore volume for Grade X is slightly larger than that of Grade Y. This is because Grade Y differs by the incorporation of 1% SLS, which finely coats the MCC particles during the spray-drying process. The fine SLS particle deposits reduce the inter-particulate porosity and hence pore volume. This is also reflected by the slightly lower median pore diameter quoted for Grade Y relative to Grade X (see Table 6.1a).

6.2 SPECIFIC SURFACE AREA MEASUREMENTS

6.2.1 Introduction

Significant work has been performed on microcrystalline cellulose, with regards to assessing its specific surface area characteristics. In all cases, the primary grade analysed has been Avicel® PH-101. A review of the literature indicates that a wide range of values have been determined for this one grade alone, namely 1.0 m^2/g (Hollenbeck *et al.*, 1978); 1.5 m^2/g (Nakai *et al.*, 1977); 1.3 m^2/g (Zografi *et al.*, 1983), and 11.2 m^2/g (Marshall and Sixsmith, 1974), using the N_2 adsorption technique and 1.3 m^2/g (Marshall and Sixsmith, 1974) by mercury porosity.

Surface area analysis was performed on the three grades of microcrystalline cellulose powder (Avicel® PH-101, Grade X and Grade Y), using the nitrogen gas adsorption technique, from which the BET multipoint surface areas (m^2/g) were determined. In addition, these results were compared with the specific surface area results obtained from mercury porosimetry data calculated in experiments performed previously, as described in Section 6.1. The objective was to determine if any differences existed between the three grades of powder and similarly between the two techniques applied, and if so, to explain them.

6.2.2 Results and Discussion

Values of specific surface area obtained for microcrystalline cellulose, using N_2 adsorption and mercury penetration under different sample pre-treatments, are given in Table 6.2a.

Table 6.2a. Specific surface area of microcrystalline cellulose measured by various methods.

Method	MCC Grade	Pre-treatment Conditions	Surface Area (m^2/g)
Hg	Avicel® PH-101	Heated at 70°C for 24 hr followed	1.42
Hg	Grade X	by vacuuming to 50 μm Hg	3.52
Hg	Grade Y		3.73
N_2	Avicel® PH-101	Heated at 70°C for 24 hr under	0.984
N_2	Grade X	vacuum followed by helium purge	2.441
N_2	Grade Y	for 3 hr at 70°C	2.947

According to Table 6.2a, above, the value determined for the average specific surface area of the Avicel® PH-101 powder, using the mercury penetration technique, is 1.42 m^2/g, which is very similar to the value calculated by Nakai *et al.*, 1977, (1.5 m^2/g) using a similar procedure, and also values determined by Zografi *et al.*, 1983, (~ 1.31 to 1.44 m^2/g) using both nitrogen and krypton adsorption data. In our case, however, the value obtained using nitrogen gas adsorption data is slightly lower with an average value of 0.984 m^2/g. This can be explained due to the presence of residual water within the powder, (Hollenbeck *et al.*, 1978). When the powder was being pre-treated, it was heated at 70°C under vacuum conditions for 24 hours, in an attempt to evaporate as much of the water present as possible. Despite this, the dried powder was exposed to atmospheric conditions within the lab for a short period of time, while it was being transferred from the oven to the helium purge, prior to attachment to the Gemini machine. During this transfer stage the powder had the potential to very rapidly reabsorb water

from the atmosphere, particularly if it was very humid. This residual moisture present within the sample froze at liquid nitrogen temperatures used during the N_2 adsorption studies. This frozen water effectively blocks access to the porous MCC structure by the nitrogen molecules, thus reducing the total volume of nitrogen adsorbed. In the case of mercury (Hg) intrusion, which was carried out at room temperature (~ 25°C), this residual water was not frozen and so the surface area determined is more representative of the true value. Further evidence for the above explanation is cited from work with asbestos (Young and Healey, 1954), which showed that complete removal of moisture was required to give the same value of specific surface area, when nitrogen and water vapour were used: with residual moisture present, values obtained with nitrogen were lower.

As mentioned previously, Marshall and Sixsmith, (1974), determined a value of 1.3 m^2/g, with mercury poresizing and 11.2 m^2/g, using nitrogen adsorption data, for Avicel® PH-101 powder. They explained this difference due to the fact that 1.3 m^2/g represent the external inter-particulate specific surface area, while values obtained with nitrogen gas reflect higher specific surface area, due to the pores not being accessible to mercury. Zografi *et al.*, (1983), have since concluded that the above data obtained using nitrogen gas adsorption was incorrect, and propose that the most likely explanation for the ten fold larger specific surface area for MCC must be due to a systematic error in calculating the values from nitrogen adsorption data.

The mercury penetration results also indicate that the specific surface areas determined for the two novel microcrystalline cellulose grades (i.e. Grades X and Y) are significantly larger than that of the Avicel powder. This is due to the smaller particle size of the novel powders, which means that an equivalent amount of powder will have significantly larger surface area available for measurement. The values for the two grades (i.e. 3.52 and 3.73 m^2/g for Grades X and Y respectively) are very similar, as reflected by their similar average particle sizes (see Table 6.1a). The slightly greater surface area quoted for Grade Y may be due to the presence of the fine particles of the 1% SLS incorporated by spray-drying, around which the mercury liquid can also penetrate. Similar trends are also

evident with the specific surface area values determined for the three powders, using the nitrogen adsorption technique, and can be explained likewise. In all cases, the specific surface area values are lower relative to those determined by the mercury technique, which is again due to the phenomenon of residual water freezing.

6.3 DSC analysis of MCC Powders

6.3.1 Introduction

Microcrystalline cellulose is prepared by controlled hydrolysis of α-cellulose, obtained as a pulp from fibrous plant materials, using dilute mineral acids. In general, acid hydrolysis destroys mainly the amorphous areas of cellulose. The result is a product of higher crystallinity and lower molecularity than the powdered microfibre cellulose product. Water vapour normally does not penetrate well-defined crystallites of cellulose, which can similarly be assumed for the microcrystalline type. Instead, cellulose-water interactions generally occur, either in intercrystalline regions (i.e. amorphous regions), or on the surfaces of the crystallites and the gross structure.

Frank and Wen, (1957), suggested that water consists of flickering clusters of hydrogen bonded molecules which are ice like. They concluded that the formation of hydrogen bonds in water was predominantly "*a co-operative phenomenon so that in most cases, when one bond formed, several would form to make a cluster and when one broke, the whole cluster broke or 'dissolved'* ". In this model, water can be visualised as an arrangement of flickering clusters of various shapes and sizes, continually dissolving and reforming. Quantitative theories have been developed from this model, for liquid water, to permit prediction of the behaviour of the liquid from the basic properties of the molecule.

There has been considerable debate over the concepts of cellulose-water interactions, which again would be equally applicable to MCC. Some concepts propose a structuring of cellulose by water, whereas others argue the opposite. Caulfield (1978), proposed that water is structured by cellulose. He speculated that, owing to the similarities and compatibilities of the spacings of the pyranose ring with those in trdymite structure of water, the adsorbed water between two cellulose surfaces can be viewed as a distorted, ice-like cluster, hydrogen bonded from one surface to the other. The cluster exhibits the flickering bond, opening and closing, associated with the flickering cluster model of water

and would be indistinguishable from bulk water in many of its properties. The clusters would be more permanent, due to the participation of anhydropyranose hydroxyl groups.

The LHS theory (i.e. water theory of Lentz, Hagler and Scheraga, 1965) categorises the short lived clusters of water molecules into two main groups:

1. A 'solid-like' component consisting of rigid hydrogen bonded ring structures (tetramer, pentamer, hexamer).
2. A 'fluid-like' component consisting of non-rigid less hydrogen bonded chain structures (dimer, trimer, star pentamer).

Goring and coworkers, (1965, 1978), on the other hand, envisaged that cellulose surfaces act as a water structure breaker, by increasing the amount of fluid-like component in the water adjacent to the interface. Thus, the surface is thought to be bonded to and to comprise part of a fluid-like layer, about one to two molecules thick. Farther away in the liquid, the ring structure pre-dominates.

Many different workers have thus shown that water sorbed by natural polymers, more specifically, cellulose based polymers, exhibit properties that are markedly different from free or bulk-like water. Instead, as described above, various theories have been proposed, indicating that water may be either structured or destructured by the presence of cellulose based polymers. In addition, it is generally accepted that absorbed water can be categorised into a number of different types as follows:

- tightly bound water, which is synonymous with non-freezable water, with properties that deviate significantly from those of normal water; mobility can set in at temperatures of around 170K. It is formed through chemical and physical interactions with the polymer matrix.
- loosely bound 'freezable' water, which exhibits properties that are nearly bulk-like.
- unbound 'free' water, which exhibits the properties of bulk water.

The bound water content is dependent on the degree of crystallinity of cellulose and MCC samples. As mentioned previously, when water adsorbs to polymers, it only diffuses into the amorphous regions of the samples. As a result, a technique capable of determining the levels of 'bound' or 'non-freezable' water in a polymeric sample will give a good indication of the overall crystallinity of that sample. There have been many techniques reported for detecting the water adsorbed onto polymers. However, Differential Scanning Calorimetry (DSC) is one of the most useful techniques for evaluating quantitatively free and bound water contents. The large number of publications, describing calorimetric methods to investigate the role of water in both natural and synthetic polymers, attests to the success of the technique, and to the scientific importance and commercial relevance of the data.

Three microcrystalline cellulose grades were used in this study, namely the original material Avicel® PH-101 and the two modified grades, Grade X and Grade Y. The hydration procedure used, as outlined in Chapter 3, involved preparing a large number of microcrystalline cellulose batches of various hydration levels, by adding a pre-determined weight of water to 5 g approx. of the cellulose, in a sealed glass bottle. After an appropriate equilibration time, a small sample was transferred to a hermetically sealed DSC pan and left for a further period of time before testing, to facilitate re-equilibration after transfer from the bottle. This method was chosen on the basis of optimisation experiments carried out by Keely (1996), in which three potential techniques were examined. The samples were scanned from 25°C to -60°C and then back to 25°C, at a scanning rate of 10 K/min. The pans were then removed, weighed to determine if any weight losses had occurred, pierced and then dried in an oven to determine the actual water content.

DSC traces portray endothermic (melting) and exothermic (solidification) features. Temperatures are in degrees Celsius, and enthalpies (expressed in various curves) are in joules per gram. Enthalpies listed in Tables 6.3a & 6.3c are in calories per gram to facilitate comparison with the broadly established convention in the literature (1 calorie = 4.17 joules). DSC traces were recorded at a fixed rate of 10 K/min. This was deemed to

be the most suitable on the basis of experiments performed by Keely (1996). This rate was decided upon by examining the smallest thermal event detectable (the region 220 - 235K), as a function of scanning rate. The compromise was to achieve the greatest temperature resolution (low scan rate) and the highest sensitivity for quantitative area analysis (high scan rate).

6.3.2 DSC of Pure Water

In order to understand the complex cellulose / water interactions, we first examined the DSC behaviour of pure water under comparable experimental conditions. The calorimeter was calibrated in terms of energy (peak area), H_{cal}, and temperature (peak onset), using a sample of pure indium. In addition, the enthalpy of HPLC grade water was used, giving a two point calibration. Initial calibration, using indium, resulted in an enthalpy of 28.6 J/g and an onset temperature of 156.65°C (see Fig. 6.3a). These values fall within the acceptable ranges of 28.45 ± 0.6 J/g for enthalpy (heat flow), and 156.6 ± 0.3°C for onset temperature, as outlined in the specifications for the DSC equipment. Verification with pure water resulted in an average enthalpy of melting for water of 83.38 ± 0.34 cal/g and an onset temperature within the range -0.88 to 0.11°C (see Fig. 6.3b). Ideally, the melting onset should occur at 0°C. Instrument calibration was performed routinely throughout the course of the study.

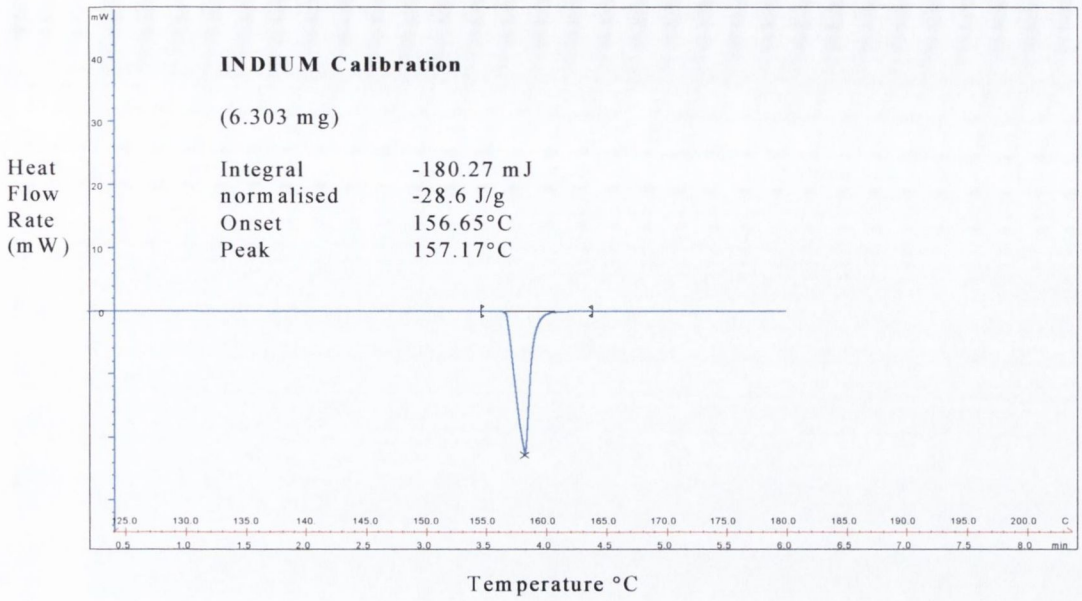

Figure 6.3a DSC instrument calibration, using the fusion peak of pure indium.

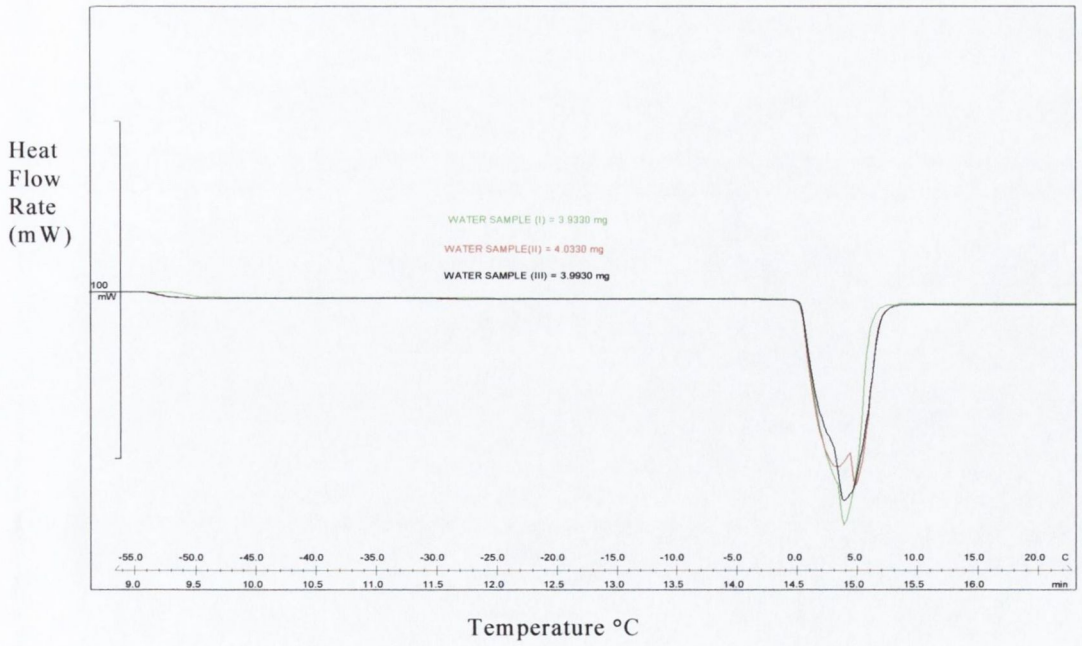

Figure 6.3b. DSC endotherms of pure HPLC grade water (approximately equal weights) recorded after equipment calibration, using indium.

Another important parameter considered was the effect of variation in water weight on the DSC data results. Fig. 6.3c depicts the recorded differences between a number of water samples, with increasing weights. It is evident from the endothermic curves, that an increase in the water content broadens the melting peak and shifts the peak maximum to higher temperatures. There is however, near constancy in the onset of the melting peak. In general, the endothermic plots illustrate one melting peak. In some instances, (i.e. see Fig. 6.3b), multiple melting peaks were observed for the pure water samples. This is due to the poor thermal contact and hence, thermal gradient variation within the samples. This effect was suppressed by ensuring that the water was evenly spread across the base of the DSC pan, before sealing it, rather than leaving it as a distinct drop within the pan.

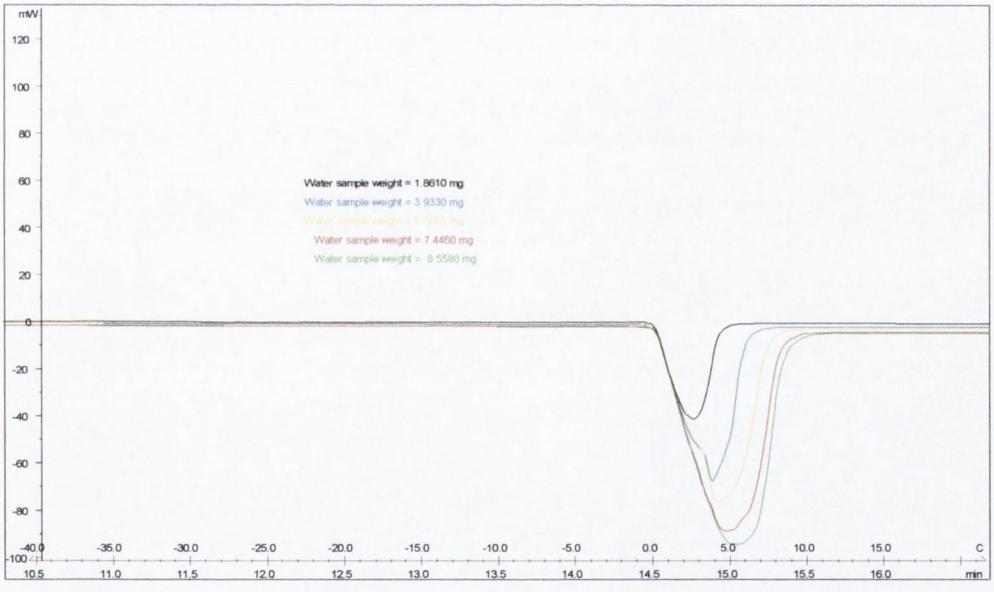

Figure 6.3c. DSC endotherms of pure water. In general, increasing sample weight results in no change in the peak onset temperature, peak broadening, and a shift in peak maximum to higher temperatures.

6.3.3 Endothermic Analysis of Hydrated MCC Powders

6.3.3.1 Qualitative Analysis of DSC Endotherms

The endotherm DSC curves for the three MCC grades are illustrated in Fig. 6.3d (I), (II) and (III). It is evident from the curves that water contents below 20 wt.% approx. produced no detectable endotherms. The water added, however, must be present somewhere. It is obvious that water cannot move to the outside of the volatile sample pans, as the pans were hermetically sealed, and no first-order transitions were observed, except for crystallization or melting in each of the cooling and heating curves. Instead, the absence of any peaks in these endotherms, below a specific water content, must be due to the fact that the water present is tightly bound to the amorphous regions of the MCC polymer. This tightly bound water is synonymous with 'non-freezable' water (Wnf). Nakamura *et al.*, (1981) have concluded from studies that this bound water, is that water which is restricted by the hydroxyl groups of the cellulose molecules. The fact that the DSC does not detect any thermal events below this moisture level does not mean that thermal events are not occurring. The properties of tightly bound water, as previously mentioned, deviate significantly from those of normal water and mobility tends to set in around 170 K. This is because, at water concentrations within the bound water regime and at temperatures below 250 K, the solidification of water is hampered by kinetic factors, arising from reduced water diffusivity and constraints imposed by the rigid polymer network (Pouchly *et al.*, 1979). DSC techniques tend to be insensitive to events below 210 K (Keely, 1996).

(I) Avicel® PH-101

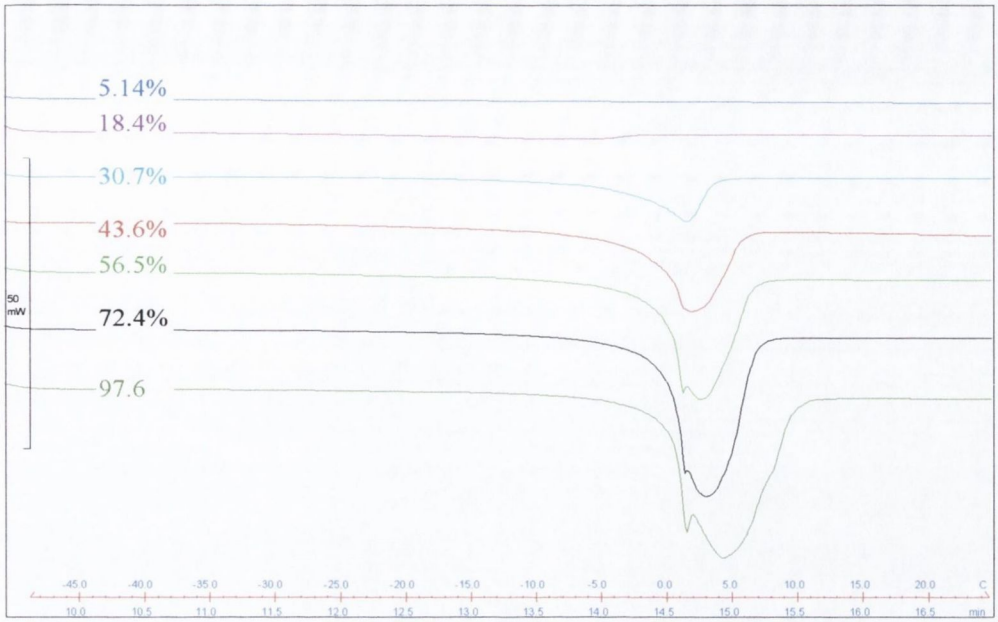

Temperature (°C)

(II) Grade X

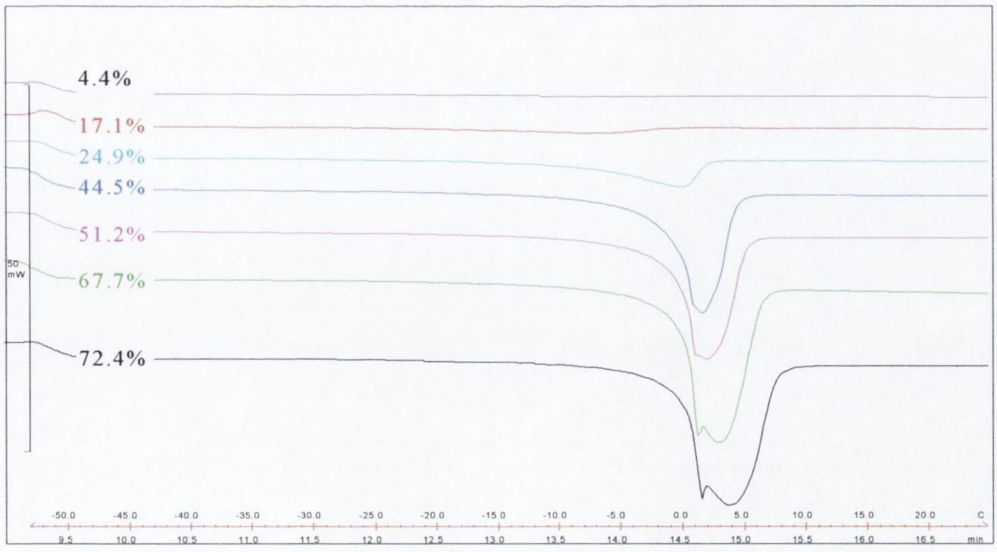

Temperature (°C)

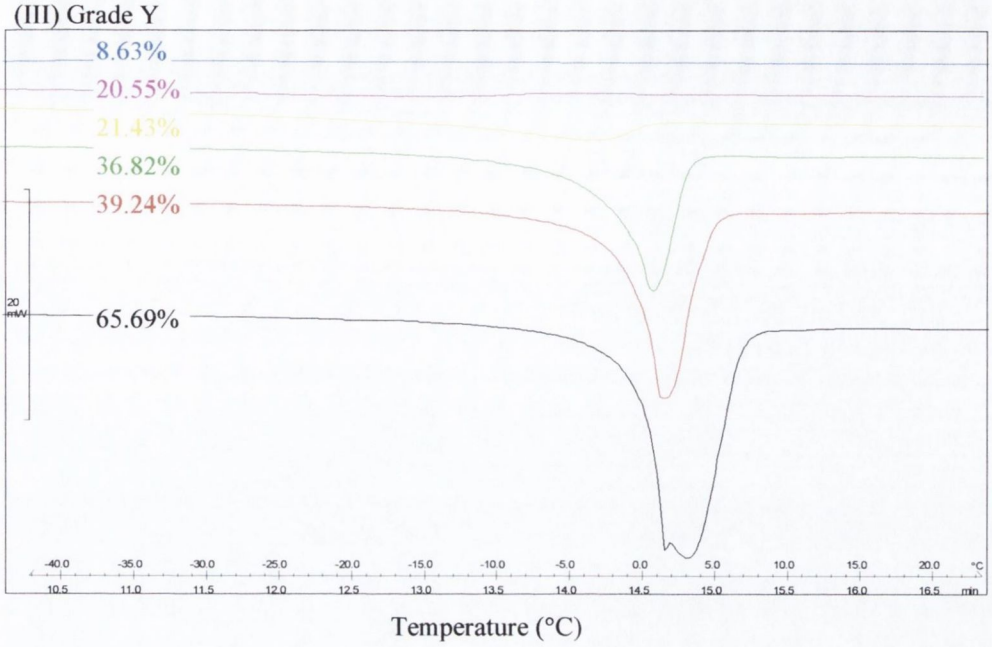

Figure 6.3d Typical DSC endotherms for hydrated MCC powder samples (Avicel® PH-101 (I), Grade X (II) and Grade Y (III), respectively) as a function of water content. The samples were heated at a rate of 10 K/min.

It is evident from the curves, that above moisture levels, corresponding to the maximum level of freezable water (W_o), the development of structure becomes apparent in the endotherm and this can be attributed to the presence of a heterogeneous distribution of water melting environments, i.e. the combined presence of both 'freezable' and 'non-freezable' water. It is the 'freezable' water that is detected by the endotherm. At low hydration levels the 'freezable' water corresponds mainly to the 'loosely bound' water and, as the overall water content increases, the 'freezable' water includes both this 'loosely bound' water and 'bulk-like' water.

6.3.3.2 Determination of ΔH_{endo}

Plots of ΔH per gram of polymer, as a function of water content (wt.%), are illustrated for the Avicel PH-101, Grade X and Grade Y, in Figs 6.3e(I), (II) and (III) respectively. The

slopes of the graph reflect the enthalpies (ΔH_{endo}) associated with the event, the calculated values of which are illustrated in Table 6.3a. Plots of ΔH per gram of water, as a function of water content, are illustrated in Appendix 5. Because water is mixed with the MCC polymer, the system exists as a mixed phase. These plots reflect the transformation of ice into water in this mixed phase (Pouchly *et al.,* 1979). Pouchly stated that an additional term exists in the system known as the 'mixing enthalpy', and which is probably negative. This would explain why the enthalpy calculated from the plots of ΔH per gram of polymer *vs.* water content, for each MCC powder grade, are lower than the calculated enthalpy of fusion of bulk water, ΔH_{bulk} = 83.38 cal/g (see Table 6.3a). This reduction of the enthalpy value, compared with that of pure water, is indicative of a progressively more dispersed water phase. It is these calculated enthalpies that are used to determine the non-freezing (W_{nf}) and freezing (W_f) water fractions. The use of ΔH for bulk water would result in an overestimation of the amount of 'non-freezable' water present.

The calculated enthalpy for Avicel® PH-101 is 79.66 cal/g. When this powder is size reduced by homogenisation to produce Grade X, the calculated enthalpy for the new grade falls to 73.3 cal/g. This suggests that the water phase is more dispersed in the Grade X MCC powder relative, to that of Avicel® PH-101. This is due to the reduced particle size of Grade X powder, which creates a more tortuous matrix or pathway, into and around which the water must spread, thus increasing the magnitude of the 'mixing' enthalpy. In contrast, the calculated enthalpy for Grade Y (82.54 cal/g) is larger than that of Avicel® and is very close to that calculated for bulk pure water. Based on the reduced particle size of Grade Y, we would expect it to have a reduced calculated enthalpy. However, here the sodium lauryl sulphate appears to have an effect. SLS appears to reduce the magnitude of the 'mixing' enthalpy (energy) associated with dispersing the water phase around the MCC particles. This is probably due to the surfactant properties of SLS, which reduce the surface tension of water and allow it to wet the MCC particles more readily, thus overcoming some of the non-equilibrium kinetic factors such as steric constraints, due to the rigid polymer matrix, which can cause reduced water diffusivity.

Table.6.3a Calculated 'non-freezable' water contents, enthalpies, and regression fits to 'freezable' water data from the endothermic DSC results for three MCC samples.

MCC Sample	'Non-freezable' Water Content (W_{nf}) (%)	ΔH_{endo} (cal/g)	Regression fit to 'Freezable' Water Data	Gradient of Curve (°)
Avicel® PH-101	18.81	79.66	$W_f = 0.98W - 17.5$	44° 25′
Grade X	15.96	73.3	$W_f = 0.98W - 15.02$	44° 25′
Grade Y	18.38	82.54	$W_f = W - 18.37$	45°

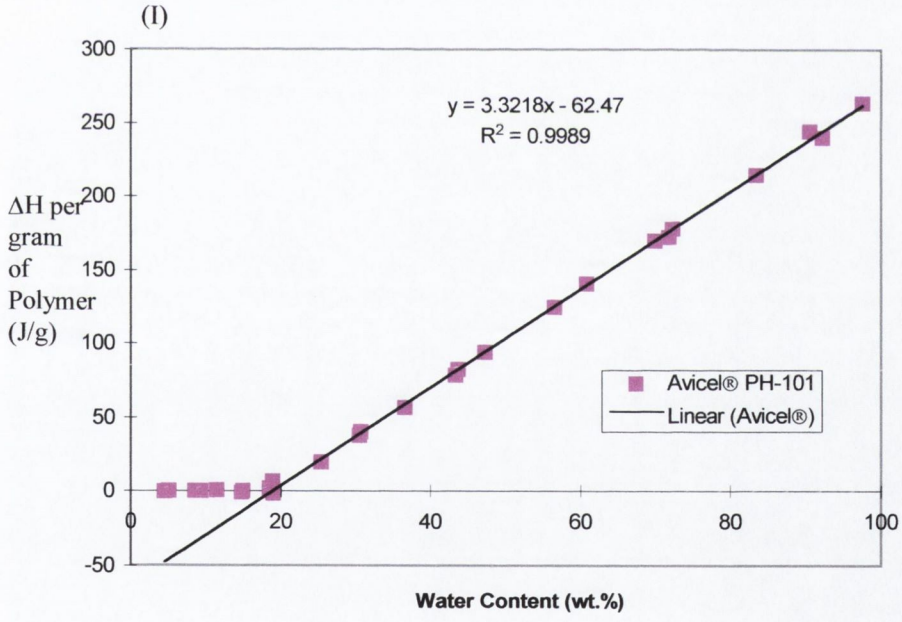

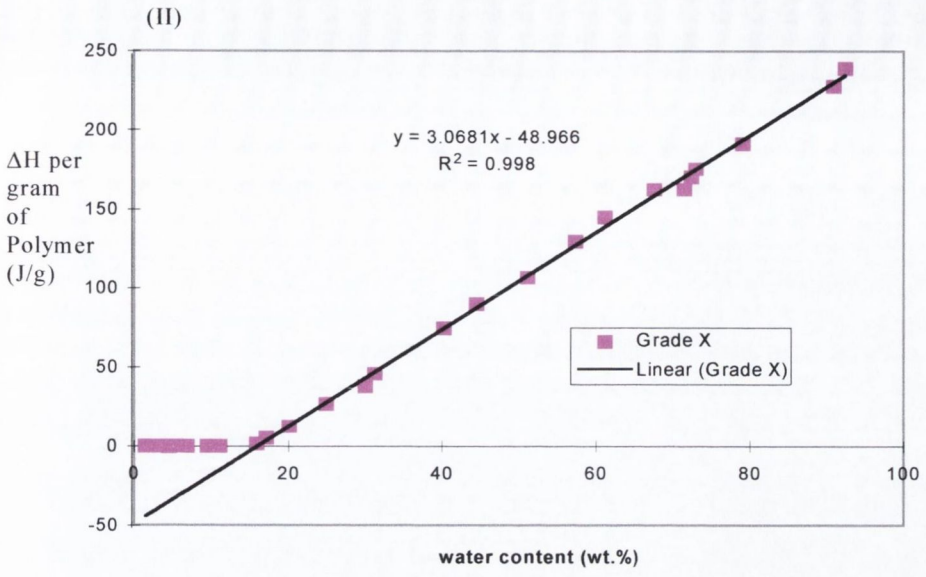

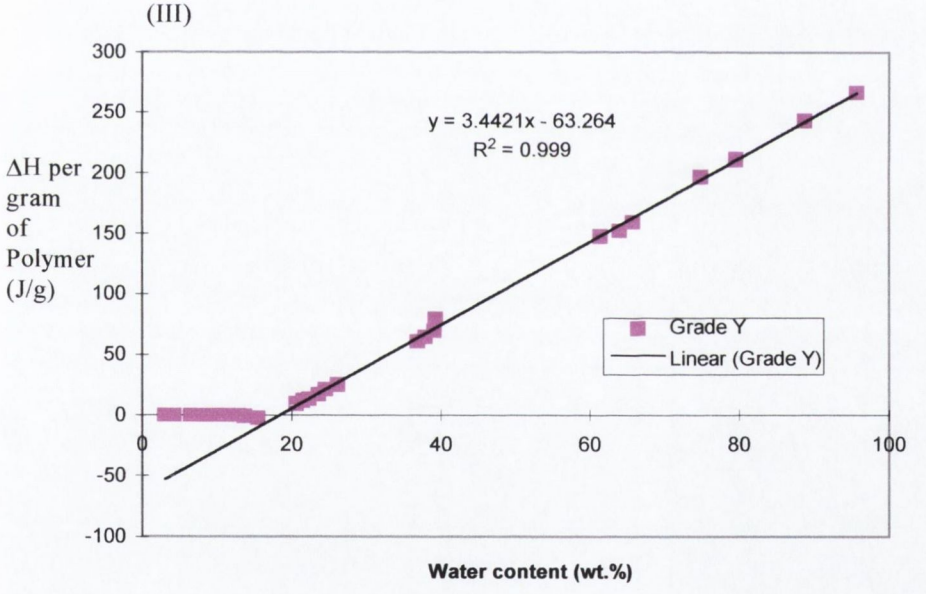

Figure 6.3e Enthalpies per gram of polymer *vs.* water content. The linear regression fits for Avicel® PH-101, Grade X & Grade Y are ($\Delta H = 3.3218W - 62.47$); ($\Delta H = 3.068W - 48.966$); and ($\Delta H = 3.4421W - 63.264$) respectively. The slopes of the graphs yield average ΔH_{endo} values for the three powders and the intercepts on the water content axes denote the 'non-freezable' water contents.

6.3.3.3 *Determination of 'Non-freezable' Water Contents and Correlation with Powder Crystallinities*

It is also possible to determine the 'non-freezable' water content, from the plots of ΔH per gram of polymer as a function of water content (wt.%), for each of the three MCC powders. The intercept on the water content axis denotes the total amount of water which is undetected, and which is synonymous with the 'non-freezable' water content (W_o). The calculated 'non-freezable' water contents for the three MCC polymers are also illustrated in Table 6.3a This value is a reflection of the degree of crystallinity of the polymer, as 'non-freezable' water is predominantly tightly bound to the amorphous regions of the polymer. As a result, a decrease in the 'non-freezable' water level would indicate a more crystalline product.

X-ray diffraction studies were performed on the three MCC powder grades in order to obtain some information on the crystallinity of the powders, using an alternative technique, and correlate it with the DSC technique. Measurements were performed at room temperature on a Siemens D500 X-ray powder diffractometer, using monochromatic Cu Kα radiation and a scanning rate of 0.5° 2θ/min, over the range 5 to 40° 2θ. Samples for analysis were prepared by pressing the powder into the cavity of a sample holder and smoothening with a glass slide.

The crystallinity index was calculated by using measured intensity measurements at 22.6° (002 peak; I_{002}) and 19.0° (amorphous background; I_{am}) 2θ according to Nelson and O'Connor (1964), as used by Chatrath *et al.*, (1991). The following equation was used to evaluate the percentage of crystalline material, % Cr,

$$\% \text{ Cr} = \left(\frac{I_{002} - I_{am}}{I_{002}} \right) X100\% \qquad \textbf{Eqn.3.3a}$$

It is important to note that this method gives only a relative set of values, but is still useful in comparing a series of samples with respect to one another.

The averaged X-ray diffractograms for the three MCC power grades are illustrated in Fig. 6.3f. It is evident from qualitative examination of the plots that all MCC grades are highly crystalline. The X-ray scans for the three grades all illustrate peaks at 15, 16, and 22.6° 2θ, which are characteristic of cellulose Type I. Cellulose Type I can be distinguished from Type II using X-ray diffraction techniques, as peaks at 12 and 20° 2θ, are characteristic of Cellulose Type II, (Landin *et al.,* 1993a). In general, cellulose I is converted to cellulose II by a vigorous manufacturing process. This suggests that the Avicel® manufacturing process performed by FMC and the subsequent homogenisation process, performed by us in the laboratory, are mild enough to retain cellulose in its native state.

Table 6.3b, below, gives the X-ray crystallinity indexes calculated from the diffractograms by the empirical formula, using the method described previously.

Table 6.3b. Crystallinity data on three microcrystalline cellulose samples

Sample Identity	X-Ray Crystallinity (%Cr)
Avicel® PH-101	84.49%
Grade X	83.93%
Grade Y	84.40%

It is evident form Table 6.3b that crystallinity values for the three powders range from 84.49 to 83.93 %. The original material, Avicel, has the highest level of crystallinity and it decreases slightly for the other two grades. This is because the cavitation forces subjected on the MCC particles, during the homogenisation process, have the effect of breaking up some of the crystalline areas in the Avicel material and rendering it more amorphous. This is similar to the phenomenon observed by Nelson and O'Connor (1964), in which they noticed that by ball-milling cellulose samples, the crystallites of the material are eventually

destroyed, converting it to an almost amorphous product. In the case of Grade Y, the reduction in the level of crystallinity is not as significant, and very closely resembles that of Avicel® PH-101. This is probably again due to the foaming effect of SLS, which as observed in Chapter 4, protects the MCC particles against the full impact of the cavitation and shearing forces experienced during homogensation.

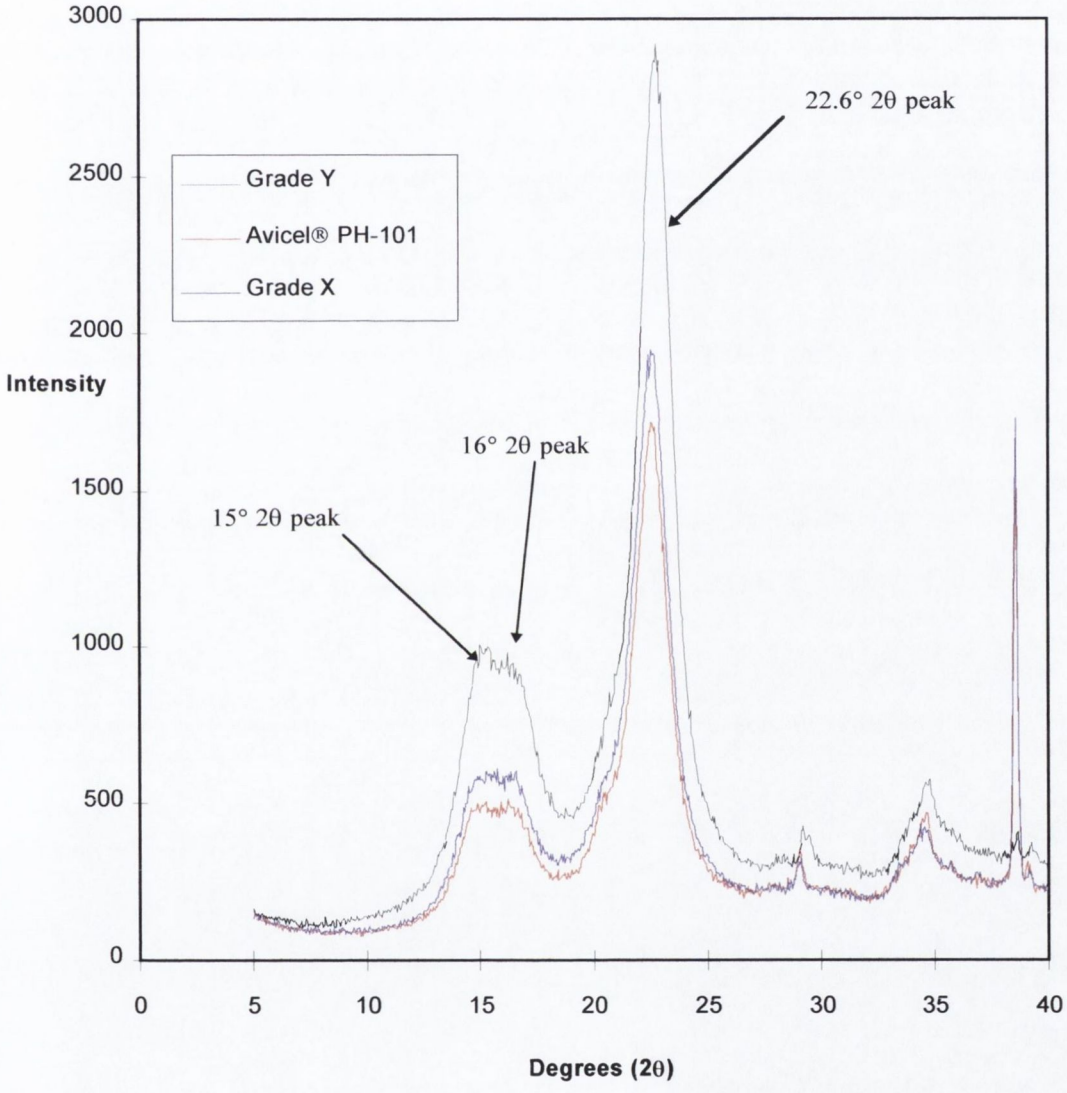

Figure 6.3f. X-ray Diffraction patterns of microcrystalline cellulose powders, namely, Avicel® PH-101, Grade X and Grade Y.

The correlation of the two techniques (i.e. XRD and W_{nf} determination), used to estimate the degree of crystallinity of the MCC powders, is illustrated in Fig. 6.3g. The plot illustrates that a linear relationship exists between the two sets of data with a good level of correlation (R^2 = 0.999). The relationship, however, is the inverse of what we expected i.e. a more crystalline material should have less amorphous regions, and hence less sites available for water to bind tightly, causing a decrease in the level of W_{nf}. In our case, however, the results indicate that in the more crystalline product, the level of 'non-freezable' water is higher than in the less crystalline products (Grades X and Y). The reason for this is probably related to the reduction in MCC powder particle size, creating a more tortuous matrix around which the water molecules must disperse. This can hinder the homogeneous distribution of water throughout all of the amorphous regions of the polymer, resulting in an underestimation of the actual amount of tightly bound water at the time of experimentation.

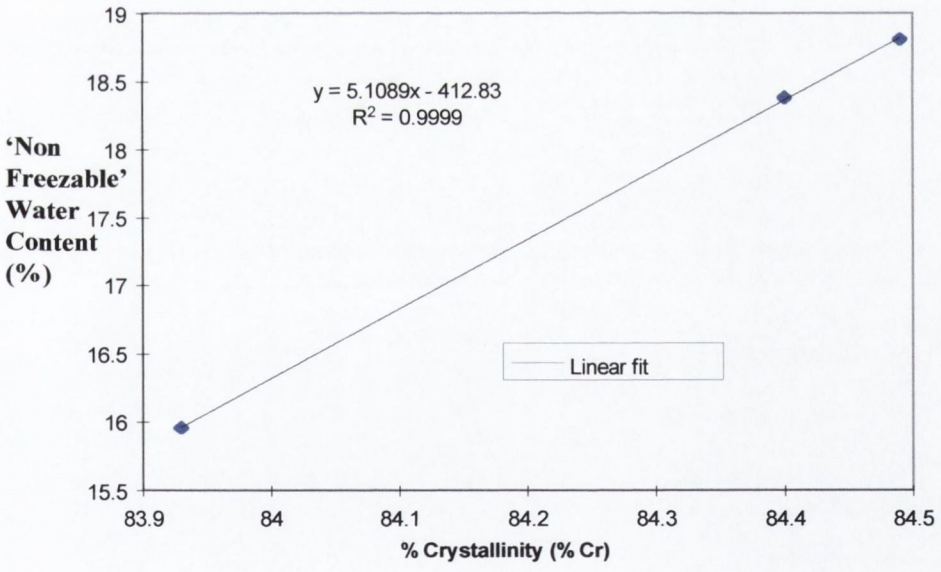

Figure 6.3g. Correlation plot between percentage 'non freezable' water content, determined form DSC data, and % crystallinity, determined from XRD data, for MCC powder samples.

As a result, if the W_{nf} results, obtained from DSC analysis, are to be directly correlated to powder crystallinity, suitable precautions must be taken to ensure similar equilibrium and non equilibrium factors apply to the different powders. Pouchly *et al.,* (1979), postulated that heavily hydrated samples may behave in a similar fashion to those with low water contents since, non-equilibrium kinetic factors such as reduced water diffusivity, steric constraints due to rigid polymer matrix, frozen bulk-like water and water coagulation, collectively influence the thermal response.

6.3.3.4 Determination of the Relative Amounts of 'Freezable' and 'Non-freezable' Water Content

The determination of the amount of 'freezable' and 'non-freezable' water, as a function of total water content per gram of polymer, provides insight into the dynamics at a molecular level, in particular the amorphous regions of MCC, where water activity is typically confined. Since the total water content is known from gravimetric measurements, the relative amounts of 'freezable' and 'non-freezable' water (in grams) can be computed by comparing the recorded endothermic heat change, H_{cal}, with the experimentally measured differential heat of fusion, ΔH_{endo}, since

$$W_c = (S_w/S_p) \times 100\% \qquad \textbf{Eqn. 3.3b}$$

$$S_f = (H_{cal}/\Delta H_{endo}) \qquad \textbf{Eqn. 3.3c}$$

$$W_f = (S_f/S_p) \text{ X } 100\% \ = (H_{cal}/\Delta H.S_p) \text{ X } 100\% \qquad \textbf{Eqn. 3.3d}$$

$$W_{nf} = W_c - W_f \qquad \textbf{Eqn. 3.3e}$$

where S_w and S_p are the weight in grams of water and the MCC polymer, respectively, H_{cal} is the total heat associated with the transition (integrated area of endotherm), W_c is the

water content per 100 grams of dry polymer (%), W_f and W_{nf} are the 'freezable' and 'non-freezable' water weight percentages respectively.

The 'freezable' water detected by DSC is charted as a function of water content, for the three MCC grades in Figs. 6.3h (I), (II) and (III). The important feature of these curves is that best fit analysis to the 'freezable' water component provides information regarding the interactions between water and the polymer. According to Nakamura *et al.*, (1981), if best fit analysis yields a straight line with a gradient $\approx 45°$, this suggests that there is no change in polymer morphology as the total water content is increased.

(I) Avicel® PH-101

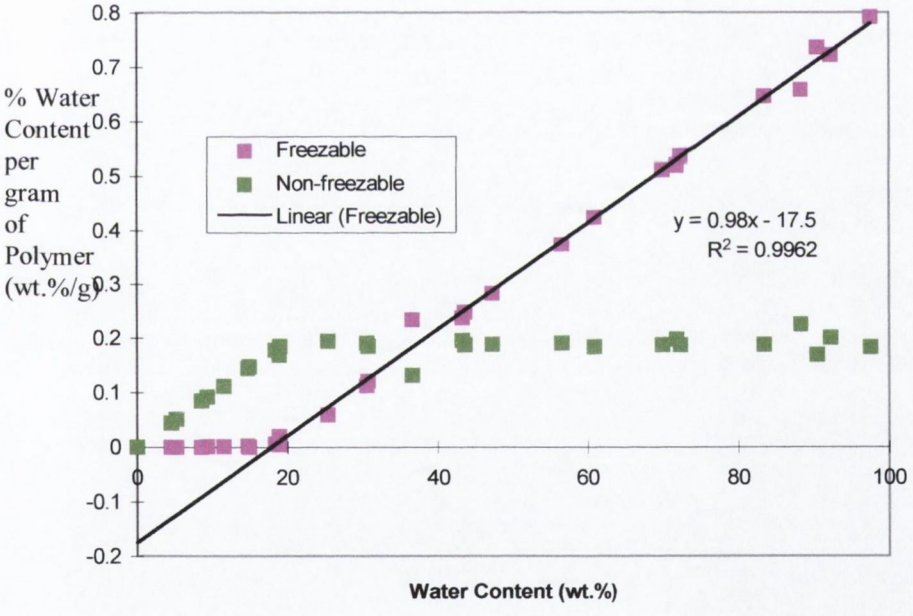

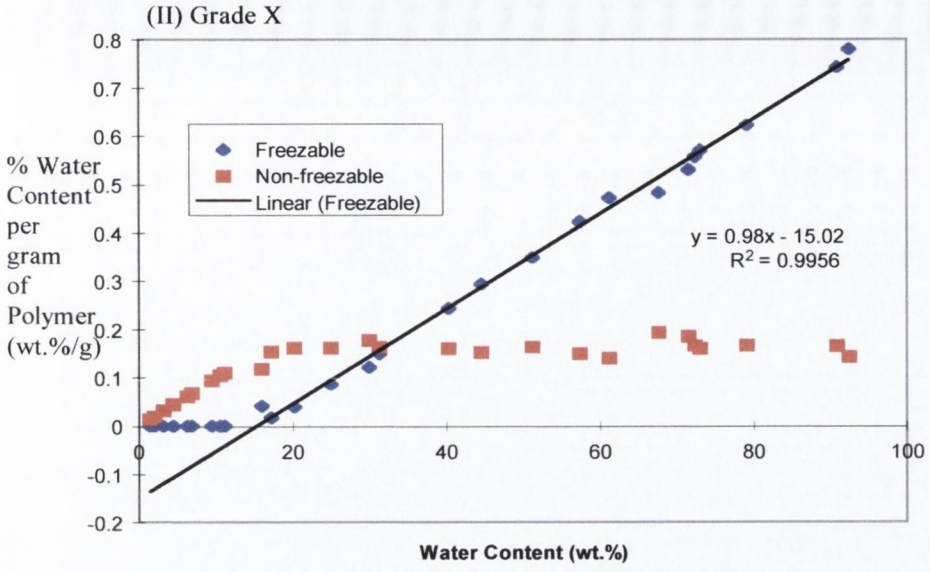

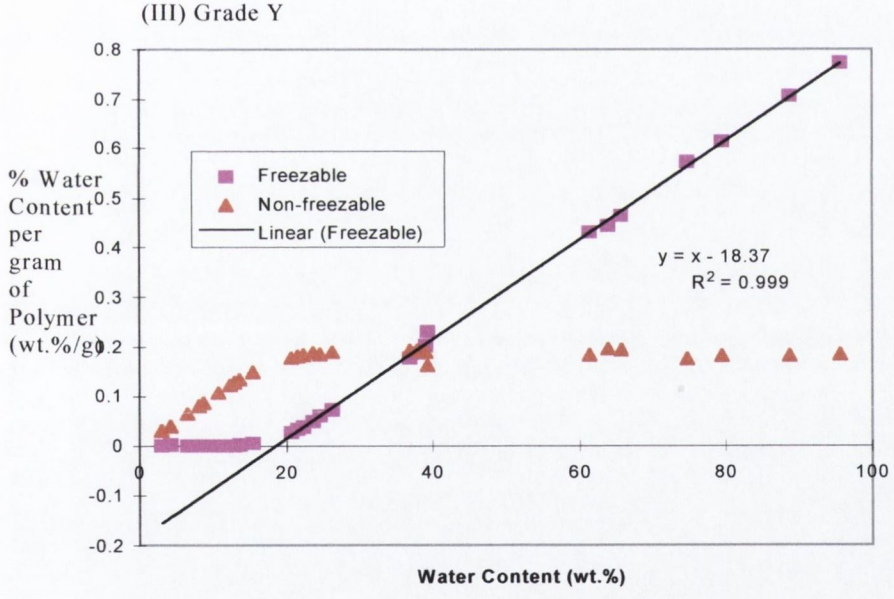

Figure 6.3h. Delineation of freezing and non-freezing water in the hydrated microcrystalline cellulose powder samples (Avicel® PH-101 (I), Grade X (II), and Grade Y (III), respectively) as a function of water content for the endothermic DSC data. A gradient of the freezing water data of 45° implies that no reorganisation of the amorphous/crystalline region occurs (see text). The regression fits to the 'freezable' water data, for the three powders, are listed in Table 6.3a.

As mentioned previously, XRD results indicated that the three MCC grades consisted of Type I native cellulose. This is further confirmed by the DSC data expressed previously in Figs 6.3h (I), (II) and (III). It is known that in the case of native Cellulose I, as it is wetted, it illustrates an increase in breaking strength (Hatakeyama, 1989), the effect of which is reversible. The effect is the opposite in Type II cellulose, the reason for which is that the amorphous region of the native cellulose becomes more ordered in the presence of water. However with regenerated cellulose, irreversible structural changes occur to the amorphous region. These structural changes result in an increase in the amorphous region, which is indicated by the increase in 'non-freezing' water content. In our case, it is evident from the above plots that the level of maximum 'non-freezable' water (W_o) remains constant, with increasing hydration levels, (or alternatively that best fit analysis to the 'freezable' water content yields a straight line with a gradient $\approx 45°$), confirming that the three MCC grades consist of Cellulose Type I.

6.3.4 Exothermic Analysis of Hydrated MCC Powders

Similar analysis was applied to the exothermic data results, as was conducted on the endothermic data. The cooling curves for the hydrated microcrystalline powder samples are illustrated in Figs 6.3i (I), (II) and (III). As in the case of the endothermic data, no exotherms are detected by DSC, for water concentrations below 18 to 20 wt.% approx., again indicating that any water present is tightly bound to the cellulose particles.

As the water levels increase, a broad, poorly resolved, low intensity peak (peak II) forms initially in the temperature range of -25 to -40°C. This peak represents the more loosely bound crystallizable water and is evident in the DSC exotherms for the three MCC powder samples. The peak shifts to higher temperature ranges with increasing amounts of adsorbed water. After a certain moisture level, a new sharp peak (peak I) appears. The shape and temperature range of peak I accords well with that for the freezing of pure

'bulk-like' water, as shown inset, although peak I is broadened slightly in the low temperature side, due to the influence of the loosely bound water. In the case of all three MCC powders, the magnitude of peak II is not very prominent. This is because the total bound water content approaches the 'non-freezing' water content, with increasing degree of crystallinity of samples, i.e. the level of loosely bound water decreases. Since our three powders are highly crystalline, the amount of loosely bound detectable water is low, and correspondingly the magnitude of peak II is low.

(I) Avicel® PH-101

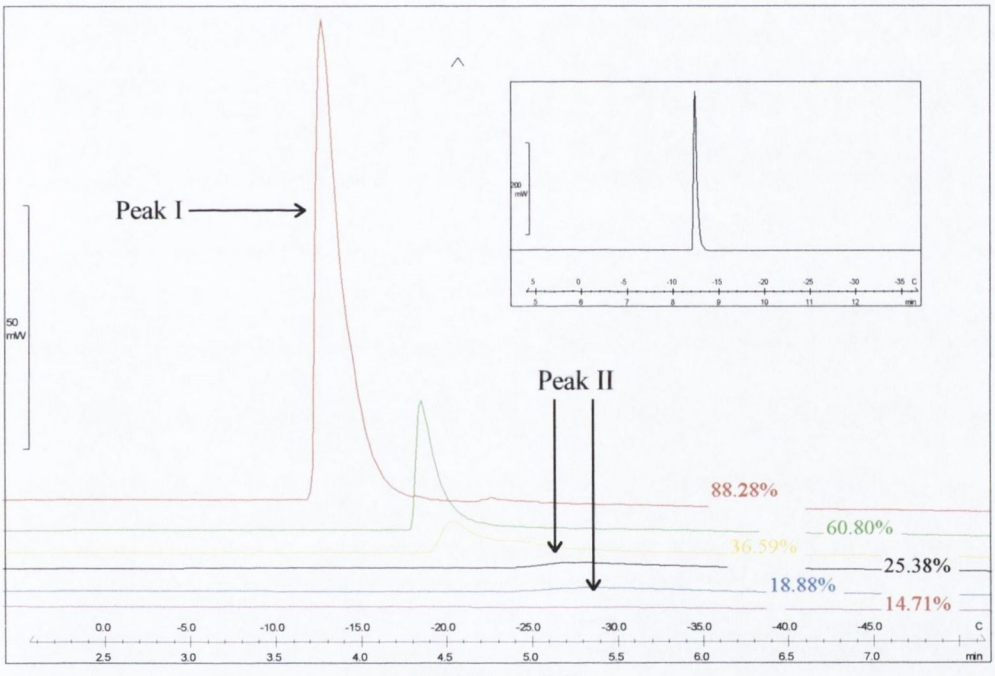

Temperature (°C)

(II) Grade X

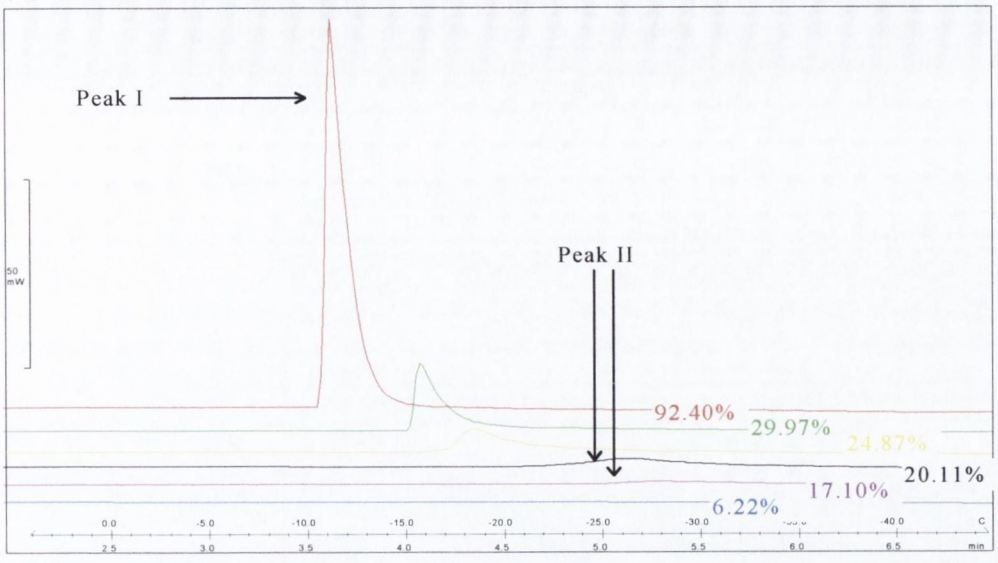

(III) Grade Y

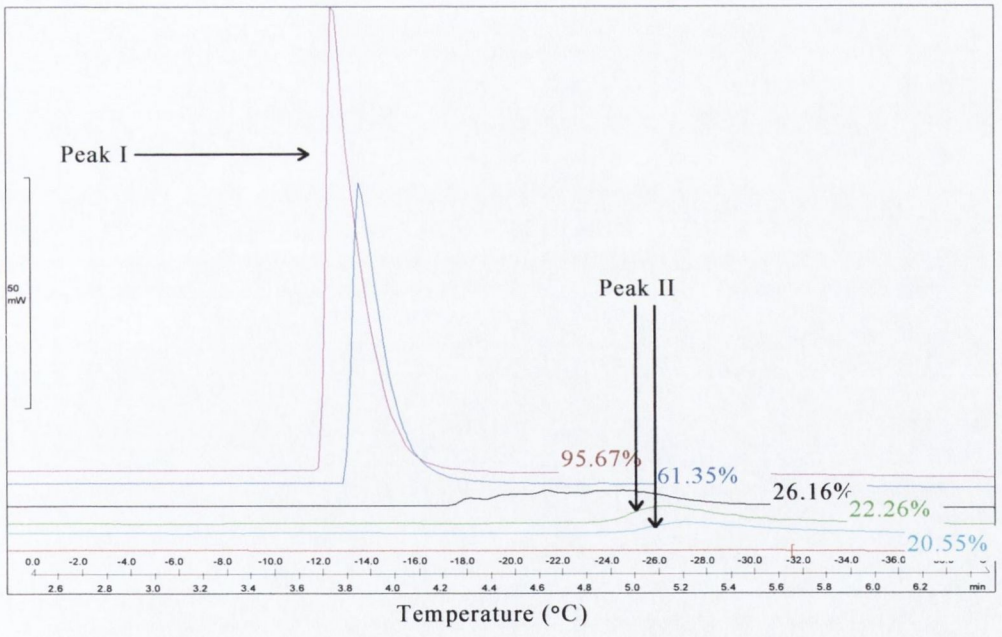

Figure 6.3i Typical DSC exotherms for hydrated MCC powder samples (Avicel® PH-101 (I), Grade X (II) and Grade Y (III), respectively) as a function of water content. The samples were heated at a rate of 10 K/min.

Similar to the observations of previous investigators, the exotherms are much sharper and correspond to smaller enthalpy changes compared to the endothermic behaviour. This is reflected by the lower calculated ΔH_{exo} values for the three microcrystalline cellulose powders, as illustrated in Table 6.3c.

Table 6.3c Calculated 'non-freezable' water contents, enthalpies, and regression fits to 'freezable' water data from the exothermic DSC results, for three MCC samples.

MCC Sample	'Non-freezable' Water Content (W_{nf}) (%)	ΔH_{exo} (cal/g)	Regression fit to 'Freezable' Water Data	Gradient of Curve (°)
Avicel® PH-101	17.74	76.69	$W_f = 0.98W - 17.22$	44° 25′
Grade X	15.37	70.53	$W_f = W - 15.36$	45°
Grade Y	17.14	77.11	$W_f = W - 17.14$	45°

(I)

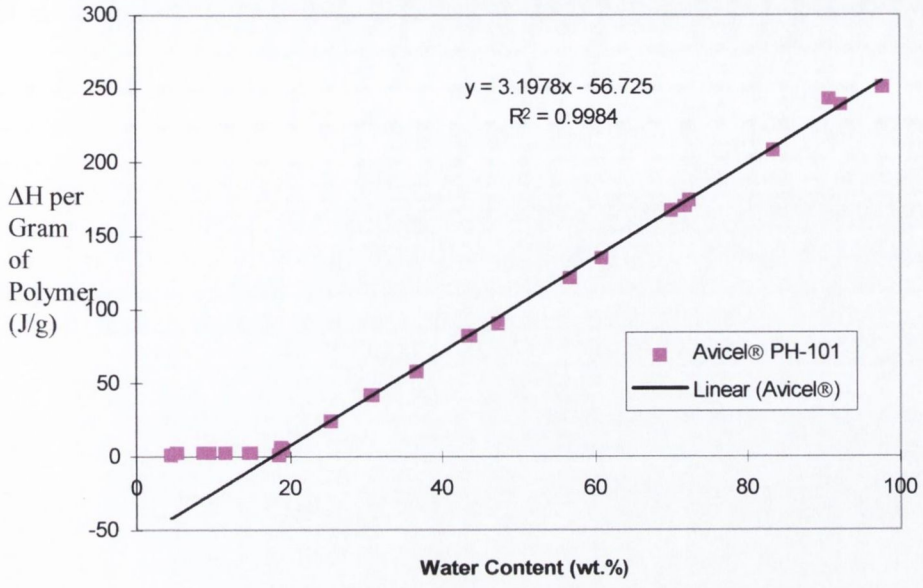
y = 3.1978x - 56.725
R² = 0.9984
ΔH per Gram of Polymer (J/g)
Avicel® PH-101
Linear (Avicel®)
Water Content (wt.%)

(II)

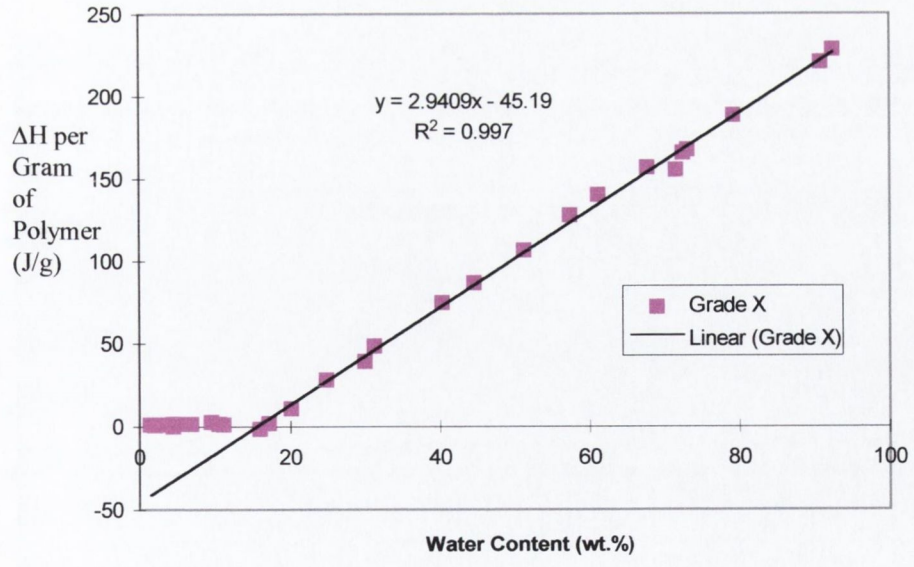
y = 2.9409x - 45.19
R² = 0.997
ΔH per Gram of Polymer (J/g)
Grade X
Linear (Grade X)
Water Content (wt.%)

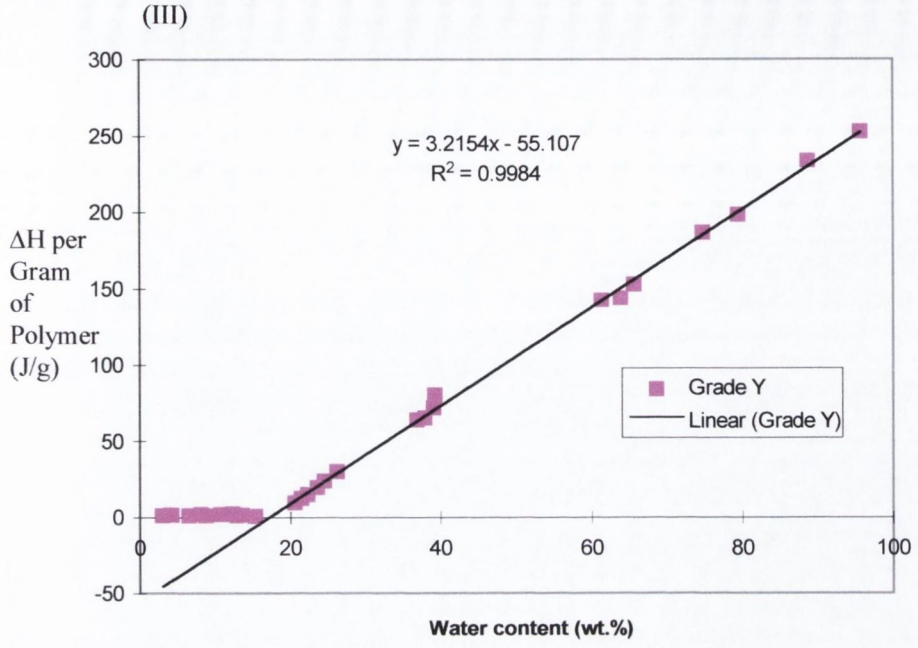

Figure 6.3j. Enthalpies per gram of polymer *vs.* water content for the exothermic data. The linear regression fits for Avicel® PH-101, Grade X & Grade Y are ($\Delta H = 3.1978W - 56.725$); ($\Delta H = 2.9409W - 45.19$) and ($\Delta H = 3.2154W - 55.107$), respectively.

As in the endothermic case, the integrated enthalpy changes for each peak per gram of polymer are plotted as a function of water content. The curves are displayed graphically above in Fig. 6.3j (I), (II) and (III). Plots of enthalpy changes per gram of water are plotted as a function of water, for the three MCC grades, and are illustrated in Appendix 5. The calculated estimates, for the bound water levels present in each polymer, are listed in Table 6.3c. The calculated 'non-freezable' water contents for Avicel® PH-101, Grade X and Grade Y are 17.74%, 15.37% and 17.14% respectively. When compared to the respective values, determined for each powder using the endothermic data, all are lower. In addition, the calculated mean integrated changes in enthalpy, ΔH_{exo},, are also lower for each powder sample, than the enthalpy changes over the heating cycle. This agrees with previous literature studies (Quinn *et al.,* 1988). It can be explained due to the phenomenon that supercooling terminates in rapid nucleation, inducing a greater change in

heat capacity to which DSC is sensitive (Coyle *et al.*, 1996). This in turn, also accounts for the slightly lower estimates of the 'non-freezable' water in the exothermic data. This lower differential heat of fusion over the cooling cycle is consistent with the significantly depressed freezing point (ie ΔT_m = 14 - 21°C), which is clearly evident from the exothermic plots, illustrated in Figs 6.3i (I), (II) and (III). A low heat of fusion and a corresponding low freezing point imply a much more dispersed water phase, (Quinn *et al.*, 1988). Corresponding plots of percentage 'freezable' (W_f) and 'non-freezable' (W_{nf}) water contents, per gram of polymer, in the hydrated MCC samples are presented as a function of total water content in Figs 6.3k (I), (II) and (III).

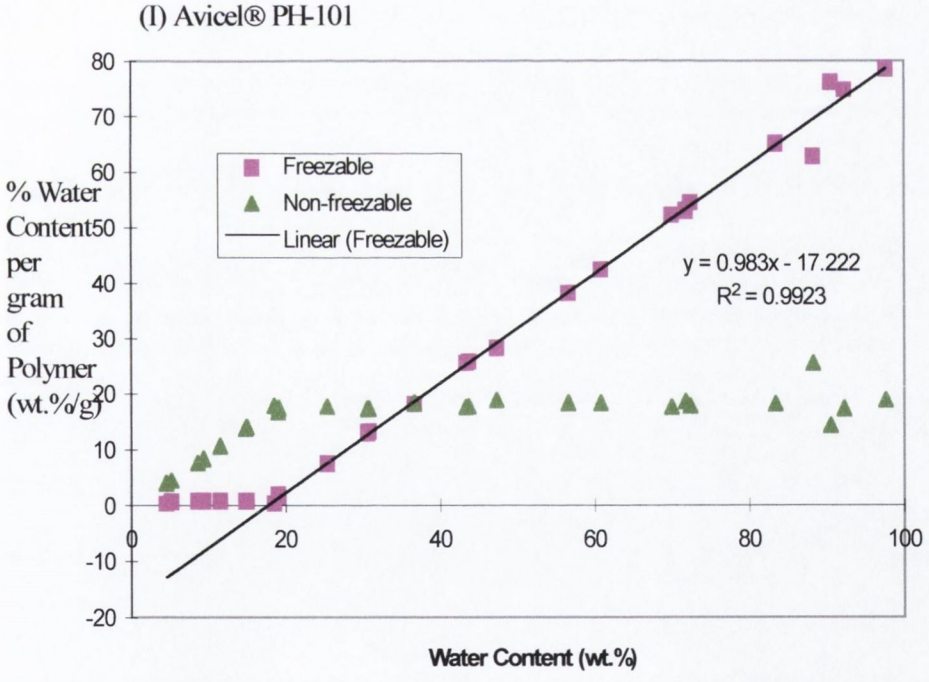

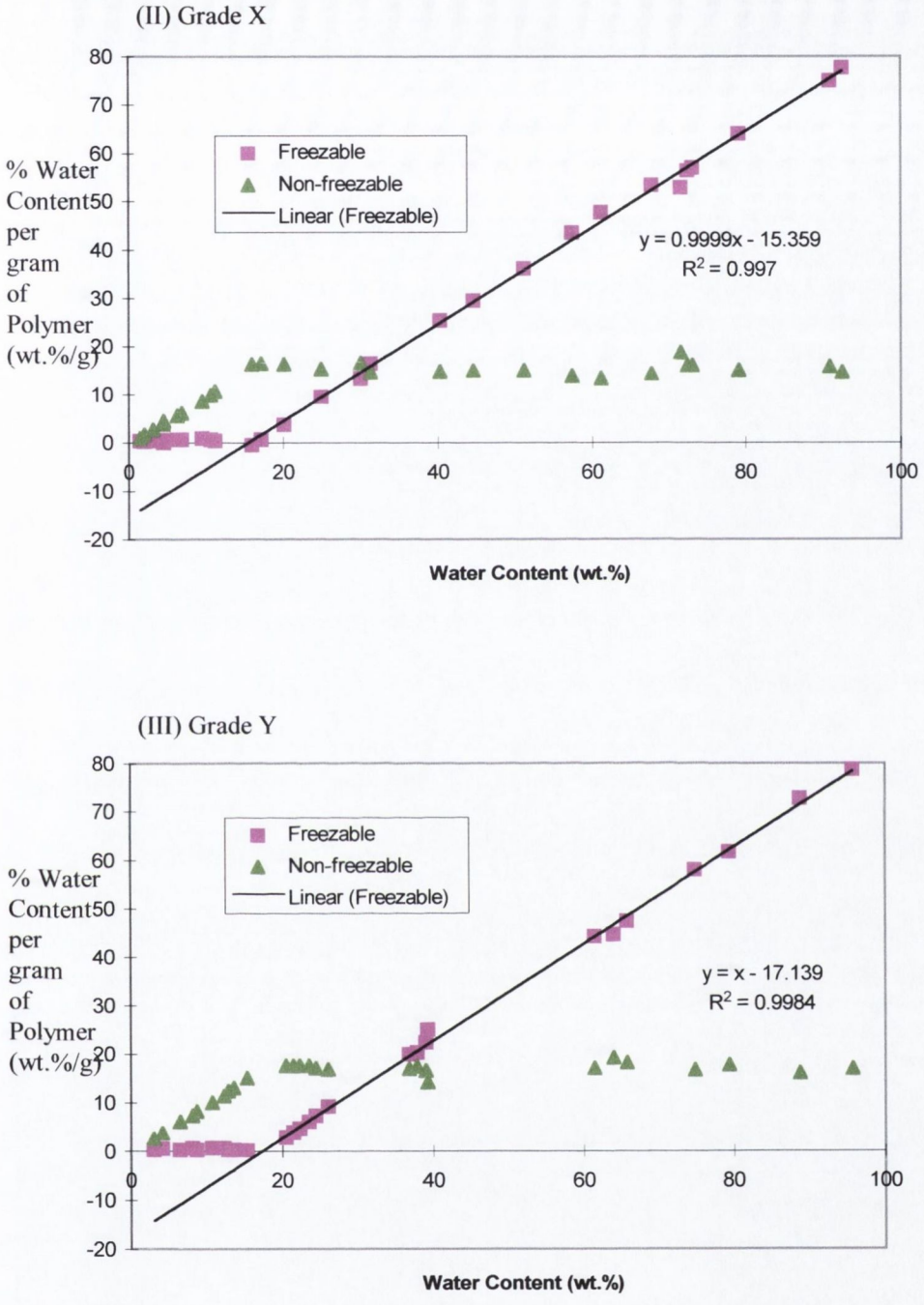

Figure 6.3k Delineation of freezing and non-freezing water in the hydrated microcrystalline cellulose powder samples (Avicel® PH-101 (I), Grade X (II) and Grade Y (III), respectively) as a function of water content for the exothermic DSC data.

6.3.5 CONCLUSION

It is appropriate to conclude from the DSC results that, when water interacts with the three MCC grades, three kinds of adsorbed water exist, i.e. 'nonfreezing' water, loosely bound freezing water and 'bulk-like' free water, the former two arising due to the interaction of polymer molecules and water. The 'non-freezing' tightly bound water illustrates no first order transition and hence, would appear to have no crystalline structure, perhaps supporting the theory of Goring and coworkers (1965, 1978), that the water structure is disrupted by the presence of the polymer.

According to the literature (Nakamura *et al.,* 1981), both bound water and 'non-freezing' water contents decrease with increasing degree of crystallinity of the cellulose samples. The reverse was evident in the case of the three MCC polymer grades, suggesting that the above observation applies to situations where the powders are examined under similar conditions, in terms of particle size and presence of other adjuvants. These factors affect parameters such as powder bed porosity, tortuosity and wettability, and can introduce stearic hindrances affecting uniform water diffusivity around individual polymer particles. In all three cases, evidence indicated the presence of a very dispersed water phase.

Estimation of the 'non-freezing' water ranged from 16% to 18.89% approx. for the MCC grades, when using the endothermic data, and from 15.37% to 17.74%, when the exothermic data was used. According to Blair *et al.* (1990), a 1:1 binding stoichiometric ratio exists (i.e. one molecule of water binds to one anhydroglucose binding site), when the level of tightly bound water approximates 19%. This would indicate that this binding stoichiometry has been achieved with our three MCC grades. This coincides with the proposed 3 stage binding model involving (1) the water binding tightly to anhydroglucose units and indeed linking adjacent units (i.e. 2 hydrogen bonds per water molecule corresponding to 10% w/w water approx.); (2) the breaking of some of the initial bonds formed between water and cellulose and addition of extra water molecules to bind at the now vacant anhydroglucose sites (19% w/w approx.). Since the samples were hydrated

for a sufficiently long period of time (ie > 1 week), before DSC analysis, this process would have proceeded almost fully to the 1:1 stoichiometry, as observed. The enthalpy associated with the breaking of bonds required to progress from a 1:2 to a 1:1 stoichiometry explains the mixing enthalpy, as observed by Pouchly *et al.,* (1979), and hence, why the associated overall enthalpies are lower than the corresponding transitions in pure bulk water. The third rapid step in the adsorption process is the onset of hydrogen bonds between water molecules (i.e. within loosely bound and 'bulk-like' water).

Chapter 7

Pharmaceutical Applications of Novel Size Reduced Grades of Microcrystalline Cellulose

(I) TABLETING APPLICATIONS

7.1 INTRODUCTION

Many uses have been suggested for microcrystalline cellulose (MCC). The largest present use is in tableting of pharmaceuticals. Here MCC is used as an excipient to assist in the flow, lubrication and bonding properties of the ingredients to be tableted, to improve the stability of the drugs in tablet form, to give rapid disintegration of the tablet in the stomach of the user and to facilitate quick bioavailability of the drug. As such MCC is widely used as a direct compression base to aid tablet production, either alone or in combination with other bases.

Four different batches of tablets were produced using the following general formula:

Paracetamol (granular)	55.1%
MCC grade	44.7%
Stearic acid	0.2%

The four batches differed with respect to the grade of microcrystalline cellulose incorporated. Two batches contained currently available pharmaceutical grades of MCC i.e. Avicel® PH-101 and PH-102, whereas the second two contained a modified grade of

Avicel® PH-101 that was homogenised as a slurry and then spray dried either in the absence or presence of SLS. The latter two experimental grades are referred to as MCC Grade X (no SLS) and MCC Grade Y (1% SLS) for convenience, the physical properties of which were examined previously in Chapter 6.

100 g powder mixtures were produced for each batch using the aforementioned formula. The powdered materials were blended together in a cube mixer for 15 min at 40 rpm. Then the powder was immediately compressed to minimise the risk of segregation. Compression was achieved, using a Manesty single punch hand operated tablet press (Model 1B 179) fitted with a 12.5 mm flat-faced punch and die set. The tablet press was initially adjusted to produce a constant compression weight of approx. 550 mg (approx. 300 mg Paracetamol), using the batch containing Avicel® PH-101. The average breaking strain was adjusted to the equivalent of approximately 10 Kp units. The adjusted die cavity depth and compression level were kept constant during the compression of all four powder batches.

7.2 RESULTS AND DISCUSSION

7.2.1 Uniformity of Weight and Thickness

The results illustrated in Tables 7.2a and 7.2b suggest that the incorporation of Avicel® PH-101 into powder blends imparts the ability to produce tablets, which are very uniform in terms of both weight and thickness. When the MCC grade is replaced by Avicel® PH-102, again very reproducible tablets are produced in terms of uniformity of weight and thickness, but their average weight is slightly lower. The F test indicates that their long run standard deviations are identical and there is no statistically significant difference in weight uniformity, as validated using the student's t-distribution with 38 degrees of freedom.

Table 7.2a. Uniformity of weight of paracetamol tablets, prepared by different direct compression bases (mean of 20 tablets weighed individually).

Vehicle	Average (g)	S.D.	C.V.%
Avicel PH 101	0.5543	0.0122	2.2
Avicel PH 102	0.547	0.0107	1.96
Test Grade X	0.4993	0.0441	8.83
Test Grade Y	0.5331	0.0317	5.95

Table 7.2b. Uniformity of thickness of paracetamol tablets, prepared by different direct compression bases (mean of 20 tablets determined individually).

Vehicle	Average (mm)	S.D.	C.V.%
Avicel PH 101	3.82	0.041	1.07
Avicel PH 102	3.83	0.023	0.60
Test Grade X	3.56	0.104	2.92
Test Grade Y	3.71	0.076	2.05

The reason for this slight decrease in weight may be the fact that Avicel® PH-102 has a larger, average, particle size of roughly twice that of PH-101, i.e. it is coarse. FMC Company literature states that Avicel® PH-101 has a typical average particle size equal to 50 μm, whereas Avicel® PH-102 has a typical size of 100 μm. Hausner (1981) explains that, when a powder mass consists of fine particles, pores between particles will be fine and vice versa. According to the work of Le Thiesse (1989), the overall porosity of Avicel® PH-102 is essentially inter-particulate (pore diameters between 10 and 100 μm). Due to the larger porosity in the PH-102 grade, it will have a lower bulk density and hence, comparable volumes of powders will result in compressed tablets with reduced weights.

In the case of the two new experimental grades (i.e. MCC Grades X and Y), they illustrated poorer potential or capability for producing tablets of uniform thickness and

weight. The average weight and thickness of the tablets for each were well below that of the tablets formed, using the previously mentioned commercial grades. In addition, their standard deviations and coefficients of variation are significantly greater. This related mainly to their poor flow properties. This is in agreement with Aboutaleb *et al.*, (1996) who state that weight and thickness variation of produced tablets are a function of the powders flowablilty. Particle size analysis of these grades, using the Malvern, indicates that their size is significantly lower with an average value of 10 μm approx., as opposed to 50 μm and 100 μm approx. for Avicel® PH-101 and Avicel® PH-102 grades, respectively. It is well known that the flow properties of MCC powders are closely related to their particle size. In general the smaller the particle size, the poorer the flow properties, which explains the above observation. Patel *et al.* (1994) stated that by increasing the size of the microcrystalline cellulose particles, which tend to interlock because of their needle like shape, their flow properties can be improved. It was to redress this problem of relative poor flowability that FMC Corp. developed the larger particle size product (Avicel® PH-102).

Of the two test grades, i.e. MCC Grade X and Y, Grade Y appears to be the better. This differs from the other, due to the incorporation of 1% SLS before the spray drying step in its production. The inclusion of SLS results in the production of tablets with an average weight and thickness, that are closer to the average values obtained for tablets containing the two commercial grades of MCC. In addition, the coefficients of variation for uniformity of weight and thickness are smaller for the batch of tablets produced using the Grade Y powder. Thus, SLS would appear to enhance the flowabiliy of the Grade Y powder, which has essentially the same particle size as Grade X. This may be due to SLS coating and reducing static effects within the powder.

7.2.2 Mechanical Properties of Tablets - Hardness/Friability

The mechanical properties of the tablets produced were tested. The results are shown in Tables 7.2c and 7.2d. From the obtained results, it is clear that Avicel® PH-101 and PH-

102 produced the hardest tablets of all four batches. Although the mean hardness differed, this did not prove to be statistically significant, again confirmed using the student's t-test with 18 degrees of freedom. The average hardness values for MCC Grades X and Y were lower and the coefficients of variation were much greater, especially in the case of Grade X (no SLS). This is again a reflection of poor flow properties, which, as previously discussed, resulted in consistently lower average tablet weights. Lower tablet weights translate directly to less powder being present within the die cavity, at the time of compression, and hence less compression force is exerted on the lesser amount of powder, during compression under constant conditions. Since tablet hardness is related to the compression force, overall tablet hardness will be lower. The large coefficients of variation indicate that these grades do have the potential to produce hard tablets, if sufficient powder is present in the die cavity during compression. Problems arose also during the compression of these new grades, in terms of die sticking. The fineness of these powder grades was mainly responsible, allowing some of it to seep down into the gap between the die and the lower punch wall, causing additional friction and sticking. The friability results obtained confirmed those of hardness. Avicel PH-101 and PH-102 tablets produced the lowest friability values, while those incorporating Grades X and Y produced the highest values. For all grades, however, only one reached values of friability considered unacceptable (>1%, BP, 1998). Tablets produced, using Grade X MCC powder, had an average friability value of 1.08%. This reflects the low hardness values for these tablets, which have been explained previously in terms of the poor flow properties of this MCC powder grade.

Table 7.2c. Uniformity of hardness of paracetamol tablets, prepared by different direct compression bases (mean of 10 tablets).

Vehicle	Average (Kp units)	S.D.	C.V.%
Avicel PH 101	10.61	1.26	11.9
Avicel PH 102	11.29	1.56	13.8
Test Grade X	7.67	3.89	50.7
Test Grade Y	8.68	2.86	32.9

Table 7.2d. Friability percentage loss of paracetamol tablets, prepared by different compression bases (mean of 3 determined using 20 tablets).

Vehicle	Average (%)	S.D.	C.V.%
Avicel PH 101	0.87	0.19	21.8
Avicel PH 102	0.79	0.11	13.9
Test Grade X	1.08	0.21	19.4
Test Grade Y	0.90	0.34	37.7

7.2.3 Compression Force / Tensile Strength Profiles

The tensile strength of compacts was measured, using the method of diametral compression of round compacts, as previously described. 400 mg samples of the four grades of MCC were compressed to form compacts, using an IR press, at pressures of 1000, 2000, 3000, 4000 and 5000 Kg. The plots of the tensile strengths of the tablets, for the four MCC grades *vs.* the compression forces used in their production, are illustrated in Fig. 7.2b.

It is evident from Fig. 7.2a that the tensile strength of all tablet compacts increases very rapidly, at low compression forces, irrespective of the MCC grade used. This is a characteristic of MCC and is one of its main advantages as a direct compression base. According to Company literature, when using Avicel®, tablets can be made harder, with lower pressures and with less increase in disintegration time, than with other excipients. In all cases a maximum tensile strength is achieved with increasing compression force. The profiles for grades Avicel® PH-101, PH-102 and MCC Grade X are very similar. The tensile strength of tablets containing PH-102 are slightly better than those incorporating PH-101, which, as Landin *et al.* (1993) suggested, is due to the greater inter-particulate bonding within the PH-102 grade. This also is in keeping with the results of Stanley-Wood, (1987), where they showed inter-particulate bonding to be greater for PH-102.

An important feature of Fig. 7.2a is that the maximum tensile strength of compacts, containing MCC Grade Y, is significantly lower than in the other cases. This may be explained by the fact that the SLS, which is in close association with the MCC particles (achieved by the spray-drying technique), imparts lubricant properties to the tablets. Much work has been performed to determine the exact mechanisms by which pharmaceutical materials bond together. For pharmaceutical tablets, three types of bonds are normally considered (Fuhrer, 1977) - solid bridges, mechanical interlocking and intermolecular forces over long distances. Intermolecular forces are believed to be the dominating bonding mechanism.

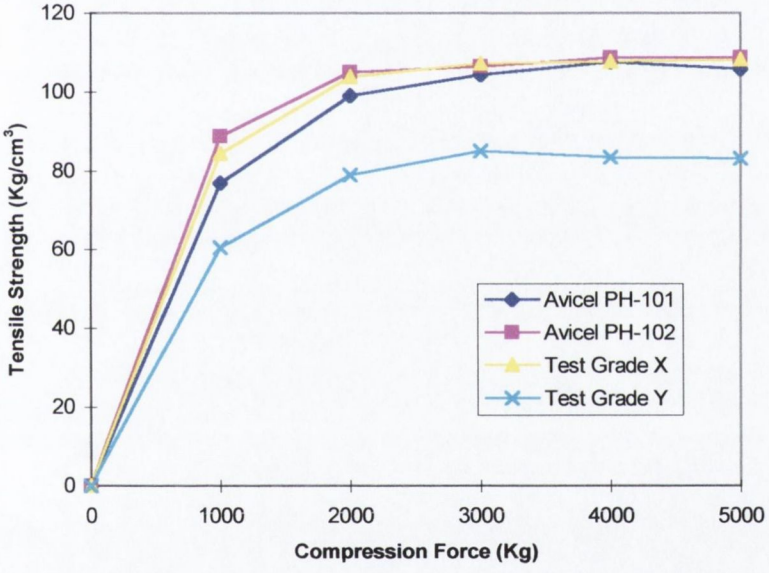

Figure 7.2a The tensile strength of tablets of four grades of microcrystalline cellulose as a function of compression force (mean of 6 determinations).

The presence of SLS produces weakened bonding between the host (MCC) particles, because the strongest bonds are formed between clean surfaces, i.e. weaker bonds result, after compression, between lubricant - lubricant molecules rather than the stronger excipient - excipient bonds (De Boer *et al.*, 1978).

The presence of lubricants also generally result in reduced penetrability of water in tablets and hence, increased disintegration times. This is because most lubricants are hydrophobic in nature. SLS, however, does not illustrate this property and in fact, reduces disintegration times relative to MCC Grade X, due to its surfactant properties which enhance water penetration.

7.2.4 Disintegration Testing of Tablets

Paracetamol tablets, prepared with all four grades of MCC, complied with the BP (1998) disintegration test. In fact, the disintegration times for all tablets, representing the four batches, were less than a minute which is very much shorter than the limit of fifteen minutes given in the BP (see Table 7.2e). Such results may be explained on the basis that the plastically deforming material, Avicel®, acts as a disintegrant. These disintegration properties in water have been attributed either to capillary action (Lerk *et al.*, 1979), or swelling (Carmella *et al.*, 1984a; Carmella *et al.*, 1984b; Ek *et al.*, 1995). Despite this, the two experimental grades did not show any improvements over the two commercial grades, and were slower to disintegrate on average. The disintegration times were also more variable for these experimental grades (evident from the large C.V. values), which is related to the variability in tablet hardness. Tablet disintegration is reduced in water, due to high crushing strength or tablet hardness.

Table 7.2e. Disintegration times of paracetamol tablets, prepared by different direct compression bases (mean of six determinations)

Vehicle	Average (s)	S.D.	C.V.%
Avicel PH 101	13	0.75	5.8
Avicel PH 102	13	0.54	4.3
Test Grade X	30	10.67	40.0
Test Grade Y	27	5.76	19.2

7.2.5 Drug Content Uniformity

The drug contents of the Paracetamol tablets prepared are shown in Table 7.3f. It was found that the average drug content for the tablets of all four batches passed the limits of

the BP (1998), which states that drug content must be between 95-105% of the stated amount. The standard deviations calculated for the two novel grades were lower than those for the commercial grades (Avicel® PH-101, PH-102), with respect to uniformity of content of active ingredient. This may be due to the drug mixing more uniformly with the novel size reduced grades, with less segregation occurring, due to differences in powder particle size.

Table 7.2f. Uniformity of content of active ingredient of paracetamol tablets, prepared by different direct compression bases.

Vehicle	Average (%)	S.D.
Avicel PH 101	100.14	4.28
Avicel PH 102	103.3	1.24
Test Grade X	104.6	1.3
Test Grade Y	104.98	0.84

7.2.6 Dissolution Testing

The obtained dissolution data is plotted in Fig. 7.2b The figures represent the plot of cumulative drug release % versus time in min.

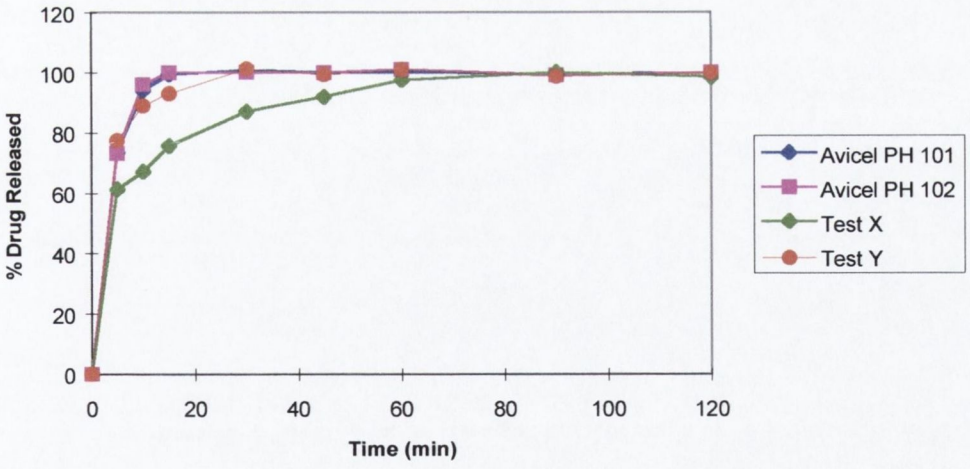

Figure 7.2b. Dissolution profiles of paracetamol tablets prepared using different direct compression bases, in McIlvaine buffer solution pH 6.8 at 37°C.

Dissolution results revealed that the dissolution rate is affected by the grade of MCC that is incorporated within the tablets. Tablets prepared with Avicel PH-101 and PH-102 showed the highest dissolution rate of all four batches. In fact, the dissolution curves for tablets produced using these commercial grades are virtually superimposable. The two experimental grades hindered the dissolution rate relative to PH-101 and PH-102. MCC Grade X hindered drug release the most, which may be due to the fact that reduced particle size may reduce porosity in the compressed tablet. This reduced porosity will then reduce capillary action, thus hindering the penetration of dissolution medium into the tablet. The dissolution profiles for the tablets composed of Grade Y were slightly faster, which may be due to the wetability effects of SLS, thereby enhancing water penetration and drug dissolution.

7.3 CONCLUSION

Overall, from these experiments and results, it is apparent that the two experimental grades of MCC are actually worse in a tablet application, compared to the two currently available commercial grades. The main drawback of these powders, for this application, is related to their poor flow properties, which are a function of the reduced powder particle size. Poor flow properties hinder consistent uniform filling of the die cavity, resulting in lower and more variable tablet weight and thickness. Variability in these physical parameters is reflected by similar variability in the mechanical properties, such as tablet hardness and friability and in other areas, such as disintegration, dissolution and uniformity of content.

However, it is apparent from the dissolution data that these new grades may have a useful application in sustained release technology, possibly involving extrusion-spheronisation. This is examined in more detail in the next section.

(II) APPLICATIONS IN EXTRUSION/SPHERONIZATION

7.4 INTRODUCTION

As well as examining the applications of novel size reduced grades of microcrystalline cellulose (MCC) in tableting, we decided to examine the feasibility of using these novel grades as extrusion-spheronization aids or enhancers. MCC has been studied extensively and employed widely as a spheronization enhancer, where it facilitates the production of spherical pellets. Spheronization enhancers are considered a requirement for effective spheronization, as they not only impart plasticity to the formulation, but they also impart binding, that is essential for maintaining pellet integrity and strength. Fielden *et al.* (1992), reported that MCC was a necessary ingredient for aqueous extrusion-spheronization, due to its ability to absorb and retain large volumes of water, despite the application of high pressures, and to control the movement of water through the plastic mass during processing. The grade and brand of MCC available can influence the quality of pellets prepared by extrusion-spheronization (Newton *et al.*, 1992).

It was recently reported by Deasy and Law (1997), that pelletized formulations of indomethacin, prepared using extrusion-spheronization technology with the incorporation of sodium lauryl sulphate (SLS), surprisingly had reduced drug release. The cause of this anomalous result was shown, by solubility studies and scanning electron microscopy, to be related to the ability of the wetting agent to promote fragmentation into small crystallites of the MCC used as spheronization aid, thus retarding drug release, due to an enhanced matrix effect.

Based on the above observation, our novel size reduced grades of MCC should similarly result in a more sustained drug release effect, due to the greater matrix effect created by the smaller particles. Seven novel grades were examined, in addition to Avicel® PH-101, which was used as a control. The seven novel grades were size reduced via ultrasonic homogenisation (using 5 cycles), as described in Chapter 5. The various grades differed by the presence or absence of three different de-aggregating agents, namely SLS, Sodium

citrate (NaCit), and Sodium hexametaphosphate (NaHMP), which were present at various concentration levels relative to the MCC content, as listed in Table 7.4a.

Table 7.4a. Grades of MCC used in the extrusion/spheronization experiments. The Table illustrates whether the MCC was size reduced and which de-aggregating agents were present.

Powder I.D. Key	MCC Size Reduced	SLS	NaCitrate	NaHMP
Control	No	-	-	-
SRP	Yes	-	-	-
SRP A	Yes	6.25%	-	-
SRP B	Yes	-	-	6.25%
SRP C	Yes	-	6.25%	-
SRP D	Yes	12.5%	-	-
SRP E	Yes	-	-	12.5%
SRP F	Yes	-	12.5%	-

SLS was chosen on the basis of the observation mentioned previously by Law *et al.*, (1997). NaCit and NaHMP were chosen for similar properties, i.e. NaCit has been used as a peptising agent for bentonite in Calamine lotion and NaHMP, (also known as Graham's salt), possesses dispersing and de-flocculating properties (Merck, 1996). The results of studies described in Chapter 5 illustrate that the above three agents allow for the recovery of a size reduced grade of MCC (10 μm approx.), without particle re-aggregation occurring.

The general formula, listed in Table 7.4b, was used to manufacture the pellet formulations, using extrusion-spheronization technology. The formulations were prepared, using three different moisture contents for each grade of MCC, in order to ascertain the moisture content for optimal pellet formulation. A primary aim of the work was to prepare formulations which gave pellet yields greater than 70%, as anything lower than this would be economically unacceptable for commercial reasons. The moisture levels used were 30%, 32% and 34%. These values were chosen on the basis of preliminary experiments and the application of Equation 4.1, which estimated optimal water content to be 32% approx.

Table 7.4b. General formulation used for preparing pellets by extrusion/spheronization.

	Indomethacin	MCC/De-aggregating agent combination	Lactose
per 60 g powder mix	30% 18 g	30% 18 g	40% 24 g

7.5 RESULTS AND DISCUSSION

7.5.1 Effect of Moisture Content on Pellet Yield

The effect of moisture content on pellet yield for each formulation is illustrated in Figs. 7.5a (i), (ii) and (iii). Optimal pellet yields arose for all grades of MCC, within this moisture range, but the exact level differed slightly, as will be discussed later.

(i)

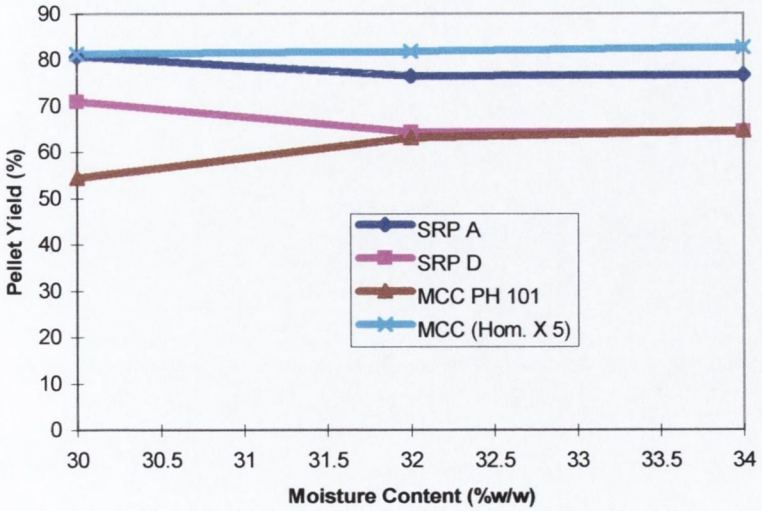

(ii)

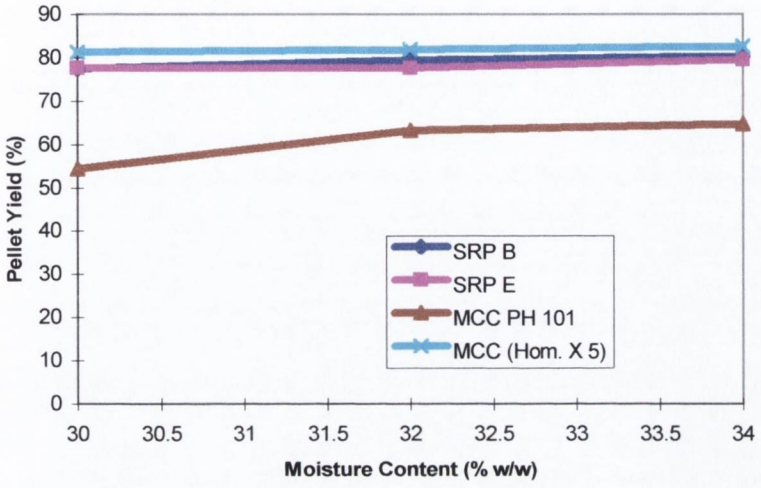

(iii)

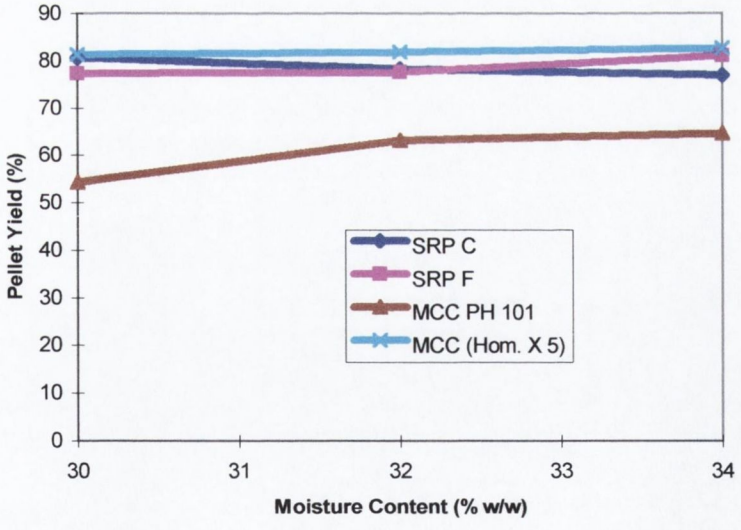

Figure 7.5a. Plot of the effects of water content on the yield of pellets, keeping spheronization time and speed constant at 10 min and 1250 rpm respectively. The key represents the identity of the formulations (Table 7.4a).

All formulations, under optimal levels of hydration, were capable of producing pellets with yields in excess of 70%, with most capable of producing pellet yields greater than 80% (see Fig. 7.5c). The main exception to this trend were the pellets produced using the control MCC grade, Avicel PH-101®, where maximum yields were 65% approx. Therefore, the novel MCC grades all resulted in an improvement in pellet yields relative to the control. The primary difference, between the novel MCC grades and the control MCC grade, is particle size. Avicel PH-101® has an average particle size of approx. 50-60 μm (Company literature), whereas Malvern analysis of the novel grades indicated the particle size to be much smaller (i.e. 10 μm approx.). Hence, it can be concluded that the reduction in particle size is primarily responsible for the increased pellet yields. This may be due to the change in intra-particulate porosity arising from size reduction. Fielden *et al.,* (1992), performed studies investigating the effect of different grades of lactose in formulations consisting of MCC and either coarse (118.0 μm) or fine grade (18.0 μm) lactose. Their ability to spheronize and also their sensitivity to moisture content were examined. Their results indicated that the pellets produced using the finer grade were less sensitive to moisture content, whereas the moisture content of the wet powder mass containing coarse lactose was shown to be critical. The results from this work seem to illustrate similar behaviour for MCC, i.e. the novel size reduced grades are less sensitive to the moisture content than the original Avicel PH-101® grade.

Despite the above, an optimal moisture content of 34%, in the case of formulations containing MCC powders SRP C, D, E, and F and 30%, in the case of formulations containing SRP A and D, was evident. This implies the existence of a 'specific moisture content level', unique to a wet powder mixture, at which optimal spherical pellets are yielded, which was observed similarly by Fielden *et al.,* (1992). They explained this phenomenon in terms of the Powder Saturation Model of Newitt and Conway-Jones, (1958), which is equally applicable to this scenario. This model suggests that the degree of moisture present in, and at the surface of, an extrudate is important, and if this level is below a specific moisture range, excessive levels of fines will be produced, whereas if

greater than this range, excessive agglomeration and large pellets are formed. This phenomenon was confirmed from our results which indicated that, as the moisture content exceeded the optimal level, the levels of large pellets increased (e.g. pellet formulations SRP A, SRP D, etc), whereas lower moisture contents resulted in a decrease in the production of large pellets, but a greater tendency to produce fines. This is illustrated for formulation SRP D, in Fig. 7.5b.

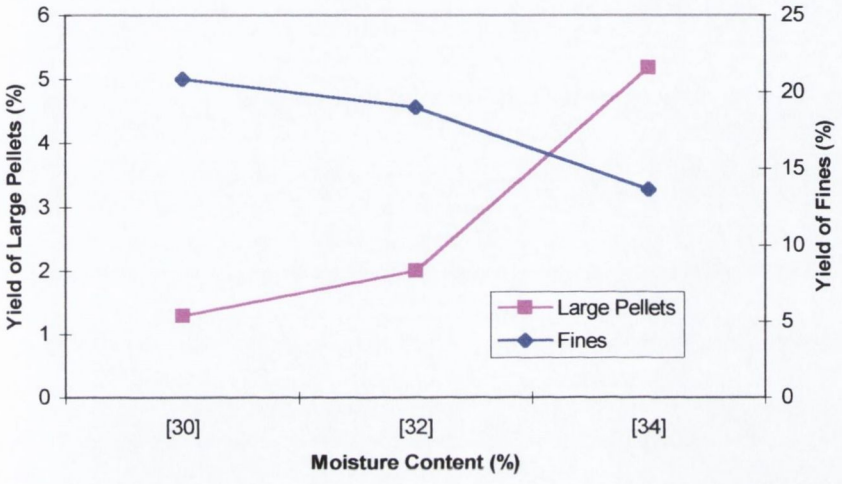

Figure 7.5b. Effect of increasing the hydration level on the yield of fines and large pellets prepared by extrusion/spheronization, for formulation SRP D.

Below the specific moisture content range, the particles in the wet powder mass are held together by discrete bridges at each point of contact in the pendular or funicular state. Satisfactory extrusion of such dry systems is unlikely, since excessive pressure is required to consolidate the material in order to remove the air voids. Extrudate, which is in this low state of saturation is brittle, will shatter generating a large quantity of fines, when broken up on spheronization and will have insufficient plasticity to form spheres. Addition of more water to the system allows the formation of bonds, which increases the tensile strength of the granule, as the mechanism of bonding changes to the capillary state. This degree of saturation achieves maximum density, since the voids are completely filled with liquid and the wet powder mass is in an ideal form for extruding. The increased plasticity

of the extrudate enables more of the impact energy on spheronization to be absorbed in deformation, with less energy available for breakage, hence the product will form satisfactory spheroids.

The results also illustrate that the yield of large pellets for the formulation consisting of the novel grades of MCC is very low, accounting for less than 10% of all pellets formed (see Fig. 7.5c). The only exceptions to this are the SRP D and control formulations, which contain size reduced MCC, in combination with 12.5% SLS and Avicel PH-101® respectively, where the large pellet yields are >20% in both cases. This suggests that the pellet formulations containing these two grades of MCC have a greater tendency to agglomerate.

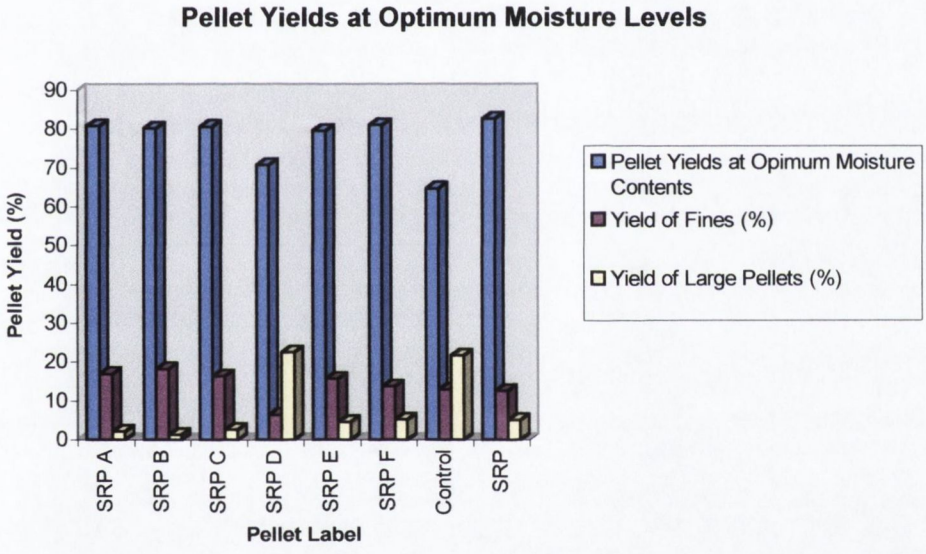

Figure 7.5c. Sieve analysis results illustrating the percentage yield of pellets, large pellets and fines, for the pellet formulations prepared, using optimum levels of hydration.

The above can be explained in terms of surface tension and capillary suction effects, due to the non-uniform liquid distribution, as discussed by Sherrington (1968). The liquid phase occupies the intra-particulate pores in a granule and creates a capillary suction, which can be expressed by the following equation, described by Rumpf (1958a,b).

$$P = T/m(Cos\sigma) \qquad \textbf{Eqn. 7.5a.}$$

where T is the surface tension of the liquid, m is the mean hydraulic radius of the pores, and σ is the solid-liquid contact angle.

Powder mixes, which consist of particles of smaller size, will have smaller intra-particulate spaces and hence the value of m in the previous equation will be greater, resulting in a larger average capillary suction pressure (P), i.e. the capillary suction pressure of the pellets formed with the novel size reduced grades of MCC will be greater than that of the pellets incorporating Avicel® PH-101. Fielden *et al.* (1993) explained that for satisfactory spheronization, it was desirable that the excess surface moisture of an extrudate should be withdrawn, since in these circumstances, the granules will not agglomerate. Larger capillary suction pressures have a greater ability to withdraw surface moisture, which would explain why the level of large pellets, produced by the formulations incorporating the novel size reduced grades of MCC, is lower than that for Avicel® PH-101 containing pellets. Sodium lauryl sulphate is a surface active agent, an inherent property of which is the ability to reduce liquid surface tension. This, according to Equation 7.5a, will reduce the capillary suction pressure leading, to greater propensity to forming more large pellet aggregates.

7.5.2 In vitro Dissolution Testing of Pellets

Figs 7.5d (i), (ii) and (iii) show the in vitro dissolution profiles for the novel pellet formulations and also include the dissolution profiles of the control pellets and pure drug, indomethacin. Indomethacin is an acidic drug, and hence it will have a greater solubility in media where the pH is greater than it's pKa (4.5), due to the presence of dissociating carboxyl groups (O'Brien *et al.*, 1984). As a result of this, McIlvaine buffer pH 6.8 was chosen as a simulation of small intestinal pH conditions, as it is well above the pKa for the

drug and hence pH dependent drug solubility will not play as big a factor in terms of drug release.

(i)

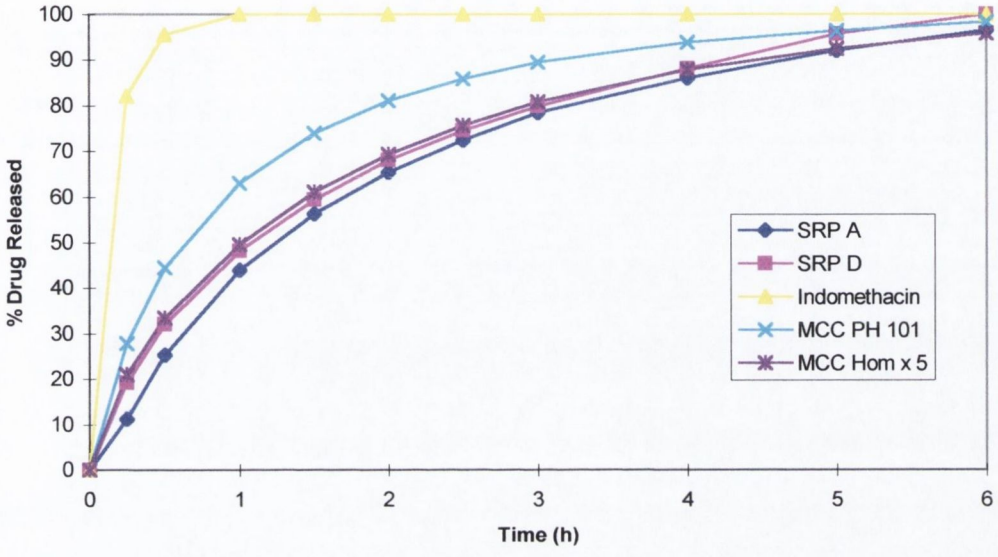

(ii)

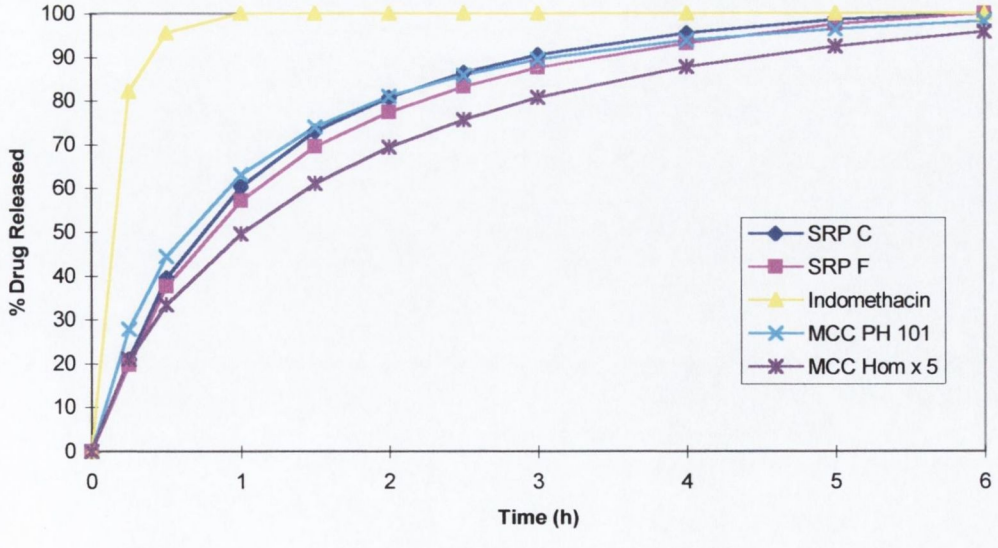

(iii)

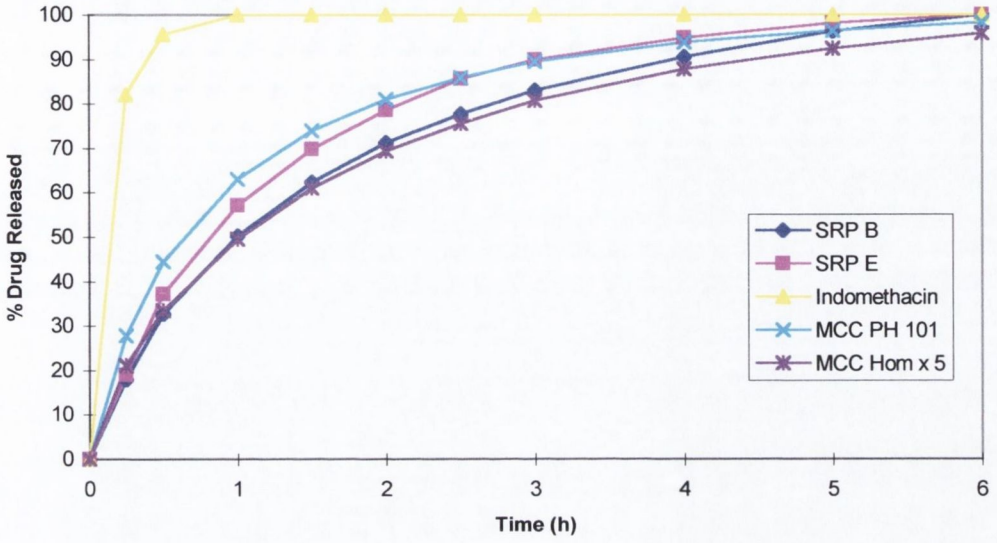

Figure 7.5d. Dissolution of Indomethacin from pellets in pH 6.8 McIlvaine buffer, for 6 h, at 37°C. The key represents the identity of the formulation used in the dissolution study (Table 7.4a). Only pellets formed under optimal moisture levels were examined.

The dissolution profile for pure drug illustrates a rapid initial rise in the amount of drug in solution during the first 15-30 min, which tapers off gradually to 100% approx. release, after 1 h. The dissolution profiles for the pellet formulations illustrated that all caused a retardation in drug release relative to that of pure drug. This was due to the matrix effect, created by the MCC incorporated into the pellet formulations. This is confirmed by the similarity factors quoted in Table 7.5a, which compare the dissolution profile for the pure drug with those of the pellet formulations. In all cases the value of f_2 was less than 50, whereas an f_2 value between 50 and 100 suggests that the dissolution profiles are similar.

Table 7.5a. In vitro similarity factors (f_2), comparing (1) the dissolution profiles of all pellets relative to that of pure Indomethacin drug, and (2) the dissolution profiles of pellets incorporating novel grades of MCC relative to the Control pellets.

Comparison between pure Indomethacin and all pellet formulations	**(1) f_2**	**Comparison between Novel pellets and Control pellets**	**(2) f_2**
SRP	21.5	SRP	51.1
SRP A	18.8	SRP A	42.7
SRP B	16.4	SRP B	51.0
SRP C	24.1	SRP C	75.9
SRP D	19.8	SRP D	49.9
SRP E	22.9	SRP E	67.3
SRP F	23.0	SRP F	63.2
Control	27.0		

Table 7.5a also illustrates the similarity factors, comparing the profiles of the novel pellet formulations to that of the Control formulation, which incorporates Avicel PH-101®. As is evident from the results, only two of the formulations result in similarity factors less than 50, suggesting a difference in release profiles, namely formulations SRP A and SRP D, which both contain SLS. It was found, however, that the release profiles for pellets SRP and SRP B were similar to those of the control, although the f_2 values for both of these formulations were very close to the lower limit of the similarity range (i.e. 50), below which the difference would be considered to be significant.

7.5.3 Pellet Intra-Particulate Porosity

Intra-particulate porosity was determined from a knowledge of the true density of the materials and pellet density, as described in the methodology. The porosity parameter can be used to describe the smoothness of the pellet surfaces, i.e. an increase in pellet density usually results in a decrease in porosity, accompanied by increased surface smoothness. The porosity values determined for the different pellet formulations are listed in Table 7.5b.

Table 7.5b. Intra-particulate porosity values, calculated for the novel pellet formulations from the powder and pellet density values.

Formulation Label	Pellet Apparent Density (g/cm^3)	Powder Apparent Density (g/cm^3)	Intraparticulate Porosity (%)
SRP A	1.365	1.369	0.3
SRP B	1.295	1.420	8.8
SRP C	1.340	1.450	7.6
SRP D	1.276	1.323	3.6
SRP E	1.41	1.456	1.03
SRP F	1.345	1.452	7.37

In general, the porosity values vary from 0.3% to 8.8%. Preparations which have the lowest porosity values are SRP A and SRP D, both of which have the incorporation of SLS as a common factor. The low porosity values reported for these two pellet preparations may be responsible for the significant delayed release observed for them from the in vitro results, i.e. the lower porosity will slow down the penetration of the dissolution medium into the pellet matrix and hence, slow down the rate of drug dissolution and release. The low porosity observed for preparation SRP E, combined with a higher rate of drug release, may be explained by the loss of matrix effect arising from pellet fragmentation during the dissolution test.

The low porosity values for pellets SRP A and SRP D may again be explained in terms of the surfactant properties of SLS. The presence of SLS reduces the surface tension of the granulating liquid, water, and thus the capillary suction pressure in the granule, as previously described. Rumpf (1958, a,b) showed that when the void space in a granule is completely filled with liquid, i.e. in the capillary state of saturation, the tensile strength of the granule as a whole is approx. equal to the average capillary suction pressure (P). Therefore, when the tensile strength of the granule is decreased, the plastic deformation increases, resulting in a smoother, rounder surface with less roughness and surface porosity. Kristensen *et al.* (1985) have shown that any means which tends to increase the deformability of moist agglomerates, e.g., by reducing their tensile strength, and/or improving their plastic deformation, also favours their agglomeration by coalescence. This

was also observed for these pellets, especially in the case of SRP D, which contains the higher level of SLS.

SLS also has the ability to produce micelles and hence, behaves as a solubilising agent. According to the Handbook of Pharmaceutical excipients, (2000), the critical micelle concentration of SLS at 20°C is 0.023% w/v. The highest level of SLS used in our pellet formulations was a 12.5% w/w combination with MCC. This combination, however, accounted for only 30% of the pellet overall weight. During in vitro dissolution testing, 200 mg samples of these pellets were placed into 1000 ml of dissolution medium. As a result, at its highest level, the SLS was only present at a concentration of 0.0008% w/v in the dissolution medium, which is well below its critical micelle concentration. Thus, the solubilisation phenomenon can be discounted, when examining drug dissolution from the pellets.

7.5.4 Mercury Porosimetry Analysis of Pellet Formulations

The porous characteristics of the pellet formulations, prepared using the extrusion/spheronisation technique, were also determined by examining plots of the cumulative pore volume intruded by mercury *vs.* the pore diameter, and plots of the incremental intrusion volume *vs.* pore diameter. The relevant quantitative results of the study are listed in Table 7.5c.

Mercury porosity data gives a much more accurate picture of the overall intra-particulate pellet porosities, compared to the technique previously described, based on hexane intrusion. In the case of the hexane technique, intrusion is based solely on solvent diffusion and, so it will not intrude into the smaller pores, for which a high pressure technique is required, such as the mercury intrusion technique. For this reason, the 'hexane intrusion' techniques gives significantly lower values for the overall pellet porosities, as is clearly evident, if the two sets of data are compared quantitatively.

Table 7.5c illustrates the total mercury intrusion for all eight pellet formulations. Intrusion values, for all pellet formulations incorporating the novel MCC grades, are very similar, with values ranging from 0.175 to 0.189 ml/g. The Control pellets, however, which incorporate Avicel® PH-101, illustrate a significantly higher mercury intrusion of approx. 0.94 ml/g. This is a 4 - 5 fold approx. higher intrusion than in the case of the novel pellet preparations, and is a reflection of the overall porosities determined for the eight pellet formulation. The porosity values for the seven novel preparations are relatively low, with values ranging between 17.7 and 18.98 %, whereas the porosity of the Control pellets is significantly larger, with an average value of 59.4%. The large observed differences in mercury intrusion volume and porosity can be related to differences in particle size between Avicel® PH-101 and the novel size reduced grades of MCC. The larger sized

Table 7.5c. Quantitative results of porosimetric study of pellet formulations SRP, SRP A, SRP B, SRP C, SRP D, SRP E & SRP F (containing novel grades of MCC) and Control pellets (incorporating Avicel® PH-101).

Formulation	Hg Total Intrusion Volume (ml/g)	Median Pore Diameter (μm)	Bulk Density (g/ml)	Porosity (%)	MCC Average Particle Size (μm)
Control	0.94	55.62	0.63	59.29	56.39
SRP	0.175	0.52	1.02	17.89	11.09
SRP A	0.182	0.44	1.04	18.92	11.28
SRP B	0.183	0.37	1.02	18.77	11.08
SRP C	0.176	0.53	1.01	17.74	11.04
SRP D	0.169	0.26	1.01	17.08	11.18
SRP E	0.189	0.29	0.99	18.81	10.65
SRP F	0.184	0.28	1.03	18.98	10.43

Avicel® PH-101 particles do not undergo as much compaction during the extrusion/spheronisation process, resulting in a greater overall pellet porosity. This is confirmed by the differences observed in the bulk densities between the novel pellet formulations and the Control pellets. The bulk density for the control pellets is 0.63 g/ml approx., whereas densities for the novel pellets are significantly higher, due to a greater compaction of the powder materials, with average values ranging between 0.99 and 1.04 g/ml for preparations SRP E and SRP A, respectively. The Hausner explanation (1981) can be extended in this situation to compacted powder masses (i.e. pellets), where pellets consisting of fine particles will have fine pores between the particles, whereas pellets containing coarse particles have coarse voids. In addition, the larger particle size results in a coarser pellet surface relative to pellets incorporating the finer novel MCC grades, which is evident qualitatively in scanning electron micrographs, illustrated in Figs. 7.5e (i) and (ii) and Figs. 7.5f (i) and (ii). Figs. 7.5e (i) and (ii) illustrate the rough surface of the Control pellets, formed using the Avicel PH-101 grade, at two levels of magnification, whereas Figs. 7.5f (i) and (ii) illustrate the much smoother surfaces and more spherical shape of the SRP D pellets, formed using the size reduced MCC grade, combined with the higher SLS content, at comparable magnifications. The coarse pellet surfaces of the Control pellets also contribute to a larger pellet porosity, as it creates surface indentations and pockets on the pellets, into which mercury intrusion is detectable and contributory to overall porosity.

The results also indicate a significant difference in the median pore diameters calculated for the eight pellet formulations. Again, the trend is consistent with the previous results, where the diameter calculated for the control pellets (~ 55.62 μm) is over 100 times greater than the diameters determined for the novel pellet preparations. In reality, the intra-particulate pores within the pellets may not differ by this magnitude, as the surface roughness of the pellet, as mentioned above, also contributes to the porosity determined for the pellets. This may have a significant influence in the calculation of the above values, thus distorting the actual pore diameter towards an artificially elevated value. In the case of the novel pellet formulations, the surface is smoother and so the values quoted are more representative of the actual intra-particulate pore diameters.

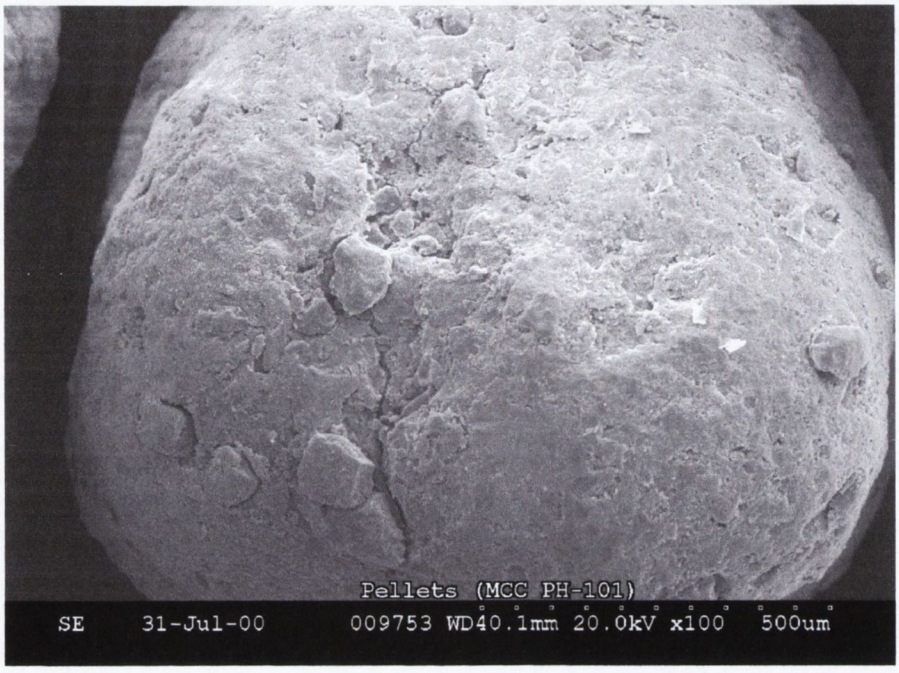

(i)

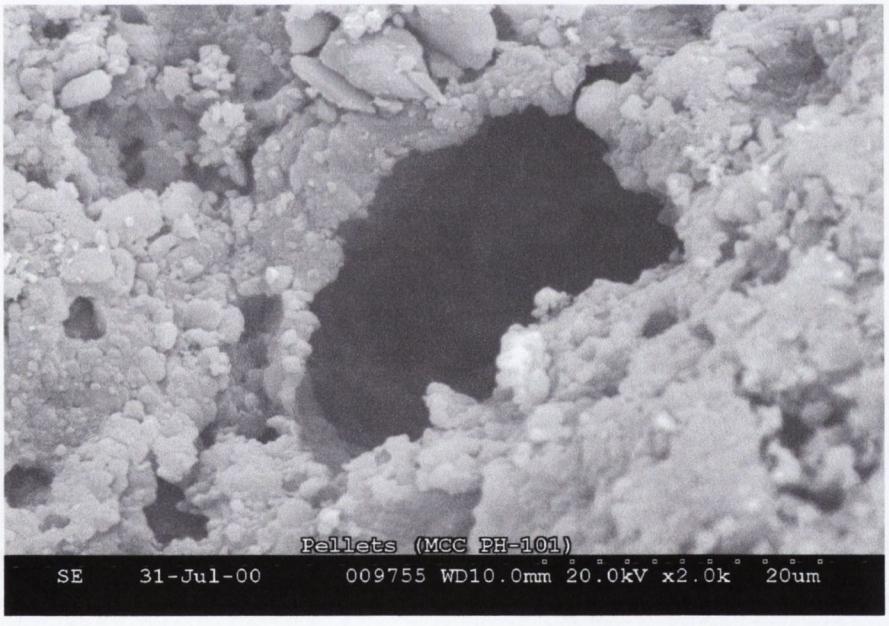

(ii)

Figure 7.5e Scanning electron micrographs of a typical pellet, incorporating Avicel® PH-101 (Control formulation), at (i) X 100, illustrating the rough surface of the pellet and (ii) X 2000, illustrating the size and shape of a typical surface pore.

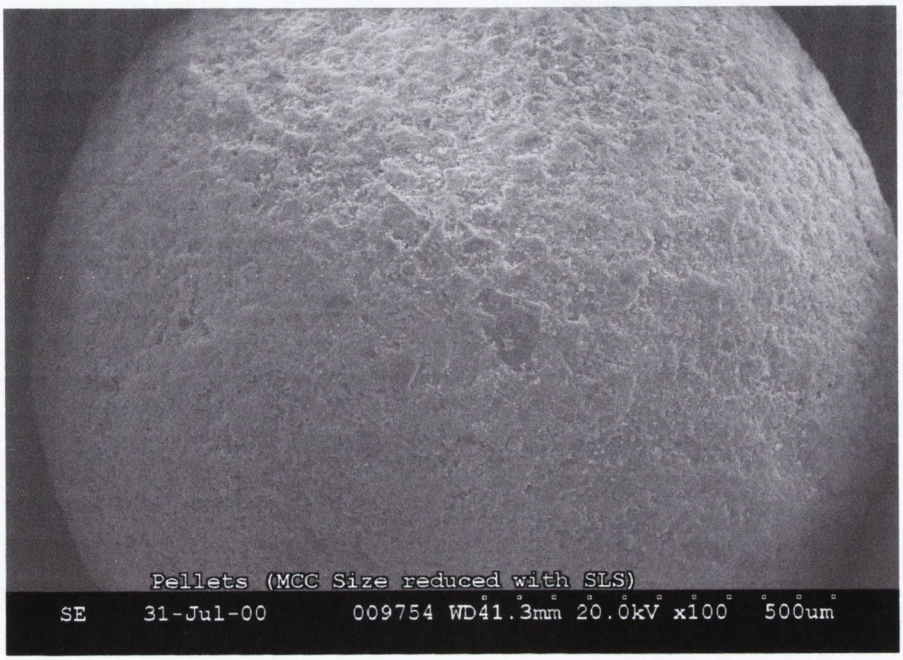

(i)

(ii)

Figure 7.5f Scanning electron micrographs of a typical pellet, incorporating size reduced MCC combined with SLS (SRP D formulation), at (i) X 100, illustrating the smoother surface of the pellet and (ii) X 2000, illustrating the smaller size and shape of a typical surface pore (when compared to the Control pellets).

The incremental intrusion curves for the pellet formulations are illustrated in Figs 7.5g and 7.5h. Fig. 7.5g represents only the pellets incorporating novel grades of MCC. In all cases the plots illustrate a bimodal distribution. Coarse pores are evident for all pellets in the range ~40 to 500 μm. This is due to the gaps which are present between the individual pellets, when they are packed together and is also an indicator of the smoothness of the pellet surfaces. The maximum intrusion of mercury in this range is 0.01 ml/g. Fig. 7.5h is similar to Fig. 7.5g, but superimposes the incremental plot for the control pellets on the previous plots. This plot also illustrates a bimodal distribution, with coarse pores between ~40 to 500 μm. The important feature, however, is that the maximum intrusion of mercury in this range is significantly higher (ie ~0.2 ml/g), confirming that the surfaces of the control pellets are very much rougher than those of the novel pellet formulations.

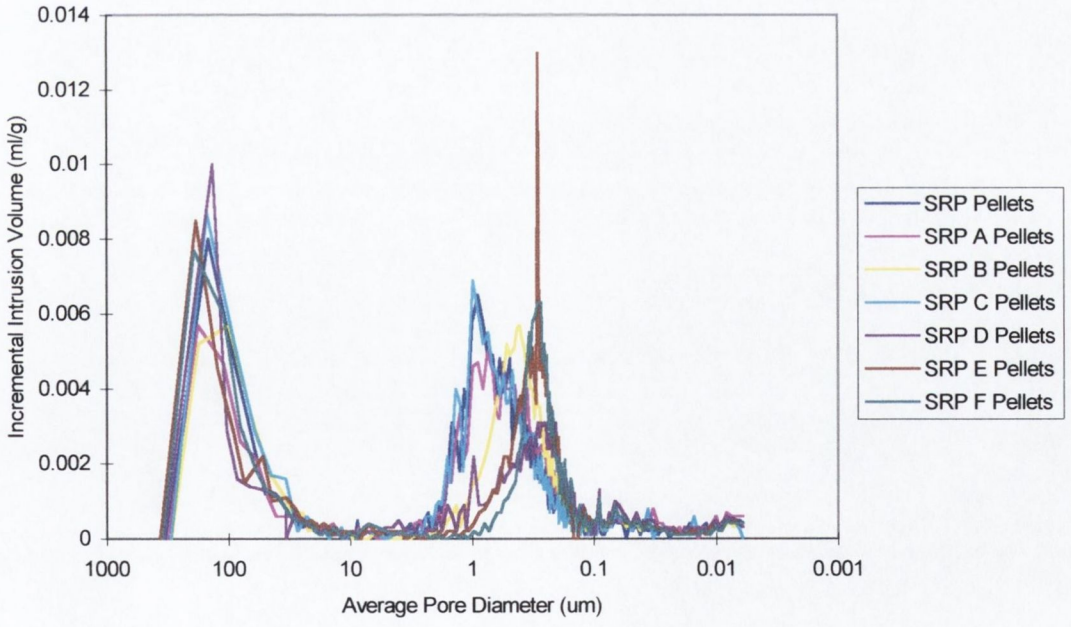

Figure 7.5g. Incremental mercury intrusion curves for pellet formulations SRP, SRP A, SRP B, SRP C, SRP D, SRP E and SRP F (containing novel grades of MCC).

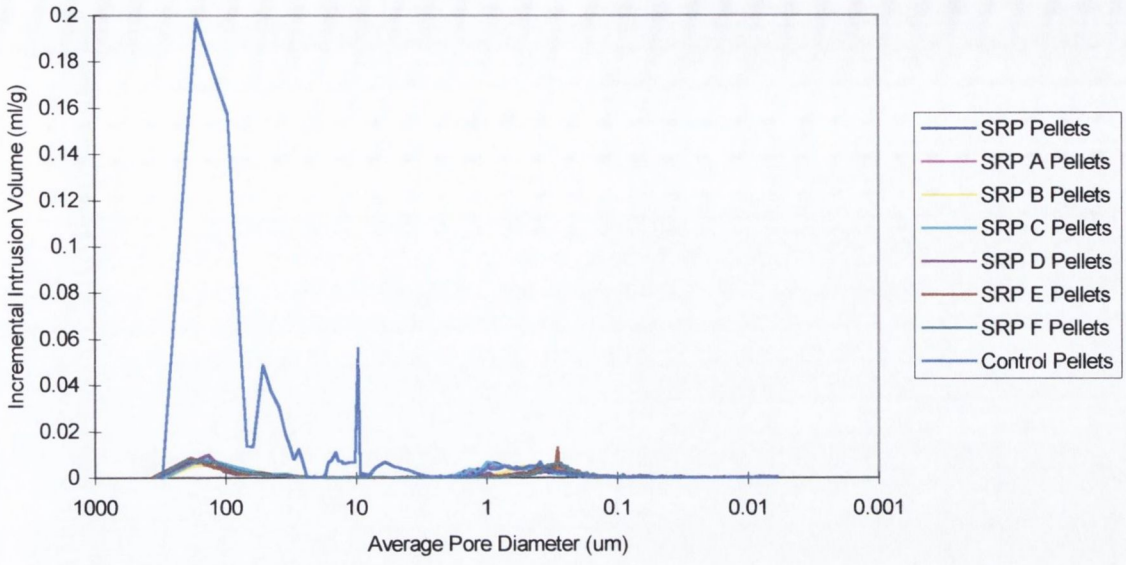

Figure 7.5h. Incremental mercury intrusion curves for pellet formulations SRP, SRP A, SRP B, SRP C, SRP D, SRP E and SRP F (containing novel grades of MCC) and Control pellets (incorporating Avicel® PH-101).

The second pore distribution, illustrated in Fig. 7.5g, extends over the range of ~ 0.1 to 1.2 μm and can be interpreted as the intra-particulate pores within the actual pellets. Penetration of dissolution medium into, and the subsequent outward diffusion of the dissolved drug from these fine pores, is responsible largely for the sustained drug release mechanism from these pellets. When the control pellet data is superimposed, as illustrated in Fig. 7.5h, its' second distribution lies within the range ~ 10 to 20 μm. This corresponds to the intra-particulate pores within the control pellets. As a result, the intra-particulate pores are significantly larger compared to those in the novel pellets. Thus, from these results, we would expect drug release to be slower from the novel pellets relative to the control pellets.

The shape of the cumulative intrusion *vs.* pore diameter curves are typically sigmoidal for all novel pellet formulations, as illustrated in Fig. 7.5i. For all pellets, a sharp increase in

intrusion occurs, when the pressure becomes high enough to fill the pores in the range ~ 0.1 to 1.2 μm.

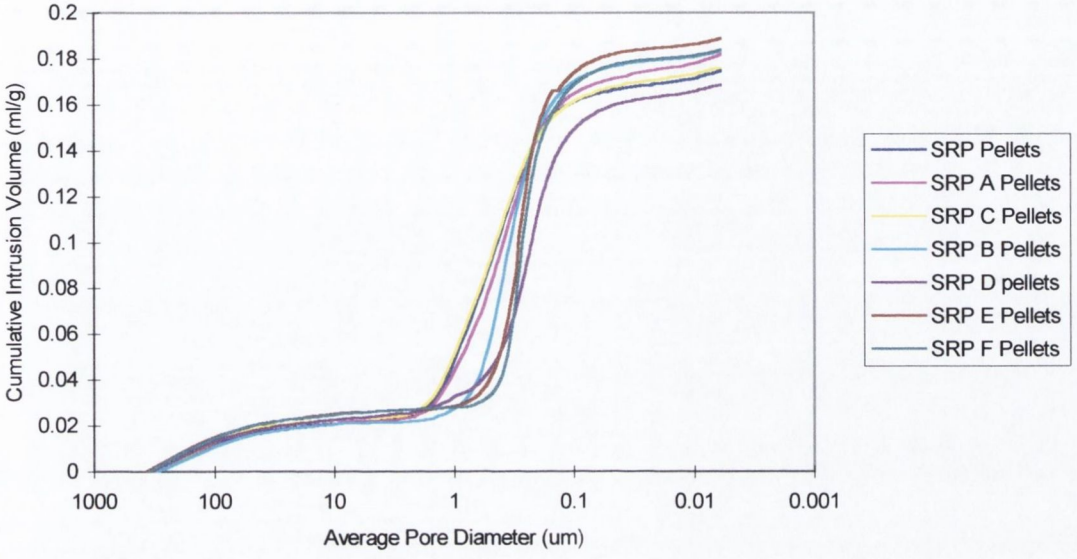

Figure 7.5i. Cumulative mercury intrusion curves for pellet formulations SRP, SRP A, SRP B, SRP C, SRP D, SRP E and SRP F (containing novel grades of MCC).

Figure 7.5j illustrates the superimposition of the cumulative intrusion data for the Control pellets on the previous data. It does not illustrate the smooth sigmoidal patterns as evident for the novel pellets. There is, instead, a rapid and significant intrusion in the range 4 to 500 μm, corresponding to the significant roughness of these pellets. Further intrusions are evident at ~ 10 μm and 0.1 to 1.0 μm, corresponding to mercury entering intra-particulate voids within the actual pellets.

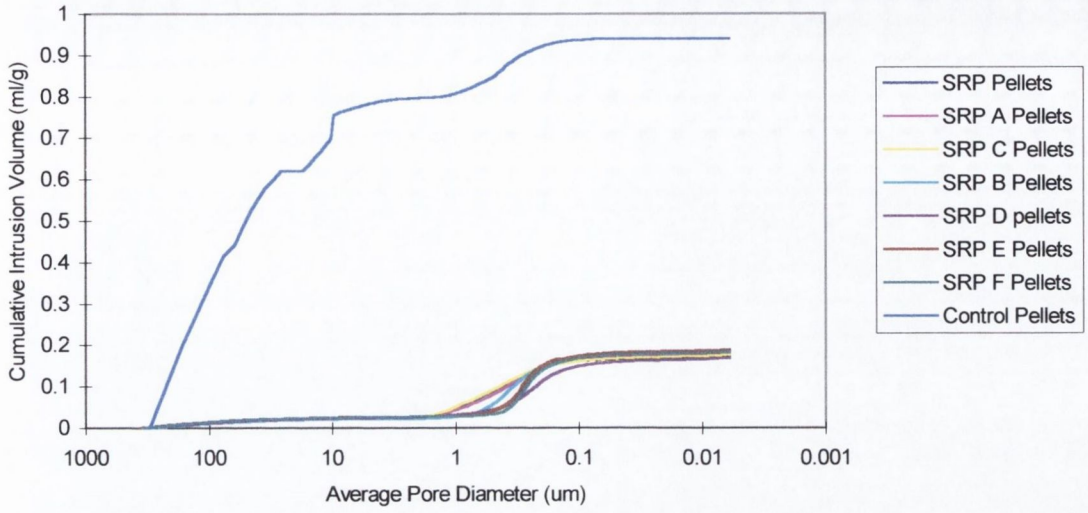

Figure 7.5j. Cumulative mercury intrusion curves for pellet formulations SRP, SRP A, SRP B, SRP C, SRP D, SRP E and SRP F (containing novel grades of MCC) and Control pellets (incorporating Avicel® PH-101).

7.5.4.1 *Presence of Ink-well Pores*

Another important feature of the porosimetry data is evidence for the presence of 'ink-well' shaped pores within the pellets. Fig. 7.5k illustrates the general pore filling mechanism for the eight pellet preparations and relates it to the intrusion and extrusion curves. The inserts in the lower half of each Fig., (i.e. inserts A through D) illustrate how mercury is forced into smaller and smaller pores as pressure is increased. Trapping of mercury appears to occur, however, during extrusion for all pellet preparations, as illustrated by inserts E, as the pressure is reduced back to a point between inserts A and B. It is possible that this is due to the presence of ink-well pores in all pellets. Pores empty when the pressure is reduced below the pressure at which the pore filled, but with these ink-well shaped pores, the small neck empties, but the larger diameter cavity remains filled, since the cavity is essentially a larger pore than the pore which creates the neck. When the pressure then falls below the pressure at which the pores of the same

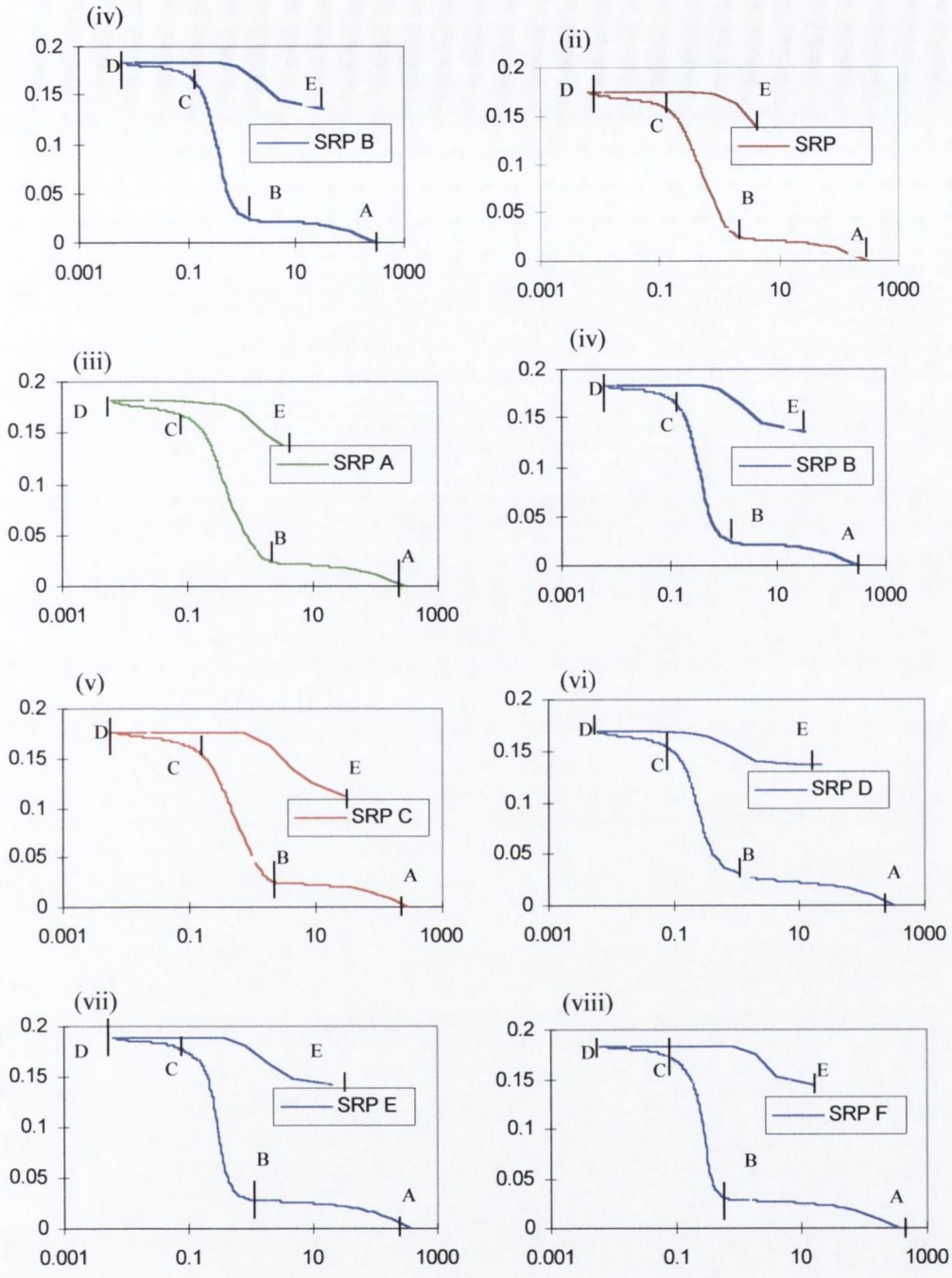

Figure 7.5k. Cumulative mercury intrusion and extrusion (ml/g) *vs* average pore diameter (μm) plots for pellet formulations (i) Control, (ii) SRP, (iii) SRP A, (iv) SRP B, (v) SRP C, (vi) SRP D, (vii) SRP E and (viii) SRP F.

diameter as the cavity empty, the mercury within the cavity attempts to extrude, but cannot due to the small neck of the ink-well, across which the mercury bridges. It is important to note, however, that according to Allen (1990), other factors can also contribute to these observed hysteresis effects. These include the fact that the angle of contact between the capillary wall and the mercury surface tend to differ during intrusion and extrusion, even though calculations are made using the same angle. Furthermore, it may arise due to mercury binding to the pore surface and also as a consequence of pore surface roughness.

7.5.5 Pellet Packing Density Analysis

Pellet density can be affected by changes in the formulation and/or process, and consequently may affect the volumetric filling of pellets into capsules, coating efficiency, mixing of different batches or types of pellets for final filling into capsules, and the gastrointestinal transit of pellets. Pellet density can be determined in a number of different ways, each technique determining a specific density value. Two commonly determined density values are the poured and tapped densities. The poured density is obtained by the division of pellet weight by the initial volume measured, after pouring the pellets into a measuring cylinder. The tapped density may be obtained, either with an automated tapper (Hellen *et al.*, 1993a; 1993b), or manual tapping, where the measuring cylinder containing a known weight of pellets is manually tapped off a laboratory bench five hundred times. The latter technique was chosen in the case of this project.

The poured and tapped density obtained can be used to estimate the flowability of the pellets, by using the values to determine Carr's Compressibility Index (Carr, 1965). The nomenclature of this index is a misnomer, since compression is not involved. The above density values can also be used to determine a similar index termed the Hausner ratio (Hausner, 1967). Hausner found that the ratio $\rho_{B\ max}/\rho_{B\ min}$ was related to interparticulate friction and as such could be used to predict powder flow properties.

The Carr's indices and Hauner ratios for the novel pellet formulations are illustrated graphically in Fig. 7.5l. Both the Carr's indices and Hausner ratios indicate that all pellet formulations have excellent flow properties. Carr's index for all pellets is less than 10%, which according to Carr is indicative of excellent free-flowing granules (i.e. within the range 5-15%). The Hausner ratios for all formulations are less than 1.2. For this ratio, Hausner explained that values less than 1.25 indicate good flow (= 20% Carr's index), while those greater than 1.25 are indicative of poor flow (= 33% Carr's Index). Hausner also showed that spheres tend to have ratios of 1.2 approx., which is in good agreement with our results.

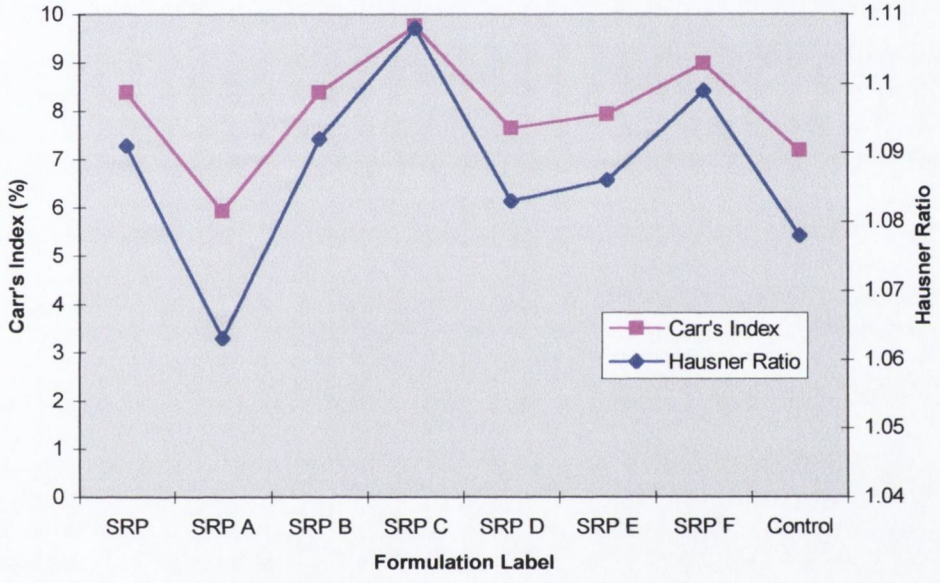

Figure 7.5l. Carr's indices and Hausner ratios calculated for pellet formulations manufactured under optimum moisture levels.

It is evident from Figure 7.5l that all pellet formulations have excellent flow properties. Both Carr's Index and the Hausner ratio are below the cut-off level indicative of free flowing granules, namely 15% and 1.25 respectively. The calculated values for the pellet formulations incorporating Avicel PH-101 are represented by the Control formulation, in the above figure. All the novel formulations illustrate reduced flowability relative to the

Control, except for formulation labeled SRP A, which incorporates SLS at the lower concentration (i.e. 6.25% of its MCC content).

7.6 CONCLUSION

All six novel grades of size reduced MCC were capable of functioning as excellent extrusion/spheronisation aids. All allowed for the formation of pellets with yields greater than 70%, and in the majority of cases greater than 80%, with minimal levels of fines and large pellets which are undesirable. The incorporation of SLS reduced the yield, especially at the higher concentration, probably due to its surfactant properties, as explained previously. In vitro dissolution testing showed that all formulations resulted in significant delayed drug release relative to the dissolution of pure indomethacin. Only those formulations incorporating SLS (namely SRP A and D) had improved sustained drug delivery relative to the Control formulation, as illustrated by their calculated similarity factors (f_2).

The reduced drug release rates observed for the pellets, incorporating the novel size reduced MCC grades, were shown to be related to a decrease in pellet porosities, the values of which were calculated using two main techniques, namely hexane and mercury intrusion. Porosity values determined, using the mercury technique, were greater due to the higher pressures generated, capable of intruding the mercury into finer pores. Porosity values were almost threefold greater for pellets incorporating Avicel® PH-101 compared to the novel grades, and were explained in terms of differences in powder particle sizes. Hexane intrusion data indicated that porosity was lowest in the pellet formulations incorporating SLS, (i.e. Preps SRPA and SRPD; 6.25 and 12.5% w/w SLS, respectively, relative to the MCC content), explaining the greatest sustained release observed for these formulations. The sustained release properties of the other pellets, also incorporating novel size reduced grades of MCC, were reduced to a degree due to their fragmentation, when placed into the aqueous dissolution media. This fragmentation was observed

visually. All pellet formulations were shown to contain ink-well pores, as indicated by the mercury intrusion data.

All pellets illustrated excellent flow properties, similar to the Control pellets, as indicated by the low Carr's indices and Hausner ratios, ie the Hausner ratios for all formulations were less than 1.2, whereas, values less than 1.25 indicate good flow properties. Formulation SRP A was the only one with improvement in flowability over the Control pellets, with a calculated Hausner ratio between 1.06 and 1.07.

It is apparent that the greatest improvements were observed for those pellets incorporating the size reduced grade of MCC in combination with SLS, of which the formulation SRP A appeared best. For this formulation, pellet yields were greater than 80% at optimal hydration levels, drug release retardation was maximal and the flow properties were improved over the Control formulation incorporating Avicel® PH-101.

(III) SUSPENSION APPLICATIONS

7.7 INTRODUCTION

In the 1960's, FMC produced a colloidal grade of Avicel®, where the particle size existed below 1 μm approx. This was termed colloidal Avicel® and was capable of producing gels, when added to water and subjected to a grinding or attrition treatment. The gel had a structure or texture which was similar to that of whipped cream or whipped potatoes. The peculiar viscosity effect was not due to the molecules, but to the small rod shaped particles which touch each other to form a random arrangement. The fact that they are stiff and touch each other accounts for the way that the gel retains its viscosity and does not sag with time.

From a rheological point of view, the gels illustrate pseudoplastic flow and thixotropy, explained in terms of the rods aligning themselves in parallel upon stress application and hence offering lower resistance to flow. If the stress is removed Brownian motion brings the rods back into a random arrangement and so viscosity increases. Experiments performed by FMC illustrated that the viscosity increased for all gels as the solids content increased, and that the smallest particles gave the highest viscosity. They also performed tests investigating the effect of the addition of sodium carboxymethyl cellulose (NaCMC) into the gels. The addition of NaCMC not only dramatically increased the gel's viscosity, but also had a big effect on its sensitivity to the rate of shear. This ultimately led to the development of an Avicel® RC grade, where the NaCMC also behaved as a protective colloid, preventing each MCC particle from hydrogen bonding to its nearest neighbour, when the two were co-spray-dried together.

Today a number of protected colloidal grades of Avicel® are commercially available. These include Avicel® RC 591, RC 581 and CL 611. They all contain NaCMC in different proportions, ranging from 8.3% to 13.8% for Avicel® RC 581 and 591, and

from 11.3% to 18.8% for Avicel® CL 611. The highest viscosities are achieved with grades RC 581 and CL 611. The various grades also differ in terms of drying treatment and hence, degree of shear that is required to disperse them, when they are being used as a suspending agent.

7.8 RESULTS AND DISCUSSION

The aim of this section was to examine the potential use of two novel size reduced grades of MCC, as suspending agents, in pharmaceutical formulations. The novel grades used were Grade X (no SLS) and Grade Y, as described in Section 7.1, which examined tableting applications. The commercial grades used for comparative purposes were Avicel® RC 591 and RC 581. The drug used in the suspensions was sulphadimidine, which was selected for its very low aqueous solubility. It is described as being very slightly soluble in water (Martindale, 1999). The drug was size reduced, using a RETSCH ultra-centrifugal mill and sieved to produce drug particles in the size range corresponding to a fine powder. Sulphadimidine suspensions (10%) were formulated, using the above four suspending agents, each at three concentration levels, namely 1.0, 0.75 and 0.5%. Each suspension was prepared in duplicate.

Prepared suspensions were placed into graduated sedimentation vessels and shaken, the time of which was recorded as t = 0. The vessels were stored on a level surface at a constant temperature of 3°C. The stability of the suspension formulations were evaluated, using the concept of sedimentation volume, expressed in terms of sedimentation height, due to a constant cylindrical cross-sectional area. This involved considering the ratio of the ultimate height (Hu) of the sediment to the initial height (Ho) of the total suspension, as it settled in a graduated cylinder under standard conditions. The larger this fraction the better is the suspendability. A particular advantage of this system is the fact that suspensions remain undisturbed.

The plots of the Hu/Ho ratios *vs.* time, for the various suspension formulations, are illustrated in Figs 7.8a (i), (ii), (iii) and (iv). From the plots it is possible to compare the different formulations. The better formulations obviously produce lines that are most horizontal and/or less steep, with Hu/Ho ratios closest to 1.0.

(i)

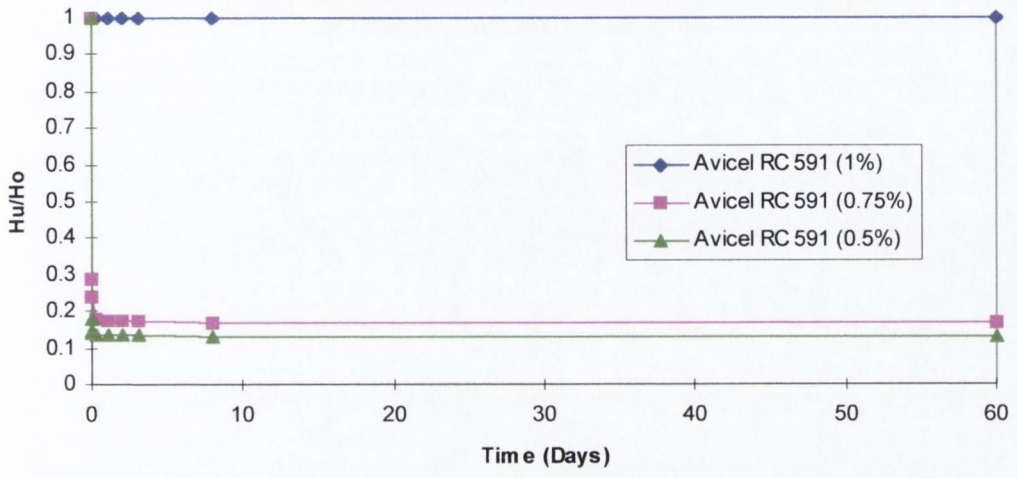

(ii)

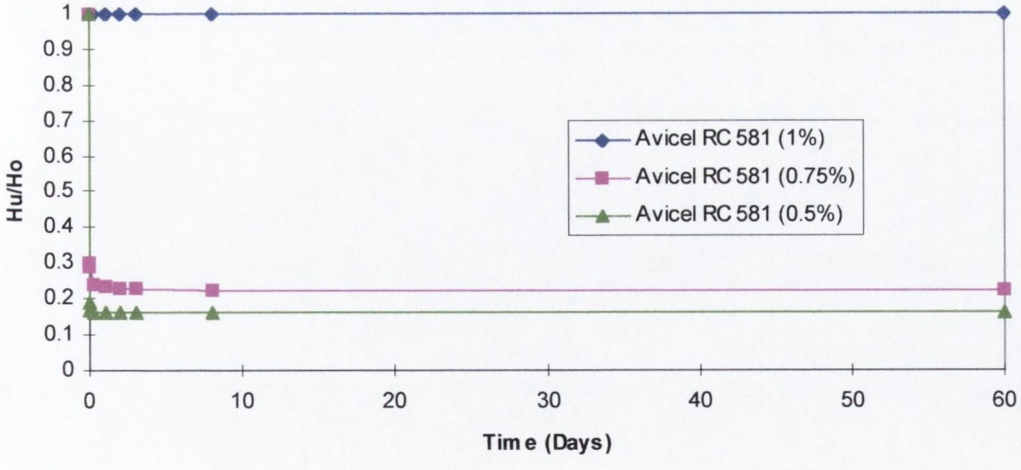

(iii)

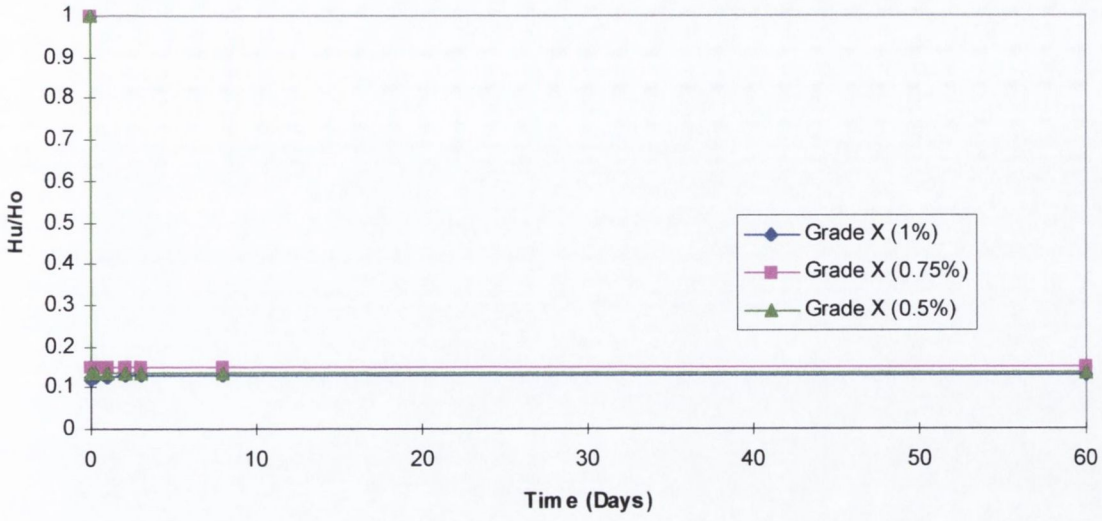

(iv)

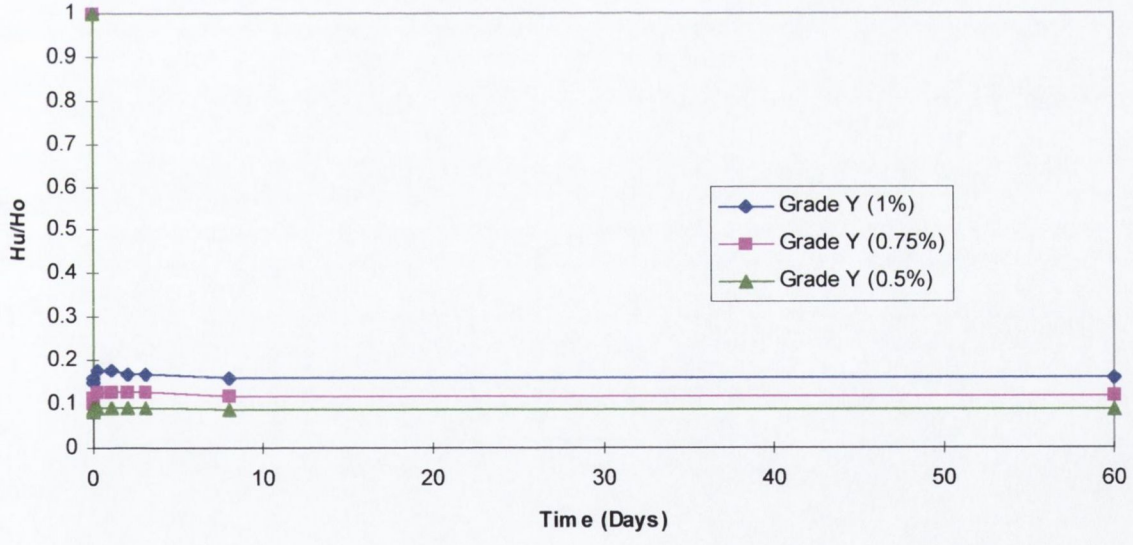

Figure 7.8a Plots of the Hu/Ho ratios vs. time for 10% Sulphadimidine suspensions, incorporating four suspending agents, namely Avicel® RC 581 and RC 591, Grade X and Grade Y, at concentrations of 1.0, 0.75 and 0.5%.

The commercial grades Avicel® RC 581 and RC 591 illustrate similar abilities as suspending agents. In both cases, when the suspending agent is used at the 1% level, permanent long-term suspensions of the sulphadimidine powder were achievable, with an absence of sedimentation. Lower concentrations, i.e. 0.5% and 0.75%, both lead to complete sedimentation occurring within 30 min approx. Because of the thixotropic properties of the Avicel gels, if sedimentation does not occur within the first 30 min, there is a low likelihood that it will occur later, as the viscosity is lowest initially, due to the shear applied by shaking the graduated vessel, but increases upon standing with time, due to the recovery of the random arrangement of particles by Brownian motion. As a result, when Avicel RC 581 and 591 were used in concentrations of 0.75% and 0.5%, the viscosities of the suspensions, after shaking, were insufficient to suspend the sulphadimidine drug particles and so complete sedimentation occurred quickly.

The plots illustrated in Fig. 7.6e also illustrate the suspendability of the novel MCC grades (Grade X and Grade Y). Both grades, at all concentrations, behave as poor suspending agents. Sedimentation occurs very quickly (within 1 min approx.) and is almost complete within 10 min approximately. In both cases there is a small increase in the Hu/Ho ratio, after approx. 30 min, which correlates to the sedimentation of the MCC particles on top of the already sedimented drug particles. This is evident visually by the formation of two distinct layers in the sediment. The ratios then decrease slightly with time, due to sediment compaction.

The novel MCC grades fail as suspending agents for two main reasons. Firstly, the particle size, although reduced relative to Avicel® PH-101, is still very much greater than the colloidal grades of Avicel that are primarily used as suspending agents. In addition, the commercial grades are protected and stabilised by the presence of sodium carboxymethyl cellulose which is absent in the case of both novel grades.

Chapter 8

Characterization of Halloysite

8.1 Introduction

Halloysite, as mentioned in Chapter 1, is a member of the kaolin group of minerals, but it differs from kaolinite in its typically tubular morphology. It also differs from kaolinite in its capability to exist in a hydrated state. The hydrated and dehydrated forms are known by a number of synonyms, which are generally termed halloysite. More specifically, the hydrated mineral endellite (halloysite) is believed to consist of well developed tubes, which split upon dehydration to halloysite (metahalloysite). An electron microscope study of the minerals of the kaolinite group has revealed that halloysite (metahalloysite) particles consist of hollow tubes, which have commonly collapsed or have split and partially or completely unrolled. It is suggested that this change in morphology explains the irreversibility of the dehydration process (Bates *et al.*, 1950).

Because this mineral exists as a hollow cylinder, it offers potential for providing a sustained drug release mechanism. Its use as a method for sustained release of biological molecules is the subject of a recent US patent (Price and Gaber, 1997). The patent refers to the invention, whereby the active agent is contained within the microtubules of the halloysite mineral. Typically, the agent is adsorbed onto the inner surface of the microtubule, the tubule having an average diameter less than 0.2 μm. The invention allows for the release of the active agent into the use environment, at a delayed rate, and over a selected time interval.

Todate, most of the work covered by the above patent is confined to the sustained delivery of anti-fouling agents for marine applications, which have been loaded into the halloysite microtubules and formulated into paint, which is then coated onto the base of naval vessels to prevent mollusk build-up. Inadequate work has been performed to investigate potential use in human and veterinary medicines. The material is chemically, though not structurally, similar to other pharmaceutically acceptable silicates such as talc, kaolin and bentonite, which are widely used in pharmaceutical products both internally and externally. Consequently, halloysites are probably pharmaceutically acceptable, particularly after clean-up procedures.

It is the intention of our research work on this mineral to attempt to characterise it both physically and chemically, the properties of which will be used to ensure minimum batch to batch variability, which is of primary concern to ensure pharmaceutical acceptability. We also intend to load a number of drug candidates into the lumen of the microtubules using a number of techniques, with subsequent coating, the results of which are described in Chapter 9.

8.2 Sourcing Halloysite

Commercially, very few high purity halloysite deposits are developed and exploited throughout the world, yet it is not uncommon in nature, being found in many subtropical and tropical soils. According to Harvey (1996), the commercial development of high purity halloysite resources is restricted to New Zealand, the Republic of Korea, and perhaps Japan. Lower grade resources are exploited in Japan, the United States (Indiana) and to a smaller extent in the Czech Republic, France, the Philippines and Morocco.

In our study, we looked at both New Zealand and Japan as potential sources. Samples were kindly provided by New Zealand China Clays Ltd (a subsidiary company of Ceramaco Corporation, Ltd) and Inagaki Clay Mining Company, from Japan. A small

crude sample of Indiana halloysite was also gratefully provided by Indiana University. Subsequent examination of the Japanese sample revealed that it was an import from New Zealand. As a result, New Zealand was the primary source of all halloysite samples used in our study.

8.3 Microscopic Analysis

We were provided with a number of small quantity samples, initially from NZ, all of which contained some of the desired cylindrical morphology. The different grades varied in terms of the tubule length, diameter, and treatment with other reagents. The three grades provided were Halloysite 'G', 'MM' and 'ultrafine'. SEM micrographs of these three grades are illustrated in Figures 8.3a (I), (II) and (III). The 'MM' grade differs from the other two in that it was treated with a reagent, rendering the mineral more hydrophobic. This would facilitate the loading of hydrophobic molecules within its core lumen. Both the Halloysite 'G' and 'ultrafine' grades were untreated in this respect (i.e. hydrophilic). Qualitative examination of the previous SEM micrographs indicated that the 'ultrafine' and 'MM' grades contain a lot of powder debris, in addition to the desired tubular minerals. The 'G' grade appeared to be the most consistent in terms of tubular content and dimensions. In addition we intended to use the highly water soluble drug, Diltiazem HCl, in drug loading studies, discussed later in Chapter 9. Therefore, due to the hydrophilic nature of the 'G' grade and its high tubular content, it was chosen for further studies and a 25 kg batch of Halloysite 'G' was subsequently obtained.

(I)

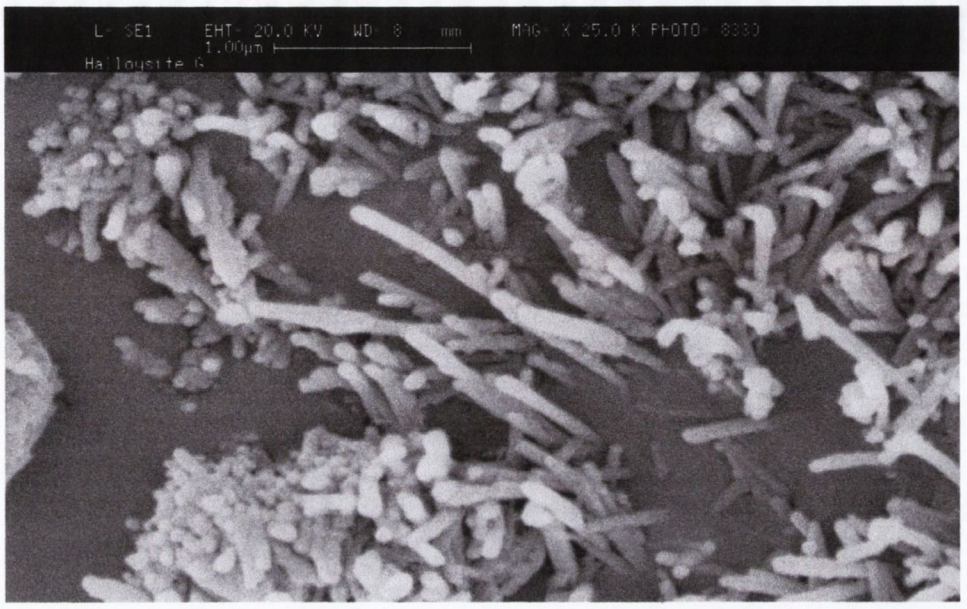
L= SE1 EHT= 20.0 KV WD= 8 mm MAG= X 25.0 K PHOTO= 8333
1.00µm
Halloysite G

(II)

L= SE1 EHT= 20.0 KV WD= 8 mm MAG= X 25.0 K PHOTO= 14224
1.00µm
Halloysite - ultrafine.

(III)

Figure 8.3a. SEM micrographs of New Zealand halloysite samples, namely, (I) Halloysite 'G', (II) 'ultrafine' and (III) 'MM', respectively.

Six 50 g samples were taken randomly from different parts of the powder batch. Each sample was subjected to a number of tests to examine the overall batch for uniformity of content. The tests included particle size analysis using the Malvern, in order to estimate the median particle size distribution, TEM analysis to qualitatively examine the tubular morphology, and SEM analysis, performed in conjunction with energy dispersive analysis, to detect the presence of any ion contamination.

TEM and SEM analysis of the six samples yielded results which were very similar and indicated that the original batch contained a lot of tubular material, as well as larger undesirable particle aggregates. The SEM micrograph for one of the samples (sample 2), is illustrated in Figure 8.3b. The average particle size for the six samples was determined to be 88 μm approx., which was probably distorted on the high side due to the contribution of the larger aggregates (i.e. the SEM micrographs indicate that the largest dimension of the individual tubules (length) is only 1 to 3 μm approx.). We decided

therefore, to sieve the six samples through a 125 μm sieve, to remove some of these large aggregates and get a more uniformly tubular product. The average yield of the desired fraction (< 125 μm) was 80% approx., indicating that the undesired aggregates only contributed a small proportion to the overall batch content. Particle size analysis of the sieved product < 125 μm, indicated an average size of 27.86 μm approx. (standard deviation = 4.75 μm) , whereas, that for the fraction > 125 μm was ~193 μm (standard deviation = 5.35 μm). The calculated standard deviation for the six sample fractions < 125 μm, as illustrated above, was low, indicating that there was good uniformity of content within the original entire powder batch.

The SEM micrograph for the sieved halloysite sample fraction (i.e. sample 2; fraction < 125 μm) is illustrated in Fig. 8.3c. The Figure clearly illustrates a more uniformly tubular product with fewer aggregates, when compared with Fig. 8.3b (prior to sieving). Both SEM images illustrated are at the same magnification to facilitate qualitative comparison of the two. As a result, this size reduced fraction of the second larger Halloysite 'G' batch was used in all subsequent characterising and drug loading studies.

Figure 8.3b. SEM micrograph of halloysite 'G'; Sample 2 - prior to sieving (magnification X 25,000).

Figure 8.3c. SEM micrograph of halloysite 'G'; Sample 2 - fraction sieved < 125 μm (magnification X 25,000).

TEM micrographs of the sieved halloysite 'G' fraction are illustrated in Figs 8.3d, 8.3e and 8.3f. TEM analysis illustrates a number of interesting characteristic structural properties of the halloysite mineral. In Fig. 8.3d, an unrolled tube is clearly evident at position A. According to Bates *et al*, (1950), dehydration of the natural halloysite (endellite) induces a structural strain in the mineral and causes the tubes to collapse, split, and commonly unroll. Such unrolling may produce a spatula-like form, if the same tube were viewed obliquely. The presence of the above unrolled mineral suggests that we were provided with the de-hydrated form of the mineral. This is further confirmed by XRD analysis in Section 8.5. It is important to note, however, that not all tubes collapse, split or unroll upon dehydration, and very often only become modified very slightly or not at all. This explains the presence of intact tubes, at positions B and C, in Fig. 8.3d, representing a tube of unit cell wall (B) and multiple unit cell wall thicknesses (i.e. several spirals (C)). Cross section of tubes are again illustrated at positions A and B, in Fig. 8.3e. These cross sections clearly illustrate the thickness of the wall and the lumen diameter. Fig. 8.3f illustrates a two layered (double) tube at position A. According to Bates *et al,* (1950), double tubes are quite common and in such particles there is often an 'empty'

space between the inner and outer tubes, and if the particles are sufficiently translucent, the inner tube can be seen running the length of the outer one or, as in our case, projecting at both ends.

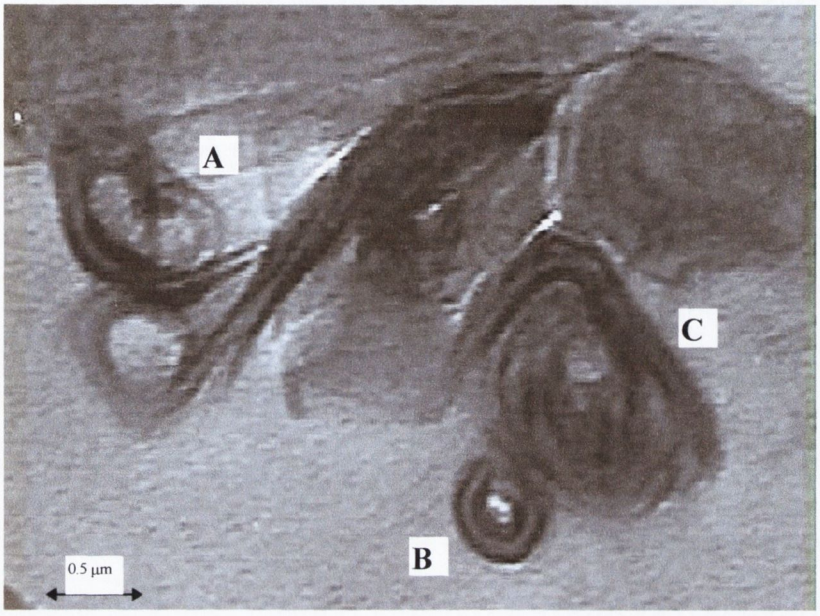

Figure 8.3d. TEM micrograph of New Zealand Halloysite 'G'. (A) partially unrolled tube; (B) end cross section of single cell walled tube; (C) end section of multiple cell walled tube (magnification X 100,000).

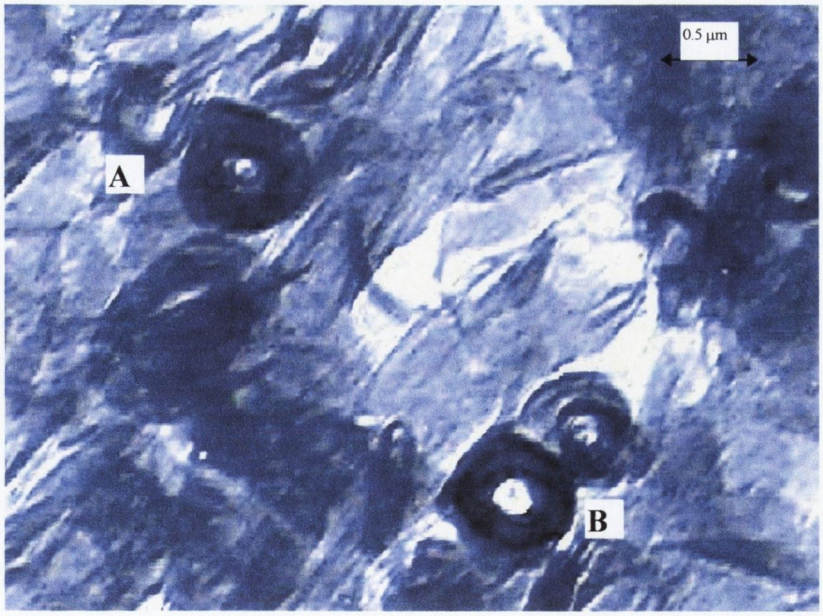

Figure 8.3e. TEM micrograph of New Zealand Halloysite 'G'. (A) and (B) are end cross sections of intact single cell walled tubes (magnification X 100,000).

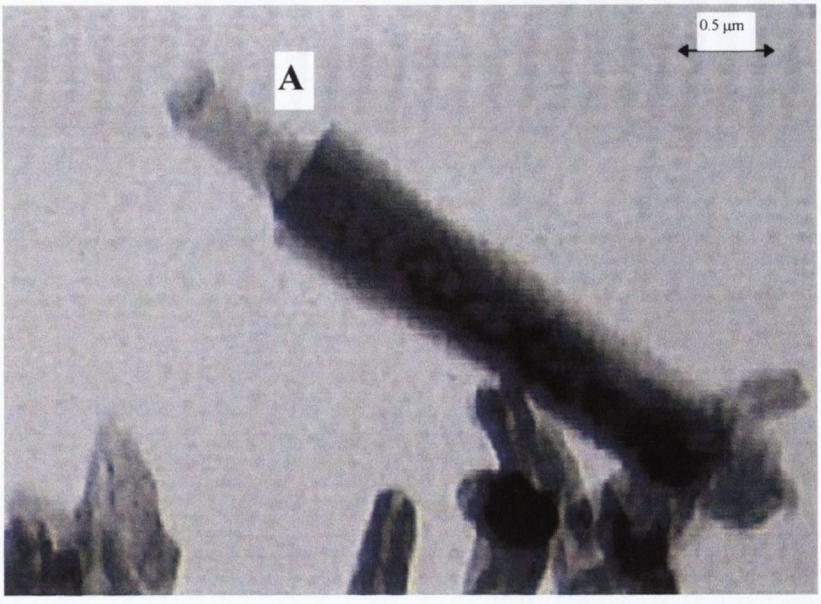

Figure 8.3f. TEM micrograph of New Zealand Halloysite 'G'. (A) double tubes (tube in tube; magnification X 100,000).

Energy dispersive analysis was also performed on the six random batch samples. This involves bombarding the elements present within a sample with high voltage electrons, which have the ability to displace electrons from the element orbitals. These displaced electrons have an associated energy, (i.e. E = hf), and emit X-rays. These X-rays are detected in this form of analysis and the associated energy behaves as a tag or marker for a particular element, which is plotted as a peak. Analysis of all six samples showed similar results. All gave sharp, well defined peaks for aluminium, silicon and oxygen, which was expected, as the mineral is composed essentially of an alumina sheet in conjunction with a silicon-oxygen sheet. Two additional very small peaks were detected, indicating the presence of iron. As mentioned in Chapter 1, larger Iron (III) atoms substitute some of the aluminium atoms in the silica layer and are responsible for a reduced curved morphology of the mineral, (Noro, 1986). In addition calcium was also detected, which was probably due to the presence of various calcium salts, such as calcium carbonate. The energy dispersion results for sample 3 are illustrated in Appendix 7.

8.4 Zeta Potential Measurements of Halloysite G

The zeta potential curve for the halloysite mineral was determined to examine the effect of different medium pH on its overall surface charge. Figure 8.4a illustrates the zeta-potential curve for halloysite 'G'. It is apparent from the plot that the surface charge of the mineral is only slightly negative in media with low pH values. As the pH increases from 2 to 6 the mineral's surface charge falls sharply to -27 mV approx., at which point the charge reaches a plateau, with subsequent increases in pH. The surface charge again becomes more negative in aqueous media with pH values greater than 10. This curve is very similar to results reported by Tari *et al.,* 1999, who carried out their work on a halloysite sample, obtained from the kaolin deposit of Sao Vicente de Pereira (Portugal), using a similar technique.

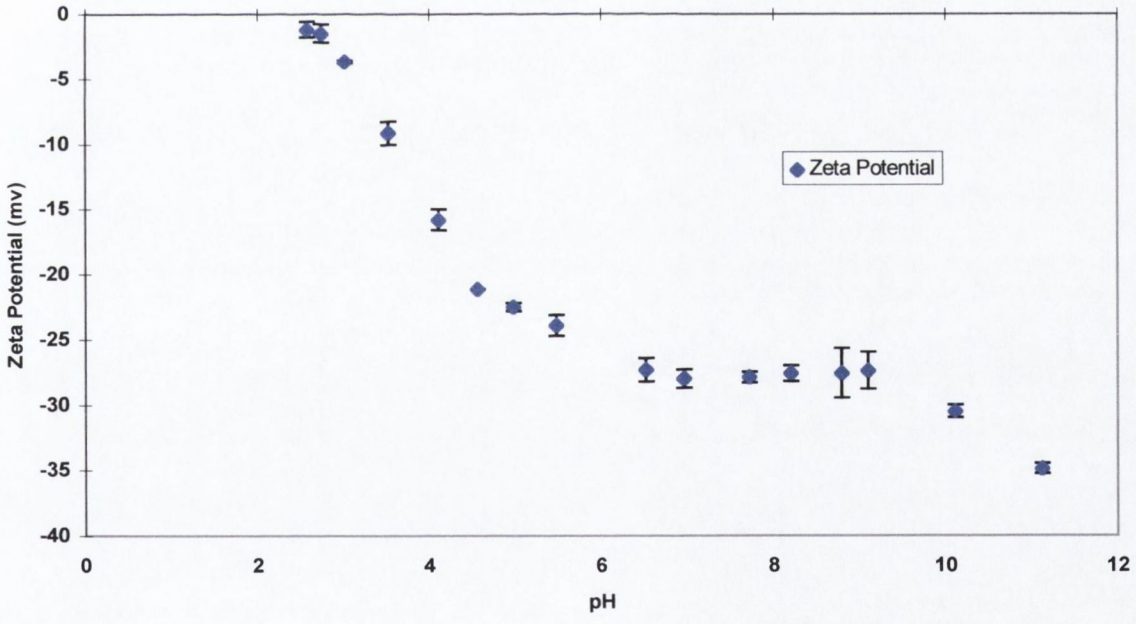

Figure 8.4a. Zeta-potential curve of Halloysite G.

The reason for the generation of this negative surface charge was explained previously in Chapter 1. As mentioned, halloysite is essentially a tubular mineral, consisting of a 1:1

structure, in which a modified gibbsite sheet is bonded to a silicon-oxygen sheet. In the curved structure, the silica is predominantly positioned on the outer surfaces of the tube, whereas the alumina is present mainly on the inner surface and edges of the tubes. Exposure of the aluminium and silicon oxides to water causes the formation of surface hydroxyl groups (Sur-OH) that can be ionised, as illustrated below.

$$\left[Sur - OH_2^+ \xleftarrow{H^+} Sur - OH \xrightarrow{OH^-} Sur - O^-\right] \qquad \text{Eqn. 8.4a}$$

Silica, being an acidic oxide, causes the second reaction on the right hand side of Eqn. 8.4a to be predominant over a substantial range of pH values, while alumina shows a more amphoteric behaviour. Since the surface is mainly silica, the surface charge will be predominantly negative over a wide range of pH, as is evident between pH 6 - 10. The full complexities of the effect of pH on surface charge are described in Chapter 1.

As a result, halloysite mineral tends to have a permanent negative surface charge. This tends to electrostatically attract cations in order to ensure the electroneutrality of the system. This phenomenon is examined in more detail for the cationic drug, Diltiazem HCl, and a number of cationic coating polymer species, in Chapter 9. When dispersed in water, these cations may be exchanged with others present in the solution, depending on their relative affinity for the particle surface, as quantified roughly in accordance with the Hofmeister scale.

8.5 XRD Identification of Halloysite G

As well as TEM and SEM techniques confirming the identity of the tubular mineral, XRD techniques were used also. As previously mentioned, halloysite is a member of the kaolin group of minerals, but differs from kaolinite, due to its tubular morphology and also its ability to exist in a hydrated state. XRD techniques were used to identify halloysite and

determine whether it was present in either the dehydrated, hydrated or partially hydrated form. The XRD plots obtained for the halloysite G mineral are shown in Fig. 8.5a.

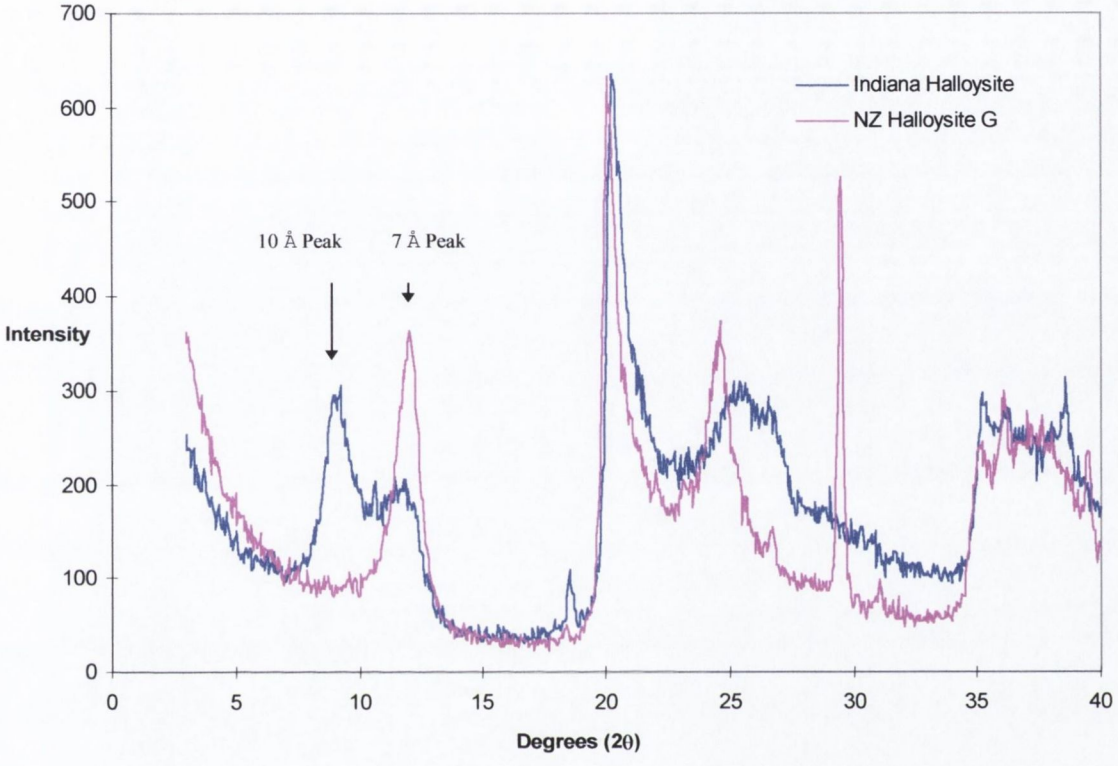

Figure 8.5a. X-Ray diffraction patterns of New Zealand Halloysite G and Indiana halloysite.

Fig. 8.5a illustrates a number of important features. The basal spacing reflections for New Zealand halloysite G indicate a sharp peak at 12.05 ° 2θ (7 Å-form), which translates to a 001 basal spacing of 7.35 Å, using Bragg's Law. There is also the absence of a peak at approx. 8.76° 2θ indicating the absence of the 10 Å-form, corresponding to the hydrated form of halloysite. Thus, it can be concluded that the halloysite supplied is fully dehydrated. This is further confirmed by the presence of the 002 basal reflection at 24.55° 2θ (equivalent to d = 3.63 Å) which is indicative of dehydrated halloysite (7 Å-form). The fact that the halloysite G is fully dehydrated is not surprising, as it is supplied in a dried powder state with a residual moisture content of 9.5% approx. (determined by drying a

sample to constant weight in an oven at 50°C). Harrison and Greenberg (1962) observed that the fully hydrated form of halloysite underwent some dehydration, even at relative humidities of 90%, as manifested by the presence of a diffuse shoulder on the high angle side of the 10.1 Å reflection. Hughes (1966) found that halloysite dehydrated rapidly in the 70-30% relative humidity region. Nagasawa (1969) suggested that the stability of the interlayer water may be related to the age of formation, ie older halloysite tends to have a less stable interlayer water.

A sample of halloysite obtained from Indiana University was X-rayed for comparison purposes. The XRD plot is also illustrated in Figure 8.5a. The main difference between it and that of the NZ halloysite G is the presence of both dehydrated (7Å-form) and hydrated halloysite (10 Å-form), which is evident as a diffuse peak between 8 to 13 degrees (two theta), and hence can be referred to as a partially hydrated mineral specimen. The Indiana halloysite sample underwent minimal treatment and drying, since its excavation from the ground, explaining the presence of some hydrated clay. The intensity of the 9.77 Å is approx. twofold the 7.4 Å peak. It is important to note that this does not correspond to the relative levels of the hydrated and dehydrated mineral present, as the 10 Å peak tends to be considerably more intense as a consequence of the L_P factor which increases, towards smaller two theta values.

8.5.1 Intercalation of Halloysite G

We are essentially interested in halloysite G in terms of drug loading and sustained release thereof. It is proposed by us that the halloysite may be loaded with drug, using three possible mechanisms. One such mechanism is the complexation of the organic drug molecules with the mineral, by intercalation. The other two involve ionic binding of cationic drug molecules to the anionic mineral surface and/or physical entrapment of the drug molecules within the tubule lumen. The formation of organic complexes of halloysite has been shown extensively (MacEwan, 1948; Carr & Chih, 1971; Churchman & Theng, 1984). In general, organic substances enter in such a way as to form a single flat molecular layer (Brindley & Brown, 1980).

Based on this phenomenon, it was proposed by us that the halloysite may be loaded with drug by this mechanism, and hence the ability of our drug candidate, Diltiazem HCl, to intercalate with the halloysite G clay, was examined. In addition, the effect of glycerol and de-ionised water were examined. Glycerol was chosen as a marker compound, as it has been shown to intercalate with hydrated halloysite in several studies (MacEwan, 1948; Carr & Chih, 1971), with a characteristic peak of 11 Å approx., ie a Δ value relative to dehydrated halloysite of 4.0 Å approx. The halloysite was treated with these compounds by grinding individually in a mortar and pestle for 20 min approx., and allowing them to stand and equilibrate with the compounds for three days. The XRD plots obtained are illustrated in Fig. 8.5b.

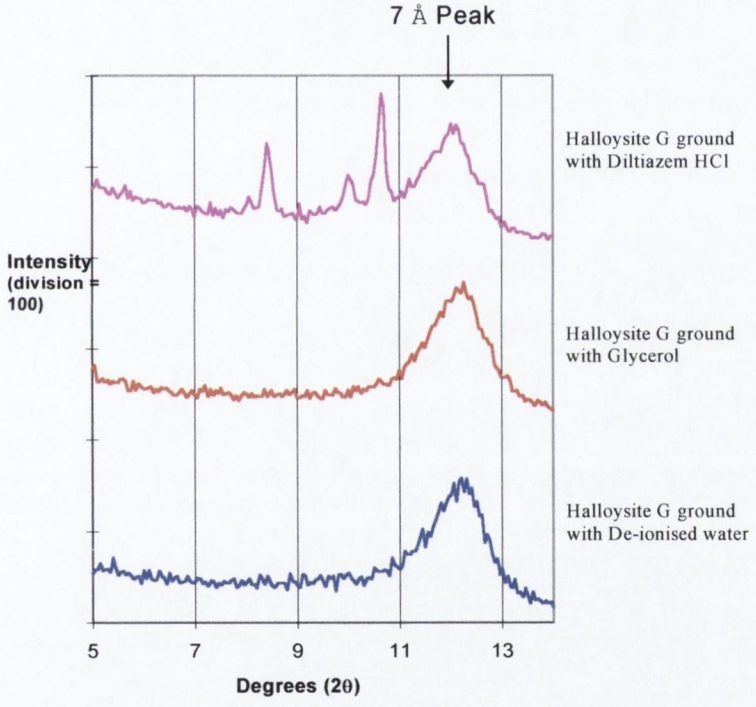

Figure 8.5b. X-Ray diffraction patterns of New Zealand Halloysite G ground with Diltiazem HCl, Glycerol and de-ionised water.

Fig. 8.5b illustrates a sharp 7.32 Å peak (12.10° 2θ) for all treated halloysite samples, i.e. there is no shift in the basal spacing reflection. It indicates that the dehydrated halloysite cannot be re-hydrated by exposing it to excess water, i.e. the dehydration process is

irreversible. This has been confirmed by past studies, whereby Harrison and Greenburg (1962) showed that halloysite dehydrated to any degree exhibits no detectable level of re-hydration, even when exposed to 100% relative humidities for up to two months. In addition, Fig. 8.5b also illustrates that the dehydrated mineral does not intercalate with Glycerol or diltiazem HCl, as again there is no shift in the basal refection (001) for the treated clay samples from 7.32 Å.

It has been observed, however, that several compounds that do not react with halloysite in its dehydrated state are capable of reacting with a rehydrated specimen. Churchman and Theng (1983) state that a high degree of interlayer hydration clearly favours complex formation, because the halloysite interlayers are then already expanded by water, enabling the organic species to be intercalated with relative ease. Halloysite cannot, as illustrated previously, be re-hydrated directly, but instead must proceed indirectly by first forming an intersalation complex with ammonium or potassium salts. In our case, Wada's procedure (1961) was adopted, which uses potassium acetate (KAOc) to form the intermediary intersalation complex. The progression of our re-hydration of the NZ Halloysite clay sample, via this technique, is illustrated in Fig. 8.5c.

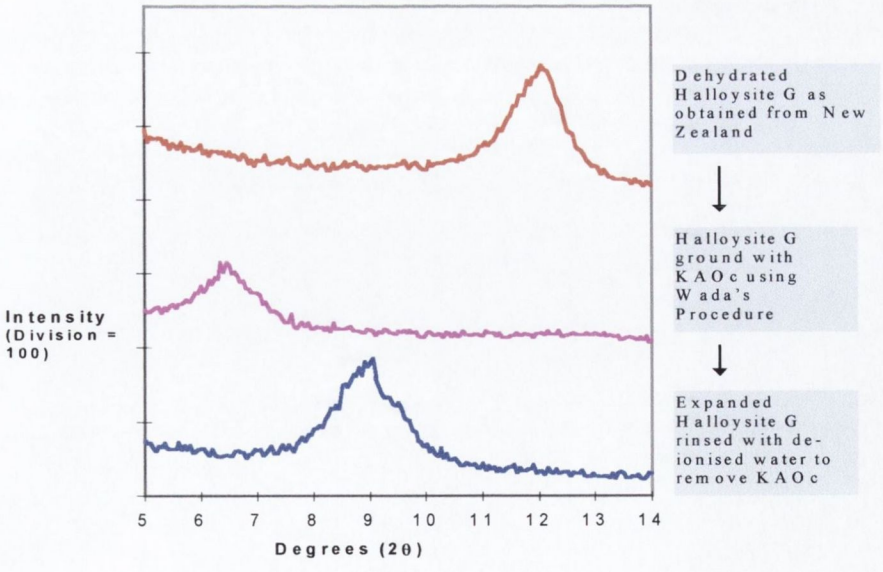

Figure 8.5c. X-Ray Diffraction pattern illustrating the progressive re-hydration of NZ Halloysite G through the intermediary formation of an intersalation complex.

The de-hydrated halloysite, for which the 7.32 Å basal peak (12.10° 2θ) is very evident, is expanded after grinding with KAOc to form a sharp peak at 13.92 Å (6.35° 2θ) representing the intersalation complex. This is in agreement with previous experimental findings (Miller & Keller, 1961). This basal peak shifts to a higher angle, corresponding to a smaller basal spacing, following washing with de-ionised water and the removal of the KAOc. The resultant basal spacing of 9.77 Å (9.05° 2θ) identifies the presence of hydrated halloysite.

The previous intercalation experiments with Diltiazem HCl and glycerol were repeated with the artificially re-expanded and re-hydrated halloysite. In addition, a number of other organic compounds were chosen, including Benzalkonium chloride (BAC), Tween 20, Polyvinylpyrrolidone (PVP) and Polyethylene glycol 400 (PEG). PEG and Tween 20 exist in liquid form at room temperature, whereas aqueous solutions were prepared using BAC and PVP. BAC and Tween 20 were chosen as they behave as surfactants and may facilitate hydrophobic drug loading into the treated clay tubule. PEG 400 and PVP were investigated due to their higher viscosities relative to water, and hence their potential ability to augment the containment of drug trapped within the mineral interlayer.

The re-hydrated halloysite was ground with the various organic liquids and solutions and allowed to equilibrate over a period of time (21 days). The treated clay minerals were examined by XRD, at one and twenty one day intervals, to examine the effect, if any, of equilibration time. The results are illustrated in Figs 8.5d (i) and (ii) respectively.

Glycerol, the marker compound, was shown to intercalate with the re-hydrated halloysite as is evident by a shift in the basal spacing from approx. 9.77 Å to 10.98 Å. This corresponds to a shift to lower angles in Fig. 8.5d (i) and (ii). In the case of all the other organic compounds, including Diltiazem HCl, no shift in the peak was observed relative to the 9.77 Å hydrated halloysite. According to MacEwan (1948), one can claim

(i)

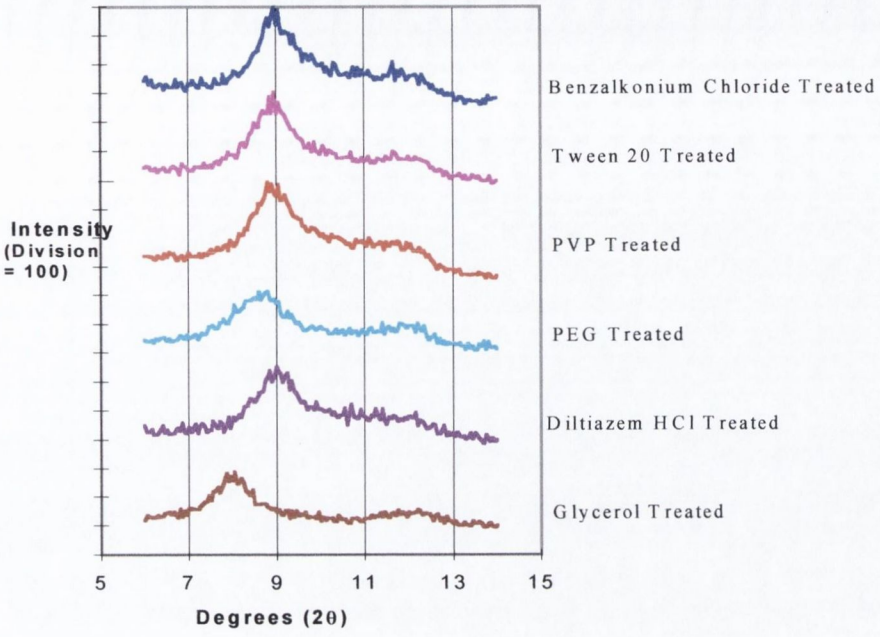

(ii)

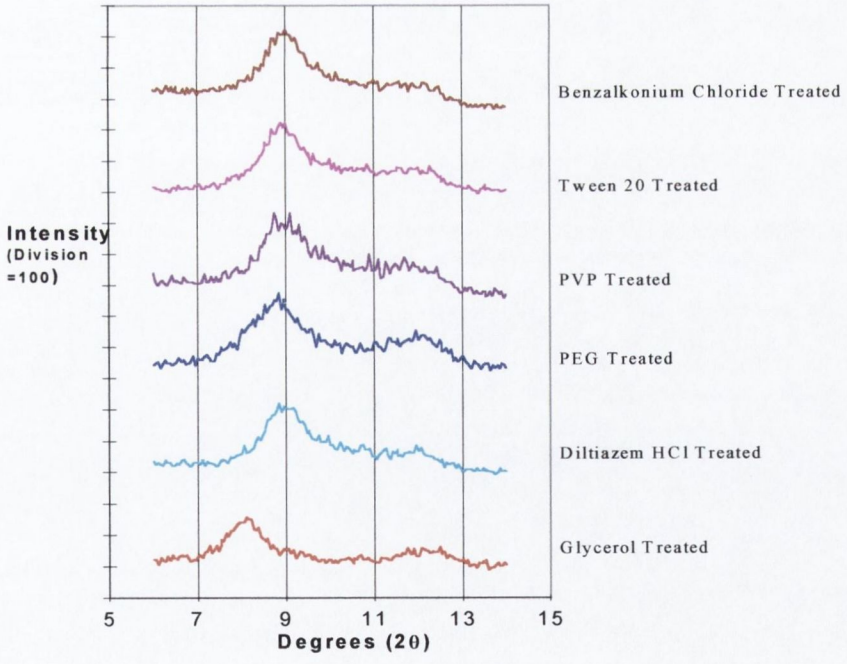

Figure 8.5d. X-ray Diffraction pattern of artificially re-hydrated NZ Halloysite G treated with BAC, Tween 20, PVP, PEG 400, Diltiazem HCl and Glycerol at (i) one and (ii) twenty one day intervals, respectively.

that definite complex formation occurs only when

$$\Delta_{product} > \Delta_{water}$$

where Δ_{water} is approximately 2.8 Å. This is only the case for the complex between halloysite and glycerol (where $\Delta_{product}$ is 3.7 Å approx.), and hence no claims can be made for the other organic compounds. It would appear, however, that no complexes are formed, as all the organic compounds are significantly larger than the water molecule and expansion would be expected if complex formation were to occur. Intercalation would appear unlikely, in agreement with the observations of Carr & Chih (1971) that in general an organic compound will only form a complex with halloysite, provided it is relatively small, contains two functional groups (preferably -OH and/or $-NH_2$) and has one functional group per two carbon atoms. Intercalation compounds do not generally include cyclic or aromatic types. The existence of these complexes lies in the ability of the organic compound to form hydrogen bonds with the halloysite structure. Since most of the organic compounds examined by us did not form complexes, the effect of equilibration time on its formation was irrelevant. In the case of glycerol, complex formation occurred quickly, within one day, and no further differences were evident with time.

8.6 Mercury Porosimetry of Halloysite Samples

8.6.1 Introduction

Halloysites include a significant concentration of fine pores. Diameters recorded for the largest concentration of pores have depended upon the resolution of the techniques used for measurement. Diamond (1970), Churchman and Payne (1983) and M^{c}Crea *et al.*, (1990), all using mercury intrusion porosimetry, found that pores in the < 50 nm range provided most of the pore volume. Jackson *et al.*, (1971), using isotherms of nitrogen and also from water sorption studies, found a sharp peak at 2-3 nm in the pore-size distribution, due to the presence of mesopores. The tubes are considered to provide the characteristic small pores, both directly from their hollow interiors, and also indirectly from the voids created, when they pack together with other tubes (Churchman and Payne, 1983).

Mercury porosimetry was used to examine the porous distribution of our New Zealand halloysite powder sample. Porosity studies were performed on three halloysite samples, one which had previously been sieved through a 125 μm sieve to remove large particulate material, a second which was both sieved and milled using an ultracentrifugal mill, and a third which was sieved and treated to remove its allophane content. Allophane removal involved boiling the halloysite with an aqueous NaOH solution, followed by appropriate rinsing with water as outlined in the methodology section. The aim of this section was to evaluate the porous structure of the halloysite samples and determine a quantitative estimate of their drug loading capabilities from the retrieved data.

Similar to studies performed on the MCC powders, the porous characteristics of the halloysite samples were determined by examining the pore size distribution, as reflected in plots of the cumulative pore volume intruded by mercury *vs* the pore diameter, or plots of the incremental intrusion volume *vs* pore diameter.

8.6.2 Results and Discussion

Table 8.6a. Quantitative results of porosimetric study of halloysite sample powders.

	'Sieved only' halloysite	**'Sieved and milled' halloysite**	**'Sieved and allophane removed' halloysite**
Ave. Particle Size of Raw Material (μm)	27.86 ± 4.75	10.18 ± 0.24	24.66 ± 1.70
Hg Total Intrusion Volume (ml/g)	0.928 ± 0.004	1.049 ± 0.008	0.827 ± 0.059
Median Pore Diameter Volume (μm)	2.089 ± 0.021	1.533 ± 0.221	3.410 ± 0.005
Bulk Density (g/ml)	0.671 ± 0.001	0.631 ± 0.085	0.702 ± 0.032
Porosity (%)	62.21 ± 0.28	66.26 ± 9.43	57.99 ± 1.49

Table 8.6a above illustrates the total mercury intrusion for the three halloysite powder samples. The levels of mercury intrusion for all samples are very similar, ranging from 0.827 ml/g for the sample treated to remove the allophane content, to a maximum of 1.049 ml/g for the Retsch® milled sample. This pattern is also reflected in the overall calculated porosities for the three samples, the values of which range from a minimum of 57.99 %, to a maximum of 66.26 % for the 'allophane removed' and 'sieved and milled' samples, respectively. The higher values for the milled sample are a direct consequence of the milling process. This breaks down any large aggregates present in the original powder bed, as well as breaking down some of the individual mineral tubules, thereby reducing the overall average particle size of the powder (i.e. reduced from 27.86 μm to 10.18 μm), with a more uniform size and shape distribution. This results in reduced powder bed packing properties, as reflected by the reduced bulk density values (i.e. 0.631 g/ml and 0.671 g/ml for the 'sieved and milled' and 'sieved only' halloysite samples, respectively) and hence, explains the higher recorded porosity and mercury intrusion values of the 'sieved and milled' fraction. The bulk density for the 'allophane removed' fraction is highest (0.702 g/ml), due to the removal of the less dense amorphous allophane content.

The median pore diameters are also shown in Table 8.6a for the three halloysite samples. They vary from a maximum value of 3.41 μm for the 'sieved and allophane removed' sample to 2.089 and 1.533 μm for the 'sieved only' and 'sieved and milled' samples, respectively. The magnitudes of the median pore diameters correlate directly with the magnitude of the powders average particle sizes. This can again be explained by Hausner's (1981) observations (similar to the MCC powders), where he states that when a powder mass consists of fine particles, pores between the particles are fine, and vice versa for larger, coarser particles.

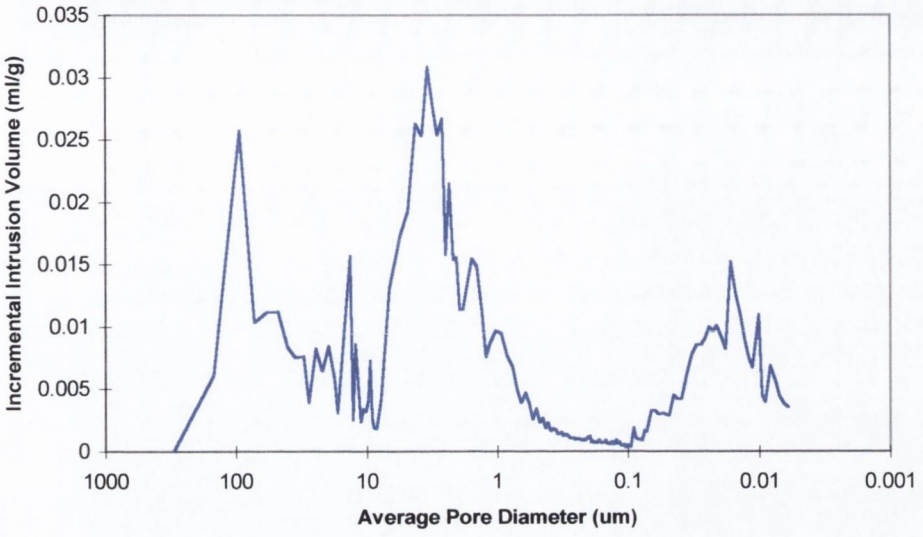

Figure 8.6a. Incremental mercury intrusion curve for 'sieved only' halloysite.

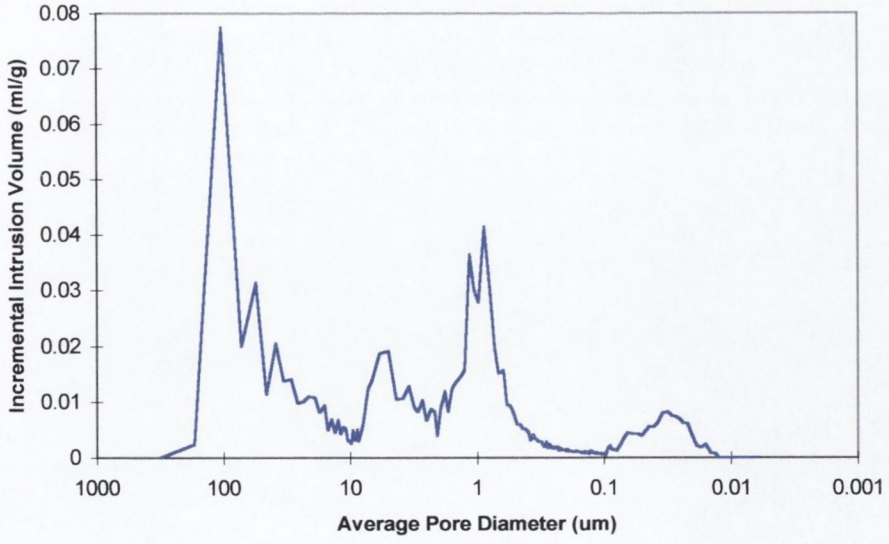

Figure 8.6b. Incremental mercury intrusion curve for 'sieved and milled' halloysite.

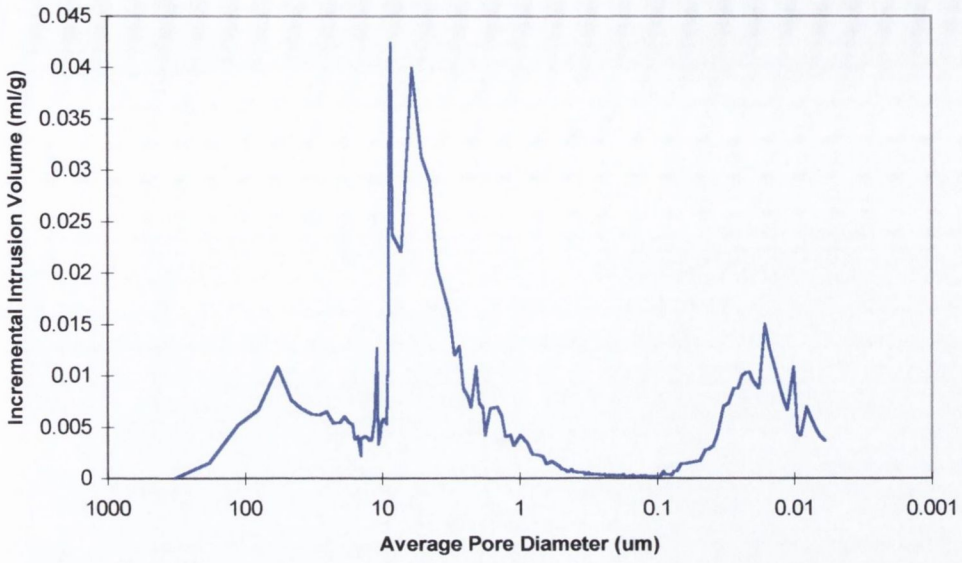

Figure 8.6c. Incremental mercury intrusion curve for 'sieved and allophane removed' halloysite.

The incremental intrusion curves for the three powders are illustrated in Figs 8.6a, 8.6b and 8.6c. All powders illustrate a tri-modal pore distribution. Coarse pores are observed in the range of ~12 to 200μm, in addition to finer pores being present in the range 0.5 to 12 μm for the 'sieved and milled' sample, and 1 to 12 μm for the other two halloysite samples. This indicates that the milling process has the effect of reducing the overall size of these finer pores. Pores within both of these ranges correspond to the interparticulate voids, (i.e. voids between individual particles), within the powder mass. In the case of all three samples, intraparticulate pores are also evident. The diameters of these pores range between ~0.006 to 0.1 μm (~6 to 100 nm) with an average size of 50 nm approx. and correspond to the diameters of the pores within the mineral tubules. Pores within the tubes consist predominantly of the luminal space and also voids created by mineral dehydration. Using an electron microscope with an environmental cell, Kohyama *et al.*, 1982, showed that dehydration of halloysite caused groups of layers to apparently shrink as a block, creating slit shaped pores between each group.

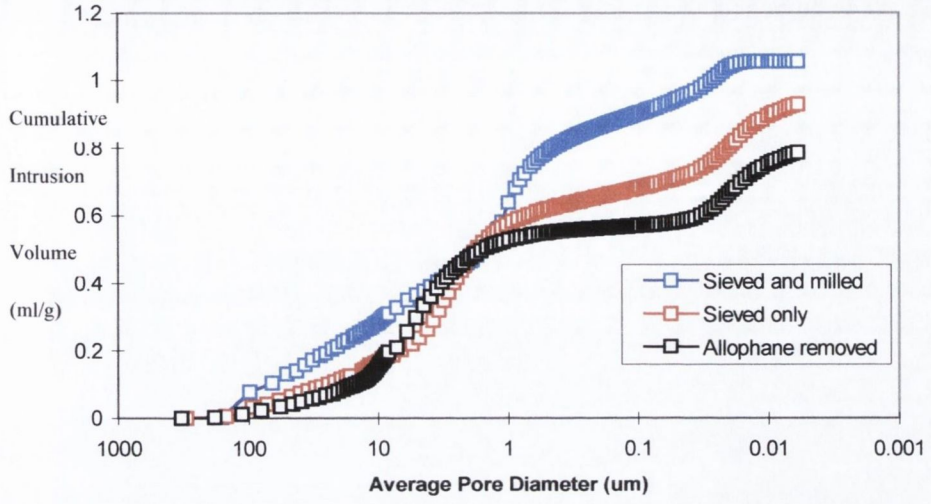

Figure 8.6d. Cumulative mercury intrusion curves for 'sieved only', 'sieved and milled', and 'sieved and allophane removed' halloysite powder samples.

The cumulative intrusion plots are illustrated in Fig. 8.6d. For all powders, there is a gradual initial increase in intrusion volume, corresponding to the filling of the coarse pores in the range 12 to 200 μm, followed by a more rapid increase in intrusion in the range 0.5 to 12 μm, corresponding to the filling of the finer interparticulate pores. In all cases, a further intrusion is evident below 0.1 μm, corresponding, as mentioned before, to the halloysite tubule pores filling with mercury. From these cumulative plots, it is possible to calculate an approximate estimate of the amount of mercury that intrudes into the tubular space per unit weight of halloysite. These values give us a guide to the potential drug loading capacities of the powders The calculated, average mercury intrusion volume values within these pores (ie < 0.1 μm) are listed in Table 8.6b.

Table 8.6b. Calculated average mercury intrusion volume estimates, within pores less than 0.1 μm in diameter, for halloysite sample powders.

	'Sieved only' halloysite	**'Sieved and milled' Halloysite**	**'Sieved and Allophane Removed' Halloysite**
Total Hg intrusion volume into pores < 0.1 μm (ml/g)	0.246	0.130	0.224

It is this inter-tubular volume that is important to us in terms of drug loading, as we intend to drug load this space and then entrap it, using various microencapsulation techniques, consequently delaying its release and creating a sustained drug delivery system. By maximising the volume of the tubule, we will be able to maximise the amount of drug that we can entrap, thereby reducing the potential amount of the formulation that will have to be administered to a patient. The values determined vary significantly, from a minimum of 0.13 ml/g for the 'sieved and milled' halloysite sample, to a maximum of 0.246 ml/g for the original 'sieved only' sample. This suggests that both treatment processes have detrimental effects on the pore volume, although this is minimal in the case of the 'allophane removed' sample. Retsch® milling probably reduces the lumen volume by smashing up some of the individual tubules, as well as the larger aggregates, into useless debris which has a low ability to entrap drug. In addition, the allophane removal treatment did not expand significantly the size of the lumen. The opposite was expected, as allophane predominantly lines the lumen of the mineral tubules, and its removal should have freed up space previously occupied by it. Based on the above poresizing results, we decided to use the 'sieved only' halloysite sample for all future, drug loading studies, the results of which are shown and described in Chapter 9.

8.7 Specific Surface Area Measurements

Surface area analysis was performed on the three halloysite 'G' samples, which were examined previously using mercury porosimetry, using the nitrogen gas adsorption technique. Values of specific surface area obtained for the halloysite powders are shown in Table 8.7a.

Table 8.7a. Specific surface area of halloysite powder samples measured by N_2 adsorption technique.

Method	Halloysite Grade 'G'	Pre-treatment conditions	Surface area (m^2/g)
N_2	'sieved only'	Heated at 70°C for 24 hr under	57.28
N_2	'sieved and milled'	vacuum, followed by helium purge	57.68
N_2	'allophane removed'	for 3 hr at 70°C.	59.86

According to Table 8.7a, the specific surface area calculated for the 'sieved only' material fraction of the original halloysite 'G' powder was 57.28 m^2/g. This value is very close to the BET surface area value of 60 m^2/g determined by Price, 1999 (correspondence), on a similar grade of the mineral, in the Naval Research Laboratory, Washington DC. It is also very similar to the value (56.2 m^2/g), determined by Churchman *et al.*, (1995), using the BET equation, on a thin tubular form of the mineral, obtained from Jarrahdale, Western Australia. This value is significantly larger than values determined for the size reduced grades of MCC, as listed in Section 6.2.2, even though their average particle size distributions are smaller, ie 12.62, 10.58 and 24.3 μm for Grade X, Grade Y and 'sieved only' halloysite powders, respectively. This is due to the highly porous, tubular nature of the halloysite mineral, which dramatically increases its specific surface area available for N_2 gas adsorption.

It is evident from the tabulated results that there is very little difference between the average surface areas for the 'sieved only' and 'sieved and milled' forms of the mineral,

even though the average particle size distributions determined, illustrate that the milling process causes a more than twofold decrease in the mean particle size (see Table 8.6a). This suggests that the milling process predominantly disrupts the mineral aggregates, within which nitrogen gas can freely flow and adsorb, and only has a smaller effect on breaking up the actual individual mineral walls, which would be responsible for increasing overall surface area. This suggests that individual halloysite tubules are very resistant to the abrasive forces experienced during ultra-centrifugal milling.

A more significant increase in surface area is obvious, when the halloysite is alkali treated to remove allophane associated with the mineral. This chemical process results in an increase of 2 m^2/g approx. of mineral to give an average value of 59.86 m^2/g for the specific surface area. This increase in the surface area can be attributed to the dissolution of the allophane associated with the mineral, to create mesopores within the mineral walls of approx. 2 to 3 nm in diameter (Jackson *et al.,* 1971). These mesopores are not detected by Hg porosity experiments, discussed in Section 8.6, as the instrument used by us was only capable of generating pressures to intrude mercury into pores of 6 nm diameter or greater.

8.8 Extrusion / Spheronisation of Halloysite Samples

8.8.1 Introduction

Halloysite was also examined as a potential extrusion/spheronisation aid, using similar technology, as described for microcrystalline cellulose in Chapter 7. It is clearly evident form SEM and TEM micrographs, that halloysite posseses an intertubular lumen, which has the potential to entrap drug molecules, thereby delaying drug release, as described earlier. The approximate volume of this lumen was quantified by mercury porosimetry studies. Drug release may be further hindered by incorporating the drug loaded halloysite into a spherical matrix. As a result, we examined the ability of halloysite to form pellets using this technology, and retain this spherical matrix, when added to dissolution media.

Halloysite G powder, which had been sieved less than 125 μm, was chosen for this study. Moistened masses of the halloysite powder were prepared at three different moisture levels, namely 17, 19 and 21%. These moisture levels were chosen, as TGA analysis of the powder indicated that the halloysite had a residual moisture content of 9.5% approx. and so the combination of this moisture and the added water levels would give an experimental moisture range of 26.5 to 30.5%, which is similar to water levels used in the MCC studies. After a suitable equilibration time (24 hr approx.), the moistened masses were extruded, using a rotary gravity-fed extruder, followed by spheronisation on a 120 mm diameter spheroniser, using a cross-hatch friction plate. The spheronised pellets were collected, dried, and analysed, using a set of standard sieves.

8.8.2 Results and Discussion

The results for pellet yields are illustrated in Fig. 8.8a below. There are a number of important features displayed. Firstly, the greatest yields of pellets occurred with the lowest of the three hydration levels (17%). The yield at this hydration level is 84% approx. At this hydration level there is also a large percentage of fines and negligible large

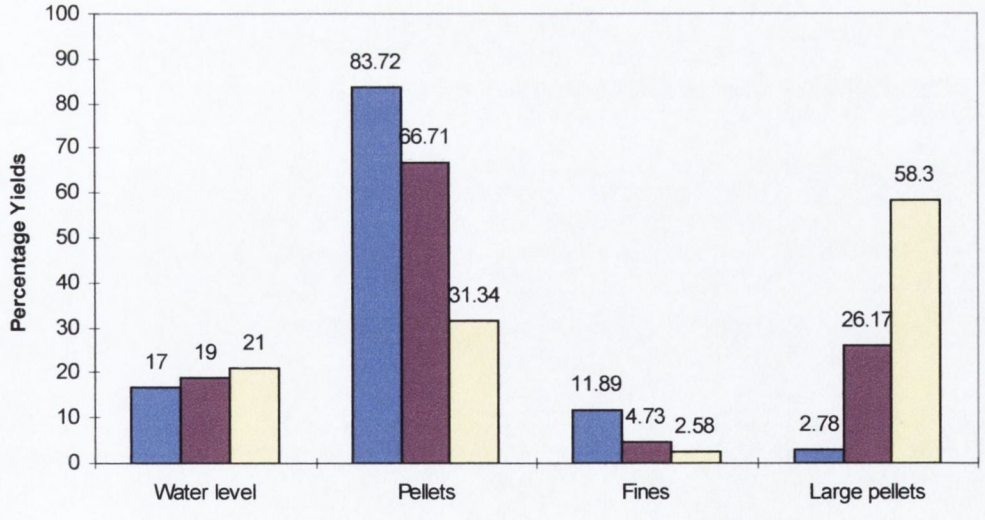

Figure 8.8a. Bar chart illustrating the percentage levels of pellets, fines and large pellets produced by extrusion/spheronisation at 17%, 19% and 21% hydration levels.

pellets. As the water level was increased the yield of pellets and fines fell. In conjunction, the percentage of large pellets increased dramatically. This is because water behaves as a binder and keeps the powder particles together as a cohesive mass. As its level increases the cohesive forces in the mass increase similarly, and so coalescence of individual pellets tends to occur during the spheronisation process, resulting in the formation of large agglomerates which are undesirable. The presence of water also confers plastic properties to the wet mass. This plasticity is desirable as it produces more spherical and smoother pellets. Visual examination of the pellets produced at the three hydration levels illustrates that the most spherical and smooth pellets were produced at the highest hydration level. As a result, a compromise between pellet yield and smoothness is apparent. Despite the above promising results, halloysite was discarded as a spheronisation aid, because when the pellets were added to water they disintegrated rapidly (unlike the MCC pellets), losing their matrix effect. Halloysite does not posses the ability to form adequate hydrogen bonds, which are responsible for retaining the matrix in the case of microcrystalline cellulose. In other applications, where rapid disintegration of spheronized pellets is desired, halloysite has interesting potential.

8.9 Conclusion

New Zealand proved to be the best source of a suitably large and uniform batch of the halloysite clay powder. Microscopic examination using SEM and TEM techniques verified that the powder consisted of an essentially tubular material with average dimensions of 5-10 μm approx. in length and 0.25-0.5 μm approx. in diameter. Various structural properties such as double tubes and split and unrolled tubes were observed, which are characteristic of the dehydrated halloysite mineral. Its identity and dehydrated nature were further confirmed by XRD analysis, which illustrated a predominant 7 Å peak indicative of the dehydrated form. Expansion of the mineral was observed using Wada's procedure, (1961), and the ability of the mineral to complex with various organic compounds, including the drug Diltiazem HCl by intercalation, was examined. Intercalation was shown to occur only with the glycerol marker compound, structural considerations probably being the reason for the lack of reactivity with the other species.

Energy dispersive analysis performed on a number of random samples illustrated strong iron, silica, and oxygen peaks, corresponding to their presence within the alumina/silicon oxide sheets, the principal building blocks of the mineral. The mineral's surface charge was shown to be predominantly negatively charged over a range of physiological pH values. Minimum negative charge occurred in acidic conditions (pH ~ 2) and conversely, was greatest within the high pH range. This negative surface charge will be manipulated in drug binding and cationic polymer coating studies, described in Chapter 9.

Mercury porosimetry studies performed on the mineral indicated a bulk density of 0.67 g/ml approx. and an overall porosity of 62% approx. for the 'sieved only' fraction of the powder. Overall, porosity was increased and bulk density was reduced, by size reducing it via milling, using an ultra-centrifugal Retsch® mill. Removal of allophane by treatment with sodium hydroxide also slightly reduced the overall porosity, but increased the powder's bulk density by removing the amorphous allophane material. Assuming that luminal pores within the mineral's tubular structure were less than 0.1 μm approx. in diameter, their intrinsic volume was calculated to be almost 0.25 ml/g. This is an important limiting factor when drug loading the mineral. Luminal entrapment volume was greatest for the 'sieved only' powder fraction and this grade was examined solely, in all subsequent drug loading studies.

Specific surface area was very large, being 57.28 m^2/ g approx., compared to only 3.5-3.7 m^2/g approx. for MCC Grades X and Y, both of which also had correspondingly smaller, average particle size dimensions. This suggests that the halloysite mineral has significant potential for binding drug species by ionic attraction forces. Its potential as a spheronisation aid proved disappointing in terms of sustained drug release, primarily due to its inability to maintain the integrity of the pellets, when immersed into an aqueous environment.

Based on the above observations, our powdered mineral showed significant potential for sustained drug release applications, by means of ionic binding of drug species to its surface or entrapment within its tubular core. These techniques are examined in detail in Chapter 9.

Chapter 9

Drug Loading of Halloysite

9.1 Introduction

As illustrated in Chapter 8, the halloysite mineral consists of small rigid hollow cylinders and fragments thereof. Because of its hollow cylindrical nature, it offers the potential for providing a sustained drug release mechanism. As mentioned previously, its use as a method for sustained release of biological molecules is already the subject of a recent US patent. Other related work by one of the inventors of the above patent, Ronald R. Price, also describes the controlled release of antifouling agents (tetracycline) from tubular structures, which were formed from lipid molecules and rigidised by a metallisation process, (Price and Patchan, 1991; Schnur *et al.*, 1994). The properties of these metallised lipid tubules are very similar to those of halloysite. Since both types of cylinder are rigid and the walls impermeable, the effective porosity is reflected in the cylinder's inner space. Despite the above studies, inadequate work has been performed to investigate halloysite's potential use in human and veterinary medicines.

It was the intention of this work to investigate the ability of halloysite to retard the drug Diltiazem HCl. This drug was chosen, as it is well-known to be highly soluble in water (i.e. greater than 50% w/v, Yang and Fassihi, 1997), has a low molecular weight and so would adequately challenge the proposed novel technology. We proposed to load the mineral with our drug candidate, using two general mechanisms, as illustrated diagrammatically in Figure 9.1a. The first (Fig. 9.1a(i)) would involve an ionic binding mechanism of the cationic drug with the anionic binding sites, which were shown to be

present on the mineral's surface by previous zeta measurements, over the entire physiological pH range. The second (see Fig. 9.1a(ii)), and potentially more important mechanism would entail trapping the drug within the mineral's tubular lumen, from which drug release would be hindered by the inherent matrix created by the lumenal structure. This entrapment could be enhanced by increasing the viscosity of the drug loading solution, using an inert polymer such as PVP, (Figure 9.1a(iii)). In addition, the release of the entrapped drug could also be delayed further by coating the mineral's outer surface with a thin polymer film or lipid matrix, which would have further inherent, limiting release rate properties (Figure 9.1a(iv)). The potential of intercalation was examined previously in Chapter 8 and was shown to have no effect.

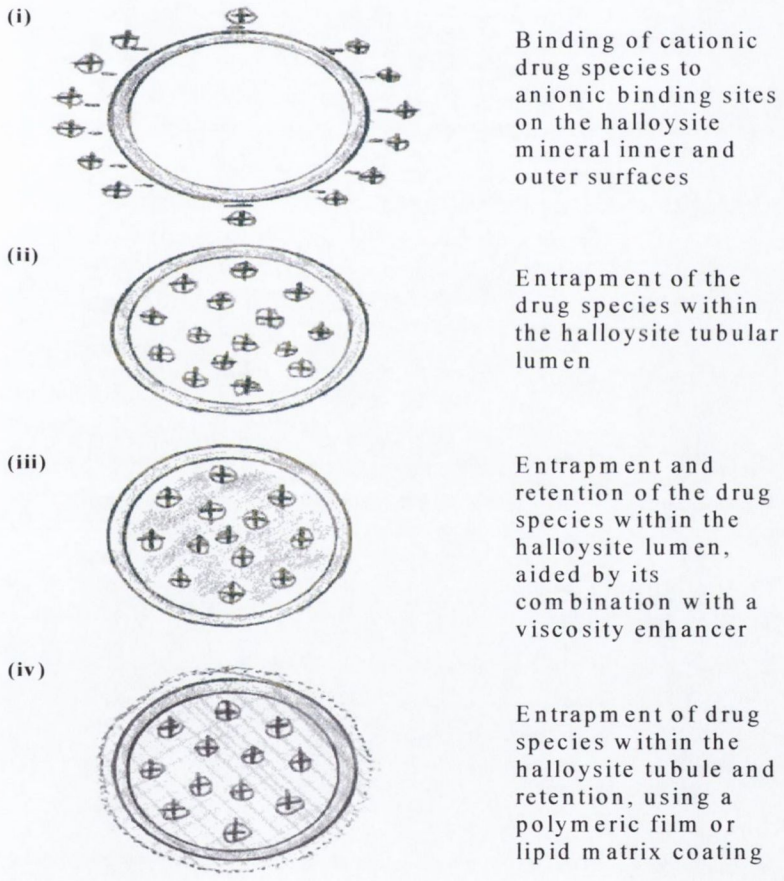

Figure 9.1a. Illustration of proposed mechanisms for loading and enhancing the entrapment of drug in halloysite.

9.2 Ionic Binding

The ionic binding profile of Diltiazem HCl with the anionic sites present on the halloysite mineral's surface was examined, as described in Chapter 3. The binding curve, as illustrated in Fig. 9.2a, is unusual, as it illustrates that, as the amount of Diltiazem HCl added to the mineral in suspension increases, the amount bound increases initially, then decreases, increases again and then reaches a plateau. The pH of the drug solutions, of varying concentrations, used for the binding studies, were monitored and ranged from a maximum of 7.43 (pure water; no Diltiazem HCl) to a minimum of 7.17 for the most concentrated drug solution used (i.e. 0.14% w/v). Therefore, the pH of the bulk aqueous environment, in which binding occurred, remained relatively constant throughout. What could not be detected, however, were the changes in pH generated within the micro-environment of the halloysite surface.

It is proposed that, initially, when low concentrations of the drug solution were added to the halloysite suspension, the pH of the mineral's surface was relatively high (i.e. ~ 7.4; pH of the bulk environment) and hence the very electronegative surface had a high binding potential with cationic species such as the ionised drug. As more drug associated itself in the proximity of the halloysite surface, with subsequent increases in the drug concentration added, the accumulation of the acidic drug caused the micro-environment around the mineral to become increasingly acidic, which, as mentioned in Chapter 8, altered the ionisation of the siloxane groups, thereby reducing the overall negative charge and hence sites available for drug binding. Eventually a drug concentration was reached, where the relative proportion of free drug was high enough to cause a net increase in drug binding again, corresponding to the upward second binding phase in the plot. Ultimately, a final plateau stage was achieved, indicating complete neutralisation of all binding sites by Diltiazem HCl. From the profile illustrated in Fig. 9.2a, it is evident that in a concentrated drug environment (i.e. > 0.14% w/v), equating to this plateau stage, 2.4 mg approx. of drug binds with 100 mg of halloysite (i.e. ~ 2.4% w/w), by ionic attraction.

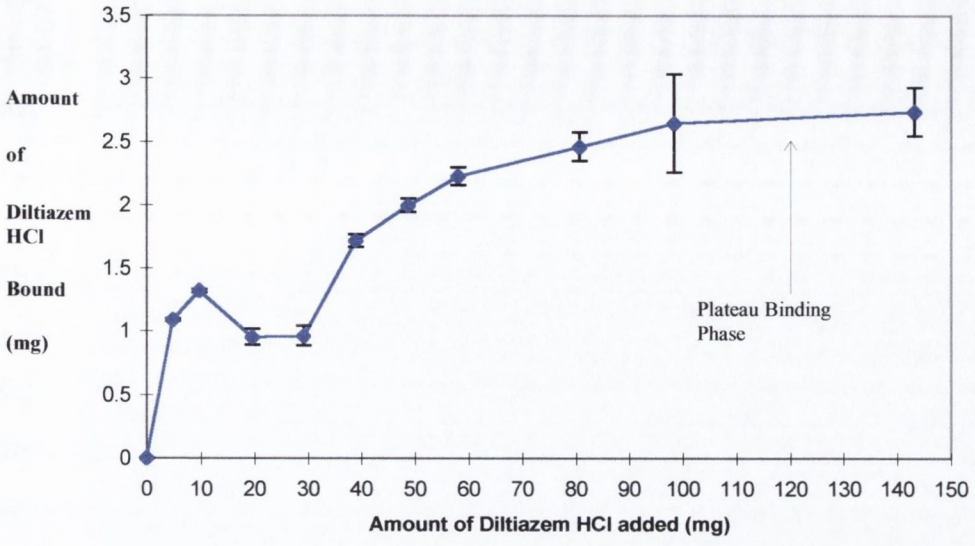

Figure 9.2a Binding profile illustrating the effect of changing amounts of Diltiazem HCl (mg) added to halloysite (100 mg), on the level of drug bound, in distilled water.

9.3 Tubular Entrapment

The potential to entrap our drug candidate within the inner mineral tubule was examined, as a means of delaying drug release. The active agent (Diltiazem HCl) was prepared as a 40% w/v aqueous solution and loaded into the tubule by vacuum, as described in Chapter 3, using a 1:1 ratio of drug solution to halloysite powder. A 1:1 ratio was found to be optimal, as higher ratios left a very wetted powder sample, even after the drug loading procedure, suggesting that not all of the drug solution was capable of being loaded within the tubule. The potential entrapment volume available (for the 'sieved only' halloysite) was calculated to be 0.246 ml/g approx., from previous Hg porosity studies. A 1:1 ratio would involve trying to entrap 1 ml of the drug solution into 1 g of the halloysite powder, i.e. more than four times the actual tubular volume available. This was achievable, however, due to the fact that the lower pressures created by the vacuum caused some of the solvent (water) to evaporate off, thereby effectively reducing the actual volume being loaded. This also had the advantage of concentrating the drug molecules within the mineral's core, to a level where they were greater than the saturation concentration of the

drug solution. This was important in order to get a high level of halloysite drug loading. Using a 40% w/v aqueous Diltiazem HCl solution, at a 1:1 ratio, the theoretical encapsulation of the drug was calculated to be 28.5% w/w of the final product, but was determined to be actually 25.6% w/w.

The release of drug from the loaded halloysite was examined, by dissolution testing, in buffer media pH 3.2 and 6.8, the results of which are illustrated in Fig. 9.3a below. Superimposed on the same plot is the dissolution of pure drug in pH 6.8. It is obvious from the profiles that by incorporating the drug into the mineral's lumen, the release rate becomes delayed relative to the non-formulated drug powder. Despite this, the loaded halloysite formulation illustrates a significant burst effect, when tested in both pH media, i.e. approx. 75.5% and 78.2% in media pH 3.2 and 6.8 respectively at t=15 min, with maximum release in both situations occurring after 4 hr approx.

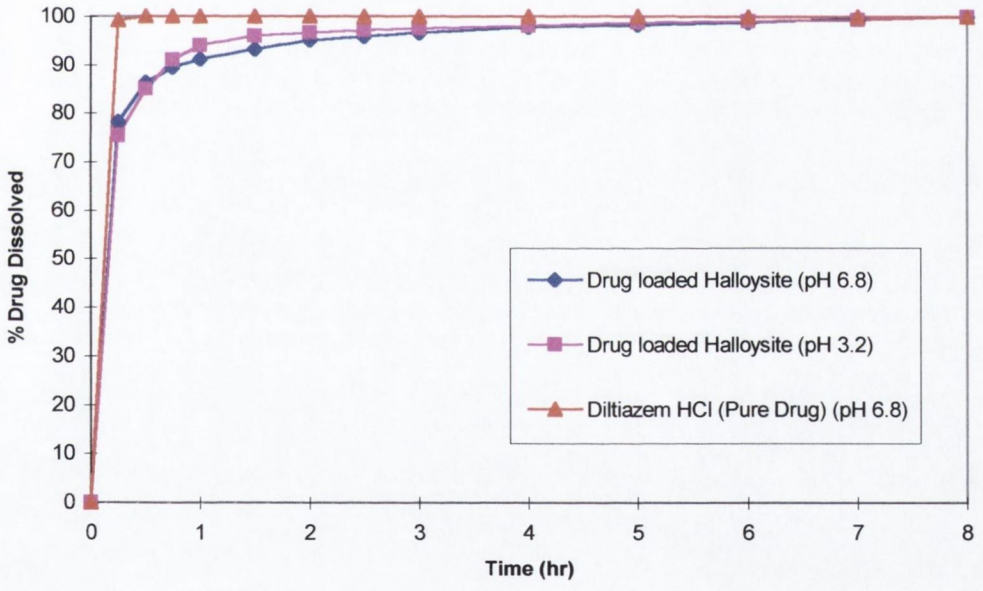

Figure 9.3a. Dissolution profiles of pure drug (Diltiazem HCl), in buffer pH 6.8, and its release from drug loaded halloysite, in buffer media pH 3.2 and 6.8, for 8 hr at 37°C.

This rapid release of drug is related to its high water solubility and later studies, discussed in Section 9.6.3, illustrate how decreasing the intrinsic solubility of the drug candidate can

dramatically reduce the burst effect and the release profiles of drug entrapped within the mineral. If we look at the dimensions of the tubule itself, its average greatest diameter is 0.1 μm approx. This dimension, although small, is still very large from a molecular point of view, and enables water molecules to readily enter the tubule in aqueous environments, by capillary forces, quickly dissolving the drug, which is then released by outward diffusion. The dissolution profiles illustrate that 90% approx. of the loaded drug content is released within the first hour, and the remaining 10% is released at a much slower rate, taking a further 3 to 4 hr approx. for complete release. The level of drug released in this final phase is very similar to that estimated previously to be bound to the mineral by ionic attraction forces, (i.e. drug loading estimate is 25.6mg / 100 mg halloysite; but 2.4 mg binds to 100 mg halloysite by ionic forces, which equates to 9.4% approx. of the total drug loading), and may account for this slower second phase of release due to disassociation.

6.4 Effect of Viscosity Enhancers

Because of the rapid drug release from the drug loaded halloysite, other techniques were examined, in an attempt to further delay the release of the entrapped drug molecules. One technique involved increasing the viscosity of the drug solution that was loaded into the tubule, the higher viscosity of which was intended to help retain the drug within the lumen, and similarly delay penetration by the dissolution medium. The viscosity was increased, by incorporating a high molecular weight polymer in with the aqueous drug solution, namely polyvinylpyrrolidone (PVP). PVP is widely used in pharmaceutical applications and has a proven non-toxic profile, (Handbook of Pharmaceutical Excipients, 2000). It has previously been used as a viscosity builder and a carrier for drugs, in concentrations of 5 to 20% w/v. In this situation the effect of its incorporation on entrapped drug release was examined, at a 5% and 10% w/v level relative to the drug solution volume, the polymer being dissolved in water initially, with the aid of heat, prior to drug incorporation.

Dissolution testing was performed at pH 6.8 on the prepared formulations, the results of which are illustrated in Fig. 9.4a below. A very small improvement in delayed drug release is observed, when PVP is incorporated at both the 5 and 10% levels, but the differences are not significant, as indicated by the calculated f_2 values, which compare them with the control formulation (no PVP present), i.e. the f_2 values are 69.50 and 73.60 for the 5 and 10% preparations, respectively, which are both greater than 50, indicating no significant difference. In both cases the burst effect is only reduced by 10% approx. from 78.2% to 68.0% and to 70.0% for preparations incorporating 5 and 10% PVP, respectively. The lack of significant improvement is probably due to the fact that the loaded halloysite powder is dried to constant weight, after loading, to remove the water content. This causes the PVP and drug molecules to precipitate out of solution within the mineral's lumen. Upon subsequent re-hydration, achieved on placing the powder into the dissolution medium, the PVP does not re-hydrate as quickly as the drug dissolves, and so the drug is leached out of the tubule, before the viscosity of the solution within it can fully increase to cause a retardant effect. PVP incorporation may have had a more beneficial effect, if the loaded halloysite powder was kept in the wetted state after loading, but since we were primarily concerned with the development of a final dry free-flowing product, which is important from compounding stability aspects, this was not examined.

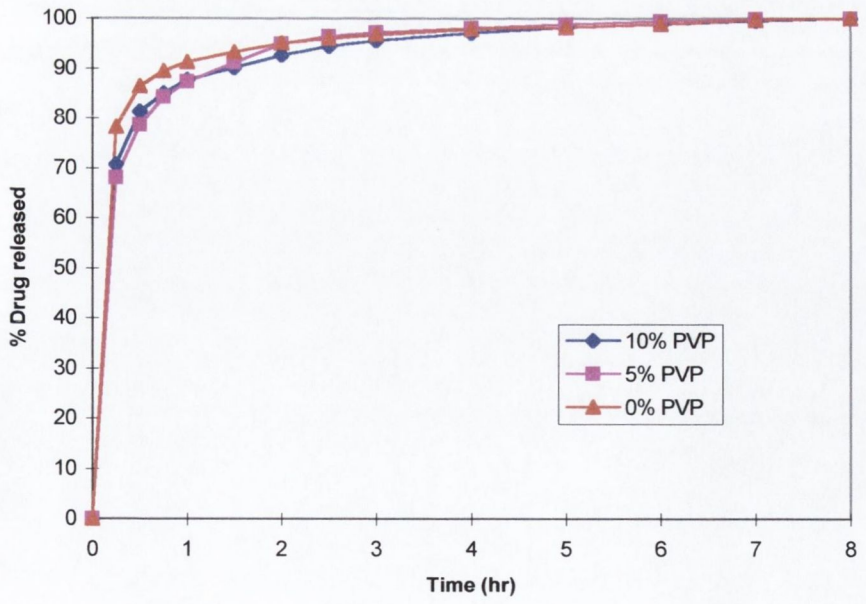

Figure 9.4a. Dissolution profile of Diltiazem HCl, from drug loaded halloysite, incorporating 0, 5 and 10% w/v PVP, in buffer medium pH 6.8.

9.5 Coating Drug Loaded Halloysite Using Cationic Polymers

9.5.1 Chitosan Coating

Chitosan is the N-deacetylated product of chitin, one of the most abundant polymers found in nature after cellulose, being a structural component of shellfish, insects and the cell walls of bacteria and mushrooms. Chitosan is a cationic polyelectrolyte and has been shown to be biocompatable and biodegradable (Hirano *et al.,* 1988, Orienti *et al.,* 1996). Due to this it has been developed for a variety of biomedical applications, including wound dressings and drug delivery systems. In the context of drug delivery, it has been used as a stabilising constituent of liposomes (Henriksen *et al.,* 1994); as an excipient controlling drug release in oral formulations (Kristl *et al.,* 1993; Denkbas *et al.,* 1999); to prepare microspheres for encapsulation of enzymes, proteins and cells (Heller *et al.,* 1996); to deliver DNA (Alexakis *et al.,* 1995) and for it's bioadhesive properties (Genta *et al.,* 1998; Yamamoto *et al.,* 2000).

As mentioned in Chapter 8, zeta potential studies illustrated that halloysite has a net negative charge, over all physiological pH ranges. Considering that chitosan is a cationic polymer, we attempted to use its polyionic interaction with the anionic halloysite, to coat the drug loaded mineral by a charge neutralisation process. It was hoped that the thin layer of chitosan, adsorbed onto the mineral's surface, would retard drug release from the reservoir created within the mineral's lumen. Polyionic complexation has been widely reviewed in the literature, observed as the formation of precipitates, on mixing cationic polymers with anionic polymers in aqueous solutions (Fuoss & Sadek, 1949; Michaels, 1965; Tsuchida *et al.*, 1974). A coulombic force is believed to be the primary binding force for the formation of these complexes (Bekturov & Bimendina, 1981).

9.5.1.1 Halloysite / Chitosan Binding Studies

In this study, we initially investigated the general properties of the polyion complex formed between chitosan and the halloysite mineral in order to get an idea of the stoichiometry of both components in the complex. Since the magnitude of the charge of both ionic species is highly pH dependent, the effect of the pH value of the media on the resultant complex was examined. Binding profiles were obtained by viscosity measurements, using a similar technique to Takahashi *et al.*,(1990), as described in Chapter 3. Chitosan, being insoluble in water, was solubilised in aqueous media containing dilute acetic acid and sodium acetate. The acetic acid quaternized the free amino group on the polymer. These stock solutions were used for the subsequent binding studies, the results of which are illustrated in Fig. 9.5a below.

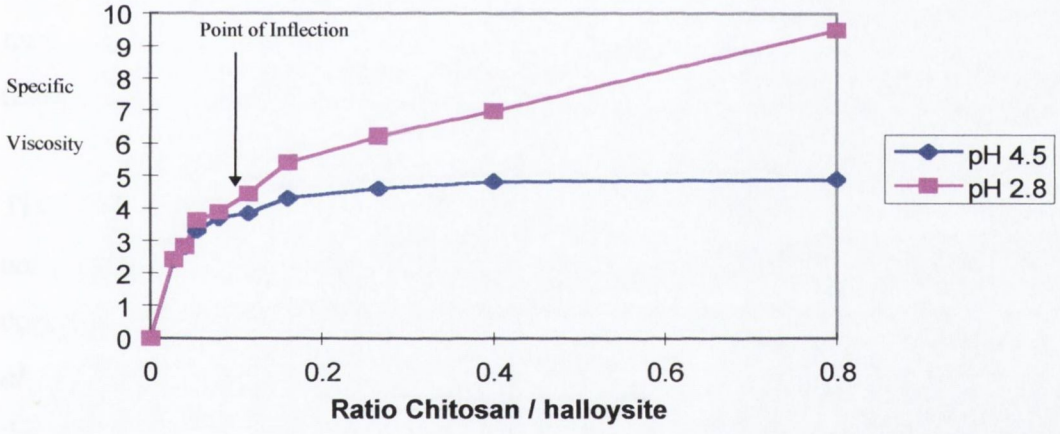

Figure 9.5a. Binding profile, illustrating the effect of changing ratios of chitosan / halloysite on the specific viscosity of the supernatant chitosan solution, in buffer media pH 2.8 and 4.5.

Figure 9.5a plots the specific viscosity of the supernatant chitosan solution, following complexation, *vs.* the ratio of chitosan to halloysite used. It is clearly evident, for both pH systems, that as the ratio increases, the specific viscosity also increases, until a point of inflection is reached and a maximum specific viscosity level or plateau is achieved. This

level is more evident when the experiment is performed in the medium of higher pH. The pattern is best explained by the fact that at high ratio levels, the amount of chitosan present is significantly greater than the amount of halloysite present. Almost all anionic sites on the halloysite mineral are fully saturated or bound, and the viscosity of the supernatant chitosan solution is very close to that of the original stock solution. As the ratio decreases (by increasing the amount of halloysite present), a point is reached (point of inflection), below which the amount of unbound anionic sites on the halloysite mineral increases dramatically, and so a greater proportion of the chitosan present is bound to the halloysite. This causes a pronounced decrease in the specific viscosity of the supernatant solution. Hence, this point of inflection reflects the ratio of chitosan to halloysite that almost fully saturates all available anionic binding sites on the mineral's surface. Ratios below this critical point represent only partial saturation, whereas those above represent near to complete saturation. The fact that the adsorption of chitosan to halloysite depends upon the total level of unbound anionic sites present on the mineral's surface (i.e. magnitude of free charge), illustrates that binding is driven by electrostatic interactions (Berndt *et al.,* 1992).

The near complete saturation ratios, as indicated by the points of inflection in Fig. 9.5a, are similar in both aqueous pH systems, and are approx. 0.1. Hence, the binding ratios are constant despite the change in pH values. A similar pattern was observed by Takahashi *et al.,* (1990), for binding between chitosan and sodium alginate. The degree of ionisation of the halloysite was considered to decrease, with decreasing pH values (see Chapter 8), whereas in contrast, the ionisation of the chitosan molecules increases, with decreasing pH values. Hence, we would have expected the unit molecular binding ratio to alter with changing pH. This was not observed and may be due to the rigidity of the halloysite mineral, which Takahashi observed to have an important role in polyion complex formation. The effects of temperature were accounted for, by performing all experiments at a constant temperature of 37°C. The overall specific viscosity is higher in the aqueous system of lower pH value (i.e. pH = 2.8). This can be explained due to the protonation of the free amino groups in chitosan, when subjected to lower pH environments. These

protonated amino groups result in a greater electrostatic repulsion between the solubilised chitosan molecules, creating more stability within the system and a resultant higher level of viscosity.

9.5.1.2 In Vitro Dissolution Testing of Chitosan Coated Halloysite

Since no significant differences were observed between the two pH systems in terms of the value of the point of inflection (saturation ratio), the higher pH system (i.e. pH = 4.5) was chosen for the subsequent coating and drug release studies. Three ratio levels were chosen for the coating studies, two being below the point of inflection, representing incomplete neutralisation and hence, film formation (i.e. 0.02 and 0.05). The third ratio chosen, 0.4, was above the point of inflection and represented complete saturation and film formation. Dissolution studies were performed at two pH levels, namely pH 6.8 and 3.2, to examine the effect of pH on the release rate through these chitosan coatings. The dissolution profiles are illustrated graphically in Fig. 9.5b & 9.5c.

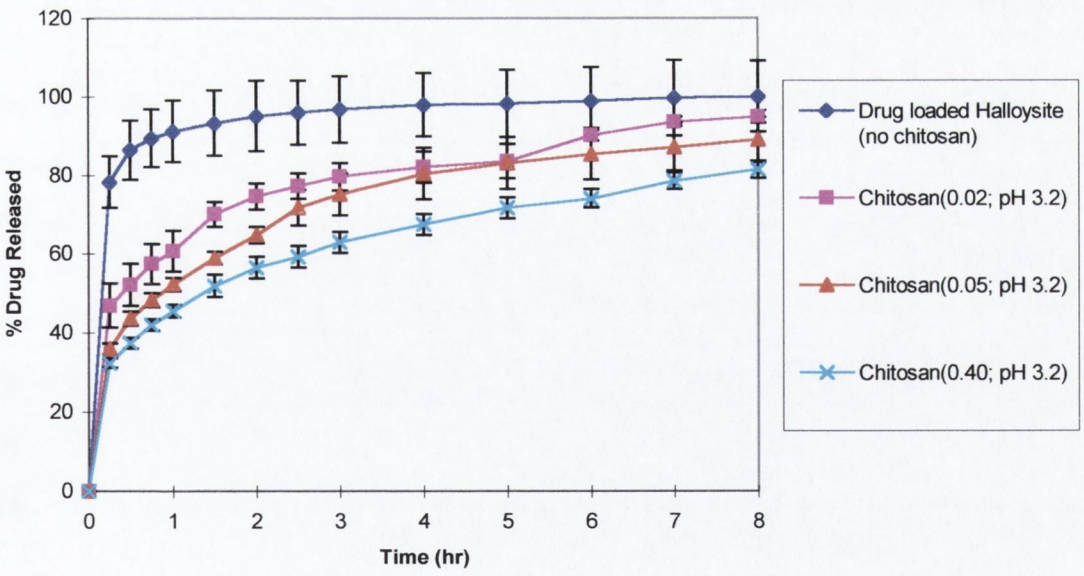

Figure 9.5b. Dissolution of Diltiazem HCL from chitosan coated (3 coating levels) and uncoated, drug loaded halloysite, in pH 3.2 McIlvaine buffer, for 8 hr, at 37°C.

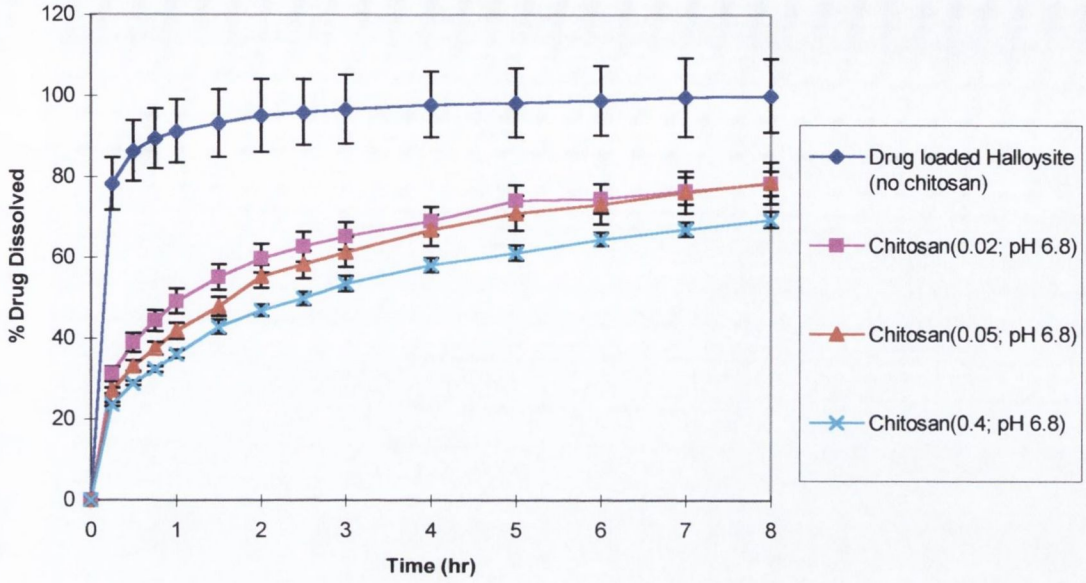

Figure 9.5c. Dissolution of Diltiazem HCL from chitosan coated (3 coating levels) and uncoated, drug loaded halloysite, in pH 6.8 McIlvaine buffer, for 8 hr, at 37°C.

Table 9.5a. % burst release and correlation coefficients calculated when the Diltiazem HCl release data, in buffer media pH 3.2 and 6.8 for the 3 chitosan coated halloysite preparations, is fitted to the Higuchi, zero order and modified zero order models, as described in the text.

Buffer pH	Chitosan / Halloysite Ratio Used	R^2 Value (Higuchi Model)	R^2 Value (Zero Order Model)	R^2 Value (Modified Zero Order Model)	% Burst Release (t = 15 min)
6.8	**0.02**	0.6899	0.6732	0.9403	31.15
6.8	**0.05**	0.8532	0.7676	0.9665	27.10
6.8	**0.40**	0.8670	0.782	0.9705	23.64
3.2	**0.02**	0.5230	0.6250	0.9707	46.87
3.2	**0.05**	0.7396	0.7015	0.9411	35.96
3.2	**0.40**	0.7806	0.7470	0.9847	32.37

Table 9.5a above illustrates the correlation values determined, when the dissolution data was fitted to various predictive models, i.e. the matrix model as described by Higuchi and the zero order model. At first glance, the data appears to fit poorly to both models with very low R^2 values obtained, i.e. all are less than 0.75. Good correlation is achievable, however, with the zero order model, if we take into account a burst effect, which is evident in the above quoted R^2 values (modified Zero Order Model). This model best describes systems incorporating membrane controlled diffusion as the rate limiting step in drug release. As a result, the chitosan coated drug loaded halloysite system can be regarded as a reservoir device, in which the active is contained within the core (i.e. tubular lumen), that is surrounded by the chitosan rate controlling membrane. Previous work by Singh and Ray, 1999, has also illustrated the controlled release of glucose through chitosan membranes to follow zero order release kinetics. The transport of drug through this membrane is dependent upon properties of the film, such as thickness and solute concentration gradient across the film, as expressed by Fick's law of diffusion.

$$J = P\frac{\Delta C}{d} \qquad \textbf{Eqn. 9.5a}$$

where J = flux of solute across the membrane, ΔC = concentration difference across the membrane of thickness, d, and P = diffusion constant..

It is evident form Figs. 9.5b and 9.5c, that the ratio of chitosan to halloysite used to coat the drug loaded halloysite had a significant effect on the subsequent release profiles. The lowest ratio (i.e. 0.02) produced the greatest release, at pH 3.2 and 6.8. This order is maintained with the other two ratio levels and the 0.4 ratio resulted in the greatest level of retardation. This is due to the fact that, when the lower ratios of chitosan / halloysite are used, the level of chitosan present is submaximal, with respect to neutralising completely all the halloysite anionic surface charges, and so the film formed is incomplete and thin. As a result, the drug more rapidly diffuses across the partial membrane, when placed into the dissolution medium. When the ratio used is increased, the film formed became thicker and more complete, thus delaying the drug release.

Table 9.5b. In vitro similarity factors (f_2), comparing the dissolution profiles Diltiazem HCl from all chitosan coated halloysite powders, relative to that those of uncoated drug loaded halloysite powder, in buffer media pH 3.2 and 6.8.

Comparison between Uncoated Drug Loaded Halloysite and Chitosan Coated Halloysite (pH 3.2)	**f_2 Value**	**Comparison between Uncoated Drug Loaded Halloysite and Chitosan Coated Halloysite (pH 6.8)**	**f_2 Value**
Chitosan Coated Halloysite (0.02)	42.54	Chitosan Coated Halloysite (0.02)	28.13
Chitosan Coated Halloysite (0.05)	34.67	Chitosan Coated Halloysite (0.05)	25.37
Chitosan Coated Halloysite (0.40)	26.95	Chitosan Coated Halloysite (0.40)	20.77

The effect of pH on the drug release profiles is also illustrated in Figs. 9.5b and 9.5c. All three chitosan coated systems show an increase in the release profiles, and hence, permeability, when the pH of the buffer system becomes acidic, i.e. shifts from pH 6.8 to 3.2. This difference is expressed by the f_2 similarity factor values, calculated when the same formulation is tested under different pH conditions. These values are 42.02 and 47.04 for the two preparations coated, using the low ratio levels (i.e. 0.02 & 0.05 respectively), suggesting that the pH effect is significant. The value determined for the 0.4 ratio formulation is greater than 50 (i.e. 51.16), indicating an insignificant difference, and hence, suggests that thicker coatings are less susceptible to changes in the pH of the dissolution media. The increases in the permeability, when the formulations are subjected to lower pH media, are again more than likely due to the protonation of the free amino groups in the chitosan (i.e. $-NH_2 + H^+ \rightarrow -NH_3^+$). Singh and Ray, (1999), argue that this causes the chitosan molecules to become uncoiled and assume more elongation, or exist in a rod like shape, ie the mutual repulsion of the charged groups supplies the uncoiling force. This increases the water absorption ability of the membrane, which in turn leads to an increase in permeability.

9.5.1.3 Burst Release Effects

For all three coating levels, the existence of a burst effect is very obvious, and arises as a consequence of the formulation process. The chitosan coat is applied in the form of an aqueous solution, which is capable of dissolving some of the entrapped Diltiazem HCl, causing it to become embedded in the coat upon subsequent drying. Thus, when the powder formulation is placed into the dissolution medium, this active agent trapped in the coat, rapidly releases from the membrane. Similar burst effects have been observed with 5-fluorouracil loaded chitosan microspheres (Denkbas *et al.,* 1999), where they observed almost 50 % of the loaded drug being released within the first hour. He *et al.,* (1999) also observed burst effects from cimetidine loaded chitosan microspheres, formed by spray-drying.

The burst effects range from 20 to 50% approx., within the first 15 min, for all the prepared halloysite formulations and are illustrated in Table 9.5a. The magnitude of the burst effects follow a similar pattern to the drug release profiles, i.e. as the chitosan / halloysite ratio increases, the burst effect decreases, again due to the thicker, more complete membranes being formed. In addition, the burst effect for the 3 formulations is greater in dissolution medium pH 3.2, which can similarly be explained due to amino group protonation and increased permeability effects.

9.5.1.4 Encapsulation Efficiencies

Table 9.5c. % drug encapsulation yields for chitosan coated (3 levels) and uncoated drug loaded halloysite.

Halloysite Formulation	**Encapsulation Yields (% w/w)**
Uncoated Drug Loaded Halloysite	25.6
Chitosan Coated Halloysite (0.02)	7.75
Chitosan Coated Halloysite (0.05)	5.6
Chitosan Coated Halloysite (0.40)	5.25

The encapsulation yields for the three, chitosan coated, halloysite formulations are listed in Table 9.5c. As the chitosan / halloysite ratio increases, the encapsulation yield decreases and is probably due to the thicker chitosan film formed around the halloysite particles. This causes the overall particle weight to increase, decreasing the relative proportion of encapsulated drug within. Overall, the encapsulation efficiencies are low, with yields ranging form 5.25 to 7.75 % w/w, indicating that the technology may be most applicable to highly potent drugs, where low drug loadings are adequate. The loading efficiency of uncoated, Diltiazem HCl loaded, halloysite was determined to be 25.6% w/w approx. This indicates that a large proportion of the drug was leached out and lost during the coating process.

9.5.1.5 Effect of Incorporating a Cross-linker

In order to obtain insoluble films, which would be capable of further delaying encapsulated drug release, glutaraldehyde was incorporated into the chitosan dispersion (0.05 ratio level only), as a cross-linking agent. The in vitro dissolution profiles from chitosan coated, halloysite micro-particles, incorporating different amounts of cross-linker, in media of different pH values, are illustrated in Figs. 9.5d and 9.5e.

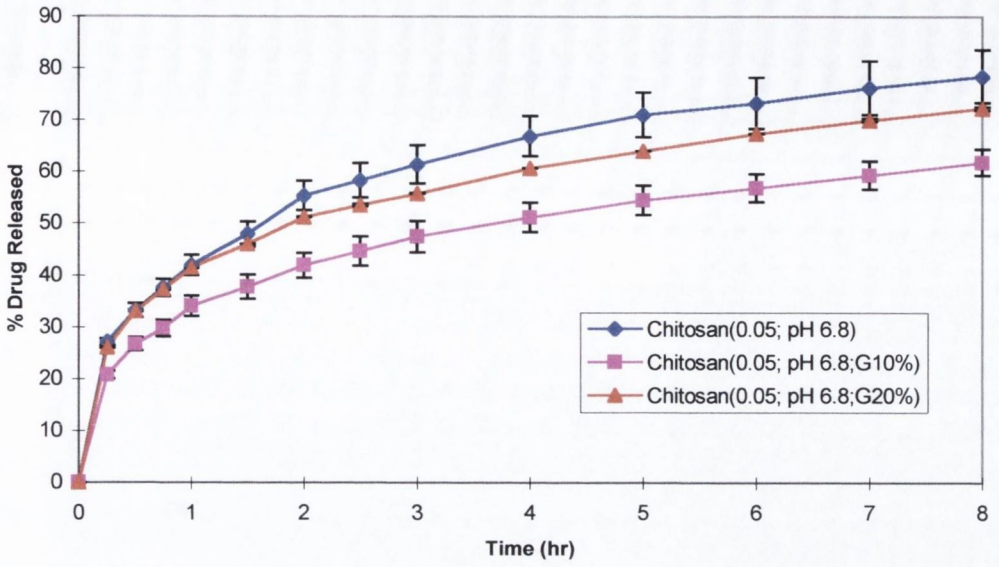

Figure 9.5d. Dissolution of Diltiazem HCl from non cross-linked and cross-linked (10 and 20% w/w glutaraldehyde) chitosan coated (0.05) drug loaded halloysite, in buffer pH 6.8.

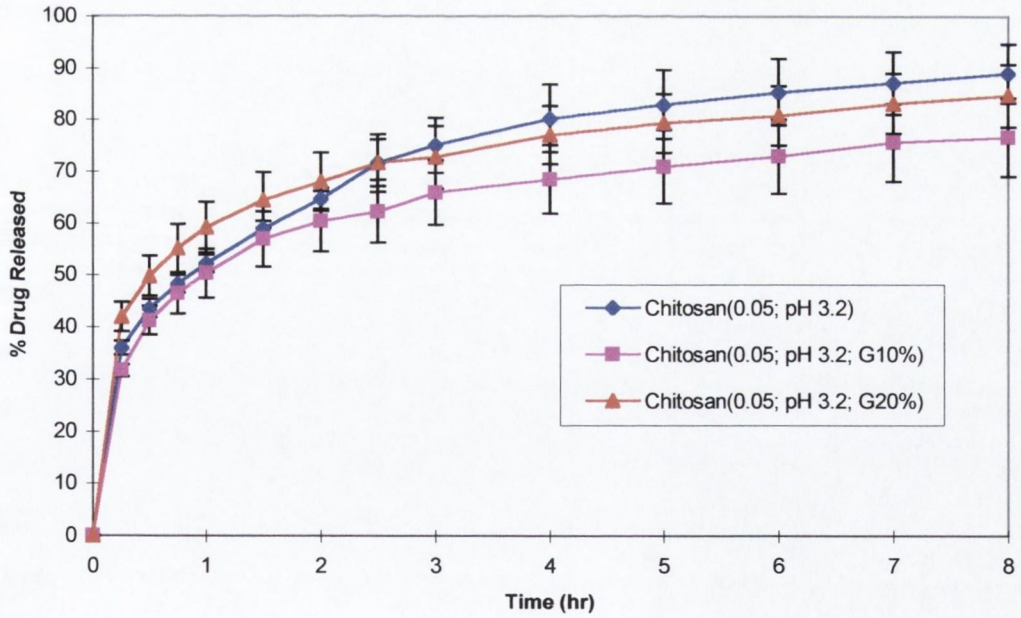

Figure 9.5e. Dissolution of Diltiazem HCl from non cross-linked and cross-linked (10 and 20% w/w glutaraldehyde) chitosan coated (0.05) drug loaded halloysite, in buffer pH 3.2.

Table 9.5d. In vitro similarity factors (f_2), comparing the dissolution profiles of Diltiazem HCl from non cross-linked, chitosan coated, halloysite powder (0.05) relative to those from cross-linked (10 and 20% glutaraldehyde), chitosan coated, halloysite powders, in buffer media pH 3.2 and 6.8.

Comparison between Non Cross-linked and Cross-linked Chitosan Coated Halloysite Powders (0.05; pH 3.2)	**f_2 Value**	**Comparison between Non Cross-linked and Cross-linked Chitosan Coated Halloysite Powders (0.05; pH 6.8)**	**f_2 Value**
10% w/w Glutaraldehyde	53.30	10% w/w Glutaraldehyde	44.12
20% w/w Glutaraldehyde	65.56	20% w/w Glutaraldehyde	66.29

It is evident from Figs. 9.5d and 9.5e that the incorporation of glutaraldehyde, at both the 10 and 20% levels (expressed with respect to the dry polymer weight), results in further delayed Diltiazem HCl release. The release profiles for the above cross-linked formulations were compared with the corresponding non-crosslinked formulation, using the similarity factor (f_2 value) for both pH media. The calculated values are illustrated in Table 9.5d. Visual examination of the plots reveals a difference to exist for the 10% cross-linker level, at both pH levels. However, it is only significant when considering the f_2 value, when dissolution testing is performed in buffer medium pH 6.8. For preparations incorporating cross-linker at the 20% w/w level, the dissolution profiles illustrate less retarded drug release, in both pH media, when compared to the 10% w/w level. A similar behaviour was observed by Ganza-Gonzalez *et al.,* (1999), which they explained in terms of the occurrence of excessive cross-linkage. This gives rise to an excessively, rigid coating structure, which swells less slowly so that drug release is less effectively retarded, i.e. when high glutaraldehyde levels are incorporated, the di-aldehyde polymerises, and so the membrane consists of a polyglutaraldehyde / chitosan copolymer. This copolymer is more hydrophilic, rigid and unable to swell, modifying the drug release properties. This suggests that there is an optimal level of cross-linker required to maximise delayed drug delivery, from the coated halloysite microparticles.

The effect of dissolution medium pH on Diltiazem HCl release, from the cross-linked formulations, illustrated a similar trend to drug release from the non cross-linked chitosan coated halloysite, i.e. all profiles illustrate an increase in the release rate, when the pH of the medium becomes more acidic, the reason for which was explained earlier.

9.5.2 Examination of Alternative Cationic Polymers

Based on the ability of chitosan to successfully bind to drug loaded halloysite and further retard drug release from within, the potential of two other cationic polymer candidates was examined, namely Eudragit E and polyethyleneimine (PEI).

(a) Eudragit E

Eudragit E has been widely used in the pharmaceutical industry, where its principal applications are in coating for taste and odour masking of tablet and capsule formulations. Its application, using the solid dispersion technique, has also been examined to obtain the controlled release of the sparingly soluble drug, Indomethacin, incorporated within its polymer matrix (Lovrecich *et al.,* 1996). Films of the polymer become water soluble by forming salts with acids and therefore, are soluble in gastric juice, i.e. pH range 2-5, (Röhm Pharma Company literature). In solutions of pH > 5, they are capable of swelling and hence, are permeable to water.

9.5.2.1 Halloysite / Eudragit E Binding Studies

Similar to the chitosan studies, the nature of the polyion complexation between halloysite and the cationic polymer (Eudragit E) was initially investigated, so as to determine the approximate stoichiometry of both components in the formed complex. Due to the insoluble nature of the polymer above pH 5, it was dissolved using a 0.1M acetic acid solution. Unlike the chitosan studies, UV analysis was used to determine the binding profiles, as described in Chapter 3, the results of which are illustrated graphically in Fig. 9.5f. Fig. 9.5f plots the amount of polymer bound (mg) *vs.* the amount added (mg), the

profile illustrating a curved shape similar to that obtained with chitosan. As the level of Eudragit E polymer added increases, the amount bound also increases, due to its complexation with the anionic binding sites on halloysite by electrostatic attraction. Again a point of inflection arises in the binding curve, corresponding to almost complete neutralisation of the mineral's surface charge. Midpoint of this inflection occurs, when 30 mg approx. of polymer is added to 100 mg of the powdered mineral, indicating a 0.3 / 1 polymer to halloysite ratio. Further binding occurs above this point, when increased increments of the amount of polymer are added, although at a reduced rate, causing complete charge neutralisation and ultimately a reversal in the coated mineral's original, surface charge. Again, all binding experiments were performed at 37°C, to account for any effects temperature might have.

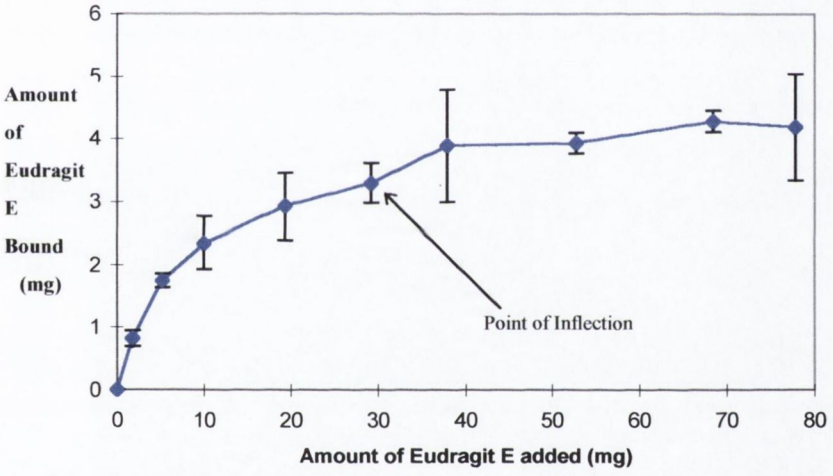

Figure 9.5f. Binding profile, illustrating the effect of changing amounts of Eudragit E (mg) added to halloysite (100mg) on the amount of polymer bound, in distilled water.

9.5.2.2 In Vitro Dissolution Testing of Eudragit E Coated Halloysite

Based on the above binding curve, three ratio levels were chosen for the coating studies, namely 0.025, 0.30 and 0.70, equating to below, approx. at, and above the inflection point, respectively. Dissolution studies were performed at two pH levels, namely pH 3.2 and 6.8, to examine the effect of pH on drug release rate through the formed films.

Testing in buffer pH 3.2 was initially performed to establish an estimate of the maximal drug release that could be expected. The dissolution profiles are illustrated in Figs. 9.5g and 9.5h.

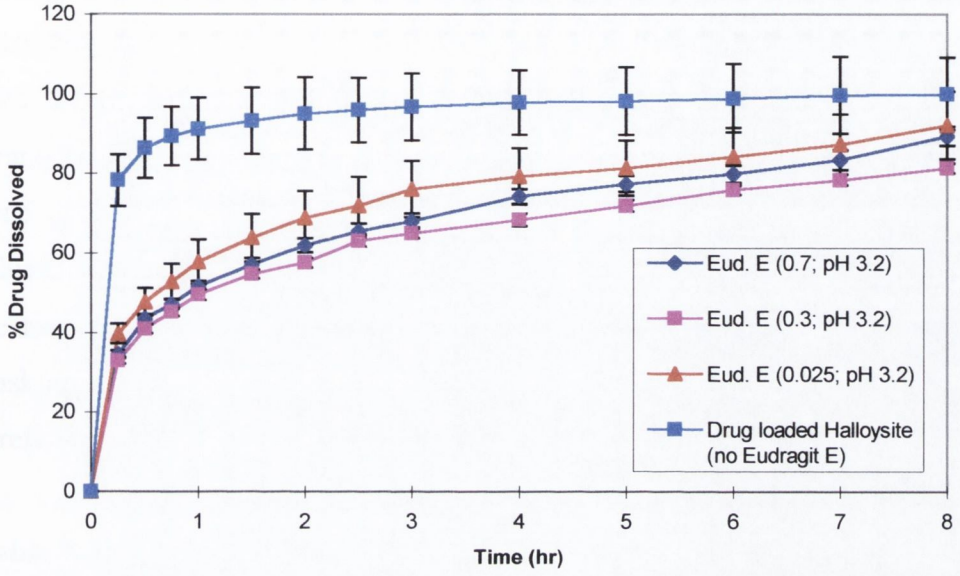

Figure 9.5g. Dissolution of Diltiazem HCl from Eudragit E coated (3 coating levels) and uncoated drug loaded halloysite, in pH 3.2 McIlvaine buffer, for 8 hr, at 37°C.

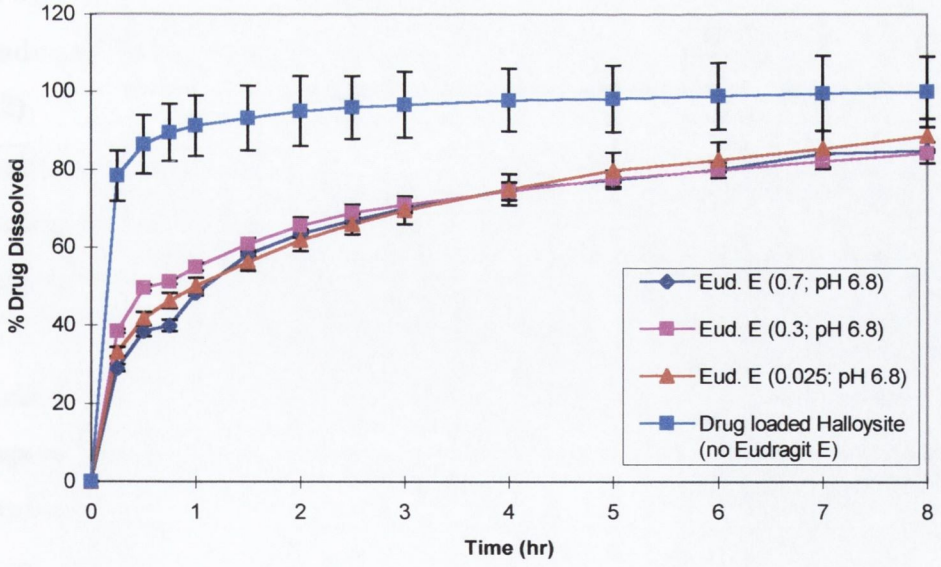

Figure 9.5h. Dissolution of Diltiazem HCl from Eudragit E coated (3 coating levels) and uncoated drug loaded halloysite, in pH 6.8 McIlvaine buffer, for 8 hr, at 37°C.

It is evident from Figs. 9.5g and 9.5h that, by coating the drug loaded halloysite with the Eudragit E polycation, significantly greater delayed release occurs relative to its uncoated control, irrespective of the pH of the buffer medium in which it was tested. This is indicated by the calculated f_2 values listed in Table 9.5e, which are all less than 50. It is interesting to note that there is no significant difference between the profiles, when the effect of media pH is examined, i.e. calculated f_2 values are 62.22, 61.17 and 72.52 for Preps 0.025, 0.3 and 0.7, respectively, when comparing the dissolution profile for the same product in buffer media pH 3.2 and 6.8. This suggests that even at higher pH values, when the polymer is relatively insoluble, it is capable of quickly expanding, creating permeability for outward drug diffusion. It is for this reason that the taste masking effects of the polymer applied to tablets, when placed in the mouth, where the pH is relatively high (i.e. ~6 to 7), only last for 30 to 60 sec approximately.

Table 9.5e. In vitro similarity factors (f_2), comparing the dissolution profiles of Diltiazem HCl from all Eudragit E coated halloysite powders relative to those of uncoated, drug loaded halloysite powder, in buffer media pH 3.2 and 6.8.

Comparison between Uncoated Drug Loaded Halloysite and Eudragit E Coated Halloysite (pH 3.2)	**f_2 Value**	**Comparison between Uncoated Drug Loaded Halloysite and Eudragit E Coated Halloysite (pH 6.8)**	**f_2 Value**
Eudragit E Coated Halloysite (0.025)	28.92	Eudragit E Coated Halloysite (0.025)	24.85
Eudragit E Coated Halloysite (0.30)	22.96	Eudragit E Coated Halloysite (0.30)	26.89
Eudragit E Coated Halloysite (0.70)	25.00	Eudragit E Coated Halloysite (0.70)	23.75

Unlike the chitosan polymer examined previously, the dissolution profiles are almost superimposable for all three coating ratio examined, especially when studied in buffer medium pH 6.8, suggesting that a near continuous film was formed with the lowest ratio level, and subsequent higher ratios had minimal effect. There is also the possibility of the existence of an ionic chemical interaction between the basic amine group of the polymer and the acidic function of Diltiazem HCl, similar to the interaction observed by Lovrecich

et al., 1996, between Eudragit E and Indomethacin. This would contribute to the delayed release of the drug, as observed.

Table 9.5f. Percentage burst release and correlation coefficients, calculated when the Diltiazem HCl release data, in buffer media pH 3.2 and 6.8, for the 3 Eudragit E coated halloysite preparations, was fitted to the Higuchi, zero order and modified zero order models, as described in the text.

Buffer pH	Eudragit E / Halloysite Ratio Used	R^2 Value (Higuchi Model)	R^2 Value (Zero Order Model)	R^2 Value (Modified Zero Order Model)	% Burst Release (t = 15 min)
6.8	**0.025**	0.9276	0.7437	0.9750	33.09
6.8	**0.30**	0.8416	0.6225	0.9850	38.41
6.8	**0.70**	0.9164	0.7205	0.9701	29.00
3.2	**0.025**	0.8689	0.6581	0.9782	39.68
3.2	**0.30**	0.8981	0.7010	0.9964	32.86
3.2	**0.70**	0.9120	0.7248	0.9818	34.44

Drug release form these Eudragit coated systems are best described, using the modified zero order model, which accounts for the presence of a burst effect (see Table 9.5f). R^2 values, in all cases, are above 0.97 and the burst release drug levels range from a minimum of 29% for preparation (0.70), in buffer pH 6.8, to a maximum of 39.68% for preparation (0.025), in buffer pH 3.2. Similar to the chitosan studies, the encapsulation efficiencies of the Eudragit E coated halloysite are reduced relative to its uncoated, drug loaded version, ie 6.15%, 4.62% and 3.26% w/w for coated preparations 0.025, 0.3 and 0.7, respectively. This is due to the leaching out of drug from the formerly loaded mineral during the coating process, which similar to chitosan, was performed in an aqueous environment.

(b) PEI

The third cationic polymer examined, namely polyethyleneimine (PEI), has been used for years in common processes such as paper production, shampoo manufacture and water purification. The polymer comes in two forms, linear and branched. More recently, it has been examined in potential pharmaceutical applications, whereby cross-linking it with carbonyldiimidazole activated poly(ethylene glycol), using emulisification / solvent evaporation techniques to form hydrophilic polymer networks, has generated the patented NanoGel™ technology (Vinogradov *et al.,* 1999). There is also currently a flurry of research aimed at this polycation's role in gene therapy, and as a gene delivery vehicle or vector (Godbey *et al.,* 1999).

9.5.2.3 Halloysite / PEI Binding Studies

The stoichiometry of its complexation with halloysite was obtained by UV measurements similar to Eudragit E, and the plot of amount of PEI added *vs.* amount bound is illustrated in Fig. 9.5i. The PEI polymer was obtained as a solution (i.e. 50% w/v aqueous solution), and so only required appropriate dilution prior to the complexation and coating studies. Again, a very similar binding profile is obtained for PEI, corresponding to the formation of the Langmuir-Blodgett film, when compared with those of Chitosan and Eudragit E. The point of inflection occurs, when 10 to 12 mg approx. of polymer is added to 100 mg of the halloysite mineral. Further binding of PEI occurs, upon subsequent addition of polymer, corresponding to charge reversal.

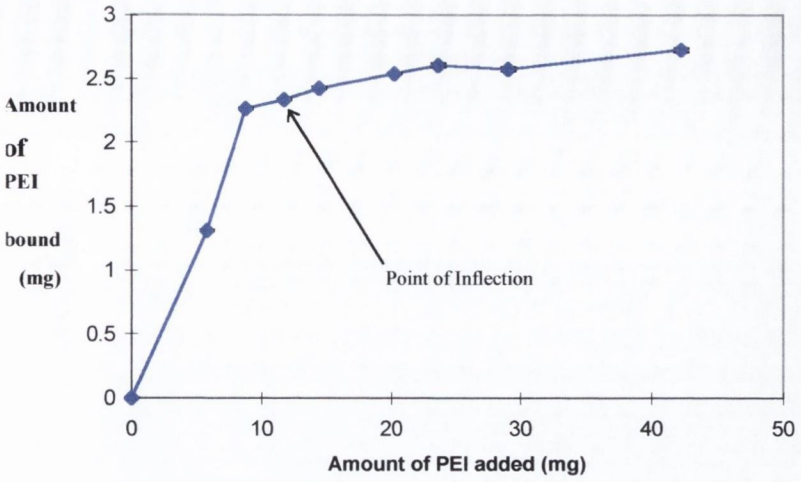

Figure 9.5i. Binding profile, illustrating the effect changing amounts of PEI (mg) added to halloysite (100mg) on the amount of polymer bound, in distilled water.

9.5.2.4 In Vitro Dissolution Testing of PEI Coated Halloysite

Based on the above profile, three PEI / halloysite ratio levels were chosen for the subsequent coating studies, these being 0.03, 0.14 and 0.28, corresponding to below, approx. at and above the inflection point, respectively. Dissolution studies were performed on the PEI coated halloysite samples, in buffer pH 6.8, the profiles of which are illustrated in Fig. 9.5j.

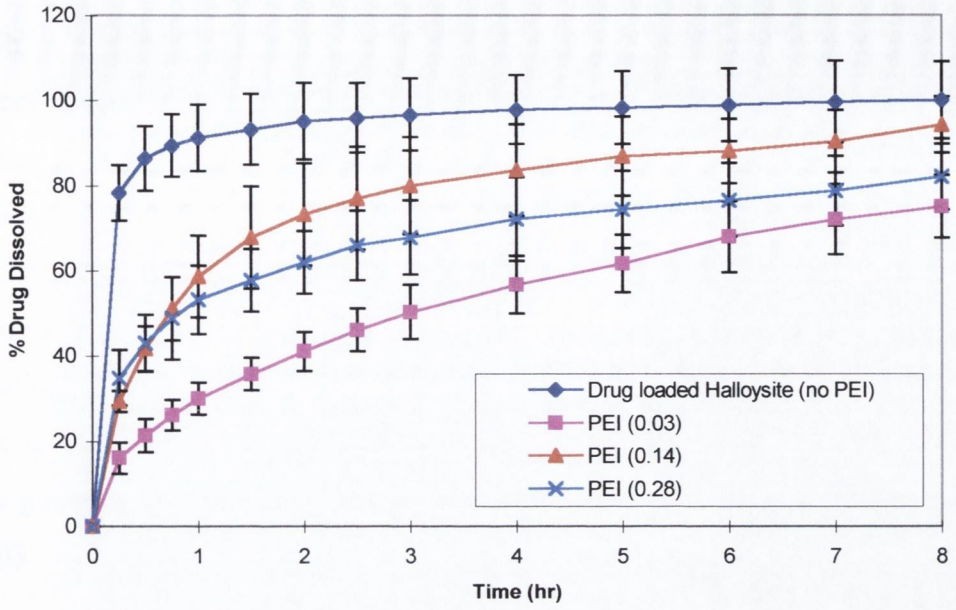

Figure 9.5j. Dissolution of Diltiazem HCL from PEI coated (3 coating levels) and uncoated, drug loaded halloysite, in pH 6.8 McIlvaine buffer, for 8 hr, at 37°C.

Table 9.5g. In vitro similarity factors (f_2), comparing the dissolution profiles of Diltiazem HCl from all PEI coated halloysite powders, relative to those of uncoated, drug loaded halloysite powder, in buffer media pH 6.8.

Comparison between Uncoated Drug Loaded Halloysite and PEI Coated Halloysite (pH 6.8)	**f_2 Value**
PEI Coated Halloysite (0.03)	15.19
PEI Coated Halloysite (0.14)	28.69
PEI Coated Halloysite (0.28)	24.63

It is evident that the coated halloysite, at all PEI ratio levels, resulted in enhanced retardation of drug release relative to the non-coated product. This delay in release was shown to be significant in all cases, as illustrated by the calculated f_2 values which are 15.19, 28.69 and 24.63 for the 0.03, 0.14 and 0.28 preparations, respectively, when compared to the uncoated sample (see Table 9.5g). The data again fitted best to the modified zero order model, which describes a constant release rate through a permeable

membrane associated with a initial burst release. The high R^2 values are quoted in Table 9.5h, all exceeding 0.97, when the burst effect is accounted for. The presence of the burst effect was again, presumably, due to drug saturation of the membrane, as a consequence of the ionic coating being applied in an aqueous environment, which dissolved some of the pre-loaded drug. Burst release, over the first 15 min, ranged from a minimum of 16% for the PEI (0.03) product to 35% approx. for the PEI (0.28) product. These results were contrary to those originally expected, as it was predicted that an increase in the level of coating polymer used would result in a corresponding decrease in the rate of drug release, due to the thicker membrane creating a longer, more hindered diffusion path. In contrast, the greatest level of retardation occurred with the lowest ratio of PEI polymer coating (ie 0.03). Higher coating ratios caused greater release rates.

Table 9.5h. Percentage burst release and correlation coefficients, calculated when the Diltiazem HCl release data, in buffer media pH 6.8, for the 3 PEI coated halloysite preparations, was fitted to the Higuchi, zero order and modified zero order models, as described in the text.

Buffer pH	**PEI / Halloysite Ratio Used**	**R^2 Value (Higuchi Model)**	**R^2 Value (Zero Order Model)**	**R^2 Value (Modified Zero Order Model)**	**% Burst Release (t = 15 min)**
6.8	**0.03**	0.9928	0.8987	0.9805	16.02
6.8	**0.14**	0.7352	0.6623	0.9742	29.36
6.8	**0.28**	0.6090	0.6476	0.9858	34.85

It is possible that the architecture of the interaction between the clay mineral and the polycation was responsible, which is affected by the relative concentration of the species at the time of interaction (Lvov *et al.,* 1996). When low concentrations of the polymer are used, i.e. PEI (0.03), the individual molecules have more room available for undisturbed movement. This allows the polycation to align with the halloysite mineral, as shown in Fig. 9.5k(i), creating a thin, but well organised and very dense film, with good retardant

properties. At higher concentration levels however, the polymer molecules are more constrained, due to stearic difficulties created from reduced space. As a result, the polymer binds the halloysite in a more random arrangement, as illustrated in Fig. 9.5k(ii). Even though the film formed appears thicker, it is looser and less dense, with the presence of water filled voids, which form pockets or holes upon drying. Hence, permeability through these coated systems, i.e. PEI (0.14) and (0.28), is increased.

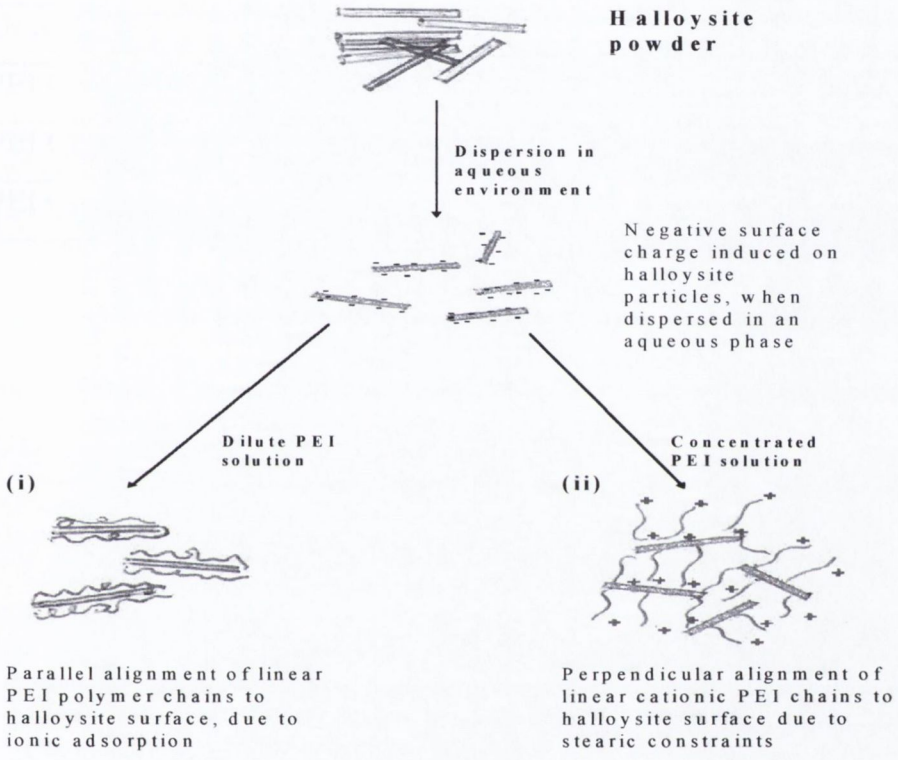

Figure 9.5k. Schematic representation of proposed binding patterns of the cationic linear PEI polymer when (i) a dilute and (ii) concentrated solution is used.

9.5.2.5 Encapsulation Efficiencies

The encapsulation yields of the PEI coated halloysite formulations are listed in Table 9.5i. Similar to the results obtained for the previous two polycationic polymers, as the ratio of polymer to halloysite increases, the entrapment yield decreases. This is again due to the formation of a thicker film causing the overall coated halloysite particle weight to increase,

decreasing the relative proportion of trapped drug within. Overall, the encapsulation efficiencies are reduced relative to uncoated, drug loaded halloysite, but are higher than those of the chitosan coated versions.

Table 9.5i. Percentage drug encapsulation yields for PEI coated (3 levels) and uncoated drug (Diltiazem HCl) loaded halloysite.

Halloysite Formulation	**Encapsulation Yields (% w/w)**
Uncoated Drug Loaded Halloysite	25.6
PEI Coated Halloysite (0.03)	15.7
PEI Coated Halloysite (0.14)	11.8
PEI Coated Halloysite (0.28)	6.6

9.6 Entrapment of Drug Loaded Halloysite within a Lipid Matrix

9.6.1 Introduction

Another technique involved examining the ability to entrap the drug loaded halloysite mineral in a solid lipid matrix (see Fig 9.1(d)). For many years solid lipid matrices have been used to produce pellets, for oral dosage forms (capsules), in order to obtain a prolonged or sustained delivery of the drug, e.g. Mucosolvon Retard invented by Dr Karl Thorme (Müller *et al.*, 1995). More recently, these matrices, when composed of physiological, biodegradable compounds (i.e. fatty acids, alcohols), have been examined as potential controlled release systems for IV administration (Schwarz and Mehnert, 1999, Müller *et al.*, 1995). The incorporation of hydrophilic drugs in these solid matrices is possible, as a dispersion of the drug crystals, where the crystals are present as a monolithic solid dispersion. At room temperature, the particles are in the solid state and, therefore, the mobility of the entrapped drug molecules is reduced which is desirable for controlled drug delivery.

In our situation, we attempted to incorporate the drug loaded halloysite powder into a solid lipid matrix, thereby forming a monolithic dispersion, as mentioned above. Drug loaded halloysite was incorporated using both the 'cold' and the 'hot' dispersion techniques. Size reduction of the solid lipid matrices has been achieved previously, by a number of techniques, ranging from the use of high speed stirrers (Speiser, 1990), to sonication of melted lipids in a sonic bath or using a titanium probe (Morris, 1982), all of which tended to form a relatively high content of particles with dimensions larger than 5 μm. More recently, the process of high pressure homogenisation has been used and, typically, leads to the formation of lipid particles with average diameters within the 80 to 400 nm range (solid lipid nanoparticles, SLNs). While the nano particle size range is ideal for suspensions which are intended for IV administration (i.e. should contain minimal particles >5μm), it was not desirable in our situation, as we intended to entrap drug loaded halloysite tubules which have an average size dimension of 10 μm approx. in length, which is significantly above the nano particle size range. Furthermore, our final product was

intended for oral administration where nano particle size requirements are not required. Instead, other quality criteria, such as the relatively low content of large aggregates (i.e. 100-200 μm) and the uniform appearance of the final product, are important. Therefore, the use of high speed stirring, achievable using an Ultra-Turrax (T25), was chosen for optimal size reduction of our solid lipid particles.

The general formulation used for the preparation of the halloysite encapsulated, solid lipid microparticles is listed as follows:

Lipid	30% w/w
Surfactant	5 or 10% w/w
Cryoprotectant	5% w/w
Distilled water	to 100%

The 'lipid' in the above formulation refers to the halloysite entrapped lipid combination. The effect of two lipids was examined, namely Precirol AT05, with a melting point in the range 53 to 57°C, and Novata E, with a lower melting point range of 34 to 36°C. Of the total lipid content, the drug loaded halloysite level was set at either 30 or 50% of it, enabling us to determine the effect of loading on drug release. The surfactant used was Pluronic F68 and was examined at 2 levels, namely 5 and 10% w/w. A second surfactant, Tween 80, was considered, but preliminary studies showed that it interfered with the lyophilisation step and prevented the recovery of a dry free-flowing powder, which was desired. This was probably due to the liquid physical state of the neat surfactant. The cryoprotectant used was glucose and was fixed at 5% w/w. Glucose was chosen, as previous research by Schwarz and Mehnert, (1997) revealed that it, along with mannose, maltose, and trehalose were the most suitable excipients used as cryoprotectants during the lyophilisation of Dynasan and Compitrol SLNs. Table 9.6a below illustrates the parameters and process conditions used in the production of the seven Solid Lipid Microparticle (SLM) preparations.

Table 9.6a. Illustration of the parameters and process conditions used in the production of the Solid Lipid Microparticle preparations.

Preparation	Technique Used	Surfactant Conc. (% w/w)	Halloysite Content (of total product weight, % w/w)	Lipid Type	Stirring Time (min)
A	Cold	5	9	Precirol	4
B	Cold	10	9	Precirol	4
C	Cold	5	9	Precirol	8
D	Cold	5	0	Precirol	4
E	Cold	5	15	Precirol	4
F	Cold	5	9	Novata E	4
G	Hot	5	9	Precirol	4

9.6.2 Particle Size Analysis of the Solid Lipid Microparticles

Suitable size reduction of all the preparations was achievable, using the high speed Ultra-Turrax. Fig. 9.6a illustrates the median particle sizes (ie d_{50} values), determined by the laser light scattering technique, for all preparations, both before and after lyophilisation. All freeze dried products were re-constituted and re-dispersed in water by sonication, using a dispersion ratio of 1:25.

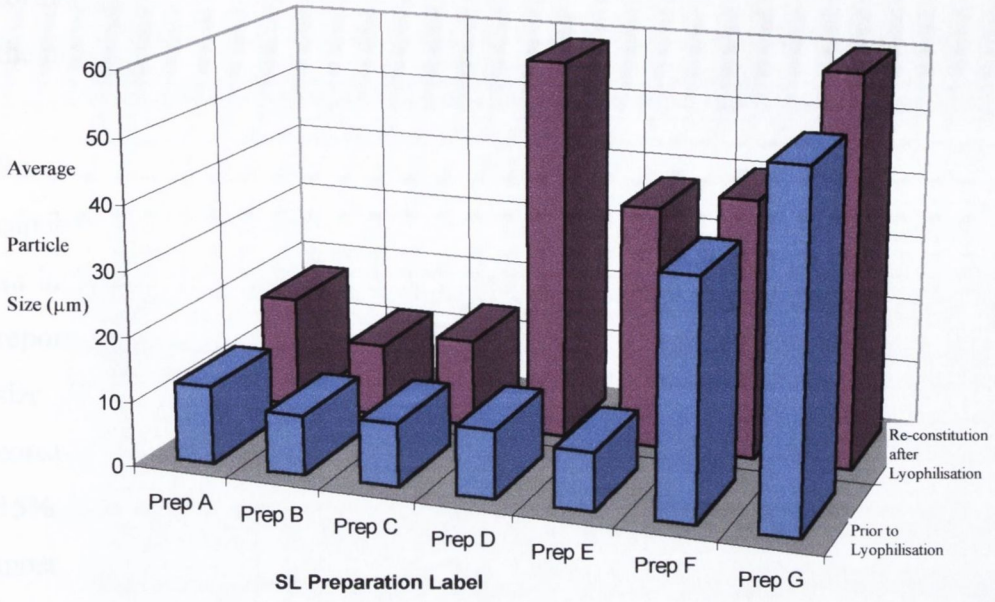

Figure 9.6a. Determined median particle sizes (d_{50} vaules) of the solid lipid preparations before and after lyophilisation.

It is evident from Fig. 9.6a that the lipid particles are reduced to a size which is almost equal to the dimensions of the clusters of halloysite tubules that are encapsulated. This suggests that the lipid forms a fine matrix coat around the mineral clusters. Greatest size reduction occurs for the Precirol lipid preparation, which is milled using the 'cold' dispersion technique, and size reduction appears to be independent of milling time, the presence or absence of halloysite and the surfactant concentration. Important parameters appear to be the type of lipid that is chosen and the type of dispersion technique used. When the lower melting point lipid, Novata E, is used (i.e. Preparation F), the lipid particles formed have a larger median particle size (36.28 μm). This can be explained in terms of the elevated temperatures, which are generated by the milling process, due to the friction created by the halloysite particles grinding against the stirrer blades and each other. These elevated temperatures are sufficiently high (~ 40°C) to melt the Novata E lipid and, hence, agglomeration of the molten lipid particles occurs, when they are left to cool and solidify. A similar explanation is equally applicable to Preparation G which was prepared using the 'hot' technique. Even though Precirol was used in this case, the

formulation was heated to a sufficient degree (~80°C), so that the lipid was molten during the milling process.

Re-constitution after freeze-drying indicated that in all cases, the lipid particles were capable of being re-dispersed into the low micrometer size range. In all cases, however, an increase in the average particle size was observed. Similar observations have been reported by Cavalli *et al.*, 1997, and Schwarz , 1997, who observed that the mean particle size of Dynasan-SLN increased from 103 nm before lyophilisation to 330 nm after re-constitution. It is apparent that the control preparation, (Preparation D), and that with a 15% halloysite loading, (Preparation E), impaired the quality of the re-constituted product most, relative to the same product prior to lyophilisation, i.e. an increase in particle size from 10.54 μm to 58.51 μm and from 8.93 μm, before lyophilisation, to 37.34 μm after re-constitution, for Preparations D and E, respectively. According to Schwarz and Mehnert, (1997), this instability can be attributed to the increase in the amount of free drug in the dispersion medium. An increase in the level of free drug arises in the case of Prep D, as there is an absence of halloysite, the tubular nature of which retards entrapped drug from being leached into the dispersion medium. In the case of Preparation E, the increased amount of loaded halloysite releases a similar percentage of drug into the dispersion medium, relative to the halloysite loading, but, which is greater relative to the overall preparation weight, when compared to Preparations A, B, C and D. During the freezing process, the water crystallizes, and so the concentration of the dissolved drug in the water increases until the eutecticum is reached. The presence of the protonated drug (electrolyte) in the water reduces the zeta potential with increasing concentration, i.e. with the progression of freezing. This reduction is considered to be the major cause of aggregation.

9.6.3 Dissolution Testing and Model Fitting

The drug release profiles of all seven solid lipid preparations were examined by dissolution testing in buffer pH 6.8, the plots of which are illustrated in Fig. 9.6b below. Preparation D functioned as a Control, as it consisted of Diltiazem HCl, entrapped in Precirol lipid,

without the aid of halloysite. All seven preparations resulted in a delayed release of the drug, over an 8 hr period, in contrast to the dissolution profile of pure drug, which is completely released within 15 min.

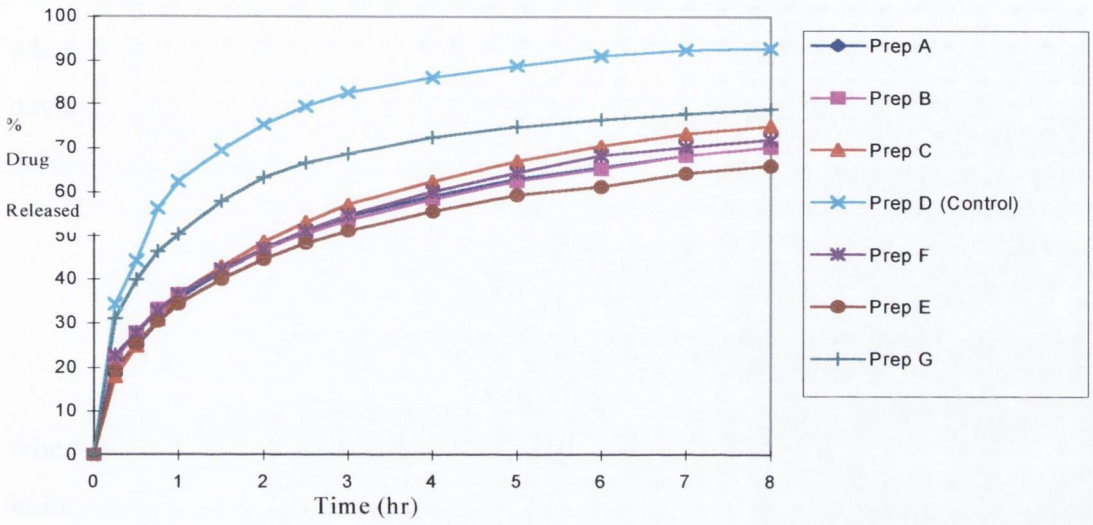

Figure 9.6b. Dissolution profiles of the release of Diltiazem HCl from the Solid Lipid Microparticles, in McIlvaine buffer media pH 6.8 at 37°C.

Table 9.6b. Correlation values (R^2) calculated when the dissolution data is fitted to various predictive release models (y = % drug dissolved; $x = t^{0.5}$).

SLN Prep	R^2 Value - Zero Order Model (using 8 hr dissolution data)	R^2 Value - Higuchi Model (using 8 hr dissolution data)	R^2 Value - Higuchi Model (using initial 2 hr dissolution data)	Higuchi Eqn. (using initial 2 hr dissolution data)
Prep A	0.7991	0.9208	0.9916	$y = 33.709\ x$
Prep B	0.7936	0.8897	0.9674	$y = 35.643\ x$
Prep C	0.8195	0.9453	0.9981	$y = 35.133\ x$
Prep D	0.6260	0.6555	0.9822	$y = 61.243\ x$
Prep E	0.7866	0.8953	0.9841	$y = 33.400\ x$
Prep F	0.8073	0.9070	0.9652	$y = 35.748\ x$
Prep G	0.6409	0.6558	0.9660	$y = 51.297\ x$

Table 9.6b illustrates the calculated R^2 values when the dissolution data is fitted to a number of predictive models, i.e. the zero order and Higuchi (matrix) models. Correlation was best, when the first 1.5 to 2 hr dissolution data was fitted to the Higuchi equation, which best describes the release of an active agent, dispersed as a solid in a monolithic device. Release kinetics from these systems can be described by Eqn. 9.6a, which was derived by Higuchi, as follows.

$$\frac{dM_t}{dt} = \frac{A}{2}\left(\frac{2C_o DC_s}{t}\right)^{0.5} \qquad \text{Eqn. 9.6a}$$

where, A is the area, D is the diffusion coefficient, C_s is the solubility of the active agent in the matrix, C_o is the total concentration in the matrix (dissolved and dispersed) and M_t is the amount released at time t.

According to Eqn. 9.6a, the release curves should maintain a square root of time dependence. Deviation from this occurs, however, when the concentration of the active agent falls below the saturation value (Heller, 1987). In our case, because of the highly soluble nature of the drug candidate (Diltiazem HCl), sub-saturation conditions occur, after 2 hr approx. of release, and so the R^2 values determined are lower, when the complete 8 hr dissolution data is used in their determination, compared to the initial 2 hr release data, as illustrated by the results in Table 9.6b.

9.6.3.1 Effect of Surfactant

The formulations were designed to enable us to examine the effect of various process conditions on the drug release kinetics from the SLM matrices. Fig. 9.6c (plot of % active release *vs* $t^{0.5}$) illustrates the effect of surfactant concentration on these release kinetics. The release profiles of Preparations A, C and D are presented. Preparation D, as

mentioned previously, was the control. Preparations A and B were similar, except for the level of surfactant present, i.e. they contained 5 and 10% w/w Pluronic, respectively.

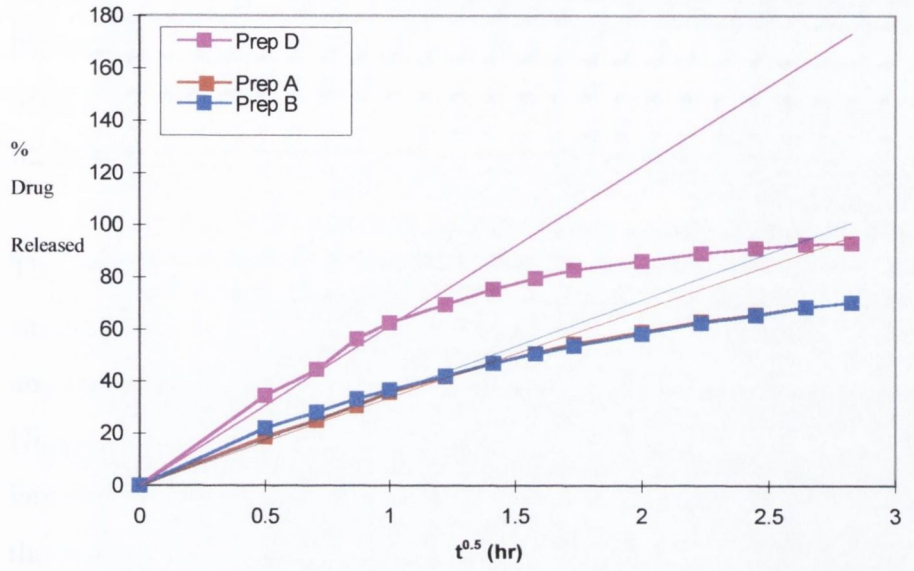

Figure 9.6c. Higuchi release profiles, describing the release of Diltiazem HCl from solid lipid preparations D, A and B, in buffer medium pH 6.8 at 37°C.

It is obvious from Fig. 9.6c that drug release from the Control preparation is significantly faster than from either preparation A or B. This is reflected by the calculated f_2 values, which are 29.75 and 30.13 for preparations A and B, respectively, (when compared to Preparation D), both of which are less than 50, indicating that a significant difference exists. Preparations A and B differ from the Control (Preparation D), in that in the case of the former two, the drug is entrapped within the halloysite tubule, prior to being incorporated into the lipid matrices. The presence of the halloysite appears to reduce the effective diffusion coefficient of the drug through the matrix into the surrounding dissolution medium. The slopes of the lines, calculated by fitting the data to the Higuchi equation, are listed in Table 9.6b, and are 61.24, 33.71 and 35.64 for preparations D, A and B, respectively. The above slope values, m, are related to the surface area, diffusion coefficients of the lipid matrix, the solubility of the active agent in the matrix (C_s), and the total concentration of drug in the matrix (C_o), as expressed in Eqn. 9.6a. Since C_o and C_s

is initially the same for all 3 preparations and the surface areas are similar (due to similar particle sizes), the diffusional coefficient is the variable constant. The diffusion coefficient is almost twice as large for the Control, suggesting that the presence of halloysite creates a physical hindrance within the matrix, introducing more tortuosity, and, thereby, retarding drug diffusion, as in the cases of preparations A and B. This effect is also evident for the other preparations incorporating halloysite.

The results clearly show that the effect of surfactant is negligible on drug release. The f_2 similarity value, comparing preparation A relative to preparation B, is 86.58, indicating any difference to be insignificant. The slopes determined for both preparations using the Higuchi equation, as mentioned previously, are also very similar. This negligible effect is interesting, as Almeida *et al.,* 1997, expected the partitioning of hydrophilic proteins into the water phase to be enhanced during the process, by the use of surfactants as emulsion stabilisers. It appears that an anomaly exists, similar to the effect of SLS, enhancing the release of Indomethacin from spherical microparticles, as discussed in Chapter 7.

9.6.3.2 Effect of Milling Time

The effect of milling time is expressed in the Higuchi plots, illustrated in Fig. 9.6d below, illustrating the Control in combination with preparations A and C, the latter two differing only by the duration of time spent milling, using the Ultra-Turrax, i.e. 4 and 8 min for preparations A and C, respectively. Again, the profiles are very similar with calculated slopes of 33.71 and 35.13 for preparations A and C, respectively. The calculated similarity factor between the same two prepartions was 75.06, a value of 100 indicating exactly superimposable profiles. Comparison of preparation C with the Control again illustrates how the presence of halloysite further retards drug release (f_2 value is 31.83 for preparation C, when compared with preparation D). The effect of milling time is negligible and the results suggest that near maximal size reduction occurs after the lower milling time of 4 min. This is confirmed by the results of Fig. 9.6a, which illustrate that

the increased milling time (8 min) only further reduces the mean particle size of the SLMs by 2 μm approx.

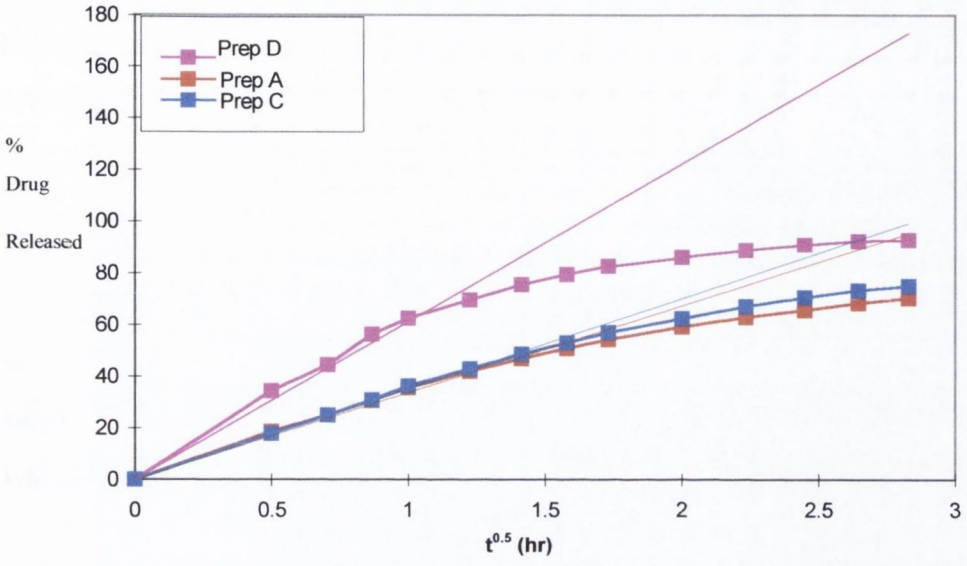

Figure 9.6d. Higuchi release profile,s describing the release of Diltiazem HCl from solid lipid preps D, A and C, in buffer medium pH 6.8 at 37°C.

9.6.3.3 Effect of Lipid Type

In order to ascertain whether a controlled release could also be obtained, using lipids with lower melting points, the drug loaded halloysite was incorporated into Novata E, as well as Precirol. The differences in melting temperature were considered an important parameter in determining the structure of SLMs. As shown by Fig. 9.6e, a delayed release of Diltiazem HCl also occurred from the matrix containing of Novata E lipid. The magnitude of the delayed release was very similar to that noted using the Precirol lipid matrix, which is evident by the high f_2 value of 82.46, when comparing the profiles of preparations A and F, and the similar slope values when the data is fitted to the Higuchi equation, ie 33.371 and 35.74 for preparations A and F, respectively. This effect is similar to the results obtained by zur Mülhlen *et al.*, 1998, who observed that they could achieve prolonged release of Prednisolone from both cholesterol loaded SLN particles and those

produced using the lower melting point lipid, Compitrol. They explained their observation as being due to the presence of a solid solution of the drug, i.e. a monolithic dispersion, throughout the entire lipid particle, combined with a slow diffusion of the drug from the matrix, and concluded that interactions between the drug and the lipid molecules play a major role in achieving prolonged release in lipid systems.

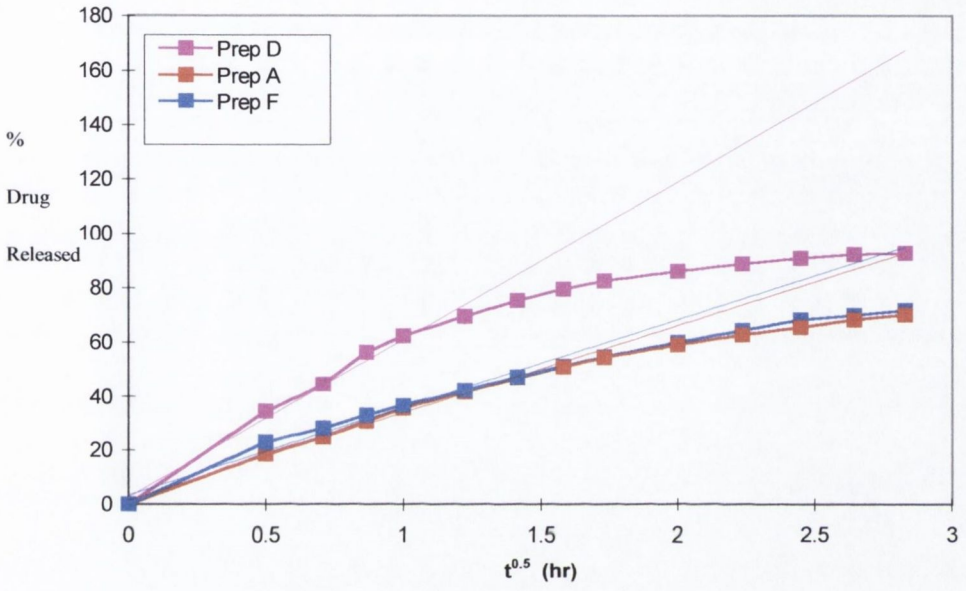

Figure 9.6e. Higuchi release profiles, describing the release of Diltiazem HCl from solid lipid preparations D, A and F, in buffer medium pH 6.8 at 37°C.

9.6.3.4 Effect of Dispersion Type

The 'cold' dispersion technique was used to prepare the SLMs for all preparations, except for that of preparation G. In this case the 'hot' dispersion technique was employed, (i.e. the lipid was milled, using the Ultra-Turrax, at a temperature above its melting point, ~ 80°C), to assess if it had an effect on the drug release profiles. The Higuchi plots for preparation D (Control) and preparations A and G are illustrated in Fig. 9.6f. Unlike the former parameters examined, it is evident that the dispersion technique used had an important effect on the release kinetics. In this case, the f_2 value comparing preparaion A

with preparation G is less than 50 (43.07), indicating that the effect is significant, as is reflected again by the differences in the slopes of the Higuchi plots, (i.e. 51.30 and 33.71 for preparations G and A, respectively). The release rate from preparation G is greater, even though the particle size results (see Fig 9.6a) indicate that the median particle size of the SL particles is larger for preparation G, and hence the corresponding specific surface area available for dissolution is less.

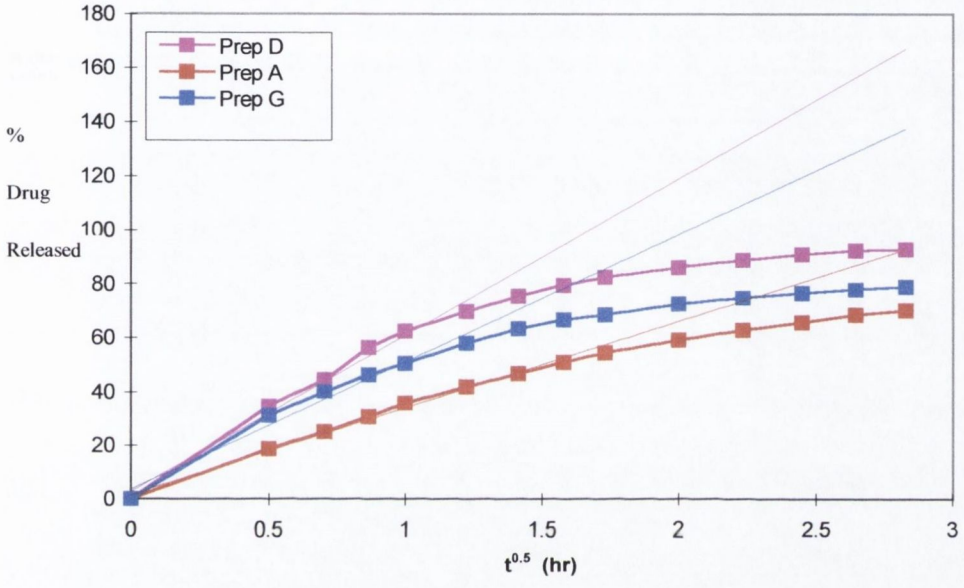

Figure 9.6f. Higuchi release profiles, describing the release of diltiazem HCl from solid lipid preps D, A and G, in buffer medium pH 6.8 at 37°C.

A possible explanation for this is the development of a shorter diffusion path due to the enrichment of drug in the outer region of the lipid particle. Such an enrichment would be a direct consequence of the 'hot' dispersion technique employed in its manufacture. Unlike the 'cold' technique, the lipid particles are in a molten state during the milling process and the viscosity of the lipid particles becomes significantly reduced. The combination of the reduced viscosity and the centrifugal forces, which are created by high speed stirring, causes the dispersed halloysite and free drug molecules to move to the outer region of lipid particles, as illustrated in Fig. 9.6g. Upon subsequent cooling and solidification of the lipid particles, an enrichment of drug is created in the outer particle

regions, allowing for faster drug release. Despite the occurrence of the above phenomenon, drug release is still slower from preparation G, compared to that from the Control, which as mentioned previously, is devoid of halloysite (i.e. a calculated f_2 value of 45.66, indicating the difference is significant).

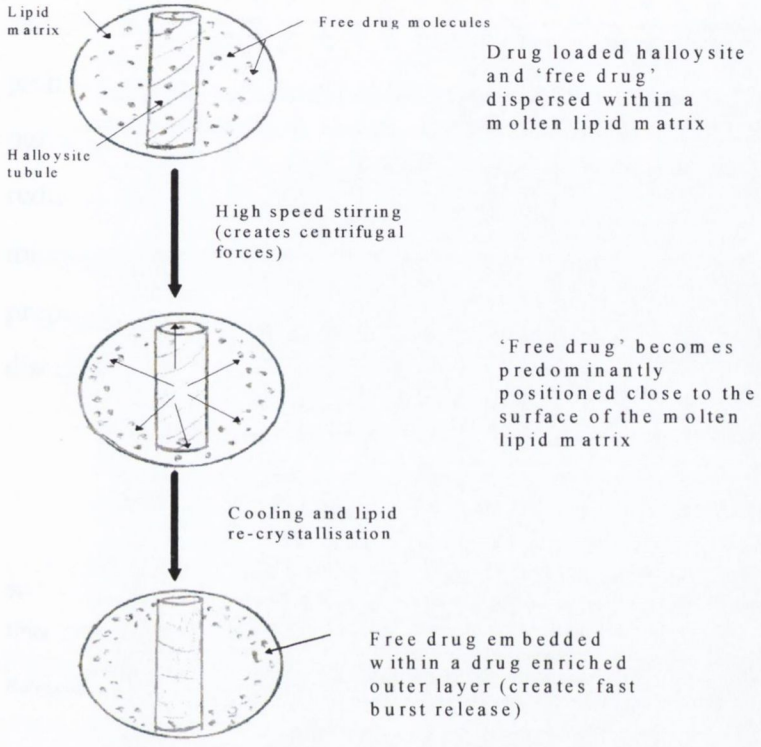

Figure 9.6g. Illustration of the proposed mechanism by which 'free drug' becomes locally concentrated in the periphery of the lipid particle matrix, when the 'hot' dispersion technique is employed.

9.6.3.5 Effect of Halloysite Loading

The final factor examined was the effect of halloysite loading. A formulation (preparation E) was prepared, with a halloysite loading of 50% w/w (relative to the total lipid weight), compared to a loading of 30% w/w used for all other formulations (except preparation D). It was believed that the higher halloysite content would reduce the amount of lipid

available to encapsulate each halloysite particle, thereby reducing the diffusional path length and increasing the rate of drug release. Despite this, the release profiles, as illustrated by the Higuchi plots in Fig. 9.6h, indicate that no significant difference exists between preparations A and E. This is confirmed by the calculated similarity factor of 76.05, which is greater than 50, and the slopes, m, of the profiles being similar at 35.71 and 35.75 for preparations A and E, respectively. In this case, the effect of any reduced path length is probably overcome by the reduction in the specific surface area of the lipid particles, across which drug molecules are available to be released. The surface area is reduced as a consequence of the greater median size diameter of the preparation E SL microparticles, being 37.24 μm compared to 17.33 μm (after re-constitution) for preparations E and A, respectively. The reason for this difference in particle size was discussed earlier.

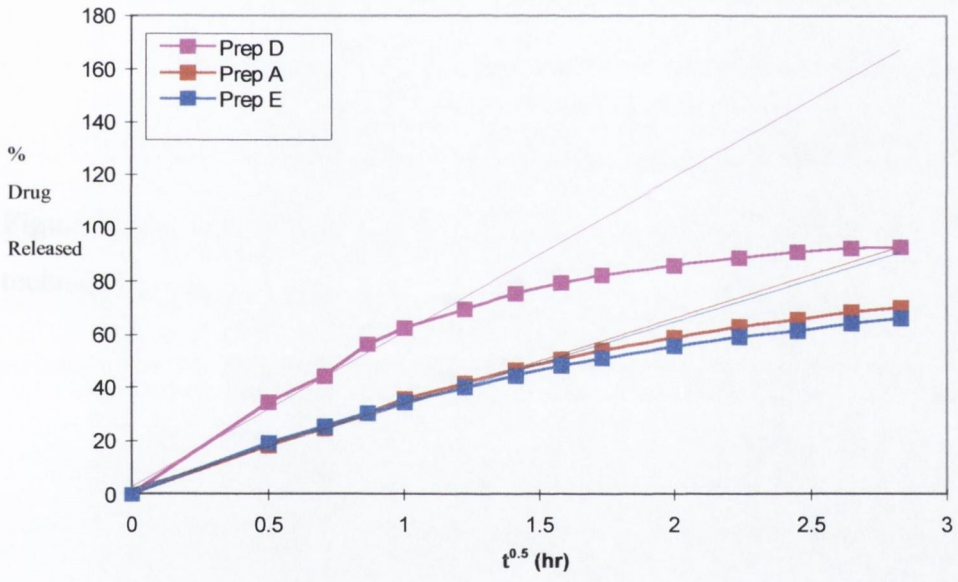

Figure 9.6h. Higuchi release profiles, describing the release of diltiazem HCl from solid lipid preparations D, A and E, in buffer medium pH 6.8 at 37°C.

9.6.4 Microscopic Examination of Solid Lipid Microparticles

The solid lipid microparticle preparations were examined, using transmission and scanning electron microscopic techniques. The TEM of preparation A (see Fig. 9.6i) illustrates a

lipid matrix (4 μm in diameter approx.), in which several drug loaded tubules are embedded, apparent as a darker shading. This indicates that some degree of aggregation of the tubules occurs within the lipid matrix. The TEM (see Fig. 9.6j) of preparation F microparticles (prepared using Novata E lipid), again illustrate clearly the halloysite embedded within the lipid matrix. It also indicates that some of the tubules project from the matrix surface (A), which might contribute to the drug release burst effects experienced with these preparations.

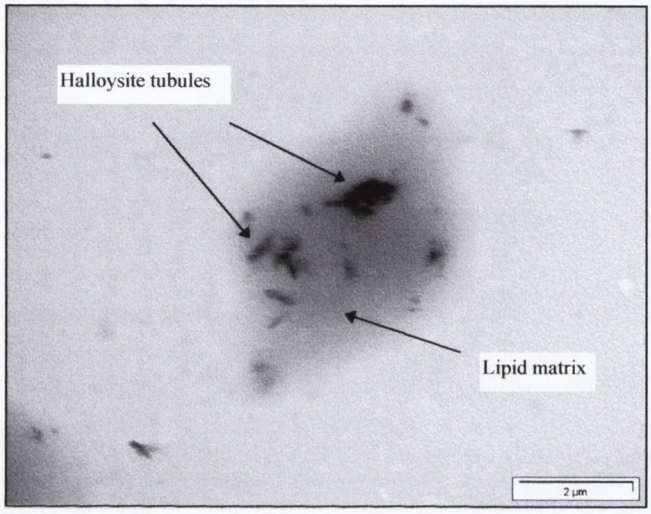

Figure 9.6i Transmission electron micrograph of preparation A ('cold' dispersion technique) solid lipid microparticles (X 20,000 magnification).

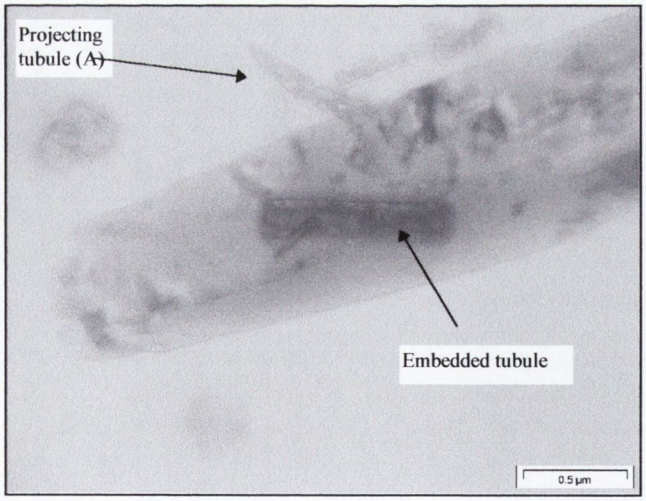

Figure 9.6j Transmission electron micrograph of preparation F ('hot' dispersion technique) solid lipid microparticles (X 70,000 magnification).

Examination of the surface of preparation A SL microparticles, using scanning electron microscopy, illustrates that it is rough, jagged and porous in nature and that the particle morphology is very irregular (see Fig. 9.6k). These characteristics, especially the jagged surface, arise from the lipid fracture technique (i.e. 'cold' dispersion technique) used to prepare them. When the 'hot' dispersion technique is used in their preparation (i.e. preparation G), scanning electron micrographs (see Fig. 9.6l) again illustrate that the lipid microparticles are irregularly shaped and very porous in nature, but the surface indentations appear to be smoother and less jagged than those of preparation A. Because the SEM images, illustrated in Figs. 9.6k and 9.6l, are of equal magnification they also illustrate qualitatively the larger size of preparation G particles relative to those of preparation A, as confirmed previously in Section 9.6.2, from particle size analysis studies.

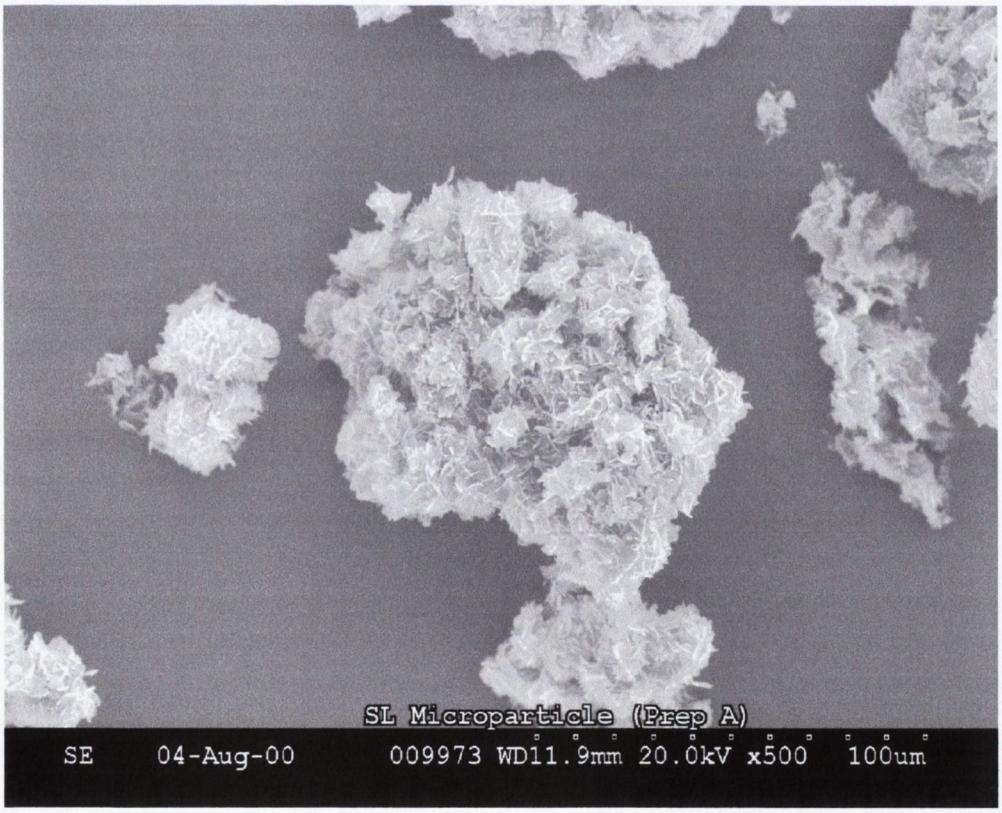

Figure 9.6k Scanning electron microscope of preparation A ('cold' dispersion technique) solid lipid microparticles (X 500 magnification).

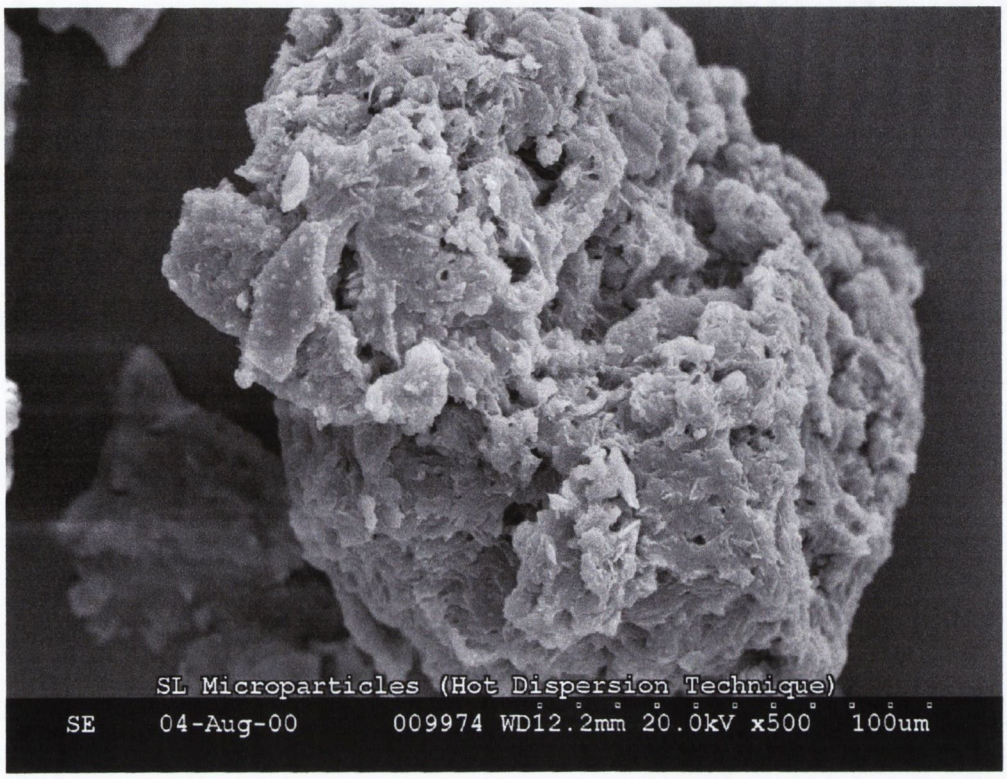

Figure 9.6l Scanning electron micrograph of preparation F ('hot' dispersion technique) solid lipid microparticles (X 500 magnification).

9.6.5 Drug Encapsulation Efficiencies of Solid Lipid Microparticles

The theoretical and actual encapsulation efficiencies of the solid lipid microparticle preparations are listed in Table 9.6c. All the actual values are less than their theoretical counterparts, indicating that some of the drug is lost during the preparation process, by adhering to the glassware and other equipment such the high speed stirring blades. When the actual loadings are calculated as a percentage of the theoretical loadings, the values range from a minimum of 94.81% for preparation B, incorporating the higher surfactant concentration, to a maximum of 99.53% for preparation D, which has an absence of halloysite. Overall, the actual loading efficiencies, when expressed as a weight percentage relative to the final product dry weight, are low (see Table 9.6c). Levels close to 10% w/w are achievable, when the higher halloysite (drug loaded) loading level is used (i.e. preparation E). Furthermore, dissolution data also illustrates that increasing the halloysite loading has no effect on the release profiles of the drug entrapped within, suggesting that

higher levels of drug loaded halloysite could be used, if higher drug encapsulation levels are required.

Table 9.6c Theoretical and actual % drug encapsulation yields for the solid lipid microparticle preparations.

Preparation	Theoretical Drug Loading (% w/w)	Actual Drug Loading (% w/w)	Actual Drug Loading (% of Theoretical Loading
A	5.75	5.55	96.46
B	5.12	4.85	94.81
C	5.75	5.61	97.44
D	6.43	6.40	99.53
E	9.60	9.42	98.09
F	5.75	5.72	99.47
G	5.75	5.72	99.39

9.6.6 Propranolol Loaded SL Particles

Since significant retardation of diltiazem HCl release was achieved by the combined technology of drug loading halloysite and then incorporating it into a lipid matrix, we decided to examine the dissolution profile if a less soluble cationic drug was incorporated, using the same technology. Propranolol HCl was chosen as a potential candidate with a significantly lower water solubility, i.e. propranolol HCl and diltiazem HCl have aqueous solubilities of 5 and > 50% w/v at 25°C, respectively, (Yang and Fassihi, 1997). We expected the reduction in drug solubility to retard the drug release rate and increase the duration of release.

Because of the intrinsic low relative aqueous solubility of propranolol HCl, we decided to dissolve it initially in methanol, for the purpose of drug loading the halloysite tubules. Using methanol, a 20% w/v drug solution was easily achievable. This facilitated the

incorporation of a higher drug loading in the mineral, i.e. the theoretical drug loading of halloysite would be 4.7% and 18.8% w/w, when using a 5% and 20% Propranolol HCl solution, respectively, assuming a 1:1 ratio of halloysite to drug solution was used. Propranolol HCl loaded halloysite (P2) was incorporated into the Precirol lipid matrix (P3), using identical formulation and process conditions to those used to prepare preparation A, as discussed earlier.

Fig. 9.6m illustrates the plots for the dissolution of Propranolol HCl in an aqueous buffer pH 6.8 system. Three plots are illustrated, the first, (P1), representing the dissolution profile of the pure drug. It is very evident that by non-formulating the pure drug, it rapidly dissolves in an aqueous environment, (i.e. 100% after 30 min), as long as it is well below saturated solubility conditions, (i.e. 100% dissolution in this case equates to a concentration of 0.01% w/v which is << 5% w/v). The P2 release profile represents the dissolution and release of the drug from the loaded halloysite mineral. It is again clearly evident that, by simply loading it into the halloysite tubule, without any further processing other than drying, a significant retardation of drug release occurs. This is reflected by the similarity factor which compares it to the dissolution profile of the pure drug ($f_2 = 20.79$). In fact, the delayed effect is so significant that only 90% approx. of the total drug loading is released after 8 hr, compared to 100% release for a similar preparation incorporating Diltiazem HCl after only 3-4 hr approx. As a result, drug solubility has a significant effect on release rate from the drug loaded mineral.

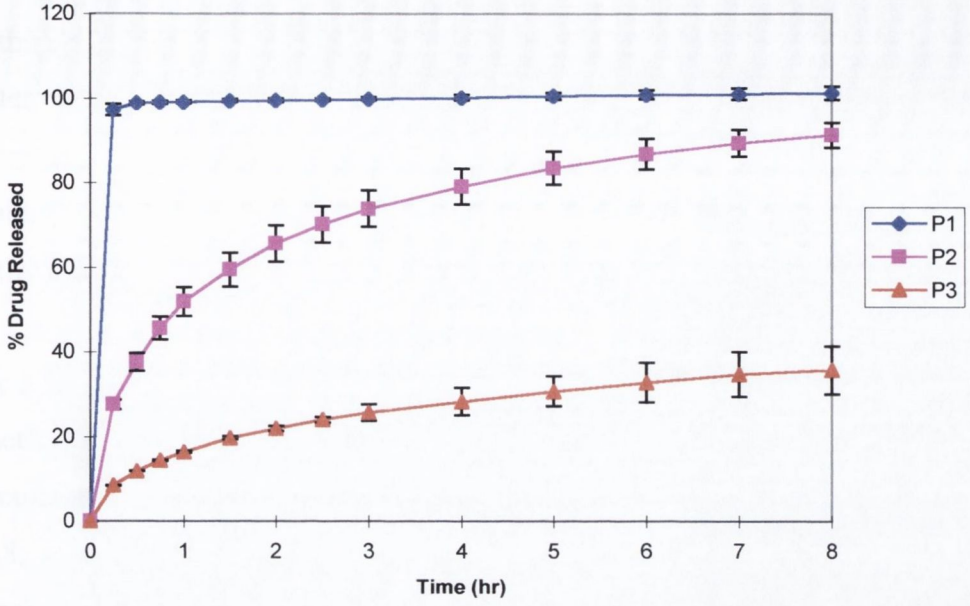

Figure 9.6m. Dissolution profiles of Propranolol HCl, (P1 pure drug; P2 drug loaded halloysite and P3 drug loaded halloysite incorporated into a SLM), in pH 6.8 McIlvaine buffer, for 8 hr, at 37°C.

The effect of drug solubility also extends to the solid lipid matrix technology, as is evident from the P3 formulation dissolution profile. By incorporating the loaded mineral into a lipid matrix, a significant further reduction in release rate occurs, (i.e. $f_2 = 5.77$), when compared to the P1 product. In the case of the lipid product (P3), only 36% approx. of the total drug loading was released over the 8 hr dissolution period. This was also a significant improvement in the level of drug retardation, when compared to the release profile of diltiazem HCl from a similar product, (i.e. preparation A), in which 70% approx. (a two fold increase) of the loaded drug was released over a similar time period.

The effect of drug solubility on the release kinetics from these formulations can be explained on the basis of the osmotic potential created by the dissolved drug. When drug solubility increases, a greater osmotic potential is created, which accelerates water penetration into the matrix created by the halloysite mineral structure and the lipid. The greater amount of water present is available to dissolve and remove drug faster, by

outward diffusion into the dissolution medium down the steeper concentration gradient. In the case of the matrix created by the lipid, there is also the possibility that the increased water penetration may also cause the polymer to swell slightly, forming more microcavities, thereby, increasing the outward diffusion constant. This swelling effect is probably minimal in the case of the drug loaded halloysite alone, due to the rigid structure of the mineral.

The release of propranolol HCl from the lipid preparation (P3) was also shown to follow kinetics, as described by the Higuchi Eqn., as illustrated by Figure 9.6n below. The slope calculated, when the first 2.5 hr of dissolution data was fitted to the Higuchi equation, was 15.8, with a correlation coefficient (R^2) equal to 0.9936. Deviation from matrix release occurred after 2.5 hr approx., again due to the concentration of the dissolved active agent falling to below its saturation value, within the matrix structure.

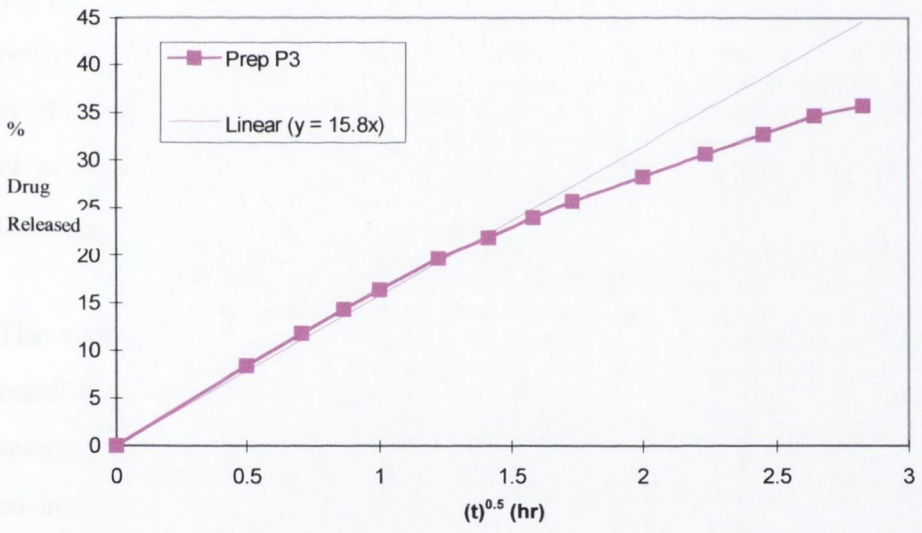

Figure 9.6n Higuchi release profile, describing the release of Propranolol HCl from the solid lipid preparation (P3), in buffer media pH 6.8, at 37°C.

9.7 Coating Drug Loaded Halloysite using Cyanoacrylate Polymers

9.7.1 Introduction

Biodegradable rate controlling membranes were formed around the drug loaded, halloysite particles by means of *in situ* polymerisation of alkyl-2-cyanoacrylate monomer units. Alkyl-2-cyanoacrylates were originally discovered by H. W. Coover, in 1951, through serendipity at Tennessee Eastman Co., and since then he started research to develop tissue adhesives based upon them. To date, their primary use in the medical area is as tissue adhesives, used in conjunction with various surgical techniques (Refojo *et al.,* 1971; Matsumoto, 1972; Vanholder *et al.,* 1993). More recently, they have also been examined as potential rate limiting membranes, controlling drug delivery from various micro and nano particle systems, (Couvreur and Vauthier, 1991; Puglisi *et al.,* 1993; Fresta *et al.,* 1996). During the preparation of the above systems, the drug may be dissolved in the polymerisation medium before the addition of the monomer (incorporation method; Puglisi *et al.,* 1993) or after the polymerisation process has completed (adsorption method; Illum *et al.,* 1986). As a result, the drug is entrapped in the biodegradable core of the nanospheres and / or adsorbed onto their surface.

The alkyl-2-cyanoacrylkates (ACA's) are highly polymerisable under neutral and basic conditions. The detailed mechanism of their polymerisation is not fully understood, but it seems likely that they polymerise via an ionic mechanism, where water molecules act as co-initiator. The ACA polymer degrades by a surface erosion process, which was illustrated by Lenaerts *et al.,* 1984, to occur by enzymatic hydrolysis of the ester side chain of the polymer. By this mechanism, the polymeric chain remains intact, but gradually becomes more hydrophilic until it is water soluble. Alcohol is a product of this degradation mechanism. A non enzymatic route of degradation was originally proposed by several authors (Leonard *et al.,* 1966), resulting in the formation of formaldehyde, but this is believed to play a minor role in the overall degradation of these polymers under physiological conditions. Indeed, Lenaerts *et al.,* (1984), showed that the quantity of

formaldehyde produced, following polymer degradation, was 5% approx. of the theoretical quantity that would have been produced, if it had been entirely degraded by this pathway. The rate of degradation is the greatest for methyl-2-cyanoacrylate, and diminishes as the size of the alkyl group increases, at pH 7.0. ACA's with branched alkyl groups also degrade faster than their straight chain homologues. Furthermore, polymers of different molecular weights, originating from the same monomers, illustrate rates of degradation inversely proportional to the magnitude of their molecular weights. The generation of formaldehyde, as a consequence of polymer hydrolysis, causes concern over their potential cytotoxicity, resulting in adverse tissue reactions. In terms of their use as synthetic tissue adhesives, the order of tolerance levels are as follows: n-decyl, n-octyl, n-heptyl, n-butyl and isobutyl 2-cyanoacrylates are well tolerated; methyl-2 cyanoacrylate is least tolerated (Refojo *et al.*, 1971).

9.7.2 Results and Discussion

Halloysite was drug loaded using a 40% w/v aqueous Diltiazem HCl solution and dried, using an air circulated oven, to constant weight. The residual moisture content of the halloysite batch was determined by TG analysis (see Appendix 6), as being ~ 1.97%. Three ACA monomers were examined, namely n-butyl, octyl (straight chained) and isobutyl (branched) CA. The method used to coat the drug loaded halloysite with ACA polymer is detailed in Chapter 3.

Table 9.7a. Correlation values (R^2), calculated when the dissolution data for the poly-CA coated, drug loaded halloysite samples is fitted to various predictive models.

CA Monomer Used	CA Monomer Conc. (% v/v)	Halloysite Residual Moisture Content (% w/w)	Polymeri-sation Reaction Time (hr)	R^2 Value (Higuchi Model)	R^2 Value (Zero Order Model)	R^2 Value (Modified Zero Order Model)	% Burst Release (t = 15 min)
n-Butyl	5	1.97	0.5	0.7106	0.3921	0.7177	61.14
n-Butyl	5	1.97	3.0	0.880	0.4847	0.9719	49.30
n-Butyl	5	1.97	8.0	0.8789	0.4875	0.9763	47.82
n-Butyl	10	1.97	8.0	0.9545	0.5944	0.9698	37.04
Isobutyl	5	1.97	8.0	0.9767	0.7139	0.9747	23.23
Octyl	5	1.97	8.0	0.8903	0.6110	0.9509	41.27

Table 9.7b. Calculated average molecular weights for the poly-CA polymer coatings used to coat the drug loaded halloysite.

CA Monomer Used	CA Monomer Conc. (% v/v)	Halloysite Residual Moisture Content (% w/w)	Polymeri-sation Reaction Time (hr)	Average Molecular Weight
n-Butyl	5	1.97	0.5	215,000
n-Butyl	5	1.97	3.0	254,000
n-Butyl	5	1.97	8.0	550,000
n-Butyl	10	1.97	8.0	382,000
Isobutyl	5	1.97	8.0	721,285
Octyl	5	1.97	8.0	572,281

9.7.2.1 Effect of Polymerisation Reaction Time

Using the n-butyl CA monomer, the effect of reaction time was examined to investigate whether it had an effect on the ultimate drug release from the coated preparations. A 5 % v/v solution of the monomer in heptane was used, and the loaded halloysite powder was allowed to stir in this solution for 30 min, 3 hr and 8 hr time intervals, followed by filtering off the heptane and drying the coated products to constant weight. The dissolution profiles, illustrating the release profiles of diltiazem HCl from the three coated products, are shown in Fig. 9.7a.

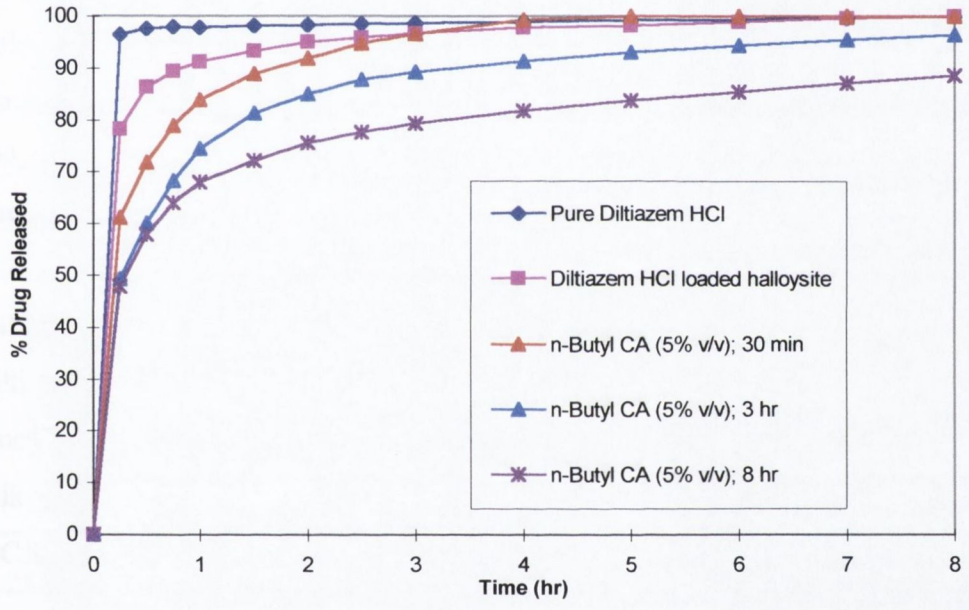

Figure 9.7a. Dissolution of diltiazem HCl from poly n-butyl CA coated (three samples with differing polymerisation reaction times, namely 30 min, 3 hr and 8 hr) and uncoated, drug loaded halloysite, in pH 6.8 McIlvaine buffer, for 8 hr, at 37°C.

The coated halloysite preparations all illustrate a reduced rate of drug release relative to the non coated, drug loaded halloysite product. This reduced rate is only significant, however, for the coated preparations, using 3 hr and 8 hr polymerisation reaction times, as denoted by the similarity factors quoted in Table 9.7b, (i.e. both are < 50 for the 3 hr and

8 hr reaction products). A possible explanation for the greatest sustained release being observed for the product coated, using the 8 hr polymerisation reaction time, was that more polymer, corresponding to a thicker membrane encapsulating the halloysite, was formed. This is supported by the encapsulation yields determined for the three preparations, being 18.51%, 18.00% and 17.83% for the products coated for 30 min, 3 hr and 8 hr, respectively. The product subjected to the 8 hr encapsulation reaction time illustrated the lowest encapsulation efficiency, yet, since the same batch of drug loaded halloysite was used in the three coating situations and diltiazem HCl is insoluble in heptane, this decrease in yield must correlate with an increase in the amount of coating polymer being formed. Furthermore, as is evident from the results of Table 9.7b, longer polymerisation reaction times also result in the formation of polymers with higher average molecular weights, i.e. the average molecular weights for the poly n-butyl CA coated samples, applied using 30 min, 3 hr and 8 hr reaction times are 215,000, 254,000 and 550, 000, respectively. These higher molecular weights are less porous and also degrade at a slower rate as mentioned earlier.

Table 9.7b. In vitro similarity factors (f_2) comparing the dissolution profiles of Diltiazem HCl from poly n-butyl CA coated powder halloysite (polymerisation reaction times 30 min, 3 hr and 8 hr, respectively) relative to those of uncoated, drug loaded halloysite powder, in buffer medium pH 6.8.

CA monomer	Polymerisation reaction time	f_2 value
n-butyl	30 min	56.34
n-butyl	3 hr	41.89
n-butyl	8 hr	34.74

The dissolution profiles are bi-phasic, similar to those observed by Puglisi *et al.* (1993), for the release of fluorescein sodium salt from poly-isobutyl-2-cyanoacrylate nanoparticles, and are best described by zero-order release kinetics (phase II), modified to account for a significant burst effect (phase I), (see Table 9.7a). Phase II equates to constant release of drug, by slow release, from the halloysite reservoir and diffusion

through the semipermeable membrane, in this case being composed of the n-butyl CA polymer. Polymer degradation is probably also a factor during this release phase (Puglisi *et al.*, 1993). This may also contribute to the explanation why the halloysite coated with CA polymer, using the longer reaction time, was shown to have reduced release profiles relative to the other coated halloysite formulations, i.e. longer reaction times correspond to higher average molecular weights (see Table 9.7b) and, hence, slower rates of degradation and rates of encapsulated drug release. The burst effect (phase I) is probably due to the presence of an amount of poorly encapsulated drug loaded halloysite. Similar burst effects of drug from dry nanocapsule systems, based on the poly-ethyl CA polymer, were observed by Fresta *et al.*, 1996. Poor correlation is observed when the dissolution data is fitted to the Higuchi model (see Table 9.7a). In the case of the preparation coated using a 5% v/v n-butyl CA monomer solution and a 30 min reaction time, the low calculated R^2 value indicates poor correlation of the dissolution data to the zero order model, even when modified to account for any burst effect. This indicates that the polymer formed in this preparation is thin and incomplete, with poor drug retarding properties. Since the most hindered release occurred for the preparation with the longest polymerisation reaction time (8 hr), this polymerisation time was used in all subsequent studies.

9.7.2.2 Effect of Cyanoacrylate Monomer Type

Using an 8 hr polymerisation reaction time, the effect of three differing ACA monomers on the resultant drug dissolution profiles, from coated halloysite preparations, was examined. The monomers examined included n-butyl CA, isobutyl CA and octyl CA, all of which were used as 5% v/v solutions in heptane. The coated halloysite products were tested in dissolution medium pH 6.8, the release profiles of which are illustrated in Fig. 9.7b.

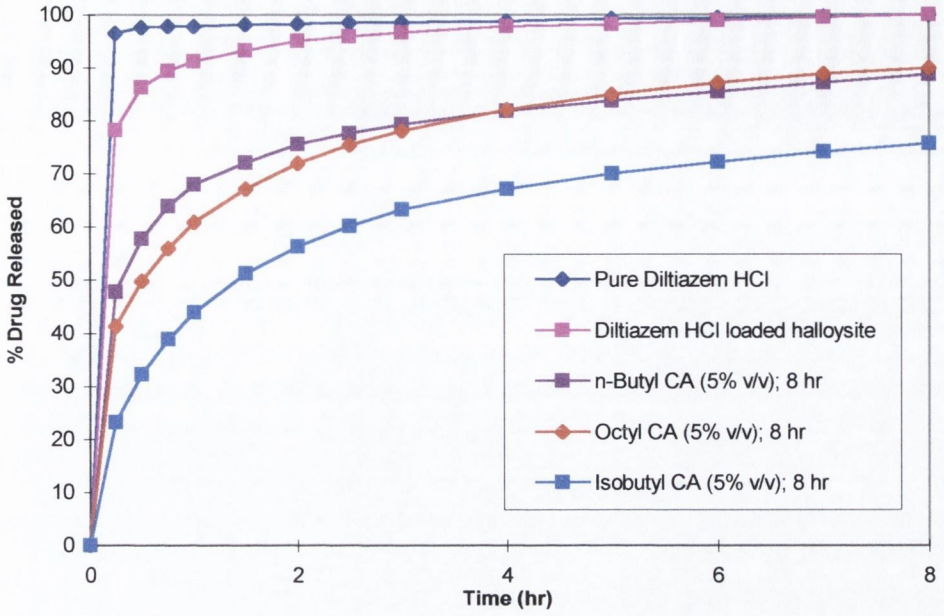

Figure 9.7b. Dissolution of Diltiazem HCl from poly n-butyl CA coated, poly octyl CA coated, poly isobutyl CA coated (using a 5% v/v monomer solution and an 8 hr, polymerisation reaction time) and uncoated drug loaded halloysite, in pH 6.8 McIlvaine buffer, for 8 hr, at 37°C.

Both the poly-octyl and poly-n-butyl CA coated preparations illustrated similar profiles, with a calculated similarity factor comparing the two being 66.43, (i.e. >50). The greatest level of sustained release occurred for the poly-isobutyl CA coated product, with similarity factors, comparing its release profile with those of the poly-octyl and poly-n-butyl CA products, being calculated as 39.99 and 36.13, respectively, suggesting that this difference is significant in both cases. When the dissolution data for the three products is fitted to the zero-order and Higuchi predictive models, drug release from the poly-octyl and poly-n-butyl CA preparations is best described as zero order release, with an associated burst effect. In the case of the poly-isobutyl CA coated product, however, release is best described as diffusion from a matrix (see Table 9.7a), in which the drug is dispersed throughout the internal structure of a matrix, this matrix consisting of an aggregate of many halloysite tubules and CA polymer molecules. This matrix effect of poly-isobutyl CA is confirmed by the transmission electron micrograph, illustrated in Fig. 9.7c. From

the TEM it is evident that the matrix is composed of a convoluted, globular shaped polymeric network, in which the drug loaded halloysite is embedded (apparent as darker shades within the globular polymer). Nearer the edges of the matrix structure, individual halloysite tubules (A) are more easily identifiable, where the polymer is less dense. The matrix consists of a high average molecular weight polymer, formed using the iso-butyl CA monomer (i.e. 721,285, see Table 9.7b). A similar phenomenon did not occur with the octyl CA monomer, which potentially could form polymers of even higher average molecular weights, as, in this instance, the polymer was supplied in combination with sulphur dioxide (i.e. contains 12.5 ppm SO_2). According to Chouinard *et al.,* 1994, when sulphur dioxide is present, dissolved in the monomer, it functions as a polymerisation inhibitor. As a result, polymerisation does still occur, but the size of the ultimate average molecular weight is limited dramatically (i.e. 572,281, see Table 9.7b).

The encapsulation yields for the poly-n-butyl, poly-isobutyl and poly-octyl CA polymer coated products are 17.83%, 18.75% and 21.46%, respectively. This indicates that the least polymer weight gain per unit halloysite mass (i.e. specific gain) occurs for the poly-octyl CA coated product, (i.e. its encapsulation efficiency is closest to that of the uncoated halloysite powder). The specific polymer weight gains by the poly-n-butyl and poly-isobutyl coated products are similar, suggesting that the predominant factor, inducing differing drug release profiles for the two, must be related to differences in their average molecular weights.

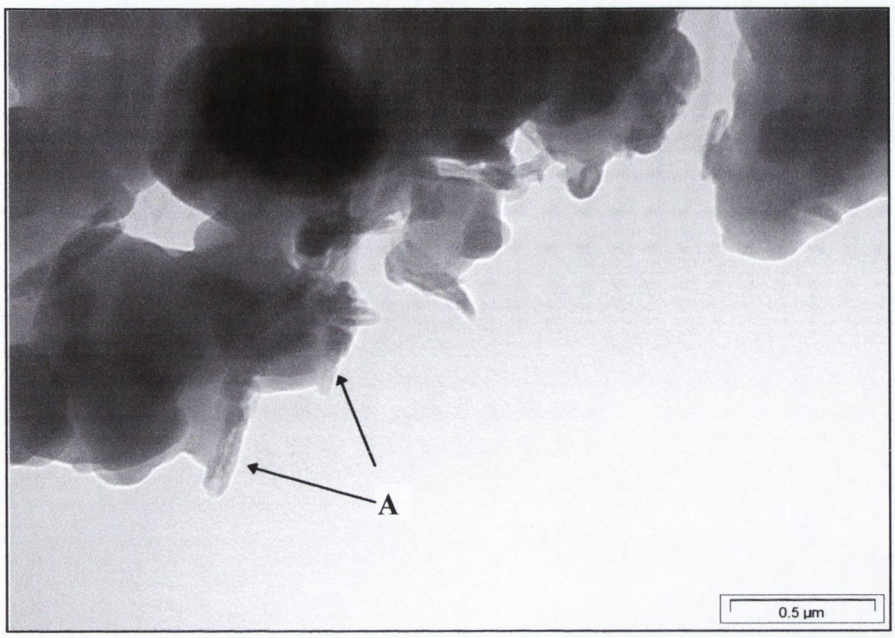

Figure 9.7c. Transmission electron micrograph of poly-isobutyl CA coated, drug loaded halloysite (X 70,000 magnification).

9.7.2.3 Effect of Cyanoacrylate Monomer Concentration

Again using the n-butyl CA monomer, drug loaded halloysite was coated, using a 5% and 10% v/v CA monomer solution in heptane, to investigate whether the monomer concentration used had any effect on the release profiles of the final product. These release profiles for the two coated products are illustrated in Fig. 9.7d.

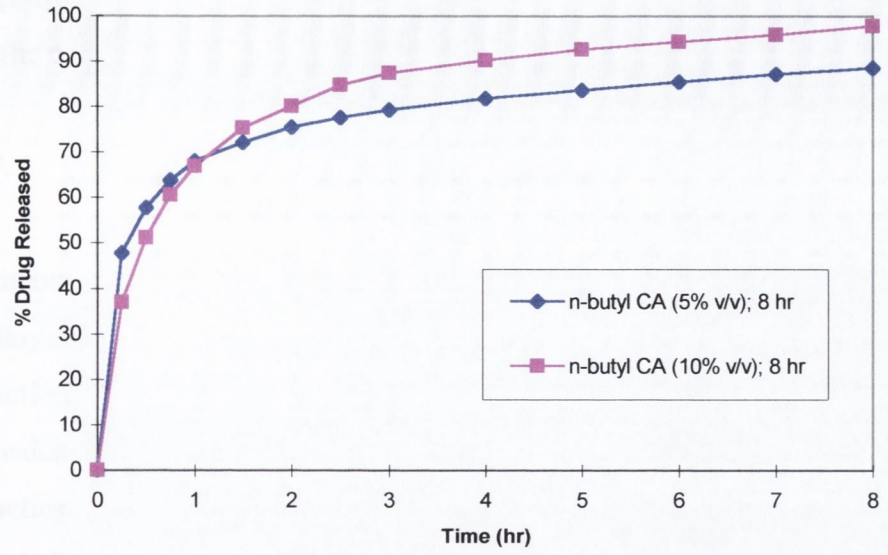

Figure 9.7d. Dissolution of Diltiazem HCl from poly n-butyl CA coated, drug loaded halloysite samples (applied using 5% and 10% v/v monomer concentrations), in pH 6.8 McIlvaine buffer, for 8 hr, at 37°C.

Comparison of the profiles, using the similarity factor, indicate that any difference that exists is insignificant (i.e. f_2 = 56.26). Visual examination of the plots suggests that the release from the product, coated using a 5% v/v monomer solution, may be slightly more delayed. This can be explained due to the fact that a higher monomer concentration (i.e. 10% v/v) correlates to a higher local concentration of monomer molecules and, hence, more initiation sites are induced. As a result, a larger number of smaller average molecular weight polymers are formed (i.e. 382,000, see Table 9.7b), in contrast to a smaller number of larger average molecular weight polymers arising (550,000, see Table 9.7b), when lower concentrations of monomer are used. The smaller molecular weight polymers degrade at a faster rate, causing a faster drug release rate. The encapsulation efficiencies for the products coated, using the 5% and 10% v/v monomer solutions, are 17.83% and 15.04% w/w, respectively, indicating that the specific polymer weight gain is much greater when the higher monomer concentration is used, although this product appears to have slightly poorer sustained release properties. This indicates that increases

in polymer molecular weight may have more significant influences on the release kinetics of the coated products, than the actual gain in polymer content.

9.7.3 Conclusion

Cyanoacrylate monomers were shown to successfully polymerise around the drug loaded halloysite particles, forming a retardant barrier to drug release. The polymerisation reaction was probably initiated by residual water present within the dried halloysite powder. In the majority of formulations, the barrier formed illustrated zero-order release kinetics with an associated burst effect, except for that coated with iso-butyl CA, where the halloysite particles became embedded within a highly convoluted globular polymer network, thereby creating a matrix, resulting in Higuchi release kinetics. This was probably due to the formation of a high molecular weight polymer. In all situations, the encapsulation yields were reduced relative to the uncoated halloysite (ie 25.6% w/w), due to the gain in polymer coating weight. From these experiments, it is obvious that a number of factors affect the final product release profiles such as polymerisation reaction time, monomer type and concentration, and whether or not it is combined with a polymerisation inhibitor such as sulphur dioxide. Suitable optimization of these parameters should allow for the development of a product with a desired release profile.

General Discussion

The aim of this work was to examine two novel excipient classes as potential candidates, offering improved functionality within the pharmaceutical technology sector. At present, because full physical characterisation of solid materials has been made possible with the help of high resolution analytical techniques on the molecular, particulate and bulk levels, there are emerging trends in the development of 'tailor-made' materials or pharmaceutical excipients. According to Pifferi *et al.,* 1999, three main approaches are followed by industry:- physical or minor chemical manipulation of materials already known, combination of two or more marketed excipients in order to reduce unwanted defects and, thirdly, preparation or use of new chemical entities, with huge investments for the toxicity studies. In our case, the first excipient class examined, i.e. novel size reduced grades of MCC (Avicel® PH-101) with the absence or presence of de-aggregating agents, falls broadly into the first two groups described above, being produced by physically combining the MCC with another marketed excipient (sodium lauryl sulphate; SLS) and then physically manipulating it by size reduction using an ultrasonic homogeniser. This grade was developed, using a systematic approach, based on observations of Deasy and Law (1997) that SLS caused fragmentation of MCC into small crystallites, affecting drug release and other properties. The second excipient class examined, namely halloysite, can be described as a new material / entity for use as a pharmaceutical excipient, although it is chemically related to kaolin, a widely used pharmaceutical excipient. Interest in this material arose from contact with Ron Price, of the Naval Research Laboratory in Washington D. C., who recently filed a patent (Price and Gaber, 1997), describing the mineral's role as an active excipient, resulting in delayed or sustained release of anti-fowling agents in marine applications. An important aspect of both the above excipient classes is their active role in delaying the release of various chemical entities, at a controlled rate, into the use environment. Because of their specific functions in the formulation, they can not be categorised as 'traditional' excipients, which are defined as being 'inert' commodities or components of dosage forms. Instead, recognition of the fact that many excipients have a specific function or role, such as the above, led to the

introduction of the more recent definition (Pharmacopoeial Forum, 1995; 21: 863), describing them as 'any component other than the active substances, intentionally added to the formulation or dosage form'.

The initial stages of work involved attempting to produce a surfactant aided de-aggregated grade of MCC, by replicating the experimental techniques used by Deasy and Law (1997), with SLS, which, according to the authors formed a more effective retardant matrix and also a greater surface area of cellulosic material for drug binding / hindering, thereby delaying drug release from pelletised formulations prepared by extrusion / spheronisation. In addition to SLS, we investigated two additional surfactants, namely Cetrimide and Tween 20. Quantitative analysis illustrated no significant particle size reduction to occur, in contrast to the results of Deasy and Law (1997), which was further confirmed by experimental replication, using an alternative MCC batch. As a result, alternative preliminary mechanical size reduction techniques were examined, namely wet grinding, using a Retsch® 'vibratory ball mill' and ultrasonic homogenisation. Results showed both techniques to be successful in achieving MCC size reduction. However, ultrasonic homogenisation proved advantageous over the former, being much faster and capable of milling relatively large quantities of suspended powder in a short time period (ie ~ 0.5 litres of material passed through the homogeniser in 30 sec approx.). It's primary limitation was the fact that it required that the MCC material be size reduced in its wetted state. However this could be overcome, by incorporating this step prior to spray-drying in the typical commercial MCC production process.

Based on the apparent success of ultrasonic homogenisation in the preliminary studies, factorial analysis was applied to optimise the process, in which three main factors were examined, namely surfactant inclusion / absence, number of homogenisation cycles and MCC suspension concentration. A full 2^3 factorial experiment was used, performed in duplicate, each replicate block of experiments being performed on separate days, enabling us to determine the magnitude of day-to-day variation. Day-to-day variation proved negligible, illustrating the robustness of the technique, and all three primary factors

examined were shown to have a significant impact on size reduction, although the number of homogenisation cycles was clearly the most important. The inclusion of surfactant was the only factor to have a negative impact on size reduction, attributable to the foam formed by the SLS surfactant, protecting the MCC particles against the full stresses caused by the cavitation and shearing forces. Subsequent to the homogenisation optimisation studies, a number of size reduced grades of MCC, in combination with two differing levels of three de-aggregating agents, were formed. In addition to SLS, sodium hexametaphosphate and sodium citrate were used, the former being chosen due to its de-flocculating properties (Merck, 1996), and the latter due to its use as a sequestering agent in pharmaceutical formulations. Quantitative analysis of the recovered MCC powders indicated that microfine grades (~ 10 μm) were achievable with the incorporation of de-aggregating agents, through a simple two-step process of homogenisation, followed by spray-drying.

The production of optimally size reduced novel grades of MCC was followed by characterisation of their physical properties such as particle size, specific surface area, crystallinity and porosity. These properties were chosen for examination, as they were considered to have a very important influence on their final use in pharmaceutical applications, particularly when used in tableting and as aids in extrusion / spheronisation. In tableting applications, ideal properties of MCC grades would include good compactability, mixing and flow properties, which are related to particle size, shape and crystallinity. When used as spheronisation aids, particle size and powder bed porosities would be important properties in terms of their influence on pellet yields, smoothness and drug release characteristics. A reduction in particle size of the novel MCC grades was confirmed, both qualitatively and quantitatively, from SEM micrographs and average particle size data collected using the Malvern, respectively. Predictable trends were also observed with the size reduced grades, when their porosities were measured by mercury porosimetry and their surface areas measured, using a combination of mercury porosimetry and nitrogen adsorption techniques. In all cases, as the average particle size of the MCC grades was reduced, their specific surface areas increased and their inter-

particulate pore diameters decreased, in agreement with Hausner (1967), who explained that when a powder mass consists of fine particles, pores between the particles will also be fine. Crystallinity values, obtained by XRD analysis, indicated minimal changes in levels of crystallinity determined for the novel MCC grades, when compared to that of the parent MCC grade, Avicel® PH-101. This confirmed that the forces subjected on the MCC particles, during homogenisation, broke up only a very small quantity of the crystalline areas in the MCC material. When the DSC data, which enables quantitative estimation of the contents of 'non-freezable' water present in hydrated MCC samples, was used to determine the relative degrees of crystallinity of the MCC grades, the calculated 'non-freezable' water contents were unexpectedly lower for the size reduced grades, indicating more crystalline products. Examination of the calculated enthalpies suggested, however, that these contrasting results, relative to the XRD data, may have arisen, due to the lower powder bed pore diameters of the novel grades creating a more tortuous network, thereby hindering uniform water distribution within the amorphous regions of the MCC polymer. This hindrance effect, against uniform water distribution, was overcome to some degree in Grade Y due to the surface wetting enhancing properties of the incorporated SLS. These contrasting crystallinity results, obtained using XRD and DSC techniques, illustrate the importance of clearly stating which technique is used, when quoting crystallinity data for various excipients and also reiterates the importance of harmonisation of testing procedures, which is currently occurring within the pharmaceutical community (Armstrong, 1997).

The novel size reduced MCC grades were examined in a number of pharmaceutical applications. At present, the largest use of MCC is in tableting, where it is used to assist in the flow, lubrication, bonding and disintegration properties of the ingredients being tabletted. Two novel grades were examined, namely Grade X and Y and it was not surprising that their use in this application proved disappointing. The two novel grades, being of smaller average particle size relative to the two most commonly used commercial grades (i.e. Avicel® PH-101 and PH-102), had very poor flow properties, which are considered vital to ensure good feed of powder material from the hopper into the tablet

die, thereby ensuring uniform die filling and uniformity of final product. This was reflected in the poor uniformity of thickness, content and hardness values determined for tablets produced using the two novel grades. Furthermore, significant sticking of the punches within the die occurred during the compression and ejection stages, which was again related to the fineness of these novel grades, allowing some of the particles to seep down into the gap between the die and the lower punch wall, creating undesirable friction. Sticking was not as problematic with Grade Y, due to the lubricant properties of the SLS present. Studies of the compression force / tensile strength profiles of the MCC powder compacts illustrated a dramatic reduction in the tensile strength of those incorporating MCC Grade Y. This was again a consequence of the SLS present interfering with the formation of strong, clean bonds between the MCC particles.

Investigations revealed that these novel size reduced MCC grades had greatest potential as spheronisation aids in the process of extrusion / spheronisation, in which application seven novel grades were examined, in conjunction with Avicel® PH-101, functioning as the Control. At optimal hydration levels all novel MCC grades produced pellets with higher yields than the Control PH-101 grade, with all yields being greater than 70% and, in the majority of cases, greater than 80%. A possible explanation for this was the improved matrix structure and finer pores created by the finer MCC particles imparting better sponge-like water retentive properties to the hydrated MCC powder agglomerates. This would result in less water being squeezed to the pellet surfaces during the extrusion / spheronisation process, the presence of which promotes particle agglomeration and the generation of large pellets. The fine intra-agglomerate pores created by the fine sized MCC particles would also generate a larger capillary suction pressure (Rumpf, 1958a,b) and, hence, binding force, helping to maintain the coherent integrity of the pellets and minimising the production of fines during the various process stages. Further evidence, supporting this theory, was the fact that the size reduced MCC grade, co-processed with the higher level of SLS, generated pellets with the highest yield of large pellets (i.e. > 20%), due to the surfactant properties of SLS reducing the surface tension and suction pressure developed within these capillary pores. Significant positive benefits were obvious

with the inclusion of SLS, its presence resulting in the formation of smoother more rounded pellets, especially when compared to the Control pellets. This was probably due to the SLS promoting a more uniform distribution of water within the MCC aggregates, causing more efficient plasticisation of the MCC particles, thereby facilitating the deformation of the pellets and the creation of smoother spherical surfaces. Fewer surface and intra-particulate pores were also apparent for pellets made using the novel size reduced MCC grade combined with SLS, compared to the Control pellets, evident both qualitatively from SEM examination of the pellets and quantitatively using mercury porosimetry. This corresponded to significantly improved delayed drug release from the former pellets. Although release was delayed from the pellet formulations composed of the other novel MCC grades, these improvements were not significant relative to the Control.

In conclusion, it was obvious that the novel size reduced MCC grades illustrated the most promising results when used as spheronisation aids. Of all the novel grades examined, those containing size reduced MCC, co-processed by spray-drying with SLS, demonstrated the best potential, capable of producing high yield pellets with improved sustained release functionality. The fact that these excipients were designed by systematic physical alteration of pre-existing excipients may also help minimise further expensive toxicological and safety studies that may be necessary, if they were to be marketed commercially. In addition, at present, a primary concern over novel excipients is the development of specific characterisation tests which can be used to ascertain their functionality within pharmaceutical applications. It is important that these tests are not generalised for excipient groups such as microcrystalline cellulose, but are, instead, tailored specifically to each grade's intended function, i.e. tests which measure MCC particle flowability may be very relevant to it's tableting applications, whereas characterisation studies performed on our novel MCC grades suggest that those that measure powder bed average particle sizes and porosities may be more relevant when intended as spheronisation aids.

The tubular mineral, halloysite was also examined for potential novel pharmaceutical applications, more specifically as a novel sustained release technology. Because this mineral had not been used to date in the pharmaceutical area, it had undergone very little characterisation in terms of relating its physical, structural and chemical properties to an ultimate pharmaceutical functionality. As mentioned in Section 8.2, the mineral is not uncommon in nature being found in many subtropical and tropical soils. However, its commercial development, according to Harvey (1996), tends to be restricted to New Zealand, the Republic of Korea and perhaps Japan. Within these individual countries, significant differences in halloysite morphology arise, depending on the exact forces of nature involved in their formation. In New Zealand, for example, Churchman *et al.*, 1995, examined a number of halloysite samples and illustrated, from TEM examination, the existence of a wide variety of morphologies, i.e. (a) thick tubular (Dunedin); (b) spheroidal (Opotiki) and (c) blocky (Te Puke). These minerals were also shown to differ significantly in terms of specific surface areas, sizes and porosities. This indicates that potentially many differing grades of halloysite are available.

At present, halloysite's primary use is within the ceramics industry, where quality criteria do not necessarily specify which mineral morphology is present. As a result commercial sources tend to produce mineral grades, which are poorly uniform in terms of average particle size and tubular content, and which also appear to contain large quantities of aggregated debris material in conjunction with intact tubules. This is illustrated by SEM examination, discussed in Section 8.3. Despite this, according to Murray (1999), improved mining techniques, and particularly new improved beneficiation methods, have resulted in higher quality and more uniform clay products. From a pharmaceutical point of view, since we intended principally to examine halloysite's ability to entrap and retain drug within its tubular structure, thereby delaying its release from this inherent tubular matrix at a controlled rate, we were interested in acquiring a highly tubular sample of the mineral. New Zealand China Clays Ltd. (the world's largest current supplier of semi-purified grades of halloysite) were contacted and supplied us with a number of preliminary sample grades, which contained high levels of tubular material, differing in terms of their tubule

dimensions, and whether or not they had been treated with a quaternary ammonium salt to render them more hydrophobic. Halloysite G was chosen for further studies due to its hydrophilic nature and apparent high tubule content, as illustrated by SEM examination and a larger 25 kg batch was subsequently obtained. SEM examination of this larger batch indicated that it was not as consistent in its tubule make-up, relative to the original smaller batch and, hence, the powder had to be sieved through a 125 μm sieve to remove some of the undesirable large aggregates prior to drug loading investigations. This suggested that significant batch to batch variability exists within similar commercial grades of the material, even when obtained from the same supplier. As a result, the mineral, as it is currently being marketed and supplied, would fall well short of the quality criteria that are now expected of pharmaceutical excipients, a primary aspect of this being good lot-to-lot or batch-to-batch reproducibility. Furthermore, very little information has been made available on the exact processes that are used to purify the mineral and separate it into different shape and size fractions, once it has been mined form the ground. Examination of our sample, using energy dispersive analysis, revealed the presence of iron and calcium ions, even though the mineral is essentially composed of alternating silica and alumina sheets. This infers the presence of other contaminants such as iron oxides, calcium oxides and perhaps calcium carbonates. Further tests would be necessary to determine their exact identities and concentrations, before setting limits on their acceptable levels. It is important that the material is well characterised by the suppliers, with the development of specific master files for the different grades of the mineral. At present, NZ China Clays and other suppliers of halloysite are unable to supply material which meets the exacting requirements of the pharmaceutical industry.

Pifferi *et al.,* (1999), lists some of the characteristics necessary of an ideal excipient, stating its necessity to be chemically and physically inert with respect to the drug and compatible with other formulation ingredients. It should be odourless and tasteless, have good flow properties, be available worldwide from many sources at an inexpensive price, be easy to store and have good lot-to-lot reproducibility. The excipient should also be pharmaco-toxicologically inactive. At present, because halloysite is mainly used in the

manufacture of ceramics, only limited toxicological and safety studies have been performed thereon. If it is going to be used as a novel excipient, in pharmaceutical applications, more rigorous and extensive studies will be necessary in this regard. This will have the disadvantage of raising the cost of the material, which at present is very inexpensive in pharmaceutical terms. These studies, however, may be minimised due to its chemical similarity to kaolin, which is currently widely used in pharmaceutical formulations and is described within the Handbook of Pharmaceutical Excipients (2000) as being harmless, when orally administered, although a disease of the lung, due to chronic inhalation of kaolin dust (silicosis / kaolinosis), has been reported. In the case of halloysite, the suppliers state that it is non-toxic if swallowed, and also recognise it as a chronic hazard respirable dust and state that a silica approved face mask should be worn, when handling the material and when dealing with spills.

Although halloysite poses a number of problems that need to be addressed if it is to be accepted for use as a pharmaceutical excipient, it was not the intention of this thesis to focus on these issues. Instead, we intended to examine the mineral's potential in a novel sustained release technology, where it could be termed an adjuvant (Pifferi *et al.,* 1999) helping the active principle to carry out its activity, by conditioning its release from the pharmaceutical form and, hence, have an important pharmaceutical function, due to the renewed interest in modified release technology. If its success as a novel sophisticated excipient could be demonstrated, then this might warrant the investment of time and money in developing better characterised, higher quality grades, as is demanded by the regulatory authorities.

As mentioned in Section 1.3.6, halloysite has the ability to intercalate with a number of organic molecules. This process is facilitated by the mineral being present in its hydrated state, although simple drying, during its extraction and clean-up processes, can result in its irreversible dehydration. The mineral, as supplied to us, was in dry powdered form and hence fully dehydrated, which restricted attempts by us to examine its potential to intercalate with various chosen organic chemicals, including our drug candidate, Diltiazem

HCl. The mineral was artificially re-hydrated and re-expanded, using the process as described by Wada (1961), yet following this, intercalation with our drug failed to occur, most likely due to its comparatively large size and inaccessibility into the interlayer space. Other mechanisms of drug loading were examined, including ionic binding of an ionisable drug species to the charged mineral surface and, secondly, physical entrapment of the drug within the mineral's hollow tubular matrix structure. As a result, halloysite was characterised in terms of surface charge and porosity, using zeta potential measurements and mercury porosimetry studies, respectively, both tests describing the previously proposed loading functions for the mineral. Zeta potential studies illustrated the mineral to have a permanent negative charge with the ability to electrostatically attract cations ensuring electroneutrality. The magnitude of this surface charge was shown to be variable, being minimal in low pH environments and increasing as the pH of the environment increased, due to ionisation of surface alumina and silica hydroxyl groups, as described in Section 1.3.7. Mercury porosimetry enabled us to distinguish between inter-particulate and intra-particulate pores, representing voids between the individual particles and aggregates, composing the halloysite powder mass, and the tubular lumenal pores running through individual mineral particles, respectively. The capacity of the intra-particulate pores was important, as it was within this volume we intended to entrap the drug. The determined available volume was optimal for the 'sieved only' halloysite fraction (i.e. 0.246 ml/g of halloysite 'G').

Diltiazem HCl was shown to bind electrostatically to the surface of halloysite, as described in Section 9.2. The choice of Diltiazem HCl was probably not optimal in this instance, as it is an acidic drug, aqueous solutions of which have low pH values (i.e. a 1% w/w solution of the drug has a pH of 4.2; Mazzo *et al.,* 1994). These low pH values have the effect of reducing the magnitude of the surface charge and, hence, number of sites available for binding. By choosing a less acidic cationic drug, higher binding levels may have been achievable (i.e. greater than 2.4 mg approx. of drug bound per 100 mg of halloysite achievable, using Diltiazem HCl at the saturation plateau binding level). The slow dissociation of this bound drug from the anionic sites contributed to a sustained

release mechanism, as illustrated in Section 9.3, which examined tubular entrapment of the drug within the lumenal matrix. Simple entrapment, without the aid of a coating of polymer of lipid, illustrated poor drug retardation (i.e. 90% release within 1 hr) due to the ready penetration of the aqueous medium causing rapid drug dissolution and outward diffusion. The second slower release phase, illustrated in the same dissolution profile (i.e. ~ 10% drug content over 3 to 4 hr), could be attributable to the slower dissociation of the tightly bound drug.

The incorporation of a viscosity enhancer (PVP) also proved disappointing as the increased viscosity effect was lost, upon drying the drug loaded product, and probably only slowly returned, upon subsequent re-hydration, by which time the entrapped drug had been mainly leached out. The use of PVP may have been more successful if the drug loaded halloysite was retained in its moist state. However this would have been pharmaceutically unacceptable for drug stability reasons, especially in the case of Diltiazem HCl, which is highly stable in its solid state, but undergoes hydrolysis to the de-acetyl product, when in solution (Mazzo *et al.,* 1994).

The most promising results were achievable by drug loading the mineral and drying, followed by coating with a suitable polymer or lipid, forming a rate limiting barrier layer around the drug loaded halloysite reservoir. A number of coating systems were examined, namely cationic polymer coatings such as Chitosan, PEI and Eudragit E, lipids such as Novata E and Precirol and the poly-alkyl-2-cyanoacrylate polymers. All coated products significantly delayed drug release relative to the uncoated halloysite formulation. In the case of the polycation coatings, the release kinetics were best described using the zero-order release model, after an initial burst release effect. This burst effect arose due to the rapid release of the drug, which became loosely embedded within the polymer film during its application. Leaching of the drug out of the tubule into the polymer was facilitated by the aqueous nature of the coating systems used. This leaching also caused a significant reduction in the actual drug loading efficiencies of the coated halloysite formulations and also made the achievement of predictable, predetermined loading levels difficult, if not

impossible. These shortcomings may have been overcome, if the polymer coatings had been prepared and applied using organic solvents in which the drug candidate had low or negligible solubility, or if the final product was dried by lyophilisation, rather than by decanting off the excess supernatant polymer solution (containing some dissolved drug), following centrifugation of the coated product. The concentration of the aqueous polycation polymer solution used for coating also had an impact on the properties of the final drug loaded formulations. In general, as the polymer concentration increased, the magnitude of the burst effect and rate of release from the respective coated products decreased, due to a correspondingly thicker and more uniform rate-limiting film being formed. In addition, the encapsulation level decreased due to a higher specific polymer weight gain per unit amount of halloysite powder. The main exception to this was in the case of the PEI polycation coated systems, where slower rates were observed for the lower coating concentrations, believed to be due to the compact arrangement of the polymer coating, whereas higher concentrations introduced molecular stearic hindrances causing more porous and less dense films to be formed. Although not illustrated, it can be accepted that the surface charge of the halloysite particles becomes reversed, as a consequence of polycation polymer binding to its surface, since polyelectrolyte concentrations used were sufficient to form a saturated layer. As a result, there is potential to further delay drug release rates from these polycation coated systems, by subsequent application of a polyanionic coating, thereby further increasing the membrane thickness, as illustrated by previous research investigating stepwise polyeletrolyte assembly on particle surfaces (Lvov *et al.,* 1996; Sukhorukov *et al.*, 1998).

More predictable drug loading efficiencies were achievable with the formulations where the drug loaded halloysite was incorporated within a lipid matrix. The release kinetics from these preparations were best described using the Higuchi model, describing drug release from a matrix created by the lipid. The actual encapsulation loadings achievable with these preparations were very close to the predicted loadings, as illustrated in Section 9.6.5. The reason for this was because the drug loaded halloysite was encapsulated within lipid, simply by melting the lipid and stirring in the halloysite to form a uniform

suspension, followed by rapid cooling using liquid nitrogen, i.e. a non aqueous system was used in which the drug had minimal solubility. An aqueous environment was only used for short time periods (i.e. 4 or 8 min), during the size reduction step, during which time the amount of drug leached would have been minimal. Furthermore, this leached drug was not lost from the preparation because it was re-crystallized and became re-embedded in the outer surfaces of the lipid micro-particles, during the subsequent lyophilisation step. Studies also illustrated that higher drug loaded halloysite loading levels were achievable in these lipid preparations (i.e. preparation E), without adversely affecting the release kinetics.

Coating the drug loaded halloysite with various cyanoacrylate polymers also further retarded the release of drug entrapped within the mineral's lumen. The magnitude of this retardation was dependent upon a number of factors such as polymerisation reaction time, monomer type and concentration, and the presence or absence of polymerisation inhibitor. Again, with this technology, similar to that involving halloysite coating using the polycation polymers, it was difficult to predict the final percentage level of encapsulated drug in the coated product. Yields, however, were closer to that of the uncoated product, as the polymer was applied using an organic solvent (i.e. heptane), in which Diltiazem HCl has negligible solubility and so none was lost to the environment, by leaching, during the coating process.

Diltiazem HCl was chosen as the main experimental drug candidate for investigation using the technology, due to its very high saturated aqueous drug solubility (~ 50% w/w; Yang and Fassihi, 1997) and so its potential to adequately challenge the use of halloysite as a novel sustained drug release mechanism. The combination of loading the drug within the mineral's lumen and coating the reservoir with a suitable membrane (lipid or polymeric), illustrated the mineral's potential in this area. The technique, involving the incorporation of drug loaded halloysite into a lipid matrix, was expanded to examine the effect of using a less soluble drug. Propranolol HCl was chosen as another cationic drug with a saturated aqueous solubility of ~ 5% w/w (Yang and Fassihi, 1997). The results obtained were very

promising and indicated that, by simply loading this less soluble drug within the halloysite tubule, without any further processing, the halloysite tubule created a suitable matrix, allowing for only 80 to 90% approx. drug release over an 8 hr period. This level of retardation was significantly improved over the similar product incorporating Diltiazem HCl, as illustrated in Figure GD.1. Matrix release was illustrated to be the predominant release mechanism for Propranolol HCl, as evident by fitting the release data to the Higuchi model, although deviations from linearity of fit occurred after 1.5 hr approx. due to the drug concentration present within the matrix structure falling below saturated conditions. When the Propranolol HCl loaded halloysite was incorporated into a lipid matrix as solid lipid microparticles, even further dramatic retardation of drug release occurred, with only 40% approx. being released over an 8 hr dissolution period.

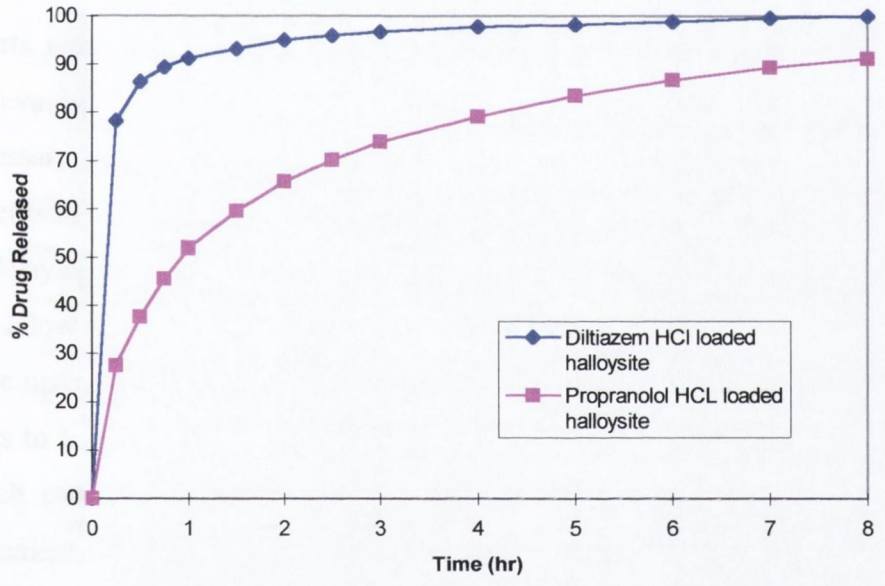

Figure GD.1. Dissolution profiles for the release of Diltiazem HCl and Propranolol HCl from drug loaded halloysite, in buffer medium pH 6.8.

It is important to note that the overall encapsulation level, achievable using this technology, is limited in terms of how much drug can be loaded within the mineral's tubular core. Mercury porosimetry data revealed that the maximum loadable volume is 0.25 ml approx. per gram of our halloysite 'G' grade. Other grades, with larger inherent

tubular volumes, may be available, but screening for these was outside the scope of this research. Optimal loading within this finite space is also limited by the fact that the drug, (in order to penetrate the tubule by capillary forces), must be in liquid form (i.e. either melted or in solution). For obvious reasons, highest loadings would be achievable if the pure drug was loaded in its molten state. However, this is limited to thermostable drugs with relatively low melting points. When loading using drug solutions, highly concentrated solutions are best for maximal loading capacity, with intermediate drying, followed by reloading from solutions. Since halloysite is chemically inert, the use of organic solutions is possible.

Despite this initial work illustrating the enormous potential of halloysite in the area of sustained drug delivery, it also suggests that much more research is necessary. Combined efforts must be made by the supplier and persons investigating specific applications to achieve better characterised, more uniform tubular grades of halloysite. Studies are necessary in optimising the mineral's drug loading capacity. Even though the improved benefits of coating the loaded mineral with various polymers or lipids are obvious, in terms of delaying release, more investigations are necessary, using alternative coating systems that allow for more predictable and higher loading yields, perhaps achievable by choosing more optimal solvents in which the drug candidate has minimal solubility. One of the best ways to test the mineral's potential is to use it to develop a specific product formulation, which can be prepared easily and cheaply, and which is capable of delivering active ingredients into the use environment, at controlled rates, which are previously defined.

FMC Corp., who supported the MCC work, are currently examining the commercial potential of the unique MCC size reduced grades. Minor modification of their current production processes, and further optimization of the approaches described, will be involved. This should enable them to introduce new grades, particularly for extrusion / spheronisation and consequently help retain their position as the major supplier of functional grades of MCC to the pharmaceutical and other industries.

In the case of halloysite, initial applications are likely to be in the non-pharmaceutical area, where constrains of excipient quality and toxicity are less stringent. Many of the techniques of drug loading and over-coating arose from extensive preliminary experimentation, not adequately described in the thesis, involving a unique hybridization of existing approaches, which is not uncommon in novel drug delivery technology. Collectively, these approaches represent unique proprietary knowledge not disclosed elsewhere in the literature. In fact, there are negligible publications in the literature describing the use of halloysite for the controlled release of active materials and none in the pharmaceutical area, as confirmed by a recent search of several major databases. Thus, the potential of halloysite generates a new and exciting area, requiring further development and commercial exploitation.

Appendices

Appendix 1

UV absorbance spectrum for diltiazem hydrochloride in phosphate buffer pH 6.8

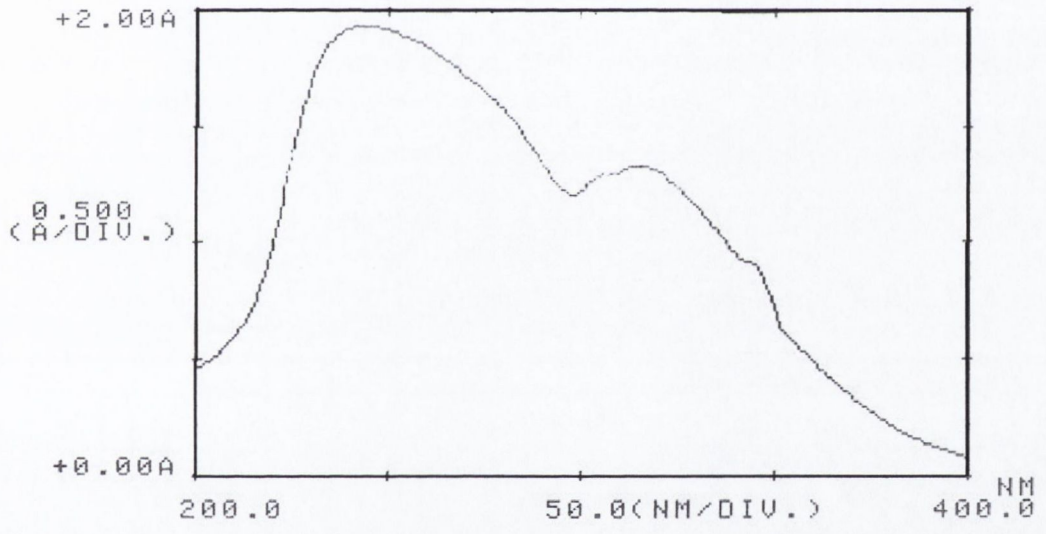

UV absorbance spectrum for propranolol hydrochloride in phosphate buffer pH 6.8

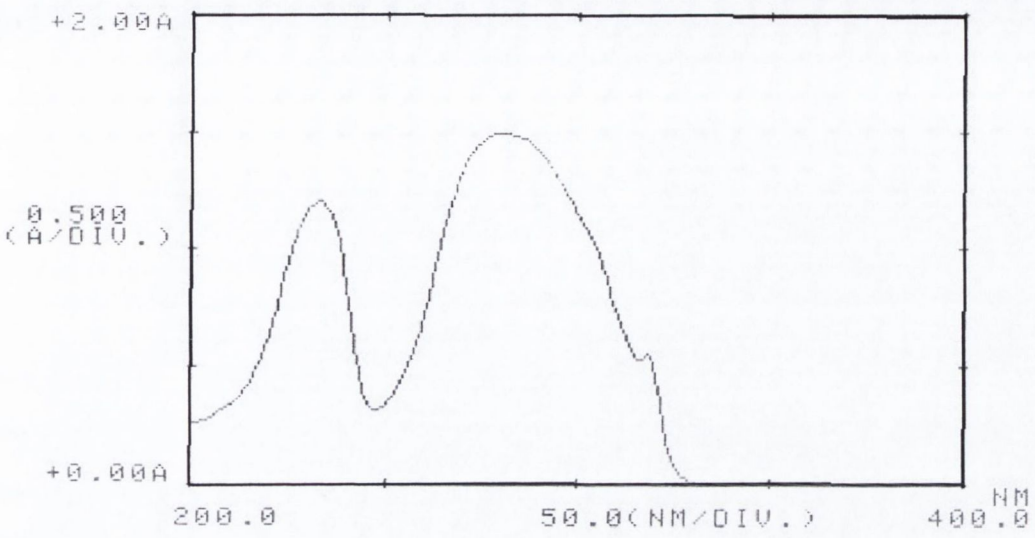

Appendix 2

Calibration curves used to determine concentration of substances in solution

UV calibration curves

(1) Paracetamol in phosphate buffer pH 6.8

Shimadzu UV 160

Analytical wavelength: 257 nm

Concentration (mg/100 ml) = (Absorbance + 0.0039) / 0.414

Coefficient of determination = 0.9998

(2) Indomethacin in phosphate buffer pH 6.8

Shimadzu UV 160

Analytical wavelength: 318 nm

Concentration (mg/100 ml) = (Absorbance + 0.0004) / 0.188

Coefficient of determination = 0.9989

(3) Diltiazem hydrochloride in phosphate buffer pH 3.2

Shimadzu UV 160

Analytical wavelength: 236 nm

Concentration (mg/100 ml) = (Absorbance + 0.0099) / 0.463

Coefficient of determination = 0.9992

(4) Diltiazem hydrochloride in phosphate buffer pH 6.8

Shimadzu UV 160

Analytical wavelength: 236 nm

Concentration (mg/100 ml) = (Absorbance + 0.005) / 0.461

Coefficient of determination = 0.9999

(5) Propranolol hydrochloride in phosphate buffer pH 6.8

Shimadzu UV 160

Analytical wavelength: 292 nm

Concentration (mg/100 ml) = (Absorbance + 0.0018) / 0.169

Coefficient of determination = 0.9999

(6) Polyethyleneimine in distilled water

Shimadzu UV 160

Analytical wavelength: 209 nm

Concentration (mg/100 ml) = (Absorbance - 0.0098) / 0.072

Coefficient of determination = 0.9998

(7) Eudragit E in 0.1M acetic acid

Shimadzu UV 160

Analytical wavelength: 229 nm

Concentration (mg/100 ml) = $59.1*\text{Absorbance}^2 + 170.7*\text{Absorbance}$

Coefficient of determination = 0.9997

Appendix 3

Pressure table used with PoreSizer 9320

Point	Pressure (Psia)	Point	Pressure (Psia)	Point	Pressure (Psia)	Point	Pressure (Psia)
1	10	45	560	89	1440	133	6500
2	15	46	580	90	1460	134	7000
3	20	47	600	91	1480	135	7500
4	25	48	620	92	1500	136	8000
5	30	49	640	93	1520	137	8500
6	35	50	660	94	1540	138	9000
7	40	51	680	95	1560	139	9500
8	45	52	700	96	1580	140	10000
9	50	53	720	97	1600	141	11000
10	55	54	740	98	1620	142	12000
11	60	55	760	99	1640	143	13000
12	65	56	780	100	1660	144	14000
13	70	57	800	101	1680	145	15000
14	75	58	820	102	1700	146	16000
15	80	59	840	103	1720	147	18000
16	85	60	860	104	1740	148	19000
17	90	61	880	105	1760	149	20000
18	95	62	900	106	1780	150	22000
19	100	63	920	107	1800	151	24000
20	110	64	940	108	1820	152	26000
21	120	65	960	109	1840	153	28000
22	130	66	980	110	1860	154	30000
23	140	67	1000	111	1880	155	29000
24	150	68	1020	112	2000	156	27000
25	160	69	1040	113	2050	157	25000
26	180	70	4060	114	2100	158	23000
27	200	71	1080	115	2150	159	21000
28	220	72	1100	116	2200	160	19000
29	240	3	1120	117	2250	161	17000
30	260	74	1140	118	2300	162	15000
31	280	75	1160	119	2400	163	13000
32	300	76	1180	120	2500	164	11000
33	320	77	1200	121	2700	165	9000
34	340	78	1220	122	2900	166	7000
35	360	79	1240	123	3100	167	5000
36	380	80	1260	124	3300	168	3000
37	400	81	1280	125	3500	169	1000
38	420	82	1300	126	3700	170	500
39	440	83	1320	127	4000	171	250
40	460	84	1340	128	4300	172	100
41	480	85	1360	129	4600	173	50
42	500	86	1380	130	5000	174	30
43	520	87	1400	131	5500	175	15
44	540	88	1420	132	6000		

Appendix 4

Endothermic and exothermic DSC data for hydrated Avicel® PH-101 powder samples

Water content (%)	Overall sample weight (mg)	Water weight in sample (mg)	Polymer weight in sample (mg)	ΔH per gram of water (J/g)	ΔH per gram of polymer (J/g)	ΔH per gram of water (J/g)	ΔH per gram of polymer (J/g)
				Endothermic data		Exothermic data	
4.50	7.799	0.336	7.463	-2.59	-0.12	30.71	1.38
5.14	8.016	0.392	7.624	-1.51	-0.08	40.43	2.08
8.51	7.666	0.601	7.065	-0.01	-0.001	35.49	3.02
9.27	7.660	0.650	7.010	-3.17	-0.29	32.01	2.97
11.42	8.159	0.836	7.323	-5.49	-0.63	22.37	2.55
14.71	8.358	1.072	7.286	-4.99	-0.73	20.17	2.97
14.90	8.203	1.064	7.139	-1.37	-0.20	17.90	2.67
18.44	8.902	1.386	7.516	-10.70	-1.97	10.22	1.88
19.00	6.907	1.103	5.804	-8.11	-1.54	25.55	4.86
18.88	7.517	1.194	6.323	-33.99	-6.42	35.34	6.67
25.38	8.131	1.646	6.485	-78.15	-19.84	96.67	24.54
30.52	8.857	2.071	6.786	-123.81	-37.79	138.12	42.15
30.68	7.625	1.790	5.835	-131.42	-40.31	138.33	42.44
36.59	6.929	1.856	5.073	-155.67	-56.95	159.39	58.32
43.29	8.871	2.680	6.191	-182.20	-78.87	189.79	82.16
43.62	8.346	2.535	5.811	-189.05	-82.47	189.46	82.65
47.21	7.858	2.520	5.338	-199.51	-94.19	191.89	90.59
56.53	8.753	3.161	5.592	-220.32	-124.54	215.99	122.09
60.80	8.204	3.102	5.102	-231.09	-140.50	223.16	135.68
69.94	8.123	3.343	4.780	-242.99	-169.94	238.92	167.09
72.36	8.687	3.647	5.070	-247.55	-178.07	242.25	174.26
71.80	8.557	3.576	4.981	-240.26	-172.49	236.71	169.94
83.40	7.536	3.427	4.109	-257.34	-214.63	249.62	208.19
92.26	8.646	4.149	4.497	-260.10	-239.98	259.31	239.24
88.28	8.081	3.789	4.292	-247.52	-218.52	227.53	200.86
97.57	8.859	4.375	4.484	-269.80	-263.24	257.73	251.46
90.52	8.181	3.887	4.294	-269.97	-244.38	269.12	243.61

Endothermic and exothermic DSC data for hydrated Grade X MCC powder samples

Water content (%)	Overall sample weight (mg)	Water weight in sample (mg)	Polymer weight in sample (mg)	ΔH per gram of water (J/g)	ΔH per gram of polymer (J/g)	ΔH per gram of water (J/g)	ΔH per gram of polymer (J/g)
				Endothermic data		Exothermic data	
2.00	7.590	0.149	7.441	-2.42	-0.048	3.91	0.08
1.44	7.176	0.102	7.074	-3.54	-0.051	9.58	0.14
3.14	7.859	0.239	7.620	-0.76	-0.024	4.19	0.13
4.40	7.870	0.332	7.538	-0.01	-0.001	3.53	0.16
4.45	7.983	0.340	7.643	-16.45	-0.73	1.09	0.05
6.22	7.581	0.444	7.137	-1.04	-0.064	2.82	0.18
6.82	7.598	0.485	7.113	-1.08	-0.073	2.56	0.18
9.44	7.444	0.642	6.802	-2.05	-0.19	2.75	0.26
10.50	7.557	0.718	6.839	-1.24	-0.13	1.69	0.18
11.06	7.936	0.790	7.146	-2.00	-0.22	1.08	0.12
17.10	7.055	1.030	6.025	-29.67	-5.07	1.05	0.18
15.88	7.690	1.054	6.636	-8.02	-1.27	8.91	0.14
20.11	7.682	1.286	6.396	-61.20	-12.30	54.87	11.03
24.87	7.360	1.466	5.894	-108.35	-26.95	113.14	28.14
29.97	7.526	1.673	5.853	-132.07	-37.75	137.63	39.34
31.25	7.317	1.742	5.575	-147.06	-45.95	155.53	48.60
40.25	7.279	2.089	5.190	-185.17	-74.53	185.77	74.77
44.51	7.568	2.331	5.237	-202.37	-90.08	195.15	86.86
51.16	7.268	2.460	4.808	-209.00	-106.93	207.75	106.29
57.36	7.459	2.719	4.740	-226.46	-129.91	222.84	127.83
61.13	7.243	2.748	4.495	-237.06	-144.93	229.43	140.26
67.67	7.054	2.847	4.207	-240.00	-157.79	231.90	156.93
71.52	7.276	3.034	4.242	-227.29	-162.56	216.96	155.18
72.41	7.286	3.060	4.226	-235.03	-170.19	228.83	165.70
73.06	7.580	3.200	4.380	-240.12	-175.19	229.40	167.60
79.11	7.127	3.148	3.979	-241.58	-191.13	238.21	188.46
90.85	7.199	3.427	3.772	-250.74	-227.80	242.92	220.70
92.40	7.092	3.406	3.686	-259.00	239.32	247.29	228.51

Endothermic and exothermic DSC data for hydrated Grade Y MCC powder samples

Water content (%)	Overall sample weight (mg)	Water weight in sample (mg)	Polymer weight in sample (mg)	ΔH per gram of water (J/g)	ΔH per gram of polymer (J/g)	ΔH per gram of water (J/g)	ΔH per gram of polymer (J/g)
				Endothermic data		Exothermic data	
2.98	7.633	0.221	7.412	-0.37	-0.011	4.28	0.13
4.18	8.659	0.347	8.312	-1.65	-0.069	4.09	0.17
6.42	6.794	0.410	6.384	-0.22	-0.014	1.86	0.12
8.07	6.843	0.511	6.332	-0.62	-0.050	2.64	0.21
10.66	8.096	0.780	7.316	-0.12	-0.013	2.15	0.23
8.63	6.940	0.551	6.389	-2.37	-0.200	1.54	0.13
12.24	7.666	0.836	6.830	-0.30	-0.036	2.08	0.26
13.56	6.976	0.833	6.143	-6.26	-0.850	1.15	0.16
12.79	7.767	0.881	6.886	-0.42	-0.054	1.04	0.13
15.36	7.570	1.008	6.562	-13.08	-2.01	6.60	1.01
20.55	7.585	1.293	6.292	-46.75	-9.61	46.33	9.52
22.26	7.723	1.406	6.317	-60.73	-13.38	67.49	15.02
21.43	6.923	1.222	5.701	-54.87	-11.76	58.71	12.58
24.49	7.005	1.378	5.627	-86.46	-21.17	97.11	23.78
26.16	7.518	1.559	5.959	-96.05	-25.13	114.16	29.87
23.57	7.487	1.428	6.059	-71.35	-16.82	82.54	19.45
36.82	7.395	1.990	5.405	-165.45	-60.92	173.97	64.05
37.86	7.141	1.961	5.180	-170.12	-64.40	173.09	65.53
39.03	7.634	2.143	5.491	-177.67	-69.34	184.84	72.14
39.24	7.700	2.170	5.530	-202.89	-79.61	204.94	80.42
63.91	7.643	2.980	4.663	-239.30	-152.93	224.87	143.71
65.69	7.254	2.876	4.378	-243.40	-159.89	232.60	152.80
61.35	7.127	2.710	4.417	-241.81	-148.36	232.14	142.43
79.46	7.207	3.191	4.016	-265.59	-211.03	249.70	198.40
88.73	7.870	3.700	4.170	-273.91	-243.04	263.28	233.60
74.76	7.228	3.092	4.136	-262.59	-197.05	249.64	186.63
95.67	7.633	3.732	3.901	-278.05	-266.00	264.53	253.07

Appendix 5

Plots of enthalpy per gram of water as a function of water content for Avicel® PH-101, Grade X and Grade Y powders, using the endothermic data

(1)

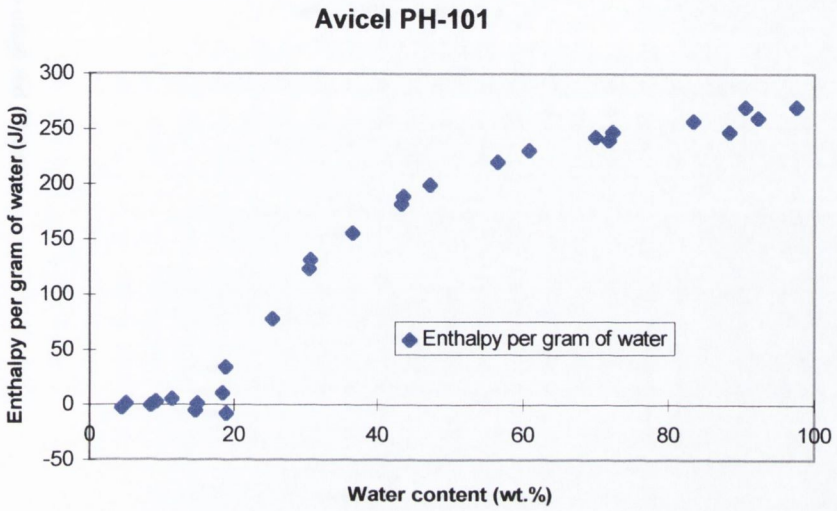

(2)

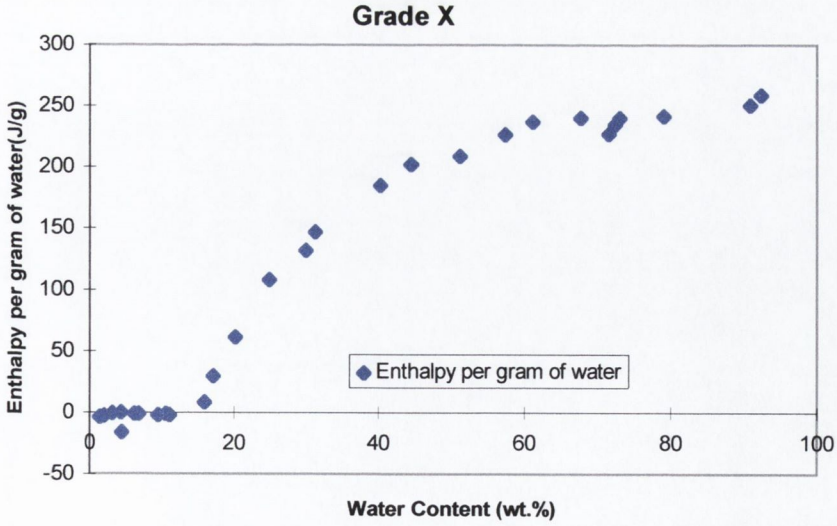

(3)

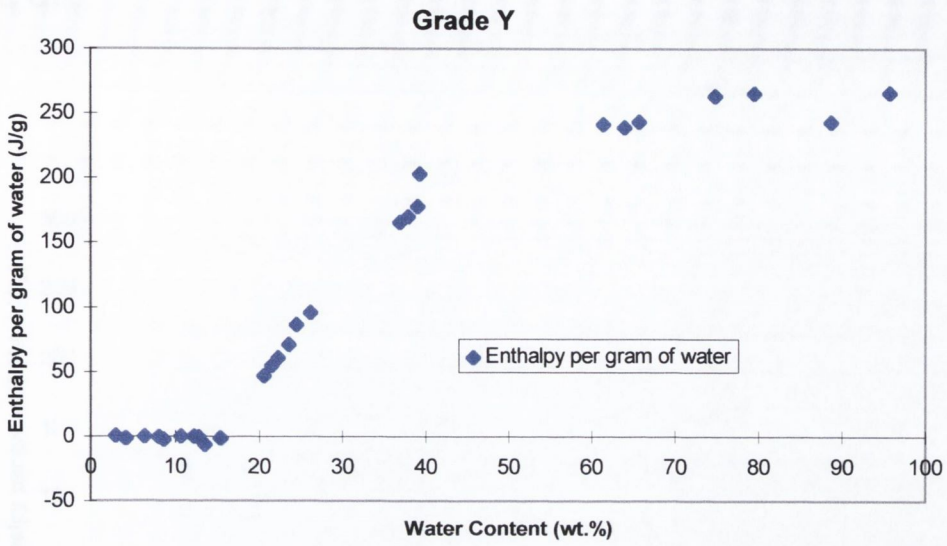
Grade Y
Enthalpy per gram of water (J/g)
300
250
200
150
100
50
0
-50
0
10
20
30
40
50
60
70
80
90
100
Water Content (wt.%)
Enthalpy per gram of water

Plots of enthalpy per gram of water as a function of water content for Avicel® PH-101, Grade X and Grade Y powders, using the exothermic data

(1)

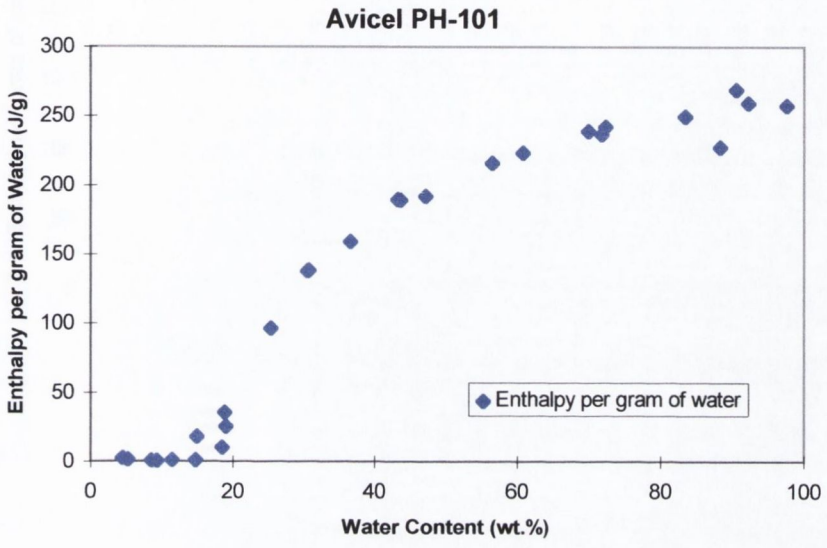

(2)

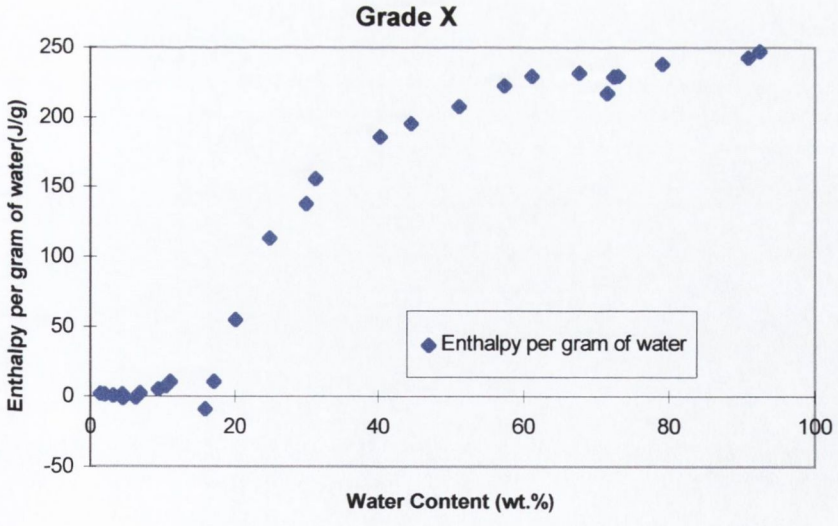

(3)

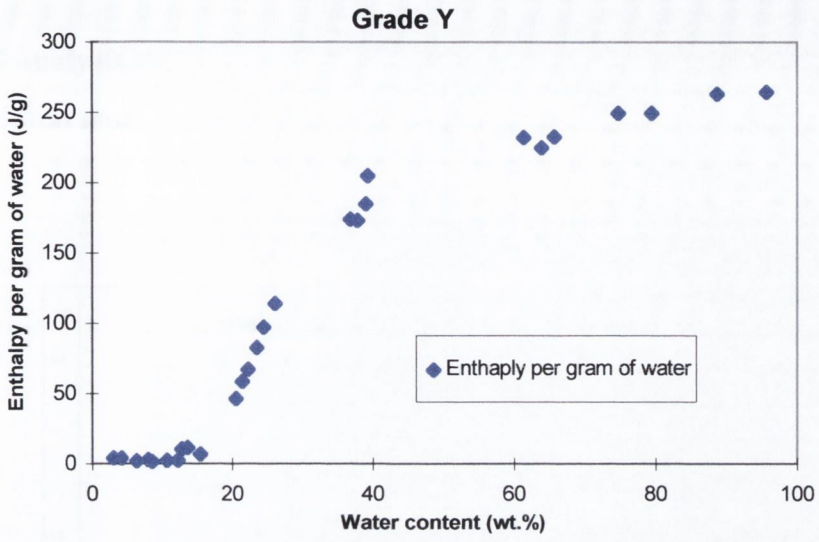
Grade Y
Enthalpy per gram of water (J/g)
300
250
200
150
100
50
0
0
20
40
60
80
100
Water content (wt.%)
Enthaply per gram of water

Appendix 6

TG analysis of diltiazem HCl loaded halloysite 'G' powder samples with varying residual moisture contents

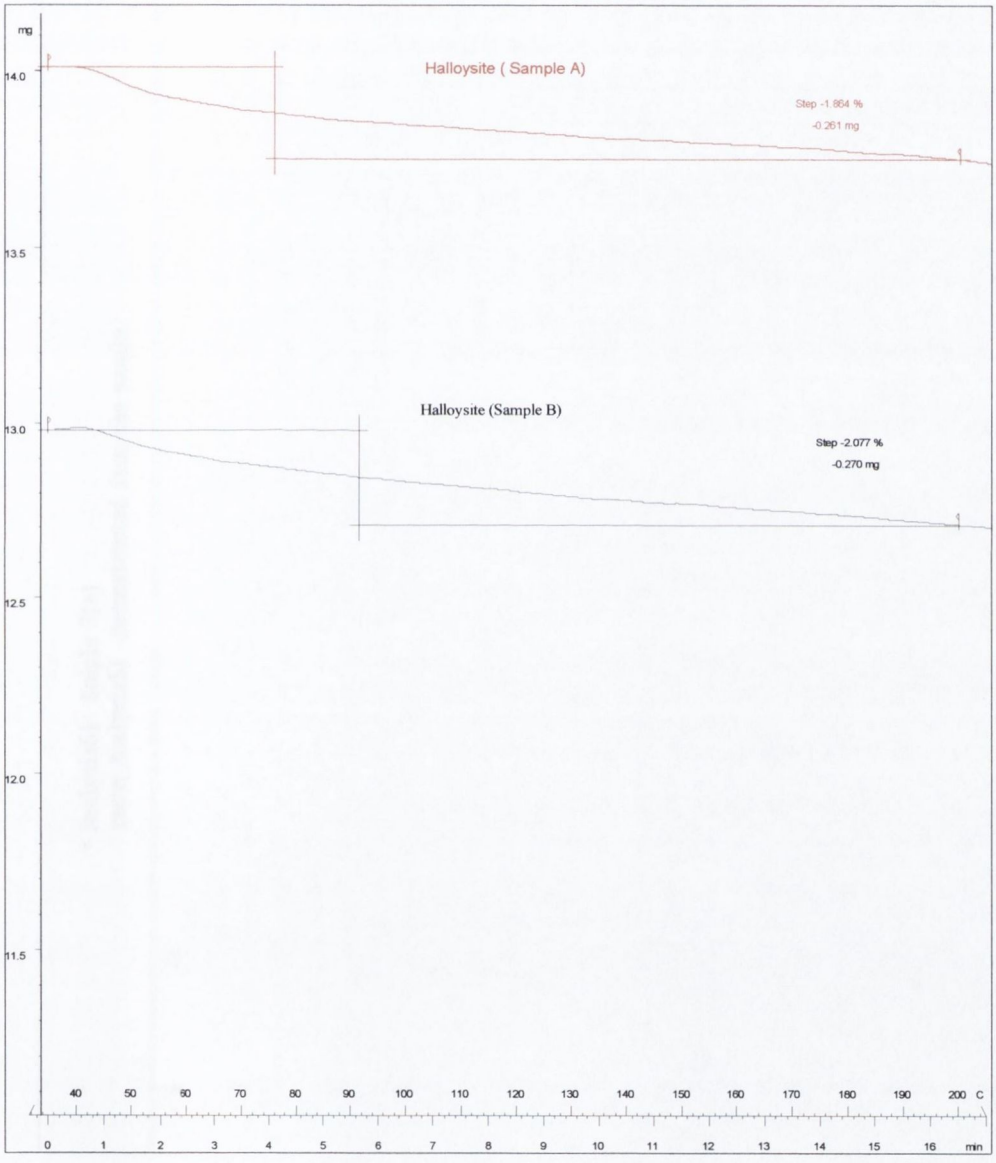

Sample Weight

Temperature (°C)

Appendix 7

Energy dispersive analysis plot of compacted Halloysite 'G' powder (Sample 3)

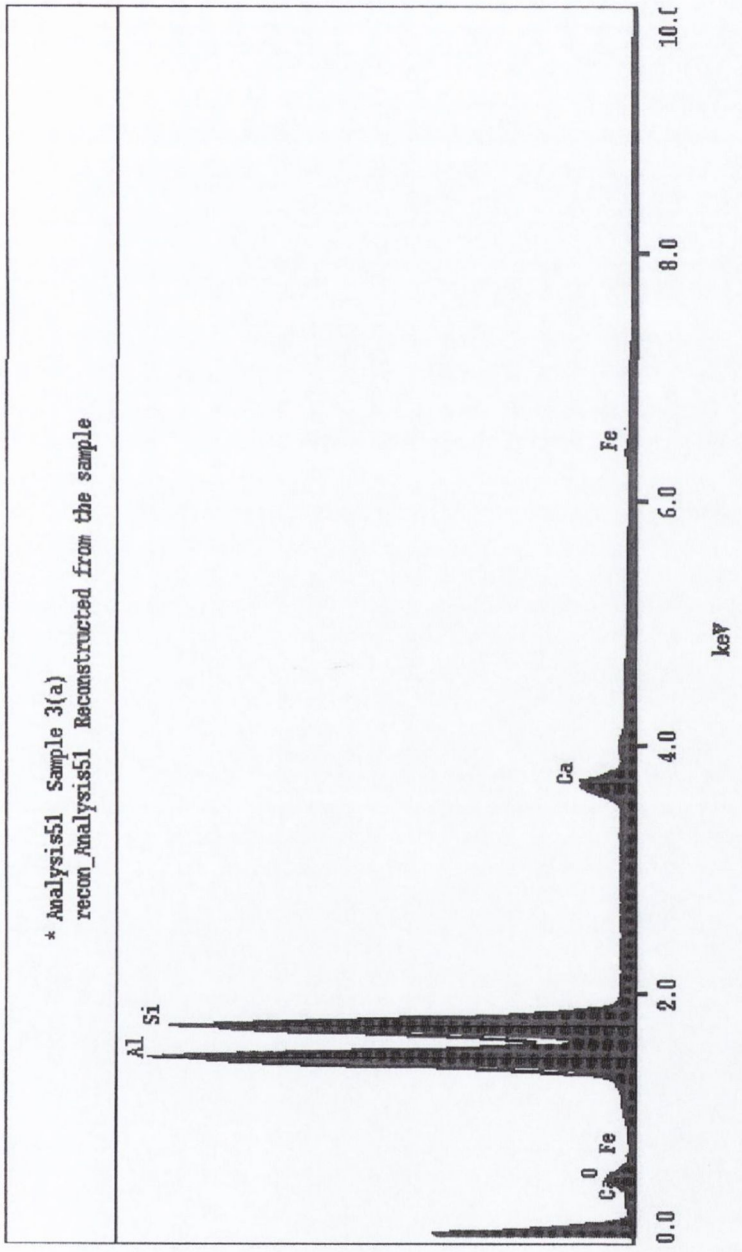

References

Aboutaleb, A. E. and Ahmed, M. O., (1986),

Preparation and evaluation of directly compressed medazepam hydrochloride tablets,

Drug Dev. Ind. Pharm. **12**, 2243-2258.

Alexakis, T., Boadi, D. K., Quong, D., Groboillot, A., O'Neill, I., Poncelet, D. and Neufeld, R. J., (1995),

Microencapsulation of DNA within alginate microspheres and cross-linked chitosan membranes for in vivo application,

Appl. Biochem. Biotechnol., **50**, 93-106.

Allen, T., (1990),

Particle Size Measurement, 4th Ed., Chapman and Hall, London, Chapter 19, 670-672.

Almeida, A. J., Runge, S. and Müller, R. H., (1997),

Peptide-loaded solid lipid nanoparticles (SLN): influence of production parameters,

Int. J. Pharm., **149**, 255-265.

Alpar, O., Deer, J. J., Hersey, J. A. and Shotton, E., (1969),

The possible use of polytetrafluoroethylene (Fluon) as a tablet lubricant,

J. Pharm. Pharmacol., Suppl. **21**, 6S-8S.

Amidon, G. E. and Houghton, M. E., (1995),

The effect of moisture on the mechanical and powder flow properties of microcrystalline cellulose,

Pharm. Res., **12**, 923-929.

Andrew, R. W., Jackson, M. L. and Wada, K., (1960),

Intersalation as a technique for differentiation of kaolin from chloritic minerals by X-ray diffraction,

Proc. Soil. Sci. Soc. Am., **24**, 422-424.

Armstrong, N. A., (1997),

Functionality related tests for excipients,

Int. J. Pharm., **155**, 1-5.

Augsberger, L. L. and Salpeker, A. M., (1974),

Magnesium lauryl sulfate in tableting,

J. Pharm. Sci., **63**, 289.

Baehr, M., Führer, C. and Puls, J., (1991),

Molecular weight distribution, hemicellulose content and batch conformity of pharmaceutical cellulose powders,

Eur. J. Pharm. Biopharm., **37**, 136-141.

Bailey, S. W., (1990),

Halloysite - a critical assessment,

Proc. 9th Int. Clay Conf. Strasbourg, 89-98.

Bates, T. F., Hildebrand, F. A. and Swineford, A., (1950),

Morphology and structure of endellite andhHalloysite

Am. Mineral., **35**, 463-484.

Bekturov, E. A. and Bimendina, L. A., (1981),
Interpolymer complexes,
Adv. Polymer Sci., **41**, 99-145.

Bergfeld, M. J. and Seifert, J., (1996),
Process for the preparation of level-off DP cellulose,
U. S. Patent, **5,543,511**.

Berndt, P., Kurihara, K. and Kunitake, T., (1992),
Adsorption of poly(styrenesulfonate) onto an ammonium monolayer on mica: A surface forces study,
Langmuir, **8**, 2486-2490.

Berthier, P., (1826),
Analyse de l'halloysite,
Ann. Chim. Phys., **32**, 332-335.

Blair, T. C., Buckton, G., Beezer, A. E. and Bloomfield, S. F., (1990),
The interaction of various types of microcrystalline cellulose and starch with water,
Int. J. Pharm., **63**, 251-257.

Bolhuis, G., Reichman, G., Lerk, C., van Kamp, H. and Zuurman, K., (1985),
Evaluation of anhydrous alpha-lactose, a new excipient in direct compression,
Drug Dev. Ind. Pharm., **11**, 1657-1681.

Bolhuis, G. K. and Lerk, C. F., (1973),
Comparative evaluation of excipients for direct compression,
Pharm. Weekbl., **108**, 469-481.

Box, G. E. P., Hunter, W. G. and Hunter, J. S., (1978),

Statistics for Experimenters. An Introduction to Design, Data Analysis and Model Building. John Wiley & Sons, Inc., USA.

Brindley, C. W. and Brown, G., (1980),

Crystal Structures of clay minerals and their X-ray identification,

1st Ed., Mineralogical Society, London.

Buckley, M. M. T., Grant, S. M. and Goa, K. L., (1990),

Diltiazem: a reappraisal of its pharmacology, properties and therapeutic use,

Drugs, **39**, 757-806.

Caillere S., Glaeser R., Esquevin J. and Henin, S. (1950),

Prepararion d'halloysite a 14 Å et a 17 Å,

C. R. Acad. Sci. Paris, **230**, 308-310.

Camp, R. W. and Stanley, H. D., (1991),

Advances in measurement of surface area by gas adsorption,

American Lab., **Sept.**: 34-36.

Carli, F. and Motta, A., (1984),

Particle size and surface area distributions of pharmaceutical powders by microcomputerised mercury porosimetry,

J. Pharm. Sci., **73**, 197-203.

Carmella, C., Colombo, P., Bettinetti, G.P., Giordano, F., Conte, U. and La Manna, A., (1984a),

Swelling properties of disintegrants,

Acta Pharm. Technol., **30**, 132-139.

Carmella, C., Colombo, P., Conte, U., Gazzaniga, A. and La Manna, A., (1984b),
The role of swelling in the disintegration process,
Int. J. Pharm. Tech. Prod. Mfr., **5**, 1-5.

Carr, R. L., (1965),
Evaluating flow properties of solids,
Chem. Eng., **72**, 163-168.

Carr, R. M. and Chih, H., (1971),
Complexes of halloysite with organic compounds,
Clay Minerals, **9**, 153-166.

Carreño-Gómez, B. and Duncan, R., (1997),
Evaluation of the biological properties of soluble chitosan and chitosan microspheres,
Int. J. Pharm., **148**, 231-240.

Carson, C. D. and Kunze, G. W., (1970),
New occurances of tabular halloysite,
Soil Sci. Soc. Am. Proc., **34**, 538-540.

Caulfied, D. F., (1978),
in *Fibre-Water Interactions in Papermaking*, Vol. 1, Fundamental Research Committee, (Eds.), The British Paper and Board Industry Federation, London.

Cavalli, R., Caputo, O., Carlotti, M. E., Trotta, M., Scarnecchia, C. and Gasco, M. R., (1997),
Sterilization and freeze-drying of drug-free and drug-loaded solid lipid nanoparticles,
Int. J. Pharm., **148**, 47-54.

Chatrath, M., Staniforth, J. N., Herbert, I., Luk, S. Y. and Richards, G., (1991),
Source-dependent polymorphism of microcrystalline cellulose,
J. Pharm. Pharmacol., **43**, 7P.

Chopra, R., Podczeck, F. and Newton, J. M., (1995),
The use of a two and three-dimensional shape factor to characterize the sphericity of pellets,
Proc. 1st World Meeting on Pharmaceutics, Biopharmaceutics and Pharm. Technology, Budapest, pp. 349-350.

Chouinard, F., Buczkowski, S. and Lenaerts, V., (1994),
Poly(alkylcyanoacrylate) nanocapsules: physicochemical characterization and mechanism of formation,
Pharm. Res., **11**, 869-874.

Churchman, G. J. and Payne, D., (1983),
Mercury intrusion porosimetry of some New Zealand soils in relation to clay morphology and texture,
J. Soil Sci., **34**, 437-451.

Churchman, G. J. and Theng B. K. G., (1984),
Interactions of halloysites with amides: Mineralogical factors affecting complex formation,
Clay Miner., **19**, 161-175.

Churchman, G. J., Davy, T. J., Aylmore, L. A. G., Gilkes, R. J. and Self, P. G., (1995),
Characteristics of fine pores in some halloysites,
Clay Miner., **30**, 89-98.

Corrigan, O. I., Holohan, E. M. and Reilly, M. R., (1985),
Physicochemical properties of indomethacin and related compounds co-spray dried with polyvinylpyrrolidone,
Drug Dev. Ind. Pharm., **11**, 677-695.

Couvreur, P. and Vauthier, C., (1991),
Polyalkylcyanoacrylate nanoparticles as a drug carrier: present state and perspectives,
J. Control. Rel., **17**, 187-198.

Coyle, F. M., Martin, S. J. and McBrierty, V. J., (1996),
Dynamics of water molecules in polymers,
J. Molec. Liquids, **69**, 95-116.

Day, R. D., Graham, G. G. and Champion, G. D., (1984),
Anti-rheumatic drug interactions,
Clin. Rheum. Dis., **10**, 251-275.

De Boer, A. H., Bolhuis, G. H. and Lerk, C. F., (1978),
Bonding characteristics by scanning electron microscopy of powders mixed with magnesium stearate,
Powder Technol., **20**, 75-82.

Denkbas, E. B., Seyyal, M. and Piskins, E., (1999),
5-Fluorouracil loaded chitosan microspheres for chemoembolization,
J. Microencapsul., **16**, 741-749.

De Souza Santos, P., De Souza Santos, H. and Brindley, G. W., (1966),

Mineralogical studies of kaolinite-halloysite clays. IV, A platy mineral with structural swelling and shrinking characteristics,

Am. Mineral., **51**, 1640-1648.

Diamond, S., (1970),

Pore size distribution in clays,

Clays Clay Miner., **18**, 7-23.

Dixon, J. B. and McKee, T. R., (1974),

Internal and external morphology of tubular and spheroidal halloysite particles,

Clays Clay Miner., **22**, 127-137.

Doelker, E., Gurney, R., Schurz, J., Janosi, A. and Matin, N., (1987),

Degrees of crystallinity and polymerization of modified cellulose powders for direct tabletting,

Powder Technol., **52**, 207-213.

Doelker, E., (1993),

Comparative compaction properties of various microcrystalline cellulose types and generic products,

Drug Dev. Ind. Pharm., **19**, 2399-2471.

Doelker, E., Massuelle, D., Veuillez, F. and Humbert-Droz, P., (1995),

Morphological, packing and flow and tableting properties of new Avicel types,

Drug Dev. Ind. Pharm., **21**, 643-661.

Ek, R., Alderborn, G. and Nyström, C. (1994),

Particle analysis of microcrystalline cellulose: Differentiation between individual particles and their agglomerates,

Int. J. Pharm., **111**, 43-50.

Ek, R., Lennholm, H., Davidson R., Nyström, C. and Ragnarsson, G., (1995),

Pore swelling in beads made of cellulose fibre and fibre fragments,

Int. J. Pharm., **122**, 49-56.

Ek, R. and Kleinebudde, P., (1998),

Microcrystalline cellulose as a sponge as an alternative concept to the crystallite-gel model for extrusion and spheronization,

J. Pharm. Res., **15**, 509-512.

Ellison, N. M. and Servi, R. J., (1985),

Acute renal failure and death following sequential intermediate dose methotrexate and 5-FU: a possible adverse effect due to concurrent indomethacin administration,

Cancer Treat. Rep., **69**, 342-343.

Evans, R. and Luner, P., (1989),

Coagulation of microcrystalline cellulose dispersions,

J. Colloid Interface Sci., **128**, 464-476.

Farmer, V. C., Smith, B. F. L. and Tait, J. M., (1979),

The stability, free energy and heat of formation of imogilite,

Clay Miner., **14**, 103-107.

Ferrari, F., Bertoni, M., Bonferoni, M.C., Rossi, S., Caramella, C. and Nyström, C., (1996),
Investigation on bonding and disintegration properties of pharmaceutical materials,
Int. J. Pharm., **136**, 71-79.

Fielden, K. E., Newton, J. M., O'Brien, P. and Rowe, R. C., (1988),
Thermal studies on the interaction between water and microcrystalline cellulose,
J. Pharm. Pharmacol., **40**, 674-678.

Fielden, K. E., Newton, J. M. and Rowe, R. C., (1992),
A comparison of the extrusion and spheronisation behaviour of wet powder masses processed by a ram extruder and a cylinder extruder,
Int. J. Pharm. **81**, 225-233.

Fielden, K. E., Newton, J. M. and Rowe, R. C., (1993),
The influence of moisture content on spheronization of extrudate processed by a ram extruder,
Int. J. Pharm. **97**, 79-92.

Frank, H. S. and Wen, W-Y., (1957),
Ion-solvent interaction; Structural aspects of ion-solvent interaction in aqueous solutions; a suggested picture of water structure,
Faraday Soc. Discussions, **24**, 133-140.

Fresta, M., Cavallaro, G., Giammona, G., Wehrli, E. and Puglisi, G., (1996),
Preparation and characterization of polyethyl-2-cyanoacrylate nanocapsules containing antiepileptic drugs,
Biomaterials, **17**, 751-758.

Fuhrer, C., (1977),

Substance behaviour in direct compression,

Labo. Pharma. Probl. Techn., **269**, 759-762.

Fukuoka, E., Makita, M. and Yamanura, S., (1986),

Some physicochemical properties of glassy indomethacin,

Chem. Pharm. Bull., **34**, 4314-4321.

Fuoss, R. M. and Sadek, H., (1949),

Mutual interaction of polyelectrolytes,

Science, **110**, 552-554.

Ganza-González, A., Anguiano-Igea, S., Otero-Espinar, F. J. and Blanco Méndez, J., (1999),

Chitosan and chondroitin microspheres for oral-administration controlled release of metoclopramide,

Eur. J. Pharm. Biopharm., **48**, 149-155.

Genta, I., Costantini, M., Asti, A., Conto, B. and Montanari, L., (1998),

Influence of glutaraldehyde on drug release and mucoadhesive properties of chitosan microspheres,

Carbohydrate Polymers, **36**, 81-88.

Godbey, W. T., Wu, K. K. and Mikos, A. G., (1999),

Poly(ethylenimine) and its role in gene delivery,

J. Contr. Release, **60**, 149-160.

Goring, D. A. I., (1978),

in *Fibre-Water Interactions in Papermaking,* Vol. 1, Fundamental Research Committee, (Eds.), The British Paper and Board Industry Federation, London.

Guyot-Hermann, A. M., (1992),

Tablet disintegration and disintegrating agents,

S. T. P. Pharma Sciences, **2**, 445-462.

Handbook of Pharmaceutical Excipients, (2000),

in *Handbook of Pharmaceutical Excipients,* 3rd Edition, A. H. Kibbe, (Ed.), American Pharmaceutical Association, Washington and Pharmaceutical Press, London.

Harrison, J. L. and Greenburg, S. S., (1962),

Dehydration of fully hydrated halloysite from Lawrence County, Indiana.

Clays and Clay Miner., **9**, 374-377.

Harvey, C. C., (1996),

Halloysite - For high quality ceramics,

in *Industrial Clays,* 2nd Edition, Kendall, T., (Ed.), London: Industrial Minerals Information Ltd., 71-73.

Hatakeyama, T., (1989),

Structure and properties of the amorphous region of cellulose, Chapter 2,

in *Cellulose. Structural and Functional Aspects,* J. F. Kennedy, G. O. Philips and P. A Williams (Eds.), Ellis Horwood Ltd.

Hausner, H. H., (1967),
Friction conditions in a mass of metal powder,
Int. J. Powd. Metall., **3**, 7-13.

Hausner, H. H., (1981),
Powder Technol., **30**, 3-8.

He, P., Davis, S. S. and Illum, L., (1999),
Chitosan microspheres prepared by spray drying,
Int. J. Pharm., **187**, 53-65.

Hellen, L. and Yliruusi, J., (1993a),
Process variables of the radial screen extruder Part III: Shape, surface, and flow properties of pellets,
Pharm. Tech. Int., **February**: 38-48.

Hellen, L. and Yliruusi, J., (1993b),
Process variables of instant granulator and spheroniser: I. Physical properties of granules, extrudate and pellets,
Int. J. Pharm., **96**, 197-204.

Heller, J., (1987),
Use of polymers in controlled release of active agents,
in *Controlled Drug Delivery; Fundamentals and Applications*, 2nd Edition, Marcel Dekker, Inc., pp. 179-212.

Heller, J., Lin-Shu, L., Ng, S., Duncan, R. and Richardson, S., (1996),
Alginate/chitosan microporous microspheres for the controlled release of proteins and antigens,
Proc. Int. Symp. Control. Release Bioact. Mater., **23**, 269-270.

Hendricks, S. B., (1938),

On the crystal structure of the clay minerals: Dickite, halloysite, and hydrated halloysite,

Am. Mineral., **23**, 295-301.

Henriksen, I., Sminstad, G. and Karslen, J., (1994),

Interactions between liposomes and chitosans,

Int. J. Pharm., **101**, 227-236.

Hirano, S., Seino, H., Akiyama, Y. and Nonaka, I., (1988),

Biocompatibility of chitosan by oral and intravenous administration,

Polym. Eng. Sci., **59**, 897-901.

Hofmann, U., Endell, K. and Wilm, D., (1934),

Röntgenographische und kolloidchemische untersuchungen über ton,

Agnew. Chem., **47**, 539-547.

Hollenbeck, R. G., Peck, G. E. and Kildsig, D. O., (1978),

Applications of immersional calorimetry to investigation of solid-liquid interactions: microcrystalline cellulose-water system,

Pharm. Sci., **67**, 1599-1606.

Hughes, I. R., (1966),

Mineral changes of halloysite on drying,

N. Z. J. Sci. **9**, 103-113.

Illum, L., Khan, M. A., Mak, E. and Davis, S. S., (1986),

Evaluation of carrier capacity and release characteristics for poly(2-butyl-2-cyanoacrylate) nanoparticles,

Int. J. Pharm., **30**, 17-28.

Jackson, B. L. J., Metcalfe, A. and Wilcock, R. J., (1971),
Adsorption hysteresis on disordered kaolinite,
Trans. Farad. Soc., **67**, 2137-2144.

Jarosz, P. J. and Parrott, E. L., (1984),
Effect of lubricants on tensile strengths of tablets,
Drug Dev. Ind. Pharm., **10**, 259-273.

Johnson, S. L., Guggenheim, S. and Koster van Groos, A. F., (1990),
Thermal stability of halloysite by high pressure differential thermal analysis,
Clays and Clay Miner., **38**, 477-484.

Kassem, M. A. A., (1975),
A technological study on direct compression of tablets,
Ph.D. Thesis, Faculty of Pharmacy, Cairo Univ., Egypt

Keely, C. M. J., (1996),
A thermal analysis and spectroscopic study of hydrated cellulose based materials,
Ph.D. Thesis, Trinity College, University of Dublin

Kelley, O. J. and Shaw, B. T., (1942),
Studies of clay particles with the electron microscope. III, Hydrodynamic considerations in relation to shape of particles,
Soil Sci. Soc. Am., Proc., **7**, 58-68.

Kelley, W. P. and Page, J. B., (1942),
Criteria for the identification of the constituents of soil colloids,
Soil Sci. Soc. Am., Proc., **7**, 175-181.

Khan, F. and Pilpel, N., (1986),

The effect of particle size and moisture on the tensile strength of microcrystalline cellulose powder,

Powder Technol., **48**, 145-150.

Khan, F. and Pilpel, N., (1987),

An investigation of moisture sorption in microcrystalline cellulose using sorption isotherm data and dielectric response,

Powder Technol., **50**, 237-241.

Kirkman, J. H., (1975),

Clay mineralogy of some tephra beds of Rotorua area, North Island, New Zealand,

Clay Miner., **10**, 437-449.

Kirkman, J. H., (1977),

Halloysite disks and cylinders,

Clay Miner., **12**, 199-216.

Kleinebudde, P., (1994a),

Shrinking and swelling properties of pellets containing microcrystalline cellulose and low substituted hydroxypropylcellulose: I. Shrinking properties,

Int. J. Pharm., **109**, 209-219.

Kleinebudde, P., (1994b),

Shrinking and swelling properties of pellets containing microcrystalline cellulose and low substituted hydroxypropylcellulose: II. Swelling properties,

Int. J. Pharm., **109**, 221-227.

Kleinebudde, P., (1997),

The crystallite-gel-model for microcrystalline cellulose in wet granulation, extrusion and spheronization,

Pharm. Res., **14**, 804-809.

Kohyama, N., Fukushima, K. and Fukami, A., (1982),

Interlayer hydrates and complexes of clay minerals observed by electron microscopy using an environmental cell,

Proc. Int. Clay Conf., Bolgna-Pavia, 373-384.

Krässig, H., (1985),

Structure of cellulose and its relation to properties of cellulose fibres, Chapter 1, in *Cellulose and its Derivatives: Chemistry, Biochemistry and Applications*, J. F. Kennedy, G. O. Philips, D. J. Wedlock and P. A. Williams, (Eds.), Ellis Horwood Ltd.

Kristensen, H. G., Holm, P. and Schaefer, I. (1985),

Mechanical properties of moist agglomerates in relation to granulation mechanisms: II. Effects of particle size distribution,

Powder Technology, **44**, 239-247.

Kristl, J., Smid-Korbac, J., Struc, E., Schara, M. and Rupprecht, H., (1993),

Hydrocolloids and gels of chitosans as drug carriers,

Int. J. Pharm., **99**, 13-19.

Kunze, G. W. and Bradley, W. F., (1964),

Occurance of a tabular halloysite in Texas soil,

Clays and Clay Miner., **12**, 523-527.

Landin, M., Martínez-Pacheco, R., Gómez-Amoza, J. L., Souto, C., Concheiro, A. and Rowe, R. C., (1993a),
Effect of country of origin on the properties of microcrystalline cellulose,
Int. J. Pharm., **91**, 123-131.

Landin, M., Martínez-Pacheco, R., Gómez-Amoza, J. L., Souto, C., Concheiro, A. and Rowe, R. C., (1993b),
Effect of batch variation and source of pulp on the properties of microcrystalline cellulose,
Int. J. Pharm., **91**, 131-141.

Landin, M., Gonzalez, M. P., Souto, C., Concheiro, A., Gomez-Amoza, J. L. and Martinez-Pacheco, R., (1993c),
Compaction of two varieties of microcrystalline cellulose as filler-binders II. Hydrochlorothiazide tablets,
Drug Dev. Ind. Pharm. **19**, 1211-1220.

Law, M. F. and Deasy, P. B., (1997),
Use of extrusion-spheronisation to develop an improved oral dosage form of indomethacin,
Int. J. Pharm., **148**, 201-209.

Lenaerts, V., Couvreur, P., Christiaens-Leyh, D., Joiris, E., Roland, M., Rollman, B. and Speiser, P., (1984),
Degradation of polyisobutylcyanoacrylate nanoparticles,
Biomaterials, **5**, 65-68.

Lentz, B. R., Hagler, A. T. and Scheraga, H. A., (1965),

J. Phys. Chem., Part C, **11**, 27.

Leonard, F., Kulkarni, R. K., Brandes, G., Nelson, J. and Mameron, J. J., (1966),

Synthesis and degradation of poly-(alkylcyanoacrylates),

J. Applied Polym. Sci., **10**, 259-272.

Lerk, C.F., Bolhuis, C.K. and de Boer, A.H., (1979),

Effect of microcrystalline cellulose on liquid penetration in and disintegration of directly compressed tablets,

J. Pharm. Sci., **68**, 205-211.

Le Thiesse, J. C., (1989),

2eme Journee Scientifique Preformulation du Medicament et Developpement Galenique, Faculte de Pharmacie, Dijon, pp. 43-89.

Li, T. Q., Henricksson, O., Klasen, T. and Odberg, L., (1992),

Water diffusion in wood pulp cellulose fibres studied by means of the pulsed gradient spin-echo method,

J. Colloid Interface Sci., **154**, 305-315.

Livingstone, J. L., (1970),

Compressed tablets,

Manuf. Chemist Aerosol News, **43**, 23-25.

Lovrecich, M., Nobile, F., Rubessa, F. and Zingone, G., (1996),

Effect of ageing on the release of indomethacin from solid dispersions with Eudragits,

Int. J. Pharm., **131**, 247-255.

Lvov, Y., Ariga, K., Ichinose, I. and Kunitake, T., (1996),

Formation of ultrathin multilayer and hydrated gel from montmorillonite and linear polycations,

Langmuir, **12**, 3038-3044.

MacEwan, D. M. C., (1946),

Halloysite-organic complexes,

Nature **157**, 159-160.

MacEwan, D. M. C., (1948),

Complexes of clays with organic compounds. 1. Complex formation between montmorillonite and halloysite and certain organic liquids,

Trans. Faraday Soc., **44**, 349-367.

Malamataris, S., Goidas, P. and Dimitriou, A., (1991),

Moisture sorption and tensile strength of some tableted direct compression excipients,

Int. J. Pharm., **68**, 51.

Marshall, K. and Sixsmith, D., (1974),

Some physical characteristics of microcrystalline cellulose I. Powders for pharmaceutical use,

Drug Dev. Comm., **1**, 51-71.

Martin, A., (1993),

Physical Pharmacy, 4th Ed., Lea & Febiger, USA.

Martindale,(1999),

Martindale. The Extra Pharmacopoeia, 32nd Edition, Parfitt, K. (Ed.), The Pharmaceutical Press, London.

Matsumoto, T., (1972),

in *Tissue Adhesives in Surgery,* Medical Examination Publishers, New York.

Mazzo, D. J., Obetz, C. L. and Shuster, J., (1994),

Diltiazem Hydrochloride,

in *Analytical Profiles of Drug Substances and Excipients, Vol. 23,* Brittain, H. G. (Ed.), American Pharmaceutical Association, published by the Academic Press Inc., London, pp. 53-98.

M^{c}Crea, A. F., Annud, R. R. and Gilkes, R. J., (1990),

Mineralogical and physical properties of lateritic pallid zone materials developed from granite and dolerite,

Geoderma, **47**, 33-47.

Mendel, E. J., (1972),

Direct compression method for producing solid dosage forms,

Manuf. Chemist Aerosol News, **43**, 43-46.

Merck Index, (1996),

The Merck Index. An Encyclopedia of chemicals, drugs and biologicals, 12th Edition, Merck & Co., Inc., New Jersey.

Michaels, A. S., (1965),

Polyelectrolyte complexes,

Ind. Eng. Chem., **57**, 32-40.

Miller, W. D. and Keller, W. D., (1961),

Differentiation between endellite-halloysite and kaolinite by treatment with potassium acetate and ethylene glycol,

10th National Conference on Clays and Clay Minerals, 244-253.

Morris, R. M., (1982),

Magnetically-localizable, biodegradable lipid microspheres,

U. S. Patent, **4,331,654**.

Morrison, J. L. and Dzieciuch, M. A., (1959),

The thermodynamic properties of the system cellulose-water vapour,

Can. J. Chem., **37**, 1379-1390.

Müller, R. H., Mehnert, W., Lucks, J., Schwarz, C., zur Mühlen, A., Weyhers, H., Freitas, C. and Rühl, D., (1995),

Solid lipid nanoparticles (SLN) – An alternative colloidal carrier system for controlled drug delivery,

Eur. J. Pharm. Biopharm., **41**, 62-69.

Müller, R. H. and Peters, K., (1998),

Nanosuspensions for the formulation of poorly soluble drugs I. Preparation by a size-reduction technique,

Int. J. Pharm., **160**, 229-237.

Murray, H. H., (1999),

Applied clay mineralogy today and tomorrow,

Clay Miner., **34**, 39-49.

Nagasawa, K., (1969),

Kaolin minerals in Cenozoic sediments of Central Japan,

Proc. Int. Clay Conf., Tokyo, **1**, 15-30.

Nakai, Y., Fukuoka, E., Nakajima, S. and Hasegawa, J., (1977),

Crystallinity and physical characteristics of microcrystalline cellulose,

Chem. Pharm. Bull., **25**, 96-101.

Nakamura, K., Hatakeyama, T. and Hatakeyama, H., (1981),
Studies on bound water of cellulose by differential scanning calorimetry,
Textile Research Journal, **116**, 607-613.

Nelson, N. L. and O'Connor, R. T., (1964),
Relation of certain infrared bands to cellulose crystallinity and crystal lattice type. Part II. A new infrared ratio for estimation of crystallinity in cellulose I and II,
J. Appl. Polym. Sci., **8**, 1325-1341.

Nevell, T. P. and Zeronian, S. H., (1985),
Cellulose Chemistry Fundamentals, Chapter 1,
in *Cellulose Chemistry and its Applications*, T. P. Nevell and S. H. Zeronian, (Eds.), Ellis Horwood Ltd.

Newitt, D. M. and Conway Jones, J. M., (1958),
A contribution to the theory and practice of granulation,
Trans. Inst. Chem. Eng., **36**, 422-442.

Newman, R. H., Childs, C. W. and Churchman, G. J., (1994),
Aluminium coordination and structural disorder in halloysite and kaolinite by ^{27}Al NMR spectroscopy,
Clay Miner., **29**, 305-312.

Newton, J. M., Chow, A. K. and Jeewa, K. B., (1992),
The effect of excipient source on spherical granules made by extrusion/spheronization,
Pharm. Tech. Int., **4** , 52-58.

Njopwouo, D., Roques, G. and Wandji, R., (1987),

A contribution to the study of the catalytic action of clays on the polymerisation of styrene I: Characterisation of polystyrenes,

Clay Miner., **22**, 145-156.

Noro, H., (1986),

Hexagonal platy halloysite in an altered tuff bed, Komaki City, Aichi Prefecture, Central Japan,

Clay Miner., **21**, 401-415.

O'Brien, M., McCauley, J. and Cohen, E., (1984),

Indomethacin,

in *Analytical Profiles of Drug Substances,* Vol. 13, Florey, K. (Ed.), American Pharmaceutical Association, published by the American Press, Inc., London, pp. 211-238.

Orienti, I., Aiedeh, K., Gianasi, E., Bertasi, V. and Zecchi, V., (1996),

Indomethacin-loaded chitosan microspheres. Correlation between erosion process and release kinetics,

J. Microencap., **13**, 463-472.

Parker, M. D. and Rowe, R. C., (1991),

Source variation in the wet massing (granulation) of some microcrystalline celluloses,

Powder Technol., **65**, 273-281.

Patel, N. K. and Reier, G. E., (1994),

An evaluation of microcrystalline cellulose and lactose excipients using an instrumented single station tablet press,

Int. J. Pharm., **110**, 203-210.

Pauling, L. C., (1930),

The structure of micas and related minerals,

Nat. Acad. Sci. Proc., **16**, 123-129.

Pharmaceutical Codex, (1994),

The Pharmaceutical Codex. Principles and Practice of Pharmaceutics, 12th Edition, A. Wade, (Ed.), The Pharmaceutical Press, London, UK.

Pifferi, G., (1995),

Qualità e performance degli eccipienti nella formulazione farmaceutica,

Rapporti GSISR, No, 9-5-95.

Pifferi, G., Santoro, P. and Pedrani, M., (1999),

Quality and functionality of excipients,

Il Farmaco, **54**, 1-14.

Podczeck, F. and Révész, P., (1993),

Evaluation of the properties of microcrystalline and microfine cellulose powders,

Int. J. Pharm., **91**, 183-193.

Podczeck, F. and Miah, Y., (1996),

The influence of particle size and shape on the angle of internal friction and the flow factor of unlubricated and lubricated powders,

Int. J. Pharm., **144**, 187-194.

Pouchly, J., Biros, J. and Benes, S., (1979),

Heat capacities of water swollen hydrophilic polymers above and below 0°C,

Macromol. Chemie, **180**, 745-760.

Price, R. and Patchan, M., (1991),

Controlled release from cylindrical microstructures,

J. Microencap., **8**, 301-306.

Price, R. R. and Gaber, B. P., (1997),

Controlled release of active agents using inorganic tubules,

U. S. Patent, **5,651,976**.

Procianoy, R. S., Garcia-Prats, J. A. and Hither, H. M., (1980),

Use of indomethacin and its relationship to retinopathy of prematurity in very low birthweight infants,

Arch. Dis. Child., **55**, 362-364.

Puglisi, G., Giammona, G., Fresta, M., Carlisi, B., Micali, N. and Villari, A., (1993),

Evaluation of polyalkylcyanoacrylate nanoparticles as a potential drug carrier: preparation, morphological characterization and loading capacity,

J. Microencap., **10**, 353-366.

Quinn, F. X., Kampff, E., Smyth, G. and McBrierty, V. J., (1988),

Water in hydrogels. 1. A study of water in poly (N-vinyl-2-pyrolidone / methyl methacrylate) copolymer,

Macromol., **21**, 3191-3198.

Radebaugh, G. W., Babu, S. R. and Bondi, J. N., (1989),

Characterisation of the visco-elastic properties of compacted pharmaceutical powders by a novel non-destructive technique,

Int. J. Pharm., **57**, 95-105.

Radoslovich, E. W., (1963),

The cell dimensions and symmetry of layer lattice silicates. VI, Serpentine and kaolin morphology,

Am. Mineral., **48**, 368-378.

Refojo, M. F., Dohlman, C. H. and Koliopoulos, J., (1971),

Adhesives in ophthalmology: a review,

Surv. Ophthalmol., **15**, 217.

Röhm-Pharma, (1996),

Eudragit E - Application in the production of pharmaceutical preparations,

in *Company literature,* pp. 1-7.

Rowe, R. C., (1988),

Interaction of lubricants with microcrystalline cellulose and anhydrous lactose - a solubility parameter approach,

Int. J. Pharm., **41**, 223-226.

Rowe, R. C., McKillop, A. G. and Bray, D., (1994),

The effect of batch and source variation on the crystallinity of microcrystalline cellulose,

Int. J. Pharm., **101**, 169-172.

Rumpf, H., (1958a),

Basic principles and methods of granulation I, II,

Chemie - Ingr - Tech., **30**, 138-144.

Rumpf, H., (1958b),

Basic principles and methods of granulation III, Survey of technical granulation processes,

Chemie - Ingr - Tech., **30**, 329-336.

Schnur, J. M., Price, R. and Rudolph, A. S., (1994),

Biologically engineered microstructures: controlled release applications,

J. Contr. Rel., **28**, 3-13.

Schwarz, C. and Mehnert, W., (1997),

Freeze-drying of drug-free and drug-loaded solid lipid nanoparticles (SLN),

Int. J. Pharm., **157**, 171-179.

Schwarz, C. and Mehnert, W., (1999),

Solid lipid nanoparticles (SLN) for controlled drug delivery II. Drug incorporation and physicochemical characterization,

J. Microencap., **16**, 205-213.

Selkirk, A. A., and Ganderton, D., (1970a),

An investigation of the pore structure of tablets of sucrose and lactose by mercury porosimetry,

J. Pharm. Pharmacol., **22** Suppl., 79S-85S.

Selkirk, A. A., and Ganderton, D., (1970b),

The influence of wet and dry granulation methods on the pore structure of lactose tablets,

J. Pharm. Pharmacol., **22** Suppl., 89S-94S.

Shaw, B. T. and Humbert, R. P., (1941),
Electron micrographs of clay minerals,
Soil Sci. Soc. Am. Proc., **6**, 146-149.

Sherrington, P. J., (1968),
The granulation of sand as an aid to understanding further granulation. The relationship between liquid phase and average granule size,
Inst. Chem. Eng. Symposium on Aggregation, 8-21.

Sing, K. S. W., Everett, D. H., Haul, R. A. W., Moscou, L., Pierotti, R. A., Rouquerol, J. and Siemieneiwska, T., (1985),
Reporting physisorption data for gas/solid systems with special reference to the determination of surface area and porosity,
Pure & Appl. Chem., **57**, 603-619.

Singh, D. K. and Ray, A. R., (1999),
Controlled release of glucose through modified chitosan membranes,
J. Membrane Sci., **155**, 107-112.

Sisson, W. A., (1966),
"Avicel Microcrystalline Cellulose, Its Production, Properties and Application,"
A series of talks given at the Avicel Distributors Meeting, Geneva, Switzerland.

Sixsmith, D., (1976),
The properties of tablets containing microcrystalline cellulose,
J. Pharm. Pharmacol., **29**, 82-85.

Smith, D. M. and Schentrup, S., (1987),
Mercury porosimetry of fine particles: particle interaction and compression effects,
Powder Technol., **49**, 241-247.

Soltys, J., Lisowski, Z. and Knapczyk, J., (1984),

X-ray diffraction study of the crystallinity index and the structure of the microcrystalline cellulose,

Acta Pharm. Technol., **30**, 174-180.

Soma, M., Churchman, G. J. and Theng, B. K. G., (1992),

X-ray photoelectron spectroscopic analysis of halloysites with different composition and particle morphology,

Clay Miner., **27**, 413-421.

Speiser, P., (1990),

Lipidnanopellets als trägersystem für arzneimittel zur peroralen anwendung,

Eur. Patent, **EP 0167825**.

Stanley-Wood, N. G., (1987),

Part. Charact. **4**, 106.

Stephens, K. (Ed.), (1992),

Micromeritics Instrument Corporation, Norcross, Georgia, USA.,

Microreport, 1st Quarter, pp.7.

Stone, J. E. and Scallon, A. M., (1968),

A structural model for the cell wall of water swollen wood pulp fibres based on their accessibility to macromolecules,

Cellulose Chem. Technol., **2**, 343-358.

Strickland, W. A., Busse, L. W. and Higuchi, T., (1956),

The physics of tablet compression XI. Determination of porosity of tablet granulations,

J. Am. Pharm. Assoc., Sci. Ed., **45**, 482-486.

Sudo, T. and Shimoda, S., (1978),

Developments in sedimentology - Clays and clay minerals of Japan, *1st Ed.*, Kodansha Ltd., Elsevier Scientific Publishing Company, Amsterdam - Oxford - New York.

Sukhorukov, G. B., Donath, E., Davis, S., Lichtenfeld, H., Caruso, F., Popov, V. I. and Möhwald, H., (1998),

Stepwise polyelectrolyte assembly on particle surfaces: a novel approach to colloid design,

Polym. Advanced Technol., **9**, 759-767.

Takahashi, T., Takayama, K., Machida, Y. and Nagai, T., (1990),

Characteristics of polyion complexes of chitosan with sodium alginate and sodium polyacrylate,

Int. J. Pharm., **61**, 35-41.

Tang, Y. and Gan, K., (1998),

Statistical evaluation of in vitro dissolution of different brands of ciprofloxacin hydrochloride tablets and capsules.

Drug Dev. Ind. Pharm., **24**, 549-552.

Tari, G., Bobos, I., Gomes, C. S. F. and Ferreira, J. M. F., (1999),

Modification of surface charge properties during kaolinite to halloysite 7A° transformation,

J. Colloid Interface Sci., **210**, 360-366.

Tazaki, K., (1982),

Analytical electron microscopic studies of halloysite formation processes - morphology and composition of halloysite,

Proc. Int. Clay Conf. Bologna-Pavia, 573-584.

Theng, B. K. G. and Wells, N., (1995a),
The flow characteristics of halloysite suspensions,
Clay Miner., **30**, 99-106.

Theng, B. K. G. and Wells, N., (1995b),
Assessing the capacity of some New Zealand clays for decolourizing vegetable oil and butter,
Applied Clay Sci., **9**, 321-326.

Thuss, A., Milano, G. and Kubar, J., (1986),
Clinical and pharmacokinetic evidence of a life-threatening interaction between methotrexate and ketoprofen,
Lancet, **1**, 256-258.

Tsuchida, E., Osada, Y. and Abe, K., (1974),
Formation of polyion complexes between polycarboxylic acids and polycations carrying charges in the chain backbone,
Macromol. Chem., **175**, 583-592.

United States Pharmacopoeia, (1995),
The United States Pharmacopoeia, XXIII. The National Formulary,
United States Pharmacopoeial Convention, Inc., USA.

UpJohn Company, (1985),
Motrin prescribing information,
Company Literature, The UpJohn Company, Kalamazoo, MI.

Van den Berg, C., (1981),

Vapour sorption equilibria and other water-starch interactions; a physiochemical approach,

Ph. D. Thesis, Agricultural University, Wageningen, The Netherlands.

Vanholder, R., Misttem, A., Roels, H. and Matton, G., (1993),

Cyanoacrylate tissue adhesive for closing skin wounds: a double blind randomized comparison with suture,

Biomaterials, **14**, 737.

Van Kamp, H. V., Bolhuis, G. K., Kussendrager, K. D. and Lerk, C. F., (1986),

Studies on tableting properties of lactose. IV Dissolution and disintegration properties of different types of crystalline lactose,

Int. J. Pharm., **28**, 229-238.

Vinogradov, S., Batrakova, E. and Kabanov, A., (1999),

Poly(ethylene glycol) – polyethyleneimine NanoGel™ particles: novel drug delivery systems for antisense oligonucleotides,

Colloids & Surfaces B: Biointerfaces, **16**, 291-304.

Wada, K., (1961),

Lattice expansion of kaolinite minerals by treatment with potassium acetate,

Am. Mineral., **46**, 78-91.

Wada, K., (1965),

Intercalation of water in kaolin minerals,

Am. Mineral., **50**, 924-941.

Wan, L. S., Heng, P. W. and Liew, C. V., (1993),
Spheronisation conditions on spheroid shape and size,
Int. J. Pharm., **96**, 59-65.

Weiss, A., Thielepape, W., Göring, G., Ritter, W. and Schäfer, H., (1963),
Kaolinite intercalation compounds,
Proc. Int. Clay Conf., Stockholm, vol. 1, 287-305.

Weiss, A., Thielepape, W. and Orth, H., (1966),
New kaolinite interlamellar complexes,
Proc. Int. Clay Conf., Jerusalem, vol. 1, 277-293.

Williams III, R. O., Sriwongjanya, M. and Barron, M. K., (1997),
Compaction properties of microcrystalline cellulose using tableting indices,
Drug Dev. Ind. Pharm., **23**, 695-704.

Yamamoto, H., (1968),
1-Acyl-indoles. II. A new syntheses of 1-(*p*-chlorobenzoyl)-5-methoxy-2-methyl-3-indolylacetic acid and its polymorphism,
Chem. Pharm. Bull., **16**, 17-19.

Yamamoto, H., Takeuchi, H., Hino, T. and Kawashima, Y., (2000),
Mucoadhesive liposomes: Physicochemical properties and release behaviour of water soluble drugs from chitosan-coated liposomes,
S. T. P. Pharma Sciences, **10**, 63-68.

Yang, L. and Fassihi, R., (1997),
Examination of drug solubility, polymer types, hydrodynamics and loading dose on drug release behavior from a triple-layer asymmetric configuration delivery system,
Int. J. Pharm., **155**, 219-229.

Yeh, T. F., Wilks, A. and Singh, J., (1982),
Frusemide prevents the renal side effects of indomethacin therapy in premature infants with patent ductus arteriosus,
J. Pediatr., **101**, 433-437.

York, P., Bassam, F., Rowe, R. C. and Roberts, R. J., (1990),
Fracture mechanics of microcrystalline cellulose powders,
Int. J. Pharm., **66**, 143-148.

Young, G. J. and Healey, F. H., (1954),
The physical structure of asbestos,
J. Phys. Chem., **58**, 881-884.

Yu, H. C. M., Rubenstein, M. H., Jackson, I. M. and Elsabbagh, H. M., (1989),
Compaction characterisation of paracetemol and Avicel mixtures,
Drug Dev. Ind. Pharm., **15**, 801-823.

Zografi, G., Kontny, M. J., Yang, A. Y. S. and Brenner, G. S., (1983),
Surface area and water vapor sorption of microcrystalline cellulose,
Int. J. Pharm., **18**, 99-116.

Zografi, G., Kontny, M. J., Yang, A. Y. S. and Brenner, G. S., (1984),
Surface area and water sorption of microcrystalline cellulose,
Int. J. Pharm., **18**, 99-106.

Zouai, O., Thomas, C. and Pourcelt-Roubeau, Y., (1996),
Microcrystalline cellulose: Investigation of porous structure of Avicel PH-102 from mercury porosimeter measurements,
Drug Dev. Ind. Pharm., **22**, 1253-1257.

Zur Mühlen, A., Schwarz, C. and Mehnert, W., (1998),

Solid lipid nanoparticles (SLN) for controlled drug release delivery – Drug release and release mechanism,

Eur, J. Pharm. Biopharm., **45**, 149-155.